Osteoblastogenic differentiation of mesenchymal stem cells through nanoscale stimulation: The conception of a novel 3D osteogenic bioreactor

Gabriel Delsol Pemberton

(BSc (Hons), MSc, MRes)

This thesis is submitted for the degree of Doctor of Philosophy at the University of Glasgow

Centre for Cell Engineering

Institute for Molecular, Cell and System Biology

College of Medical, Veterinary and Life Sciences

University of Glasgow

United Kingdom

G12 8QQ

“If you want to find the secrets of the universe, think in terms of energy, frequency and vibration!”

- Nikola Tesla

Abstract

Throughout this body of work low amplitude high frequency (500 Hz – 5000 Hz) mechanical stimulation and its effect to induce osteogenesis on bone marrow derived MSCs has been investigated. Due to the nanolevel amplitudes of these high frequency vertical vibrations the term nanokicking appeared to be appropriate and was subsequently used throughout this thesis to refer to these high frequency sinusoidal stimulations provided by the bioreactor. In the first instance this work was performed in 2D and biological analyses to determine osteogenesis were carried out at a transcript (mRNA), protein and mineralisation level. Affirmative results for osteogensis were observed from genes and proteins (RUNX2, osteocalin, osteopontin) related to the osteoblast phenotype by qRT-PCR, in cell western, and immunostaining. To determine the prescence of inorganic osseous minerals, more specific techniques such as Raman spectroscopy, micro-computed tomography and histological stainings (Von Kossa/Alizarin Red) were further employed. The results observed remained in line with previously published material (Gentleman et al., 2009) drawing the conclusion that calcium phosphate ($Ca_{10}(PO_4)_6$, through nanokicking,was formed *in vitro*.

The natural progession of this research meant that a novel vibrational bioreactor was conceived and designed, through the use of Lean and Six Sigma principles (Andrew Thomas, 2004; Caldwell, 2006), in order to assess the potential of nanokicking in 3D. Here collagen was employed as a biomimetic scaffold and affirmative results for osteogenesis were observed.

The bioreactor was unique in that long term (up to 46 days) sterile culture was achieved, it was easy to use and there was no requirement for osteogenic media, growth factors or complex chemistries (e.g. dexamethasone, rhBMP2) in order to induce osteogenesis. The cost of use and maintence was relatively cheap compared to available commercial bioreactors (Rauh et al., 2011b).

It is envisaged that this technology may one day have real world use for ossesous tissue regeneration and care in a GMP and clinical setting, or for the preparation of autologous tissue for medical testing in the burgeoning field of personalised medicine.

Table of Contents

List of Tables

Chapter I: General Introduction

Chapter II: Validation of a 2D nanokicking osteoblastic bioreactor

Chapter III: Osteogenesis using the 2D bioreactor – nanotopography & nanokicking

Chapter IV: Validation of a novel nanokicking bioreactor for use with 3D collagen gels

Chapter V: Osteogenesis in collagen gels by nanokicking using the 3D bioreactor

List of Figures

Chapter I: General Introduction

Chapter II: Validation of a 2D nanokicking osteoblastic bioreactor

Chapter III: Osteogenesis using the 2D bioreactor nanotopography & nanokicking

Chapter IV: Validation of a novel nanokicking bioreactor for use with 3D collagen gels

Chapter V: Osteogenesis in collagen gels by nanokicking using the 3D bioreactor

Chapter VI: General discussion

List of Abbreviations

BGLAP	Bone gamma carboxyglutamate protein
OCN	Osteocalcin
OPN	Osteopontin
Runx2	Runt-related transcription factor 2
ONN	Osteonectin
PPARγ	Peroxisome proliferator-activated receptor gamma
BMP	Bone morphogenetic protein
COL I	Collagen Type I
ALKP	Alkaline phosphatase
BSP	Bone sialoprotein
TGFβ	Transforming growth factor beta
SDF	Stromal cell-derived factor
IGF	Insulin-like growth factor
VEGF	Vascular endothelial growth factor
TSG	Tumour necrosis factor inducible gene 6 protein
GAPDH	Glyceraldehyde 3-phosphate dehydrogenase
HPRT1	Hypoxanthine phosphoribosyltranferase
GUSB	β-glucuronidase
TFRC	Transferin receptor
PCL	Polycaprolactone
MSC	Mesenchymal stem cell
HSC	Hematopoietic stem cell
ESC	Embryonic stem cell
iPSC	Induced pluripotent stem cell
pES	Parthenogenetic embryonic stem cell
gPS	Germline derived pluripotent stem cell
MG-63	Human osteosarcoma cell line
ECM	Extracellular matrix
JNK	C-jun N-terminal kinase
FAK	Focal adhesion kinase
MAPK	Mitogen activated protein kinase
ERK	Extracellular signal regulated kinase
PCR	Polymerase chain reaction
RGD	arganine-glycine-aspartic acid
cDNA	complementary deoxyribosenucleic acid
ANOVA	Analysis of variance
SD	Standard deviation
mRNA	Messenger ribonucleic acid
2D	Two-dimensional
3D	Three-dimensional

ROCK	Rho associated protein kinase
RhoA	Ras homoog gene family A
v/v	Volume by volume
mL	Milli-litre
BSA	Bovine serum albumin
FBS	Fetal bovine serum
PBS	Phosphate buffer saline
w/w	Weight by weight
mM	Milli-Molar
nm	Nanometre
Pa	Pascal
V	Voltage
T	Tesla
Khz	Kilohertz
Hz	Hertz
Rpm	Rotations per minute
LZT	Lead zirconate titanate
Htert	human telomerase reverse transcriptase
GMP	Good manufacturing practice
FDA	Food and drug administration
DMEM	Duldeco's modified eagle medium
NSq-50	Near square 50
Qrt-PCR	Quantitative reverse transcriptase polymerase chain reaction
OSM	Osteogenic media
CD	Cluster of differentiation
SSEA	Stage specific embryonic antigen
Micro-CT	Micro-computed tomography
HLA	Human leukocyte antigen
MHC	Major histocompatibility complex
cAMP	Cyclic adenosine monophosphate
LINC	Linker of nucleoskeleton and cytoskeleton
FFT	Fast fourier transform

Oral Presentations/ Publications / Patent / Awards

- Gabriel D Pemberton, Peter Childs, Stuart Reid, Nikolaj Gadegaard, Adam SG Curtis and Matthew Dalby (2015). Low amplitude osteogenic inducement of mesenchymal stem cells in 3D. The Wellcome Trust International Conference - The biology of regenerative medicines.

- Gabriel D Pemberton, Peter Childs, Stuart Reid, Habib Nikukar, P Monica Tsimbouri, Nikolaj Gadegaard, Adam SG Curtis and Matthew Dalby (2015). Nanoscale stimulation of osteoblastogenesis from mesenchymal stem cells: nanotopography and nanokicking. Nanomedicine, Vol. 10, No. 4, Pages 547-560, ISSN:1743-5889, DOI:10.2217/NNM.14.134.

- Gabriel D. Pemberton, Peter Childs, Stuart Reid, Nikolaj Gadegaard, Richard Burchmore, Adam S.G. Curtis, Matt Dalby (2014). Nano-Kicking Stem Cells into Making Bone. 11TH Tissue and Cell Engineering Society (TCES) annual national conference.

- Gabriel D. Pemberton, Habib, Nikukar, Peter Childs, Stuart Reid, Nikolaj Gadegaard, Richard Burchmore and Matt Dalby (2013). High Frequency Piezo Stimulation of Mesenchymal Stem Cells. Doctoral Training Centre (DTC) – College of Medical Veterinary and Life Sciences Conference, University of Glasgow.

- Paper written for publication - Gabriel D. Pemberton, Peter G. Childs, Vineetha Jayawarna, Adam S.G. Curtis, Stuart Reid, Matthew J. Dalby. Conception of a novel nanovibrational bioreactor for 3D osseous tissue engineering.

- Patent application submitted to the UK patent office Title: Nanomechanical Bioreactor.

➢ Prize won at the 2014, 11th Tissue and Cell Engineering Society (TCES) national conference, for the runner up oral presentation award.

Acknowledgements

I acknowledge the supervision and guidance provided during my PhD by Professor Mathew Dalby, Professor Nikolaj Gadegaard, Professor Adam Curtis, and technical advice and guidance rendered by Dr. Mathias Riehle and Dr. Stuart Reid.

I would also like to thank Dr. Habib Nikukar, Dr. Monica Tsimbouri and Carol-Anne Smith for their technical support and help in becoming adept in biological/stem cell culture and biological analysis. I also thank Carol-Anne Smith and Josie McGhee for their assistance in the laboratory which made all the experiments possible.

I acknowledge Mr. Peter Childs, who performed the ANSYS modelling used during by 2D bioreactor assessment and also helped me perform the interferometry measurements and calibrations. I also acknowledge him for helping me invent and optimise the 3D bioreactor from the 2D bioreactor system, and also building the 3D bioreactor along with Dr. Stuart Reid.

I acknowledge Dr. Robert Wallace who performed the micro-CT testing and analysis used during my PhD.

I acknowledge Dr. Peter Cheung who helped me perform the Raman spectrometry analysis.

I would also like to acknowledge Dr. Vineetha Jayawarna whose guidance assistance and training allowed me to perform the rheology assessments.

I would also like to acknowledge the late Professor Chris Wilkinson along with Professor Adam Curtis whose unique intuition and biological insight and understanding, first proposed that a piezovibrational bioreactor could be used to induce osteogenesis.

My heartfelt thanks and gratitude to the DTC in Cell & Proteomics technologies, funded by EPSRC and the BBSRC which made my studentship possible.

In addition I also thank the MRC, STFC, the Royal Society of Edinburgh, The University of Glasgow and the University of West of Scotland for additional financial support, materials and for the equipment which was used.

Author's Declaration

The research reported within this thesis is the original work of the author except where the assistance of others has been acknowledged and at the time of submission is not being considered elsewhere for any other academic qualification.

Gabriel Delsol Pemberton

September 2015

Dedication

I dedicate this thesis to Yahshua the Messiah, to my parents and to my grandparents: Lattie, Paul, Verallia and Arthur

Chapter I: General Introduction

1.1 Introduction

Throughout the 19th and 20th century we have seen various technological revolutions and advancements which have profoundly changed and improved (for the most part), the life of man. It can be argued that the first came in the field of chemistry in the Victorian Age at the turn of the 19th century and has continued up to this day. We are now able to manipulate reactions and processes to produce compounds and polymers like plastics and silicon (contact lenses, microprocessors) with unique properties and structures that can be used in everyday life. Towards the early to mid 20th century the next technological epoch came in physics where scientists, such as Boltzmann and Einstein proved that atoms truly existed and this knowledge could be used to calculate more efficient thermodynamics. This climaxed with the atomic age/fission and nuclear power whereby generating thousands of times more energy per mass compared to coal; the main energy source of the time. Presently, it could be said that we are on the threshold of another technological revolution that can profoundly improve the life of man. This time it is in the field of the biological sciences and regenerative medicine; whereby mastery of the stem cell and the human genome/proteome could help prolong not just life but also its quality. With this technology it could be said that western medicine would see a paradigm shift from, for the most part, not just alleviating the symptoms of chronic ailments to actually remedying debilitating conditions at their core.

1.2 Tissue engineering and regenerative medicine

Human beings are living longer than ever before and although positive, one of the downsides of this is the inevitable deterioration of a biological system, which is not intrinsically designed to last forever or moreover has limited regenerative capacity in main organs like the heart, brain/neural tissue and kidneys (Morishita, 2014). Dr. Micheal Lysaght was among the first to define this arena, its challenges and potential for downstream therapy for replacement of damaged tissue and organs (Lysaght, 1995; Lysaght and Hazlehurst, 2004; Lysaght and Reyes, 2001).

Although it is becoming more difficult to unmarry the two it could be said that tissue engineering encompasses the use of auto / allografts and biomaterials while regenerative medicine can use biomimetic scaffolds and repairing modulating endogenous factors, with multi or pluripotent stem cells playing a crucial part, i.e. being able to differentiate into parenchymal or functional cell types to replace that which has been damaged (Fisher and

Mauck, 2013). The idle goal of regeneration is the partial or complete restoration of damaged specialized tissues and/or organs returning full function and anatomical structure without the formation of fibrosis or scar tissue (Candiani et al., 2008; Lewis et al., 2009). Surgery and the bodies innate healing abilities repairs but does not necessarily regenerate. As adults we have passed this physiological chronological development stage where we once had this full regenerative potential in the form of an embryo with toti and pluripotent cells (de Kretser, 2007; Mintz, 1985; Morgani et al., 2013).

A present rationale of note, in the use of grafts and tissue engineering which is making advancement is to devitalise an extra cellular matrix (ECM) and then revitalize this matrix with autologous cells. Several works have shown positive results; for example in 2009 a life was saved through the first transplantation of an engineered airway using a devitalised cadaveric implant in vivo (Macchiarini et al., 2008), and in animal models this rationale has also been used with varying levels of success for the regeneration of the lungs (Ott et al., 2010; Petersen et al., 2010), the liver (Uygun et al., 2010), the perfusion of vascular allograft from cadaveric tissue (Wilshaw et al., 2012), and synthetic polymer scaffolds (Dahl et al., 2011). Interestingly, there have also been publications on the re-enervation of musculo-skeletal tissue (Kang et al., 2012) and preparation of skeletal allografts to support mesenchymal stem cells vitalization for further mineralisation (Coquelin et al., 2012).

Commercial regenerative research to address unmet medical needs (so called neo-organs and neo-tissues) in urologic, renal, gastrointestinal and vascular diseases has also gone on to form spin-out companies like Tengion Inc. with early phase I and II clinical trials for real world application of this technology (Basu et al., 2011; Basu et al., 2012; Kelley et al., 2010). The burgeoning linkage between gene therapy and cell therapy/regenerative medicine has also seen the onset of research using induced pluripotent stem cells in UK companies like ReNeuron (Damasceno-Oliveira et al., 2007; Finger et al., 2007; Myers et al., 2007) and actual clinical trials using adult neural stem cells in US companies like Neuralstem Inc. for treatment of conditions such as stroke, Alzheimer's and Parkinson's disease (Bautista et al., 1994; Miyauchi et al., 1991). Also in the realms of Big Pharma the UK based company Glaxosmithklein has also invested in cell and gene therapy autologous hematopoietic stem cells with indications for ADA-SCID, WAS, MLD and Beta Thellassemia.

1.3 Bionanotechnology

As mans engineering ability continues to improve and become more precise we are now realising benefits that have emerged in moving from the macro to the microscale, and now from the micro to the nanoscale for biological applications (Crowder et al., 2013). Bionanotechnology is the field of biology which uses devices or implementations in the range of the nanometre (nm - 10^{-9} m) to interact with cells in order to maintain, diagnose or improve health (Etheridge et al., 2013; Nie, 2009). Collectively for bioloigical therapeutic use; this arena has been termed nanomedicine – nanotechnology, biology and medicine (Bharali et al., 2013; Mason and Dunnill, 2008). These include but are not limited to peptoid nanosheets (Morgani et al., 2013), nanocrystals (nanoparticles/quantum dots) (Cauffman et al., 2009; Cifarelli et al., 2013) and carbon nanotubes (Mintz et al., 1984) for drug delivery and diagnostics.

Traditionally the definition of nanotechnology has been limited to the range of 1-100 nm as described by the National Nanotechnology Initiative, a US federal government enterprise for the advancement of nanoscale research (Goldfarb and Morgan, 2013; National Research Council (U.S.). Committee to Review the National Nanotechnology Initiative. and National Academy Press (U.S.), 2006). At that scale we observe quantum restriction taking hold and the properties of compounds favourably being altered compared to their macroscale. For example much more refined absorption and emission spectra (Allan and Delerue, 2005; Larson et al., 2003) and increased physiochemical interaction and bioavailability of nanocrystals (Van Eerdenbrugh et al., 2008). However in the range above 100 nm, we observe the Plasmon-resonance (the frequency at which photons match the resonance frequency of surface electrons in a nanoparticle) and this phenomena is being assessed in clinical trials using gold nanoparticles at 150 nm to thermally treat tumours (Etheridge et al., 2013).

Liposomes and nanoparticles around 200 nm also show beneficial in vivo persistence in blood plasma and the passive targeting of specific in vivo sites using the enhanced permeability and retention effect (EPR) (Litzinger et al., 1994) with particles in the range of 400 nm proving to have favourable specificity (extravasation) for tumour tissue (O'Neal et al., 2004) . We also observe conjugated quantum dots/nanoparticles being designed with payloads, (streptavidin and specific antibodies) being able to interact with cells on a genetic level through

short-interfering RNA (siRNA) (Yezhelyev et al., 2008) as well as active cancer (Wu et al., 2003) and neural tissue targeting (Vu et al., 2005). Although of great promise, much work still remains to characterise toxicity; pharmacodynamics and pharmacokinetics of these nanoparticles and devices in vivo (Karin and Mintz, 1981; van der Kamp et al., 1984).

Noteworthy is the ambition in bionanotechnology to create nanomachines by the year 2025. It is envisaged that these nanomachines will possess 'theranostic ability' i.e. have the combined capacity of therapy and diagnostics all in one nano-device (Hauptman A, 2005).

1.4 The stem cell

The stem cell is the focal point of most modern tissue engineering approaches and it can be described as a cell which has the ability to self renew and has clonogenic properties, i.e. one parent stem cell has the capacity to proliferate and give rise to an entire colony of daughter cells (Lanza, 2006). They can also do this and remain undifferentiated after several cycles of cell division (by symmetric as well as asymmetric cell division). Finally, they can also be described as being potent i.e. are able to differentiate into the different cells which make up an organism (through asymmetric division). The potency of a cell can be categorised by the degree of its differentiation ability (Gomez-Lopez et al., 2014). During the development of a human being stem cells eventually give rise to all the organs and systems of the body, as shown diagrammatically in **(Figure 1.1)**.

The different stem cell potencies include a totipotent cell which is a zygote or fertilised ovum divided up to the 8-16 cell stage of the *morula*, these cells are truly able to form any cell which makes up an organism including cells of the placenta (Surani and Tischler, 2012). The pluripotent stem cells of a *blastocyst/embryoblast* (comprising of 70-120 cells) has the power to later form into any of the three germ layers which make up a very early stage embryo and goes on to form an entire organism. They include the endoderm or interior embryo which later gives rise to the stomach lining, gastrointestinal tract, and lungs etc; the mesoderm, the mid layer of cells which forms the muscle, bone, blood, urogenitalia of an organism and the ectoderm which later forms epidermal tissues and the nervous system. These cells fall short of the term totipotent as they lack the power to form extra-embryonic tissue such as the placenta and the umbilical cord. The ability of stem cells from one germ layer e.g. the mesoderm to give rise to cells which originate from a separate germ layer e.g. liver or lung tissue which

usually originate from the endoderm is referred to as plasticity or transdifferentiation (Krause et al., 2001). The plurioptent cells which were discussed in the last sentence are generally referred to as embryonic stem cells (ESC), and reprogrammed cells such as induced pluripotent stem cells which will be discussed later in more detail.

Multipotent cells or *progenitor cells* can differentiate into several different types of cells, however they begin to commit to particular lineages e.g. stromal, circulatory or neural tissues and the progenitor cells lack the capacity of unlimited self renewal as is the case with ESC. Bipotency is the ability of progenitor cells to differentiate only into a few different cell types, due to an increased level of lineage commitment compared to multipotent cells. These can include the epithelial stem cells of the mammary glands which have the potency to give rise to myoepithelial and luminal cells (Hassiotou et al., 2013). Finally, there are unipotent cells such as spermatogonial stem cells (De Rooij and Griswold, 2012) which are referred to as *blast* or *precursor cells*, these cells can only form one cell type. In an adult organism stem cell differentiation is usually restricted by particular lineages or their tissue environment and do not usually display greater differentiation prowess than multipotency.

The fact that harnessing the power of the stem cell has the potential to provide almost limitless regeneration of any tissue from almost any injury is indeed revolutionary as at the beginning of the 20th century this notion would have been thought of as impossible (Chistiakov, 2012; Kuwabara and Asashima, 2012; Teo and Vallier, 2010). Certain difficulties such as control of stem cell renewal and differentiation must first be overcome however before the true promise of tissue engineering can be realised. Due to the fact that the most regenerative potential is promised from multipotent and pluripotent stem cells, and the majority of research and clinical trials is performed using them, these two types of stem cells will be elaborated upon in more detail.

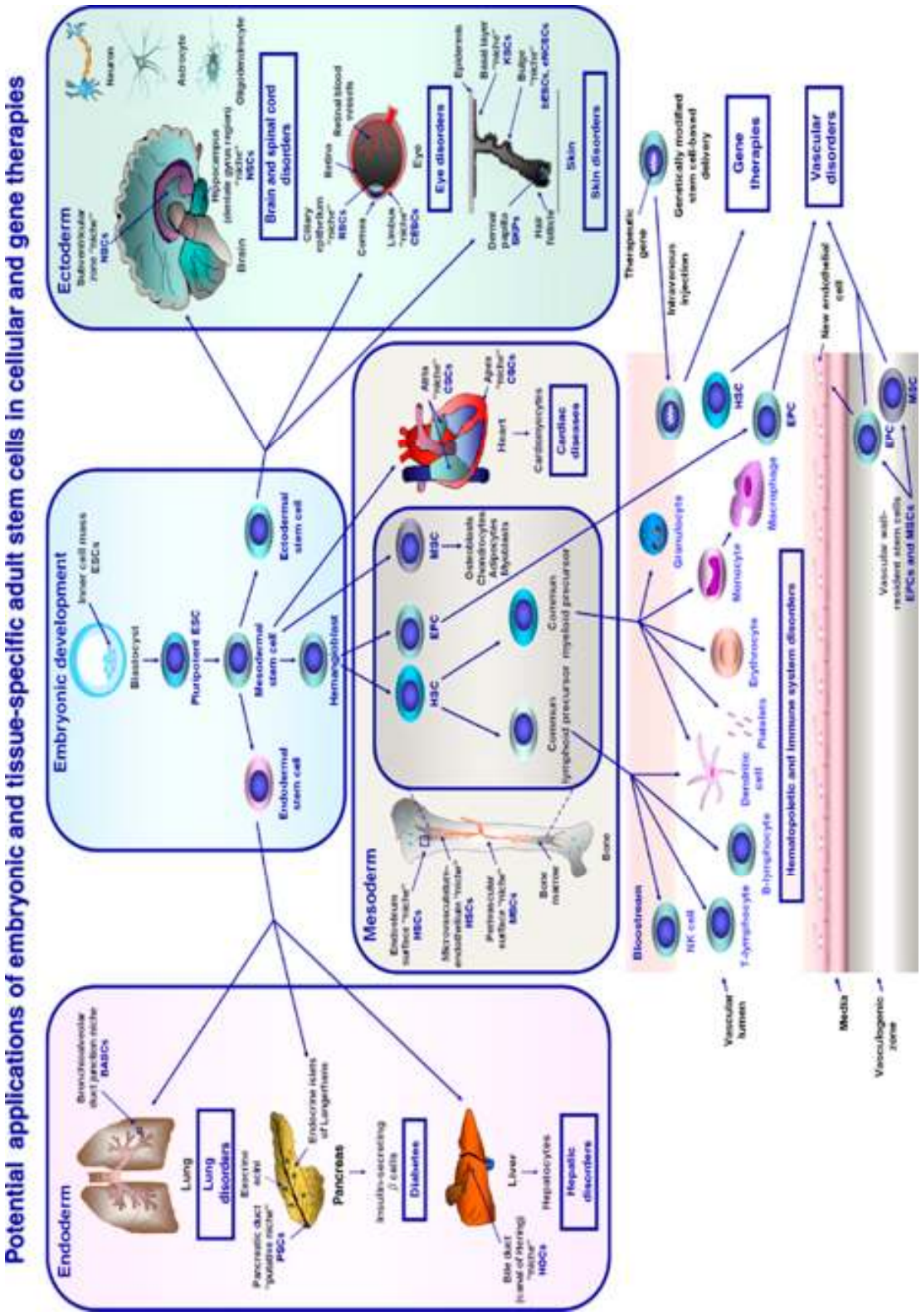

Figure 1.1: Developmental origins of the human organism and the presence of stem cells of different potencies along that development spawning from the embryonic ectoderm, endoderm and mesoderm, with permission from publisher (Mimeault et al., 2007).

1.4.1 Multipotent stem cells

The term covers adult autologous stem cells which can be isolated from most tissues in the body. Their differentiation capability is limited to lineages associated with the tissues or organs in which they take up residence, although there are now papers published proving multipotent stem cell plasticity (Conese et al., 2014; Zhang and Alexanian, 2014). Generally their occurrence in a specific tissue is approximately 1 in 10,000 cells, a limiting factor in their therapeutic use (Hipp and Atala, 2008). At present the vast amount of research and clinical trials that involve multipotent stem cells, use either mesenchymal stem cells (MSCs) or haematopoietic stem cells (HSCs).

1.4.1.1 Mesenchymal stem cells

Mesenchymal stem cells were first described by Friedenstein et al in the sixties as cells which could form colonies with a fibroblastic appearance, and hence they were first designated as colony-forming unit-fibroblasts (CFU-Fs) (Friedenstein et al., 1968). Since then there has been some controversy as to the precise origin of MSCs and although for the most part it is agreed and was first published that they originate from the mesodermal layer (Caplan, 1991, 1994) work since then also suggests that the neuroepithelium may play a role in MSC origin (Takashima et al., 2007) and indeed this notion may be given credence by papers which state that MSCs are a heterogeneous population of cells which also show plasticity in their ability to form somatic cells from the ectodermic germ layer (Taran et al., 2014; Zhang and Alexanian, 2014). Further research also suggests that MSCs are also related to pericytes and that their true *niche* is perivascular (within small indentation/fenestrations on sinusoidal capillaries) and the resulting loss of stemness and efficacy in vitro after each passage is due to the loss of this perivascular environment (Crisan et al., 2008).

MSCs have now been characterised using three main criteria issued by the International Society of Cellular Therapy. They can be isolated due to their affinity for plastic, they express specific phenotypic markers; CD-73, CD-90, CD-105, STRO-1 and more recently CD-271(Etheridge et al., 2013) and lack expression of CD-45, CD-34, CD-14, CD-11b, CD-79, and HLA-DR which is a leukocyte antigen (MHC class II cell surface receptor). Finally they have the potency to differentiate into mesenchymal lineages namely osteoblasts, adipocytes and chondrocytes (Dominici et al., 2006) .

Further to these three criteria MSCs also have immunomodulating/anti-inflammatory (Krampera et al., 2006; Sharma et al., 2014) and immunosuppressive (Ren et al., 2011; Su et al., 2014) ability (paracrine properties – expression of nitric oxide, indoleamine 2,3-dioxygenase, IL-6 for example), both on the innate and adaptive immune system, as well as being proangiogenic and antiapoptotic (Nascimento et al., 2014). It is thought that a further benefit of using allogeneic MSCs is a lower level of expression of major histocompatibility complex (MHC) related antigens (hypoimmunogenic) compared to somatic cells, furthermore novel research suggests that improved therapeutic efficacy can be gained by matching MHC in allogeneic MSCs, reducing donor specific T-cell and B-cell response (Lee et al., 2014; Schu et al., 2012).

MSCs possess the capacity to home to a site of injury by responding to chemokines/ proinflammatory cytokines (IFN-γ, TNF-α, IL-1α) released by injured cells (Krampera et al., 2006; Spaeth et al., 2008) subsequently overseeing the repair process (Phinney and Prockop, 2007). They are also characterised as having further regulatory and supportive effects on hematopoietic stem cells both *ex vivo* (proliferation, maintenance of stem cell viability) (Dewey et al., 1977; Krikorian and Steward, 1978) and *in vivo* (e.g. RANK ligand production /osteoclast formation) while not becoming hematopoietic in their natural state (Dewey et al., 1978).
Although we now understand that MSCs are present in all adult and fetal tissues in the vasculature as part of the pericyte population (Crisan et al., 2008); as far as harvesting a sufficient number of adult MSCs for expansion and implementation in regenerative medicine the main sources remain the bone marrow stroma and adipose tissue although other potential candidates include the blood, dental pulp cavity, placenta, cord blood/wharton's jelly and amniotic fluid, (Pappa and Anagnou, 2009; Pozzobon et al., 2013).

Research suggests that both adipose derived (AD-MSCs) and bone marrow derived mesenchymal (BM-MSCs) stem cells have comparable properties in most parameters such as clonogenecity, proliferation rate and differentiation potential, but differ with the presence of certain surface markers, for example BM-MSCs show an increased expression of CD-146 and AD-MSCs are positive for CD-34 and CD-54 which are not present in BM-MSCs (De Ugarte et al., 2003b; Zhu et al., 2012b). That being said however after *in vitro* culturing AD-MSCs quickly loose this CD-34 surface mark (Maumus et al., 2011; Sengenes et al., 2005). Also of

note, *in vitro* passaging of BM-MSCs begun to show features of senescence (loss of cell viability) in almost half the time as AD-MSC, and the use of serum added media can also alter MSCs characteristics (Dmitrieva et al., 2012b).

Another favourable trait of MSCs as a regenerative tool is their ability to release bioactive factors (trophic properties) which affect neighbouring cells indirectly and directly, while themselves remaining undifferentiated by this process (Shabbir et al., 2010; Shabbir et al., 2009). In the trophic properties too we observe differences in secretion levels of MSCs with BM-MSCs showing a higher level of expression of vascular endothelial growth factor (VEGF), stromal cell-derived factor-1 (SDF-1) and transforming growth factors/bone morphogenetic protein-2 (TGF-β/Bmp2) compared to AD-MSCs (Dmitrieva et al., 2012b). Interestingly, as well as all of these attributes new data is also coming to light which suggests that MSCs may also have the benefits of an analgesic (Pang et al., 2014).

MSCs will be paramount for the future pursuits of regenerative medicine and immune disorders and this is helped all the more by the fact that good manufacturing practices (GMP) for on scale clinical-grade production are coming into main stream use in line with the regulatory bodies such as the US Food and Drug Administration (FDA) and in Europe under Commission Directive 2003/94/EC (Sensebe et al., 2011; Sensebe et al., 2013). Despite these achievements a lasting hurdle which remains in the clinical translation of a MSCs treatment is the heterogeneity of results from different batches of cells in different patients, notwithstanding the need for serum free media and the secondary effects different batches of FBS may also confer on MSCs. Here too steps are being made, in finding novel specific surface markers such as Tumour necrosis factor-inducible gene 6 protein (TSG-6) , which inhibit inflammatory responses in microglial cells (Song et al., 2014) and syndecan 2 CD-362, recently discovered by Orbsen Therapeutics, which also appears to confer immunosuppressive wound healing qualities to MSCs (Vlashi and Pajonk, 2014). The expediency of these novel markers suggests that they do not only characterise the presence of a MSC for clinical use, but that they also begin to give some information into the potential efficacy which may be observed in future clinical trials using MSCs for therapy.

1.4.1.1.1 The osteoblast

Critical to this body of research has been the MSCs potency to be able to differentiate into osteoblastic cells; a process referred to as osteogenesis or osteoblastogenesis in the literature (Xie et al., 2014). A key function of osteoblasts is the secretion of osteocalcin (OCN) which is an extracellular (calcium binding) mineralisation protein (Lee et al., 2007). Osteopontin is another calcium binding extracellular matrix glycoprotein secreted by osteoblasts, which also expresses a specific amino acid sequence (arginine, glycine, aspartic acid - RGD ligands) facilitating cellular adhesion through integrin attachment (Bautista et al., 1994; Zou et al., 2013). The up-regulation of these key mRNA and proteins as well as bone morphogenetic protein 2 (Bmp2), osteonectin, alkaline phosphatise (ALKP), runt-related transcription factor 2 (RUNX2), and its effector also an osteogenic transcription factor; osterix (Matsubara et al., 2008) is accepted as validation of MSC differentiation into osteoblasts (McNamara et al., 2010; Nikukar et al., 2013).

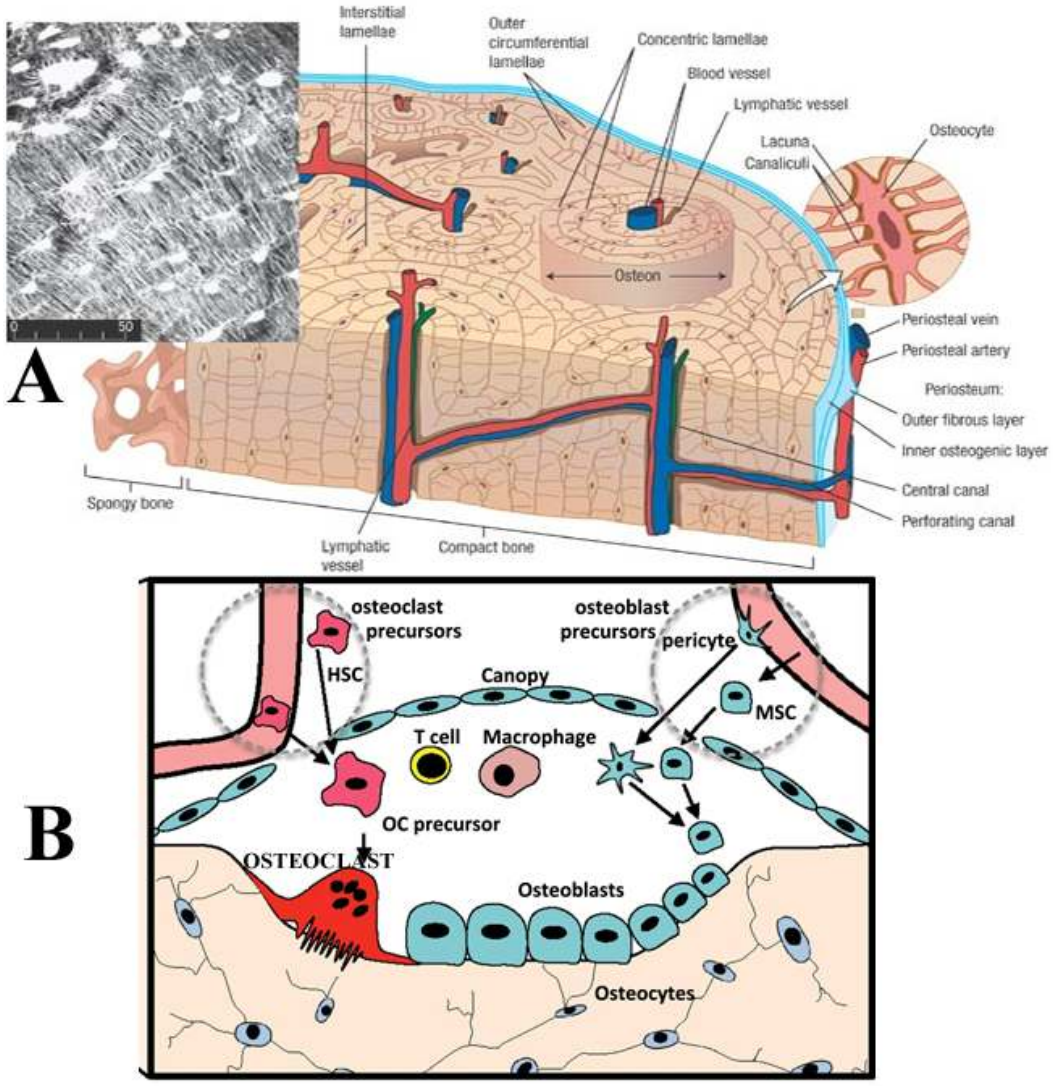

Figure 1.2: Diagram showing (A) cross sectional framework of bone and (B) the interplay between osteoblasts, osteoclasts and osteocytes. Figure reproduced with modification from (A) nature article (Taylor et al., 2007) and (B) nature article (Sims and Martin, 2014). With permission from the publisher.

The osteoblast can further be characterised by responding to the presence of parathyroid hormone (cyclic adenosine monophosphate (cAMP pathway) for calcium homeostasis, the production of alkaline phosphatase for ECM modulation (Ozaki et al., 2005) and the secretion of Collagen I, which comprises 90% of the organic nature of bone (Wildemann et al., 2004). Osteoblasts do not only respond to mediating factors but also have a autocrine/paracrine effect in facilitating the regulation of skeletal tissue and cells, and to that end release cytokines (IL-6, osteoprotegerin, TNF-α RANKL)(Gowen et al., 1990; Ishimi et al., 1990; Steeve et al., 2004) and growth factors (VEGF and TGF-β) (Liu et al., 2012; Robey et al., 1987; Spector et al., 2001).

The osteoblast, along with the osteoclast and osteocyte are the cells which model bone, as represented in **(Figure 1.2)**. While the osteoblast synthesise hydroxyapatite, forming matrix mineralisation (initial formation of an osteoid), the osteoclast (formed from a hematopoietic lineage) carry out resorption. The osteocytes are formed from osteoblast after being cemented into matrix and reside in lacuna. They are connected to osteoblasts and osteoclasts through channels called canaliculi, and are thought to have a regulatory designation (Bonewald, 2007). It is suggested that the osteocytes interpret mechanical stimulation by a differing mechanism compared to osteoblasts, i.e. through the cell body or dendritic processes instead of through the filapodia or polygonal protrusions and the signal is mediated through gap junctions and hemichannels resulting in the release of signalling compounds such as prostaglandins into the bone fluid (Jiang et al., 2007; Klein-Nulend et al., 2013b). This is unsurprising as it has been published that prostaglandins have the effect of not just regulating cyclic AMP levels which is important in many cell processes, but also the ability to regulate calcium movement (Yamasaki, 1983).

Matrix mineralisation by osteoblasts is a complex process which involves several extracellular matrix proteins for cell proliferation (Bmp2,c-Jun,RUNX2), matrix maturation (alkaline phosphatase, collagen) and the eventual mineralisation (osteocalcin, osteopontin), i.e. calcium phosphate deposition, which occurs after approximately 28 days, as represented by **(Figure 1.3)** (Sanchez Alvarado and Yamanaka, 2014; Stein and Lian, 1993). Note c-jun will be discussed later in more detail, in reference to the ERK/MAPK pathway. Figure 1.3, only provides a guide to the chronological timeline of mineralisation, this would change depending on the type of chemical or mechanical stimulation being carried out, nevertheless, the

chronological order of genes starting with BMP2 and RUNX2 would for the most part remain the same.

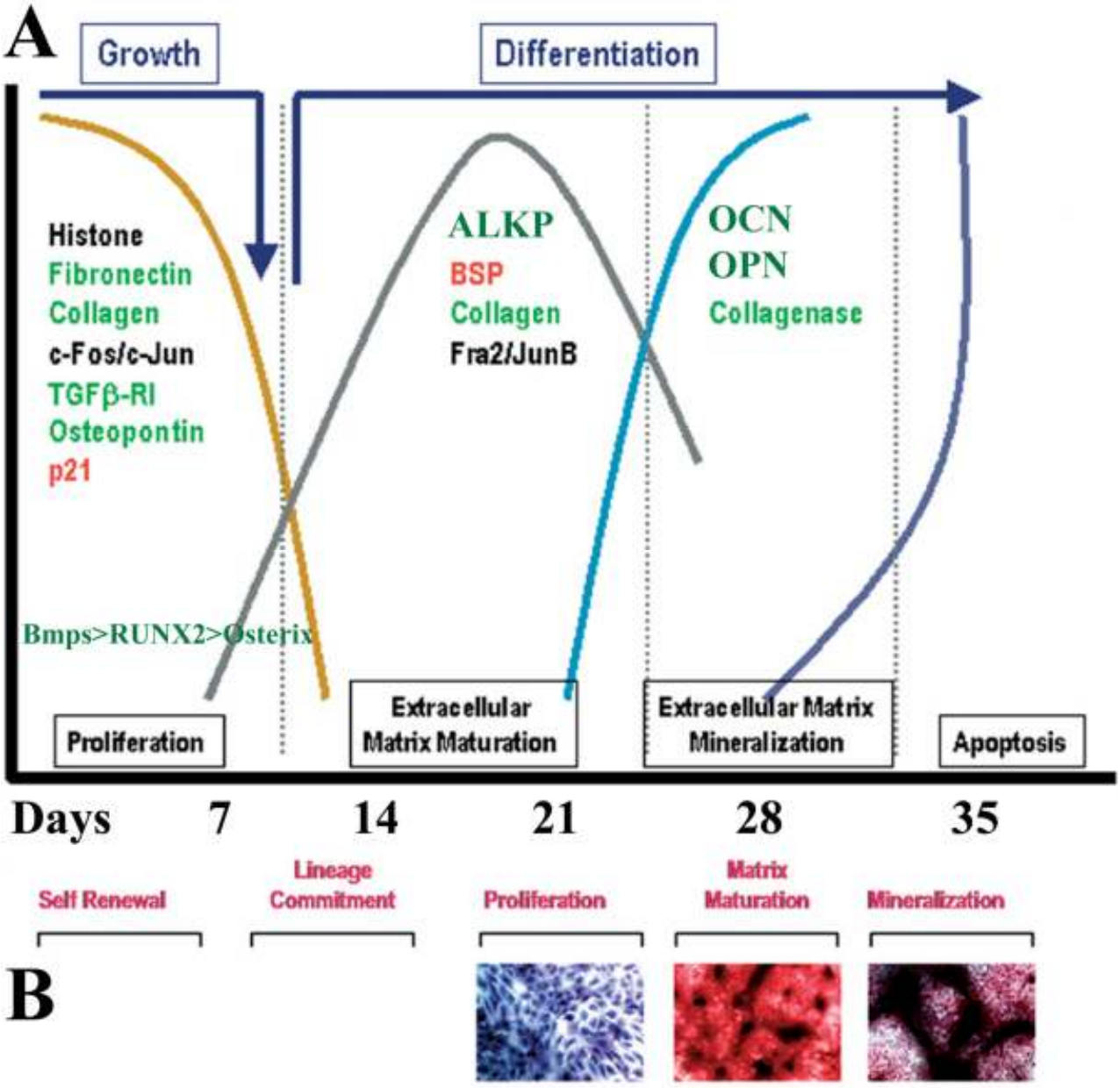

Figure 1.3: A.) Diagram showing the key osteogenic related proteins involved in proliferation, maturation and mineralization of the osseous extracellular matrix in a chronological manner dependant on the master transcriptor RUNX2 – upregulated proteins shown in green, and down regulated bone sialoprotein (BSP) shown in red. B.) Histological representation of proliferation to matrix minerlisation, figure used with permission from the publisher (Stein et al., 2004).

1.4.1.2 Hematopoietic stem cells

These multipotent stem cells originate from the mesoderm and reside in the bone marrow giving rise to the cells that make up the blood (haematopoiesis); including myeloid (innate immunity) and lymphoid (adaptive immunity) progenitors. This capacity makes hematopoietic stem cells (HSCs) useful therapeutically in leukemia and immune related conditions and subsequently it has been found that umbilical cord blood, which can be cryopreserved at birth, may also be a useful source of HSCs for treatment in later life (Stephen J. Szilvassy Albertus W, 2013). Prominent surface marker identifiers of hematopoietic stem cells are CD-34, CD-45 and CD-15 (Dominici et al., 2006).

Self renewal and viablility of HSCs in vitro can be maintained by co-culture with primary or immortalized stromal cells, i.e. MSCs (Fei et al., 2007) and stromal free expansion can be aided by culture with hematopoietic soluble factors such as angiopoietin like proteins (Himburg et al., 2010). HSCs are putatively one of the first and hence, best characterised adult stem cell (Weissman, 2000) and as a result clinical trials are now underway to treat conditions such as critical limb ischemia/arterial disease, being pioneered by commercial firms such as Aastrom Scientific (Kondo et al., 2003; Ledford et al., 2013; Powell et al., 2011).

They also show therapeutic promise for use in patients who may have undergone high dose irradiation, as would have been observed, for example in the Chernobyl disaster (Bishop, 1997). This type of therapeutic capacity is made all the more poignant in light of the more recent Fukushima incident.

1.4.2 Pluripotent stem cells

By definition a plurioptent stem cell will form a teratoma if introduced into an organism without first undergoing partial differentiation, they require a supportive or feeder layer of cells to remain viable in vitro (although research into serum free and feeder free culture is on the way (Jungreuthmayer et al., 2009), and they have the potential (ESC) to spontaneously form a spheroid mass of cells referred to as an embryoid body. In the case of ESC they are also harvested from the inner cell mass of a developing *embryoblast.* Furthermore, in humans ESC have an increased expression of E-Cadherin (Kurosawa, 2007), alkaline Phosphatase and SSEA-4 as cell surface protein markers (Takahashi et al., 2007) and transcription factors Oct-4, Nanog and sox2 which are necessary for the maintenance of their pluripotency (Ling et al., 2012) .

While in the past the pluripotent stem cell almost instantly meant ESC; this is no longer necessarily the case. Due to ethical concerns and through biological engineering research into pluripotent stem cells is now a wide and varied group which will be discussed briefly.

Parthenogenetic embryonic stem cells (pES) involve the derivation of stem cells which have solely come from an oocyte which has not undergone fertilisation by male gametes. This involves their activation to form a *blastocyst* through electrofusion and the use of media containing activating chemicals (e.g. ethanol) (Kaufman et al., 1983) or dimethylamino-purine (Mai et al., 2007)). pES show promise in the study of diseases e.g. some cancers are theorised to be related to imprinting, the silencing of an allele from a particular parent in the offspring (Feinberg et al., 2006) and pES may hence aid in the understanding of the regulation of epigenetic imprinting in humans (Hernandez et al., 2003).

Similar to pES, germline-derived pluripotent stem cells (gPS) can be derived from reproductive cells, however in this case they would usually be sourced from the spermatogonial stem cells which are initially unipotent. It has been published that culture of these cells under ES conditions (without splitting, the use of ESC media, and on embryonic fibroblast feeder cells), intriguingly facilitates the formation of pluripotent stem cells. These cells could have the potential for use in autologous regenerative therapies (Kim et al., 2014; Ko et al., 2009).

Although being researched to a lesser extent pluripotent stem cells derived through therapeutic cloning or somatic cell nuclear transfer (SCNT) also shows promise as another therapeutic source of autologous artificially produced pluripotent stem cells (Tachibana et al., 2013) .

In the use of artificially produced pluripotent stem cells, induced pluripotent stem cells (iPSC), are at the forefront of research. Induced pluripotent stem cells were first pioneered by Yamanaka for which he received the 2012 Nobel Prize in Medicine. He discovered that pluripotency could be induced by the expression of 4 master transcription factors (Oct3/4, Sox2, c-Myc, and Klf4) using a viral vector. With culture under ESC conditions they reverted differentiated somatic fibroblast cells to a more primordial pluripotent chronological state," in effect biologically winding the clock backwards" (Takahashi and Yamanaka, 2006). Since then several different somatic cells including hepatic, blood, epithelial and gastric, have shown the width of this technology (Zhou et al., 2012).

Also of note, research using mice has shown that the expression of microRNA (miR-291-3p, miR-294 and miR-295) which is specific to ESC also improves the efficiency of iPSC by modulating reprogramming by Oct4, Sox2 and Klf4. Interestingly, these microRNA are promoted by c-Myc suggesting that it is a downstream effector of the c-Myc transcription factor (Judson et al., 2009).

As c-Myc and Klf4 are known to be oncogenic, research has shown that iPSC can be formed without these transcription factors (Huangfu et al., 2008). Considering the use of a virus and stimulation of potential oncogenes would certainly pose pharmaceutical regulatory questions in their own right, it is significant that Zhou and his colleagues have been able to form what has been termed protein-induced pluripotent stem cells (proteins introduced into the cells via poly-arginine anchors (Zhou et al., 2009)). Further to this the use of small compounds which mimic the effect of transcription factors such as valproic acid (Huangfu et al., 2008) and Thiazovivin (Lin et al., 2009) have also been shown to improve the reprogramming efficiency of the process 100 and 200 fold respectively, compared to Yamanaka's original process.

In 2014 the first human clinical trials using autologous iPSC was initiated in Kobe Japan by the Ministry of Health, for treatment in age-related macular degeneration (RikenCenter, 2013).

1.5 Stem cell differentiation

In vivo it has been found that natural microenvironments (niches) are used to orchestrate the life and phenotype of the stem cell dictating whether it maintains homeostasis, (a state of inactivation yet maintaining genetic and biological viability known as quiescence) whether it begins to self-renew, migrates to new locations or differentiates into specific tissue to aid regeneration (Dmitrieva et al., 2012b; Kshitiz et al., 2012). A key component which creates a microenvironment from which the stem cell receives the instructions which governs its role; includes the ECM such as collagen, laminin, fibronectin and proteogylcans. This is coupled with respective naturally occurring cell mediating compounds (e.g. cytokines, growth factors, hormones) specific for the type of lineage tissue or cell to be formed (Schmeckebier et al., 2013; Yu et al., 2012; Zolochevska et al., 2012), as well as mechanical cues described as mechanotransduction and nano-stimulation (Dalby et al., 2014b), and oxygen tension (Pimton.P, 2013).

It is now thought that the fate of stem cells (including changes between different potencies during development), are not just due to information from their base genetic sequence (genotype), but is also orchestrated through epigenetic cues such as DNA methylation, messenger RNA (mRNA) methylation, histone modification /acetylation, and the resultant changes in the expression levels of microRNA (Guo et al., 2014).

In vitro experimentation with biomaterials seek to mimic these physical environments found *in vivo* to interact with cell surface receptors for intracellular signalling, gene expression and adhesion in order to regulate cell function. Of particular relevance to this body of work and to this thesis is the process of osteogenesis. The process of osteogenesis has been induced in MSCs through several mechanisms including nanotopography described in seminal papers from Dalby et al. (Dalby et al., 2007b; Dalby et al., 2007c; Dalby et al., 2006a; Dalby et al., 2006b), geometrical manipulations (Kilian et al., 2010; McBeath et al., 2004), hydrostatic pressure or fluid shear stress (Henstock et al., 2013; Liu et al., 2009a; Liu et al., 2009b), parathyroid hormone and transforming growth factors (TGF) (Yu et al., 2012), ambient

hydrogel stiffness (Engler et al., 2006), pulsed electromagnetic field stimulation (Cronmiller and Mintz, 1978) and hypergravity (Kacena et al., 2004; Prodanov et al., 2013). Surfaces with a high (biological) Young's modulus (40 kPa) and nano-patterns in elaborate formations facilitate the development of large focal adhesions bringing about up-regulation in the G-protein RhoA and the ROCK (RhoA kinase) pathway. As a result of this the actin cytoskeletal is fortified through phosphorylation increasing the cytoskeletal tensile strength that is required to support the large osteoblastic cells; the resultant cell type of osteogenesis (del Rio et al., 2009; Sawada et al., 2006; Vogel and Sheetz, 2006). This process also facilitates cell motility with actin (contractility through RhoA) and myosin working in tandem with integrin containing micro protrusions known as filopodia locating attachment sites (Miller et al., 2014).

1.5.1 Mechanotransduction

The process by which mechanical forces occurring extracellularly are perceived and interpreted by biologically active cells, resulting in intracellular (nuclear deformation) changes; facilitating adaptation to these mechanical changes in their environment is referred to as direct mechanotransduction. Indirect mechanotransduction would be brought about through biochemical stimulation and the two very often can work in tandem (Dalby, 2005).

The physical antennae which senses these changes and can respond by clustering are the integrins (heterodimer α and β subunit transmembrane receptor) and they are physically attached to a specific amino acid sequence (RGD ligand) found on extracellular matrix proteins like OPN and fibronectin. On the opposing end of these integrin transmembrane receptor are protein complexes (paxillin, vinculin, talin) which form focal adhesions intracellularly. These focal adhesion complexes interact and can regulate focal adhesion kinase/Src (or protein tyrosine kinase), and are also attached to the cell cytoskeleton via F-actin, **(Figure 1.5).**

F and α- actin dictate the physical structure or shape, integrity and motility of the cell (actin microfilaments) along with tubulin (microtubules). In the mechanotransductive flow, the actin cytoskeleton also comes into contact with the lamin nucleoskeleton (intermediate filaments) through linkers of nucleuskeleton and cytoskeleton (LINC) complexes. The nucleoskeleton interacts with chromosomes (telomeres) mechanically influencing their repositioning and as a result, gene transcription (Ostlund et al., 2009).

Hence, focal adhesions can instigate a mechanistic cascade which downstream can cause the up-regulation in transcription factors responsible for self-renewal, migration, or differentiation (adipogenesis or osteogenesis (phosphorelated RUNX2), see **(Figure 1.4 and Figure 1.5)** for a diagrammatic representation of the mechanotransductive flow believed to be involved in nanokicking which has been described above (Dalby et al., 2014b), (Wang et al., 2009b).

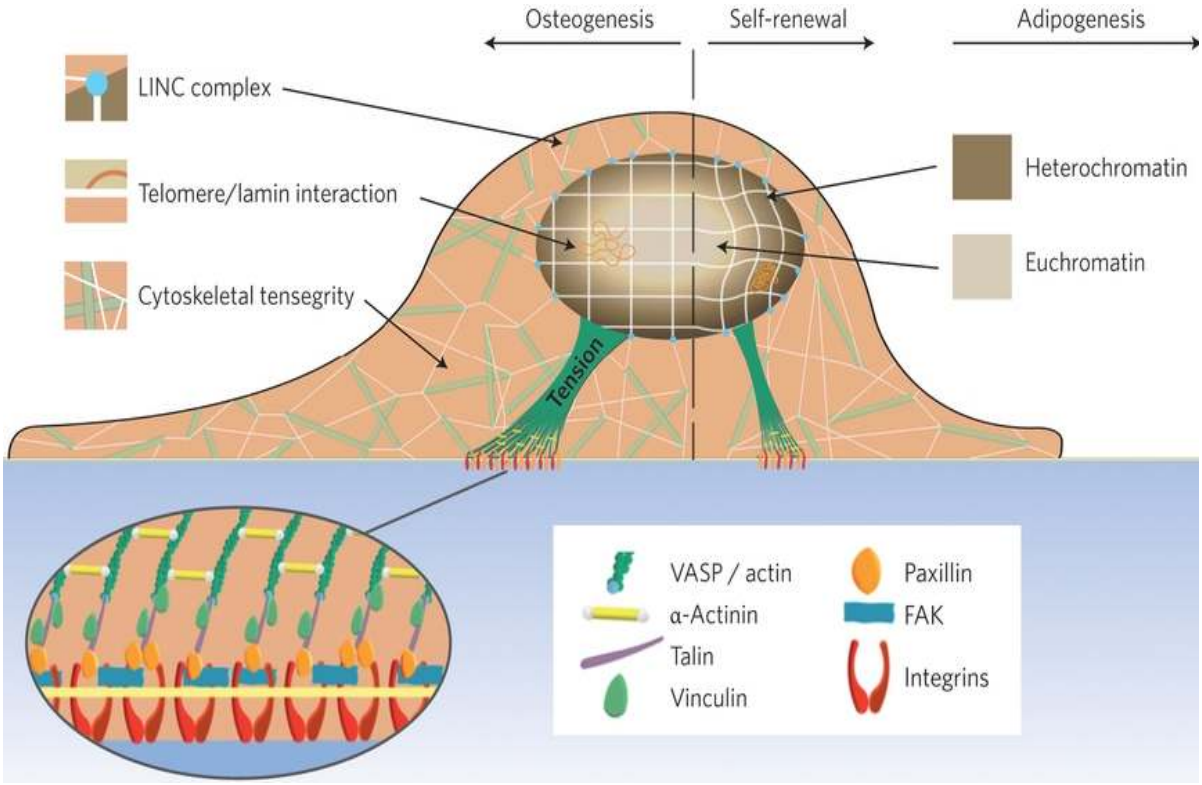

Figure 1.4: Diagrammatic representation of the cell mechanotransduction and the resulting differentiation through focal adhesion attachment, cytoskeletal and nuclear/chromosome activation. Figure reproduced with permission from the publisher (Dalby et al., 2014b).

In terms of osteogenesis it has been published that larger well spread focal adhesions (super mature or fibriller focal adhesions > 5 μm) can bring about osteoblast differentiation through increased cytoskeletal tensegrity, instigated by RhoA (Ras homolog gene family, member A - which is a small GTPase protein) mentioned above (Tay et al., 2013). The extent of ossification or mineral deposition during remodelling can be effected by mechanical stimuli or weight bearing, which has also been theorised by Wolff's Law (Klein-Nulend et al., 2013a).

The integrin, focal adhesions, also activate the MAPK extracellular-signal related kinases (ERK, chiefly ERK 1/2) by stimulating Ras (similar to RhoA) and the pathway is further regulated by p38 MAP kinase (which phosphorylates subsequent mitogenic kinases), and c-jun-n-terminal kinase (JNK) which phosphorylates the transcription factor c-jun, to name but a few kinases involved. Downstream the ERK/MAPK pathway can also bring about osteogenesis (Nikukar et al., 2013; Tsimbouri et al., 2012b).

Fundamentally the loci for the alleles coding for osteogenic related genes can be found on larger chromosomes (osteopontin 4q22, alkaline phosphatise 2q37, osteonectin 5q31, osteocalcin 1q25-31) which have greater telomeric mechanosensitivity, hence possibly facilitating access to these genes by transcription factors promoting the osteoblastic phenotype (Tsimbouri et al., 2013). This potentially makes focal adhesions a poignant agonist of nanokicking related osteogenesis (Nikukar et al., 2013).

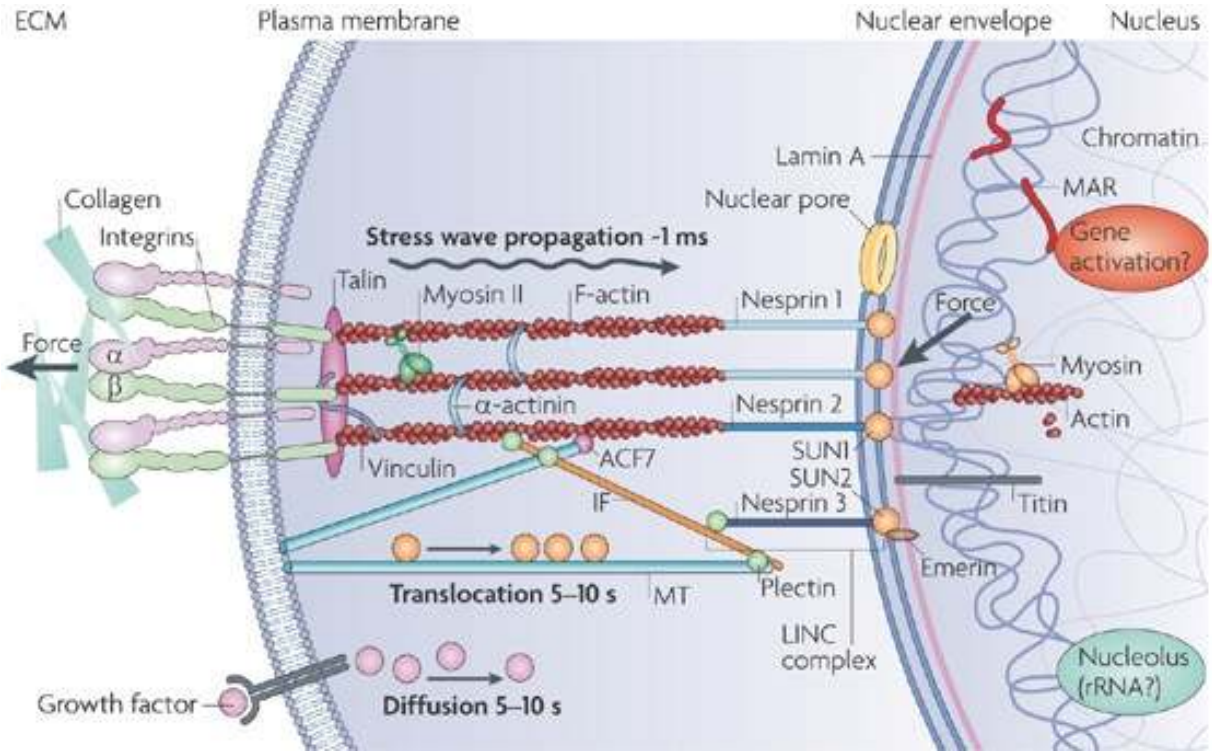

Figure 1.5: Mechanostransduction through mechanical stimulation: Potential mechanism of the flow of mechanical force (such as high frequency vibrations - nanokicking) originating outside of the cell transduced intracellularly causing a physiochemical (and genetic) change downstream (Wang et al., 2009b). Used with permission from the publisher.

When discussing direct mechanotransduction as well as taking into account the mechanical forces, discussed previously, which undoubtedly are a major contributor in a technology like nanokicking; it should also be considered that there are other mechanistic routes such as ion channels and primary cilia which facilitate the mechanotransductive process. These routes are not necessarily mutually exclusive and could potentially work hand in hand. The primary cilium is a singular microtubule which protrudes out of the cell like an antenna and is restricted in movement. It stands out from apical surfaces from nearly every cell in the body (including bone related cells) (Singla V, 2006). Interestingly it has been published that cilia have a role as a mechanosensor and could bend under fluid shear stress. The bending of the cilia seemed to be directly proportional to the extent at which Ca^{2+} ions would be taken through ion channels. Further work also showed that in bone related cells (osteoblast/osteocytes), weight bearing and mechanical stimuli such as pressure and vibration was also sensed by the micro cilia and it appeared that this may cause an increase in the upregulation of genes related to osteogensis such as OPN and COX2. Further still it was observed that the cilia (4-9 μm in length) would deflect and recoil under the application and cessation of sub-physiological flow and an oscillatory fluid flow (OFF) which caused an upregulation in osteogenic gene expression and may play a part in the overall regulation of bone formation and resorption (Malone A, 2007; Lee K, 2010; Hoey D, 2012). Also of note in relation to chondrogenesis, Wann and his colleagues showed that primary cilia has a critical role in the formation of the cartilage ECM and the upregulation in its synthesis. It was found that the primary cilia also had the functional ability to induce Ca^{2+} signalling mediated release: downstream of compression (Wann A, 2012).

In relation to mechanotransduction it has also been published that mechanically activated ion channels appear to be sensors of physical force. Key ion channels of note which have been published to play a crucial role in ion channel related mechanotransduction include Piezo 1, Piezo 2, TREK, TRAAK and TRPN, although there are others (Ranade S, 2015). In osteoblast like cells (osteosarcoma cells) there have been observed three classes of mechanosensitive ion channels and these could be classed on the basis of conductance, ion selectivity (in particular K^+ and Ca^+) and sensitivity to membrane tension, and it is thought that these can orchestrating a physiological response in bone through mechanical loading (Davidson R, 1990).

1.5.2 Nanotopography and vibrational stimulation

Very interesting research from the Centre for Cell Engineering in Glasgow has endeavoured to assess the use of nanotopographies and to interrogate the possible effect various patterns may have on MSCs.

They have embossed 120 nm diameter and 100 nm deep nanopits into PMMA over 1 cm^2 , using electron beam lithography. Five different patterns were investigated as a substrate platform for stem cell growth, and all had absolute or average centre-centre spacing of 300 nm.

The patterns assessed included a square array, hexagonal array, disordered square array with nanopits displaced randomly by up to 50 nm, (i.e. the NSq-50), the same again but with 20 nm displacements (i.e. NSq-20), and nanopits placed randomly over a 150 um by 150 um field, repeated to fill the 1 cm^2 area. A simple planar surface was used as a control. The cells were grown on these different topographies over a 21 day period followed by staining for expression of bone specific ECM proteins; osteopontin and osteocalcin, see **(Figure 1.6)** for the results obtained from the work. Further assessments also included a 28 day Alizarin red staining for calcium, and a qRT-PCR determination for osteospecific genes. In subsequent tests dexamethasone was utilised as a corticosteroid that induced bone formation; and was used as an osteogenic media sample (OSM) or positive control (Dalby et al., 2007d).

The results showed that highly ordered nantopographies, such as square and hexagonal array gave negligible osteblastic differentiation and reduced cell numbers compared to the control (especially on the hexagonal pattern). The cells on a more random topography, such as NSq-50 actually differentiated as far as to give bone nodule formation. The random nanopits showed the development of good cell populations but with low expression of osteopontin and osteocalcin proving osteogenesis to a lesser extent than the NSq-50 topography (Dalby et al., 2007d) . It was theorised that a great deal of the differentiation or lack thereof observed on the different topographies could have been attributed to the type and distance of the focal adhesions the MSCs were able to attain. This as a result, directly affected cytoskeletal tension and mechanotransductive pathways which may have an effect on chromosome positioning during cell division and subsequently gene expression (Dalby et al., 2007a; Engler et al., 2004; Wang et al., 2012; Wingate et al., 2012).

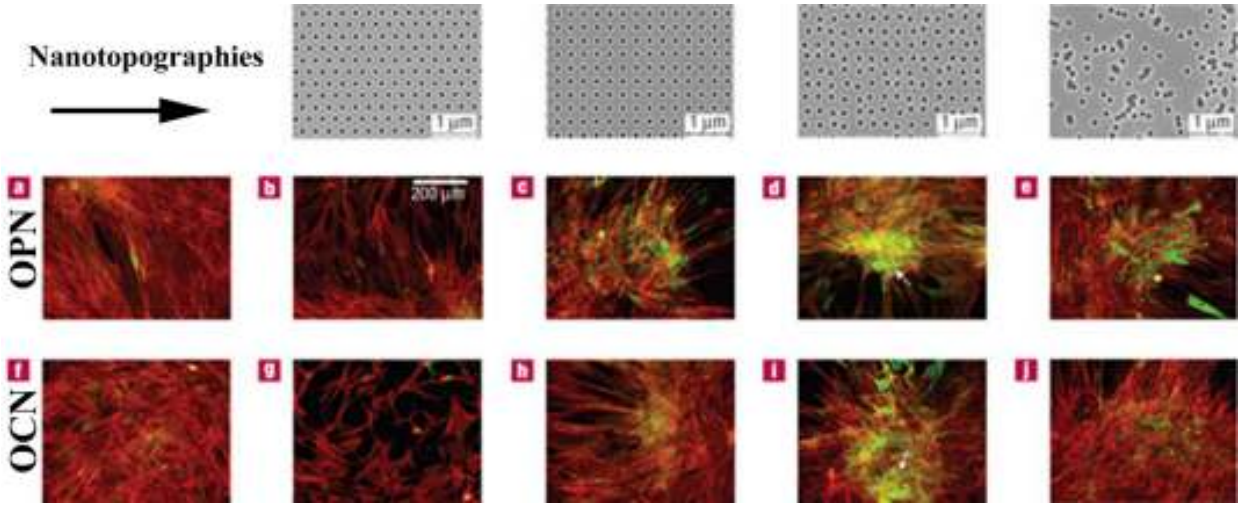

Figure 1.6: Showing the different types of nanotpograhical patterns and their osteogenic effect on cultures MSCs after 21 days, staing for OPN and OCN, without the use of OSM. From left to right, a square array, hexagonal array, disordered square array with nanopits displaced randomly by up to 50 nm, (i.e. the NSq-50), the same again but with 20 nm displacements (i.e. NSq-20), and nanopits placed randomly. With permission from M.Dalby (Dalby et al 2007d).

As well as facilitating differentiation further work also suggested that certain surfaces can help maintain self renewal and hence maintain a viable stem cell population. By reducing the level of offset to as close to zero as possible and forming an absolute square lattice symmetry; there was a resultant switch from osteogenic differentiation to a surface conducive to MSCs growth and replication. This was shown to be the case over an 8 week period, while the NSq-50 and OSM samples showed osteogenic induction strongly. The planar polycaprolactoen (PCL) surface gave a mixed population of MSCs and differentiated cells (McMurray et al., 2011).

Recent work by D. Pre and his co-workers also proved that low amplitude high frequency (30 Hz) vibrational treatment was also able to induce adipose derived stem cells to differentiate into osteoblasts after as little as 14 days with stimulation. Compared to controls which did not undergo mechanical vibration the level of key bone matrix proteins such as collagen, osteopontin, bonesialoprotein and fibronectin were found to be increased as much as 10 fold when assessed by qRT-PCR and ELISA (Pre et al., 2011b). Further to this, Curtis et al also showed that nanoscale vibrations within the region of 1 – 50 Hz implemented by a piezo actuator (a device which converts electrical energy to mechanical energy) to endothelial cells

were able to up-regulate the expression of endothelin-1 and Kruppel-like factor 2 and subsequently increase cell adhesion (Curtis et al., 2013b).

Lau et al found that low magnitude high frequency vibrations (LMHF) in vitro culture of mouse derived MSCs did not have an osteogenic effect, when stimulation was provided 6 x over a duration of 1 hour at 0.3 g and 60 Hz. This was carried out over a 2 week period. It was hypothesised that this stimulation was not for a long enough duration or at a high enough frequency (Lau et al., 2011). Stimulation at 200 Hz had been assessed, however osteogenesis was not the goal but instead it was to determine the viability of MSCs (observed to be 96%) cultured under these conditions (Gaston et al., 2012). Kim et al too attempted LMHF vibrations and found an affirmative response to osteogenesis and deemed that the success of the experiment was dependant on the culture method. 3D cultures showed the most positive results through an increased expression of collagen I, osteoprotegerin (decreases expression of RANK and hence osteoclasts), and VEGF. Their best results occurred at an acceleration of 0.3g and vibrations of 30 – 40 Hz (Kim et al., 2012).

A further seminal and insightful paper from the Centre for Cell Engineering at the University of Glasgow also investigated high frequency low amplitude vibrations. They researched the effect of even higher vibrational frequencies (1000 Hz) driven by a piezo actuator, to induce osteogenesis. These results corroborated the increased effect of focal adhesions and the fortification of the actin cytoskeleton for osteoblast differentiation (Nikukar et al., 2013). High frequency piezo vibrations also at a frequency of 1000 Hz showed microarray genomic changes relating to the cytoskeletal structure and an increased proliferation in adhered mouse embryonic fibroblast cells (Ito et al., 2011). These data together give credence to the future promise and potential of this technology.

1.6 Bone tissue engineering

The need for a ready source of skeletal tissue becomes more apparent as people become advanced in age, and a spate of osseous defects becomes more prevalent in the elderly. These conditions may include osteoarthritis, osteoporosis and all too often severe breaks and fractures due to falls. These conditions are further compounded by the fact that a limited skeletal regenerative capacity is observed in the elderly as stem cell population decreases (Garvin et al., 2007).

At present one of the most common forms of regenerative aid employs the use of donor derived bone grafts. These include autologous, allogeneic or xenogeneic/heterologous and they all have their failings including donor site morbidity, availability, rejection and cost to the healthcare system (Hashimoto et al., 2013). This makes apparent the need and urgency for successful bone tissue engineering (bone TE) protocols. Bone TE approaches can either take the form of cell only (regenerative cells), cell free (osteoinductive constructs) or a combination of the two (Bueno and Glowacki, 2009).

A combined engineering approach first requires a source of regenerative skeletal cells which would very likely be MSCs, and as discussed in section 1.4.1.1, these could be patient specific and sourced from adipose tissue, bone marrow or even the blood (Pozzobon et al., 2013). However, one of the limitations of MSCs is their replicative senescence when cultured *in vitro* / *ex vivo*, and to that effect the use of human telomerase reverse transcriptase (hTERT) ectopically expressed has been shown to increase their longevity (Bjerre et al., 2011).

For successful tissue engineering these cells also require a complimentary extracellular matrix for seeding, proliferation and expansion, i.e. scaffolds or polymer coatings with conducive physiochemical and mechanical attributes which may also be biodegradable (collagen, hyaluronic acid, alginate) (Stevens, 2008). This matrix would further expedite the delivery of the MSCs or even more favourably differentiated osteoblasts to the site of damage for regeneration and remodelling. Apart from these scaffolds, also of note has been the use of demineralised bone matrix as well as bioactivated glass (Schepers et al., 1991).

It has been published that these scaffolds would be required to induce an osteoblastic phenotype or be osteoconductive, to that end, osteoinductive 3D scaffolds (silicates, calcium phosphates, calcium carbonates, hydroxyapatite constructs) which can simulate the *in vivo* skeletal environment have been investigated (Bjerre et al., 2011; Wang et al., 2009a). These would of course be more expensive, time consuming and would cause discomfort to the patient hence why the introduction of a biodegradable 3D scaffold with differentiated osteoblasts would be far more favourable and expedient to the healing process. Osteogenic scaffolds would also be required to have sufficient gaseous exchange, supply of nutrients and waste removal for long term culture, approximately 28 days **(Figure 1.3)**. The added attribute of having osteogenic and/or vascular trophic (rhBMP2, VEGF) ability (Kanczler et al., 2010) or an environment that would shift the biochemical gradients away from resorption (addition

of bisphosphonates to induce downregulation in osteoclasts) is also desirable (Bobyn et al., 2009).

In an attempt to meet the clinical demand for osseous tissue, specific bioreactors for bone tissue engineering, (with the aim of providing autologous *in vitro*/*ex vivo* engineered grafts) have been investigated. The extent of the technology to date will now be considered.

1.6.1 Bone bioreactors

Bioreactors for the seeding, expansion and differentiation of MSCs into an osteoblastic lineage can be divided into various types. These systems which involve the induction of a hydrodynamic stress (shear force) would include perfusion bioreactors and those that employ centrifugal force would include a spinner flask and rotating bioreactors. Apart from the three bioreactors mention in the last sentence, less well lauded systems entail the use of mechanical stimulation (bending, contraction, stretching, compression) and pulsed electromagnetic fields (PEMF). Interestingly, since bone is piezoelectric, mechanical deformations can generate an electric potential (Bjerre et al., 2011), what's more bone appears to have a selective EMF frequency of approximately 15 Hz which also appears to be osteogenically effective. It is noteworthy that to date some successes have been observed from the perfusion bioreactors. These employ the use of the flow of the media or fluid over cells for the movement of nutrient and gaseous diffusion. Further to this some success has also been attained through shear stress. The perfusion bioreactor will be briefly discussed in section 1.6.1.3 (Rath et al., 2012; Yeatts et al., 2013).

1.6.1.1 Spinner flask bioreactors

The spinner flask utilises convection currents which are generated by a magnetic stirrer at the bottom of the flask. This design can make use of cells seeded on a 3D scaffold (e.g collagen and silk) (Korin et al., 2009), attached to a needle like apparatus protruding from the top, and passing through its centre with the cells and 3D construct being stimulated by the flowing medium. This can be altered by varying the speed of the magnetic stirrer. Oxygen is allowed to diffuse through the bioreactor by the use of filtered angled side arms, preventing contamination. The entire unit is intended to be kept at optimum environmental conditions by using an incubator.

Published work has reported an affirmative osteogenic effect by an early up-regulation in the ALKP maker in human MSCs, where a stirring velocity of 50 rpm was employed. An increase in proliferation and osteogenic marker genes was observed relative to static controls (Korin et al., 2009). A further stated positive of this bioreactor design is that it is relatively inexpensive compared to others which will be discussed in this section and what's more it can be used for dynamic seeding (Wang et al., 2013). That being said however, a shortcoming of the use of 3D constructs with the spinner flask is the formation of more and less dense areas of cells which can impede gaseous and nutrient transfer in varying regions (particularly the centre) of the scaffold. Furthermore, it has also been noted by users of the spinner flask that this design lends itself to varying convection current gradients, with lager convection forces being found at the bottom of the flask in closer proximity to the magnetic stirrer bar (Bjerre et al., 2011). This may have a varying osteogenic effect at different regions.

1.6.1.2 Rotating bioreactor

The origins of the design of this bioreactor can be found in the rotating wall vessel implemented by the National Aeronautics and Space Administration for the simulation of microgravity conditions (Bjerre et al., 2008). In this bioreactor we observe the use of dynamic shear stress, (created by laminar flow) for the successful diffusion of nutrients, oxygen and waste products along a horizontal axis. Different designs have also been used with some using discs rotating in a horizontal position to create a shear force; in this case the cells were seeded upon these discs (3D constructs). Other derivative designs have utilised the attachment of scaffolds to the outer vessel wall in a free-fall and uniform manner, i.e. the rotating wall and rotating bed bioreactors.

Using the rotating bioreactor Pollack and his colleagues published that they observed an up-regulation of ALKP as well as an augmented effect for maturation and mineralisation of the ECM when contrasted against static controls (Pollack et al., 2000). Using a rotating wall vessel bioreactor, Song too also saw an affirmative result for the expansion of osteoprogenitors (Song et al., 2013).

However mixed results using the rotating bioreactor have been published as Goldstein et al have reported seeing a decrease in ALKP levels and no change for osteocalcin using precisely the same model as Pollack (Goldstein et al., 2001). This negative result was further reasserted by Sikavitsas and his co-workers who also saw decreased levels of calcium and ALKP when

using a rotating wall vessel system (Sikavitsas et al., 2002). Interestingly, the rotating bed bioreactor designed and developed by Zellwerk GmbH, was not only found to provide osteoblastic differentiation but was also built with GMP compliance in mind (Anton et al., 2008).

Disadvantages of the rotating wall vessel bioreactor include unwanted traction between the scaffolds and vessel walls which may result in the destruction of the scaffold and damage to proliferating cells, that being said however, this limitation could be overcome by using the rotating bed design of the bioreactor. An overall failing though of the rotating design is that an osteogenic effect generally seems to be limited to the outside of the scaffold and resistance issues to mass (nutrient) transport to internal sections of the scaffold may be observed (Sikavitsas et al., 2002).

1.6.1.3 Perfusion based bioreactor

This design of bioreactor implements the use of laminar media flow for gaseous exchange and nutrient transport. The system comprises of a central container or cartridge which houses the cells and scaffold set up, with medium pumped through the construct via a peristaltic roller. Oxygen, gaseous transfer and renewal can either be transitioned through the system provided by a reservoir and waste vessel or by implementation of a closed loop system (Fang et al., 2014). The perfusion bioreactor laminar flow system can either be separated into direct or an indirect design. In indirect systems the central construct and scaffold is loosely sealed which facilitates the flow of media in regions of least resistance usually found on the sides of the scaffold construct, this design includes commercial bioreactors such as the MINUCELLS and MINUTISSUE Vertriebs, **(Table 1.1)**. In direct bioreactor systems however, the setup forces the flow of media only through the centre of the cells and scaffold construct, brought about by the reduction of limitations which arise from internal mass transfer (Hathout, 2014). It has been published that a shear stress of 5×10^{-5} Pa was found to have a positive effect on cell proliferation and expansion and that increased shear forces beyond this pressure had an increased effect on osteogenic related genes(Deng et al., 2014). It is also noteworthy that the commercial OsteoGen perfusion bioreactor (Tissue Growth Technologies **(Table 1.1)** has utilised 3D cultured scaffolds which have delivered positive results *ex vivo* matrix mineralisation, while using micro-computed tomography for online monitoring (Porter et al., 2007).

Disadvantages of the perfusion bioreactor include its complexity for use and set up, and the need to scale up the bioreactor in order to engineer clinically relevant sized grafts also provide substantial engineering difficulties. What is more it may take several weeks to artificially engineer osseous tissue and maintenance of a sterile environment using a complex set up during this time may prove challenging (Gardel et al., 2014). The scaffold too; its geometry, porosity, dimensions, material make up and potential manufacturing defects will directly affect high flow and stresses of the media. This can adversely affecting cell viability, proliferation and subsequently mineralisation; not to mention having a deleterious effect on biodegradable scaffolds such as collagen (Meinel et al., 2004; Rauh et al., 2011b; Voronov et al., 2010). It has also been perceived that another limiting factor to engineered bone grafts becoming mainstream is the present cost of bioengineering grafts, which is estimated at $10,000 - $15,000; much of which would be due to the cost of building and operating bone bioreactors which are presently on the market (Salter et al., 2012).

Although these bioreactors discussed may work, it appears that cost, complexity and maintenance of a sterile environment long term, may limit their use and uptake. This fact highlights the prevailing requirement for a cheaper option which can utilise a 3D scaffold, is easy to use, can conform to GMP standards and maintain a sterile environment.The most important requirement to the modern healthcare system will inevitably be the reduction of the overall cost of engineering autologous osseous tissue and or osteoblasts in a 3D matrix, and this will be “the make or break” consideration.

Company	Product	Type (Features, options)
Bellco Biotechnology (Vineland, NJ)	Bell-Flow™	Spinner flask
Corning® Lifesciences (Lowell, MA)	ProCulture® glass spinner flask	Spinner flask (disposable or autoclavable)
MINUCELLS and MINUTISSUE Vertriebs GmbH (Bad Abbach, Germany)	Tissue engineering container	Perfusion bioreactor (indirect perfusion)
Tissue Growth Technologies (Minnetonka)	OsteoGen Bioreactor	Perfusion bioreactor (pulsatile fluid flow stimulator, μCT)
Zellwerk GmbH (Oberkrämer, Germany)	BIOSTAT® Bplus RBS 500 System, Z® RP cell and tissue culturing systems	Rotating bed bioreactor (GMP conform)
Synthecon, Inc. (Houston) B. Braun Biotech International GmnH (Melsungen, Germany)	STLV Bioreactor Medistat RBS	Rotating wall vessel Rotating bed bioreactor (GMP conform)
Flexcell International Corporation (Hillsborough, NC)	e.g., BioPress™ Compression Plates, Fkexcell® FX-5000™ Compression System	Systems using tension, compression and shear stress
GMP - Good Manufacturing Practice; RBS- rotating bed system; STLV - slow turning lateral vessel; μCT - micro-computed tomography.		

Table 1.1: Commercially available bone tissue engineering bioreactor systems, adapted from (Bjerre et al., 2011; Rauh et al., 2011b). Note this is not an exhaustive list, but a guide to some of the other bioreactors which have been developed.

1.7 Hypothesis

It is well known that mesenchymal stem cells derived from the bone marrow have the potency to differentiate into osteoblasts, or bone forming cells under given conditions, however much work remains to characterise new and efficient means to bring this about. It is hypothesised that the new technology in this field of piezo mechanical stimulation, can induce osteogenesis in mesenchymal stem cells using high frequency (≥ 1000 Hz) low amplitude (in the nanometre range) sinusoidal vertical displacements in 2D, and what's more there may be a potential to augment this effect by complementing it with an osteogenic nanotopographical surface, a disordered pattern of nanopits, referred to as an NSq-50.

It is further hypothesised that these piezo mechanical vibrations can also be transferred in a 3D environment through a biodegradable scaffold such as collagen I, and hence can also provide an osteogenic effect in an environment or extracellular matrix which is biomimetic, resembling the osseous condition of the *in vivo* skeletal framework. This 3D bioreactor would have the ability to expand and differentiate MSCs in a GMP sterile environment, would be cost effective and would be very easy to maintain and use at the hands of the clinician.

1.8 Aim

In the first instance the aim of this PhD was to create and characterise a 2D bioreactor which employs high frequency sinusoidal displacements and nanotopographical stimulation as a combined mechanical cue to bring about osteogenesis in bone marrow derived mesenchymal stem cells. The bioreactors mechanical integrity would first be validated as well as the integrity of mesenchymal stem cells to undergo high frequency piezo driven stimulation (nanokicking) without deleterious effect. The proof of concept would be determined by assessing the transcript (mRNA) and protein landscapes and subsequent mineralisation to confirm the presence of calcium phosphate deposition through osteoblast differentiation. This aim was then further extrapolated into the development of a 3D bioreactor with the potential to engineer *ex vivo / in vitro* calcium phosphate deposits in a collagen I extracellular matrix in a sterile, GMP, cost effective and easy to use manner.

Chapter II: Validation of a 2D nanokicking osteoblastic bioreactor

2.1 Introduction

In this chapter we begin to examine the construction of a 2D bioreactor which was used to induce osteoblastogenesis in mesenchymal stem cells. In order to have confidence in the mechanical integrity of the apparatus which had been designed; it was necessary to subject it to a rigorous assessment using techniques such as interferometry to determine that the displacements, even on the nanoscale, were indeed consistent, reproducible and uniform. The questions were further asked; would over heating also be a consequence of high frequency vibrations and could the cells respond positively to such high frequencies (≥ 5000 Hz) and not undergo adverse effects, i.e. what was referred to as the biological integrity of nanokicking.

2.2 Piezotechnology and the piezo device

The piezoelectric phenomenon was first investigated using crystals of boron silicate; tourmaline by the Curie brothers back in the late 19th century, when they found that it had unique mechano-electrical properties. Simply put a piezo device or piezo actuator is a material which has the physical ability to convert mechanical force or deformation into electrical energy, or electrical energy into mechanical force. The conversion of mechanical force into electrical energy is termed the direct piezoelectric effect, and is caused by the crystals physically deforming causing the negative and positive poles found in the polarised material to move more closely together. At the same time this allows a charge to move to the surface of the material and a potential difference to form between the poles allowing electrons to flow. The strength of the charge or the number of electrons that flow is related to the level of deformation (pressure applied). The formation of mechanical deformations from electrical energy is termed indirect or reverse piezoelectric effect in which changes in electrical dipoles and charge density causes mechanical deformations (Ballato, 1998).

Both organic and inorganic materials have been found to possess a piezoelectric capacity including tourmaline, bone/collagen, tooth/dentine, quartz and even sugarcane. There are also artificially prepared ceramics such as barium titanante, which employ lead zirconate titanate (LZT) as the piezo active material. Lead zirconate titanate is presently the most commercially used material for piezoelectric exploit (Minary-Jolandan and Yu, 2009). For the purposes of this body of research use was made of the ability of the piezo actuator to convert electrical energy into high frequency low amplitude mechanical displacements in order to vibrate cells on an aluminium platform, see **(Figure 2.1)** for a diagram of the piezo actuator which was

used in the 2D bioreactor. Modified LZT and barium titanate was used by the German company PI to make the piezo actuators which were utilised for this PhD. These devices had resonant frequencies between 200 kHz and 10 MHz which was well above the usable scope of this research which hence meant suitability.

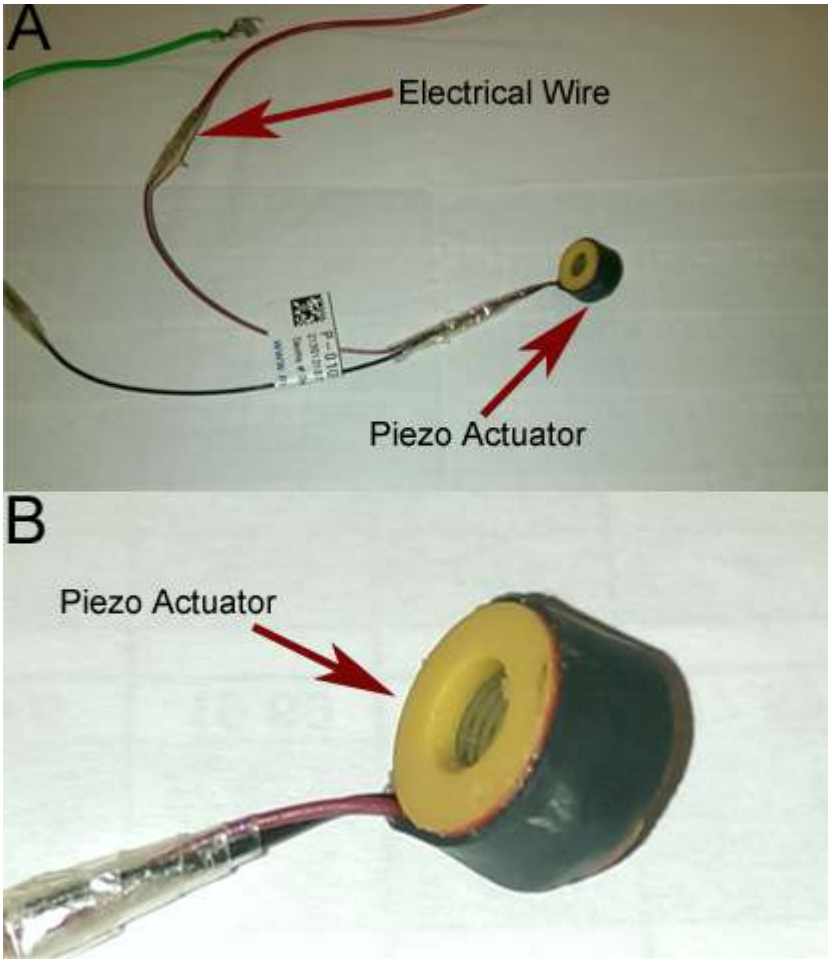

Figure 2.1: (A) Diagram showing piezo actuator with wire attachments, (B) showing magnified view of the piezo actuator device.

2.3 Materials and methods

2.3.1 Materials

Materials and Reagents	Source / Supplier
Human mesenchymal stem cells, from bone marrow	Promocell GmBH, Germany
Fetal Bovine Serum (FBS)	Sigma Life Science F9665
Penicillin streptomycin	Centre for Cell Engineering, University of Glasgow
Versene	Centre for Cell Engineering, University of Glasgow
Trypsin	Centre for Cell Engineering, University of Glasgow
Fixative	Centre for Cell Engineering, University of Glasgow
Ethanol (Ethanol:H20/70:30)	Centre for Cell Engineering, University of Glasgow
Phosphate buffer saline (PBS)	Centre for Cell Engineering, University of Glasgow
1% BSA in PBS	Centre for Cell Engineering, University of Glasgow
Rnase free water	Qiagen, UK
Quantitech reverse transcriptase kit	Qiagen, UK
Spectrophotometer	Nanodrop ND-1000
7500 Real time PCR system	Applied Biosystems – S/N:275007079
Dulbeccos modified eagle medium (DMEM)	Sigma Aldrich, UK
Sodium Pyruvate	Sigma Life Sciences – S/N: S8636
Nonessential amino acids	Gibco Life Technologies – S/N:11140-035
Minisart hydrophilic sterile 0.2 μm filters	Sartorius Stedim
Accurepette – pipette gun	VWR – AE5453
Syringes 20 mL & 50 mL	BD Plastipak P/N: 300613 & 300866
Triton X-100	Sigma S/N:T-9284
Ascorbic Acid	Sigma A-7506
Dexamethasone	Sigma D2915-100MG
Tween 20	Sigma Aldrich P9416-100mL
Permeability buffer	Centre for Cell Engineering, University of Glasgow
Piezo Actuator	Physik Instrumente GmBH Germany P/N: P-010.00H
Thermal IR Detector	Thermovision A40 supplied by FLIR systems
Signal generator	Agilent 33210A
DC offset box	Mastech PSU - P/N: HY3003
Laser Interferometer Vibrometer	SIOS Meβtechnik GmBH Germany SP-S120

Table 2.1: Table of materials and reagents used for chapter II

2.3.2 NSq-50 polycarbonate substrate fabrication

A silicon master was utilised to form a permanent impression or imprint on a substrate material made out of polycarbonate. The disordered but not random pattern which was impressed into the polycarbonate had a near square nanotopographical geometrical pattern of pits and was called an NSq-50, see **(Figure 2.2C)**. The imprinting was carried out by the process of hot-embossing (i.e. raising the temperature of the polymer substrate, polycarbonate, slightly above its glass transition temperature (Tg), but lower than its melting temperature (Tm), hence facilitating imprinting). The NSq-50 nanopits were spaced over a 120 nm diameter; the pits were 100 nm deep with an average centre spacing, which did not exceed of 300 ± 50 nm from a perfect square. To serve as a negative control flat surfaced polycarbonate substrates which did not have disordered patterns were also fabricated.

2.3.3 Setup of functioning 2D bioreactor

An Agilent 33210A function generator served as the power source for the piezo actuator from being plugged into the mains. Continuous sinusoidal nano-displacements were output by the function generator to the petri dish which contained the MSCs. A direct current (DC) voltage was provided by a DC offset box i.e. Mastech PSU (part number: HY3003) and this was employed to ensure that all voltages would be positive, resulting in a uniform displacement in a single direction. The German engineering company Physik Instrumente was used to source the piezo actuator device, part number: P-010.00H, as shown in **(Figure 2.1)**. The resulting sinusoidal nano-displacements which were introduced into the petri dish were controlled and reproducible.

A 20 mm^2 polycarbonate substrate, which was either the NSq-50 pattern see **(Figure 2.2 C)** or a flat unpatterned surface (control), was first plasma treated for approximately 20 seconds in order to facilitate cell attachment. So as to ensure a physical connection between the polycarbonate substrate and the 60 mm diameter polystyrene petri dishes used, polycaprolactone beads (FDA approved) were heated on a hot plate to approximately 90ºC and served the purpose of a biocompatible adhesive. An aluminium disk (52 mm in diameter with a 3 mm thickness) was securely adhered via epoxy to the outer base of the petri dish to allow uniform displacement of the entire petri dish. An aluminium block was used as a solid support and a stationary foundation onto which the piezo actuator was glued. The aluminium block was of dimensions 315 x 100 x 50 mm, and it facilitated the transference of the piezo

displacement into the dish instead of out into the ambience. A complete illustration of the 2 D piezo bioreactor is provided in **(Figure 2.2 A-B)**.

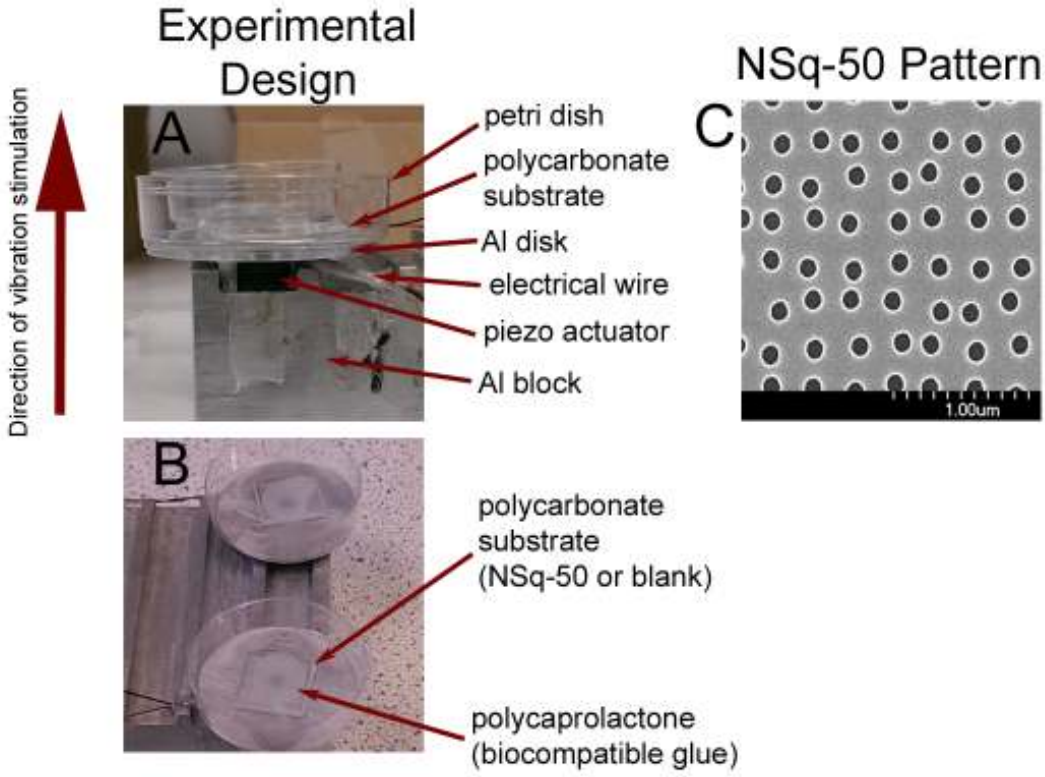

Figure 2.2: Nanokicking vibrational apparatus setup – The 2D bioreactor: (A) cross section view of setup showing the petri dish with the aluminium disk and piezo glued to the aluminium block which facilitates displacement vertically upwards into the petri dish. (B) Aerial view of setup showing the polycarbonate substrate (either NSq-50 or blank surface) adhered to the inside of the petri dish using melted polycaprolactone as a rigid biocompatible adhesive. (C) Near square disordered nanopits (NSq-50) used as an osteogenic surface for MSC differentiation. The nanopits are 120 nm wide and 100 nm deep with an average centre-centre spacing of 300 nm in a square arrangement, but with up to a ± 50 nm offset in X and Y positioning. Figure used with permission from the publisher (Pemberton et al., 2015).

2.3.4 Cell culture and media preparation

Promocell, Germany was used to source human MSCs. The cells were grown and used for culturing in passages 1-3. The basal media which was used to maintain the cells during experiments and for proliferation was DMEM (Sigma-Aldrich) supplemented with 10% FBS, 1% sodium pyruvate - Sigma (11 mg/ml), 1% MEM NEAA – Gibco (amino acids) and 2%

antibiotics (6.74 U/mL penicillin-streptomycin, 0.2 µg/mL fungizone). The initial volume of the DMEM used was 500 mL and all solutions, save the sterile DMEM, were first filtered through a 0.2 µm hydrophilic filter to make the finished basal media.

For the preparation of osteogenic media which served as a positive control, the DMEM basal media was also substituted with 100 µMol ascorbic acid and 10 nMol dexamethasone (Sigma). For this preparation 0.0088 g ascorbic acid was added to 500 mL basal media. A stock of dexamethasone was prepared by adding 0.081 g in 5 mL deionised H_2O (41.3 mMol), 24.2 µL of this stock was added to 1 mL of deionised (1 mMol) and subsequently 5 uL of this stock was added to 500 mL basal media (10 nMol).

The population of MSCs used for seeding was approximately 1×10^4 per petri dish, (with approximately, 60% of that quantity being seeded on the 2 cm^2 polycarbonate flat or NSQ-50 substrate). All culture was performed in an incubator at 37ºC with 5% CO_2, the basal media being changed every 2-4 days.

2.3.5 Laser vibrometry and nanokicking bioreactor displacement characterisation

A laser interferometric vibrometer supplied by SIOS Technology Corp. part number: SP-S120 was used to calibrate individual piezo actuators for accurate nanoscale displacements. For reference two individual piezo actuators set up for calibration are shown in **(Figure 2.2 B)** and a diagram of the interferometer, (laser vibrometer) used to perform the measurements is shown below in **(Figure 2.3)**. The piezos were calibrated from 500 Hz to 10000 Hz with a varying amplitude range from 2 to 20 volts. A continuous helium neon laser beam at wavelength 632.8 nm and at a continuous wave power of 5 mW was shone from the laser vibrometer onto the surface of the polycarbonate substrate and was subsequently reflected back into the laser vibrometer off a fused silica mirror which was attached to the substrate surface. This reflectance beam created an interference pattern which was then related to a reference beam. To align the reflectance beam accurately back into the laser aperture an internal oscillating signal was tuned and this was displayed as a resolved circle on the monitor of the oscilloscope. INFAS Vibro (Interferometer Analysis Software for Vibrometers) computer software supplied by SIOS Meβtechnik GmbH was used to acquire the interference

output and convert the information by fast fourier transform; representing it in terms of amplitude or displacement in frequency space. The mean of 4 piezo actuators were used to determine nanolevel displacement for the different frequencies relative to an increase in voltage, see **(Figure 2.6 A)** for these results.

The calibration of increasing number of piezo actuators connected in series to the same signal generator was further assessed to determine if this would have an effect on the displacement output, see **(Figure 2.6 B)** for these results.

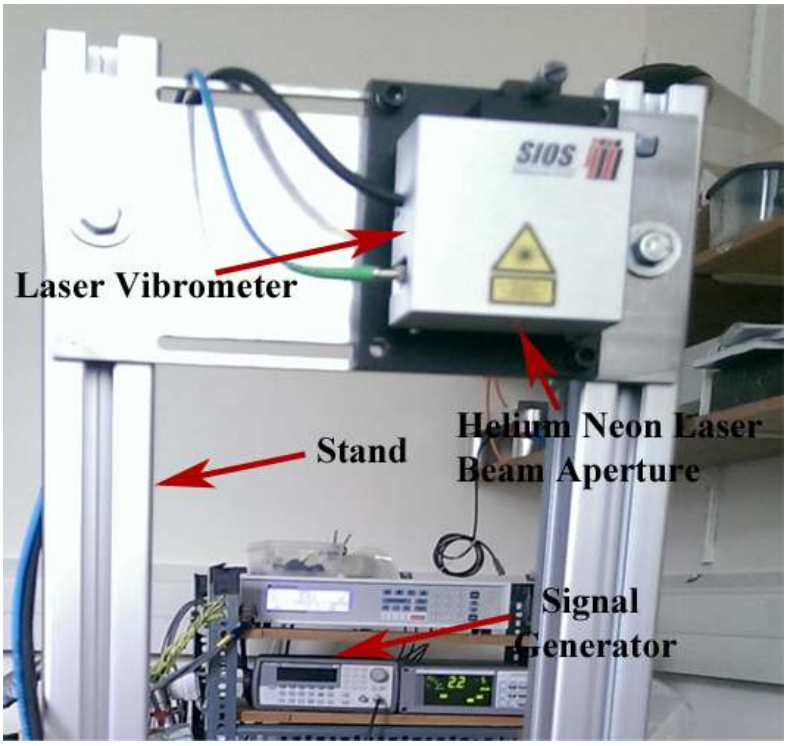

Figure 2.3: Laser vibrometer used to perform interferometric experiments in order to calibrate the bioreactor (displacements were assessed at the nanometre level). A helium neon laser beam is shone from the laser vibrometer to the piezo activated surface of the polycarbonate substrate in the centre of the petri dish. The laser was reflected from the surface of a statically adhered fused silica mirror back into the laser vibrometer to make an interference pattern related to a reference beam. The INFAS Vibro, (i.e. the Interference Analysis Software for Vibrometers) was used to construe the results. Fast fourier transform (FFT) computer software was used to assign an amplitude of the displacement relative to the frequency at a given voltage, vertical resolution = 0.02 nm. FFT reading was determined approximately every five seconds by the software and five readings were also recorded at each voltage for a particular frequency.

2.3.6 Thermal assessment

In order to confirm that at high frequency vibrations the generation of heat would not be an issue thermal characterisation was carried out. Infrared thermal imaging was performed using the Thermovision A40 supplied by FLIR systems, (User Manual: Publ.No. 1557813Rev.a72-October 29, 2004). The potential for heat conduction from an activated piezo actuator at high frequency (5000 Hz) through the aluminium disc and into the culture media could theoretically affect the viability of the MSCs.

An initial or starting time point in which the piezo actuator was inactive was first determined. Next one activated piezo actuator (bioreactor) was compared concomitantly to an inactive bioreactor at the frequency of 5000 Hz for 5 mins. Subsequently as an extreme condition an activated piezo actuator at 5000 Hz and 20 V peak to peak was concurrently compared against an inactive actuator with exactly the same set up. All these experiments were performed with and without the presence of culture media in the petri dish to determine if heat which could potentially be generated would alter the media temperature through convection. **(Figure 2.4)**, provides the results of these experiments.

Note as well as performing thermal analysis an investigation into the possibility of shear force being a contributing variable in the experimental set up was also investigated by previous analysts. This was performed by determining the movement of fine particulate fluorescent dyes in an active nanokicking bioreactor, for this work see reference (Nikukar et al., 2013).

2.3.7 Quantitative real-time (qRT-) PCR

2.3.7.1 Pelleting of cells after experimental culture

- Triplicates of triplicates (initially 45 samples brought down to 15 with triplicates) were cultured for a given period of time. The sample populations were as follows:
- **Group A: No exposure to nanokicking**
  I) MSCs grown in osteogenic media a 1 cm^2 flat polycarbonate substrate-(Positive Control).
  II) MSCs grown on a 1 cm^2 flat polycarbonate substrate - (Negative Control)
  III) MSCs grown on a 1 cm^2 NSq-50 nanotopography polycarbonate substrate
- **Group B: Cells exposed to nanokicking**
  IV) MSCs grown on a 1 cm^2 flat polycarbonate substrate
  V) MSCs gown on a 1 cm^2 NSq-50 nanotopography surface
- For all the samples, the 1 cm^2 polycarbonate base was removed and placed into a 10 cm Petri dish.
- The 1 cm^2 base was inverted so that the top (the surface on which the MSCs were grown) was facing down. To this was then added 1 mL trypsin/versene mix (0.5 mL/20 mL). The 3 triplicates were then placed in the incubator for between 5-10 mins, with observation for detachment. After this time, 500 µL DMEM media was then placed into each Petri dish to quench the trypsin catalysis reaction.
- While working in a fume hood, a scraper was then used to thoroughly scrape all the cells from each 1 cm^2 surface, combining the contents of 3 surfaces into 1. A syringe was then used to carefully take up the 1.5 mL solution containing the suspended cells, this volume was placed into a 1.5 mL Eppindorf tube.
- Each triplicate per sample group was then centrifuged for 5 mins at 14000 rpm.
- A pellet was observed and the media was removed using a pipette without disturbing the pellet, leaving behind the pellet in as little media as possible.
- The samples were immediately placed on dry ice (CO_2) at -100ºC, and then stored overnight at -70 ºC.

2.3.7.2 RNA extraction

- When dealing with RNA at the qRT-PCR kit, nitrile gloves were used at all times to prevent contamination of the very labile RNA samples.
- Firstly, the necessary solutions as dictated by the Qiagen qRT-PCR kit were made.
- Ethanol:H_2O / 70%:30% (deionised Millipore water)
- Ethanol:H_2O / 80%:20% (deionised Millipore water)
- Buffer RLT: by adding 450 µL B-mecaptoethanol (B-me) to the 45 mL Buffer RLT provided by Qiagen. (i.e. 10 µL B-mecaptoethanol per 1 mL Buffer RLT).
- Buffer RPE (concentrate supplied): 44 mL ethanol (absolute) to 11 mL buffer RPE concentrate, to give 55 mL buffer RPE working solution.
- The samples were taken from the -70ºC storage back onto dry ice and brought to the working lab. To each sample from on ice (while still frozen) was added 350 µL Buffer RLT to the Eppindorf tube with the pellet. This was then vortexed for 5-10 secs to ensure mixing.
- To each solution was again added 350 µL 70% ethanol solution. It was then agitated using the pipette to mix.
- This solution was then added to a special MinElute spin column, which was placed into a 2 mL flow through collection tube (both supplied by Qiagen).
- The samples were then centrifuged for 60 secs at 10000 rpm. The flow through was then discarded.
- To the MinElute spin column cartridge was then added 350 µL buffer RW1. The samples were then centrifuged for 60 secs at 10000 rpm. The flow through was then discarded.
- At this point it is necessary to resuspend the DNase I (provided in powder form by Qiagen). To make the DNase I incubation mix 10 µL DNase I stock was added to 70 µL RDD (supplied by Qiagen) for just one sample. In order to make, for example, sufficient quantities for 15 samples, 16 times the amount of the incubation mix was prepared.

  For this 550 uL RNase free H_2O was added to the DNase I stock, and the solution was agitated gently by inverting. No vortexing was used as the DNase I was sensitive to physical denaturation.

160 µL DNase I stock solution was then added (10 x 16 samples) to 1120 µL Buffer RDD solution. The solution was then mixed with gentle inverting to form DNase I incubation mix. 70 µL of this mix was then added directly to each sample MinElute spin column membrane.

- The samples were then left to incubate for 15 minutes at ambient temp (20-35ºC).
- Next 350 µL Buffer RW1 was added to the RNeasy MiniElute spin column cartridge. The lid was closed and the tube centrifuged for 60 secs for at 10000 rpm. This was used to wash the spin membrane. Both the flow through and collection tube were then discarded.
- The MinElute cartridge was then placed into a new 2 mL collection tube (supplied by Qiagen). To the cartridge was added 500 µL Buffer RPE to the spin column. The lid was closed and the tubes centrifuged for 60 Secs at 10000 rpm. This washed the spin column membrane and the flow through was discarded.
- Then 500 µL 80% ethanol was added to the MinElute spin column cartridge. The lid was closed and the tubes centrifuged for 2 mins at 10000 rpm. Both the flow through and collection tube were then discarded.
- The cartridge was then placed into a new 2 mL collection tube. The lid of the spin column cartridges were then opened, and centrifuged at 14000 rpm for 5 mins. Both the flow through and collection tubes were then discarded. This step was used to dry the spin column membrane, since residual ethanol would interfere with downstream reactions. Centrifuging with the lids opened ensured that no ethanol was carried over during RNA elution.
- The MinElute cartridge was placed into a new 1.5 mL collection tube. To this was then added 14 µL RNA free water. This was carefully added directly to the centre of the column cartridge membrane. The lid was closed and the Eppindorf tube was centrifuged at 14000 rpm for 2 mins, in order to elute the RNA. The dead volume of the RNeasy MinElute column was 2 µL, hence 14 µL only yield a 12 µL volume of RNA.
- At this point if necessary the RNA was frozen at – 70ºC, or directly tested on the Nanodrop system for quantification of the RNA content (concentration).

2.3.7.3 RNA quantification

- Quantification of the levels of RNA in each sample was performed using a spectrophotometer Nanodrop system (UV detection). By the following process.
- Firstly, a P2 – 2 µL Pipette was used.
- The nucleic acid setting was chosen on the nanodrop software.
- The UV analysis mount was cleaned with 2 µL RNA free water, and the system was background initialised.
- ng/µL units of concentration was selected.
- The top was wiped and 2 µL RNA Free water was placed on the analyser, and a blank determination was performed.
- Each triplicate set of samples was then analysed by adding 1.5 µL of volume directly on the analyser pin hole
- Once a result report was printed all the values of the RNA samples were normalised to be at the same level as the lowest sample concentration, by adding different volumes RNA free water (supplied by Quiagen).
- Note, the comparison absorption between the wavelengths of 260/280 nm and 260/230 nm were used for the quantification of the RNA.

2.3.7.4 Reverse transcription process

- 12 µL of the normalised dilutions for each sample were added to a 0.2 mL (200 µL) reverse transcription PCR – Cup (supplied by Qiagen).
- To each of the samples was then added 2 µL gDNA wipeout buffer, (provided by Qiagen).
- Following this each sample was run at 42ºC for 2 mins, on the thermal Cycler (PCR) Master cycler system.
- The Stock solution was then made as given in **(Table 2.2)** below (allowing for 15% extra)

	1 x Mix	16 x Mix
Quantiscript reverse transcriptase	1 µL	16 µL
Quantiscript RT buffer	4 µL	64 µL
Primer mix	1 µL	16 µL

Table 2.2: qRT-PCR Reverse transcription solution volumes

- 6 µL of the Stock Solution was then added to each well, to give a total volume of 20 µL.
- The second program was then run to reverse transcribe the RNA into cDNA. This took approximately 20 mins.

Temp	Time
42ºC	15
93ºC	3
4ºC	Hold

Table 2.3: qRT-PCR reverse transcription thermal program

- Once complete the cDNA, if necessary was stored at 4˚C.

2.3.7.5 Analysis of qRT-PCR

- Where necessary the samples were taken out of storage and to each of the (200 µL size) reverse transcription PCR cups was added 30 µL DNA free water (supplied by Quiagen), to give a total volume of 50 µL.
- Master mixes were then prepared, one for the house keeping gene Glyceraldehyde 3-phosphate dehydrogenase (GAPDH - used as an internal reference standard gene) and the other genes being assessed, see **(Table 2.5)** for a list of the genes determined. These were prepared with 10% extra volume.

	1x	16x stock Mix
SYBR Green PCR Kit	33 µL	528 µL
Forward primer (100 µM)	0.33 µL	5.28 µL
Reverse primer (100 µM)	0.33 µL	5.28 µL
DNA free water	25.74 µL	411.84 µL

Table 2.4: Volumes of primers and PCR kit solutions used for the PCR cycle analysis.

- 59.4 µL of the Master mix was placed into a 1.5 mL Eppindorf tube. To this was then added 6.6 µL of cDNA from each of the samples. This was then used to create 3 triplicates of each sample, as a result there were 9 wells corresponding to each sample.
- 20 µL of the each was then aliquoted into the correct well on a PCR 64 well plate. Once this was done for the GAPDH gene, it was then repeated for the genes being assessed placing the samples in a different but known location on the plate.
- Following this a negative control or Blank was also placed in a known location on the 64 well plate corresponding to each gene. This comprised of 18 µL of the Master mix and 2 µL of DNA free water.
- The wells were then covered with a specific thin plastic and sealed tightly using a scraper.

Gene	Forward Primer	Reverse Primer
GAPDH	TCAAGGCTGAGAACGGGAA	TGGGTGGCAGTGATGGCA
Beta-Actin	CCAACCGCGAGAAGATGA	CCAGAGGCGTACAGGGATAG
HPRT1	TGACCTTGATTTATTTTGCATACC	CGAGCAAGACGTTCAGTCCT
TFRC	TGGCAGTTCAGAATGATGGA	AGGCTGGAACCGGGTATATGA
GUSB	CGCCCTGCCTATCTGTATTC	TCCCCACAGGGAGTGTGTAG

Table 2.5: Primers for genes used to perform qRT-PCR, housekeeping screen experiment, the culture time for the housekeeping gene experiment was for 3 days at 10000 Hz.

Note:

glyceraldehyde 3-phosphate dehydrogenase - (GAPDH)

hypoxanthine phosphoribosyltransferase - (HPRT1)

β-glucuronidase - (GUSB)

transferrin receptor - (TFRC)

The 7500 Real Time PCR system was used to perform the amplification and GAPDH served as the internal reference standard gene (housekeeping gene) against which the expression of the target genes were assessed. For accurate PCR quantification the $2^{-\Delta\Delta Ct}$ method was used to determine gene expression and amplification of 3 triplicates from an unstimulated control (the negative control sample listed in section 2.3.7.1) was compared against the stimulated sample conditions.

2.3.8 Statistics

To determine significance between controls and test samples the probability values have been quoted to an accuracy of 95% and 99% (*$p < 0.05$ and **$p < 0.01$ respectively**),** as an acceptable way to quote significant data. Kruskal-Wallis ANOVA, for use with non-parametric data, was used to compare significance in PCR experiments, using the Prism software package. Tukey's post hoc test was further performed for comparison of significance of the control to multiple test samples.

2.3.9 Finite elemental modelling (ANSYS)

Simulated models of Corning petri dishes, and the bioreactor materials were developed in ANSYS finite element software (ANSYS, Canonsburg, PA). Models were developed in ANSYS Workbench v14.0 with analysis involving use of the Harmonic Response package to provide values for deformation at user defined frequencies.

The culture plate component was modelled with a polystyrene dish bonded to an alumium disc adhered by epoxy. A similar method was used to model the piezo actuator attached to the aluminium block and the polycarbonate NSq-50 substrate adhered within the polycaprolactone. For this analysis, a vibration frequency of 1000 Hz with 28 nm amplitude was applied to the models to compare amplitude consistency. Throughout all the analysis, mesh relevance was set at 0 giving a medium mesh density.

Harmonic response analysis was used to study the frequency dependant effects of deformation of the construct taking into account all the different materials. Vibration condition was set in the range of 500 to 10000 Hz at 20 nm to encompass the experimental value of 1000 Hz. Harmonic response analysis is strictly linear so accuracy would be limited to the linear range of the material. Meshing size was set to coarse to reduce computational time. The additional impact of gravity was incorporated through an inertial acceleration of 9.81 ms^{-1}. Note the ANSYS modelling was performed by Mr. Peter Childs, as stipulated in the acknowledgements.

2.4 Results

2.4.1 Thermal analysis of the piezo actuator

The thermal analysis carried out showed that the ceramic material which was used to build the piezo actuator by PI was in fact an excellent insulator, and that the piezo actuator could be vibrated at high frequencies without generating a noticeable heat increase between activated and inactive bioreactor set ups. What's more even at the extreme condition of 5000 Hz and 20 V peak to peak amplitude, which would also be used to test the onset of osteogenesis; no noticeable increase in heat was observed. It is worth noting that the experiment was only determined for a maximum of 10 mins although culturing could be carried out for weeks. The rationale here; after discussion with expert physicists was that if after 5-10 mins of activation no heat was detected, it could be accepted that this would be status quo through the duration of culture. Observe **(Figure 2.4)** for a summary of the thermal imaging results determined.

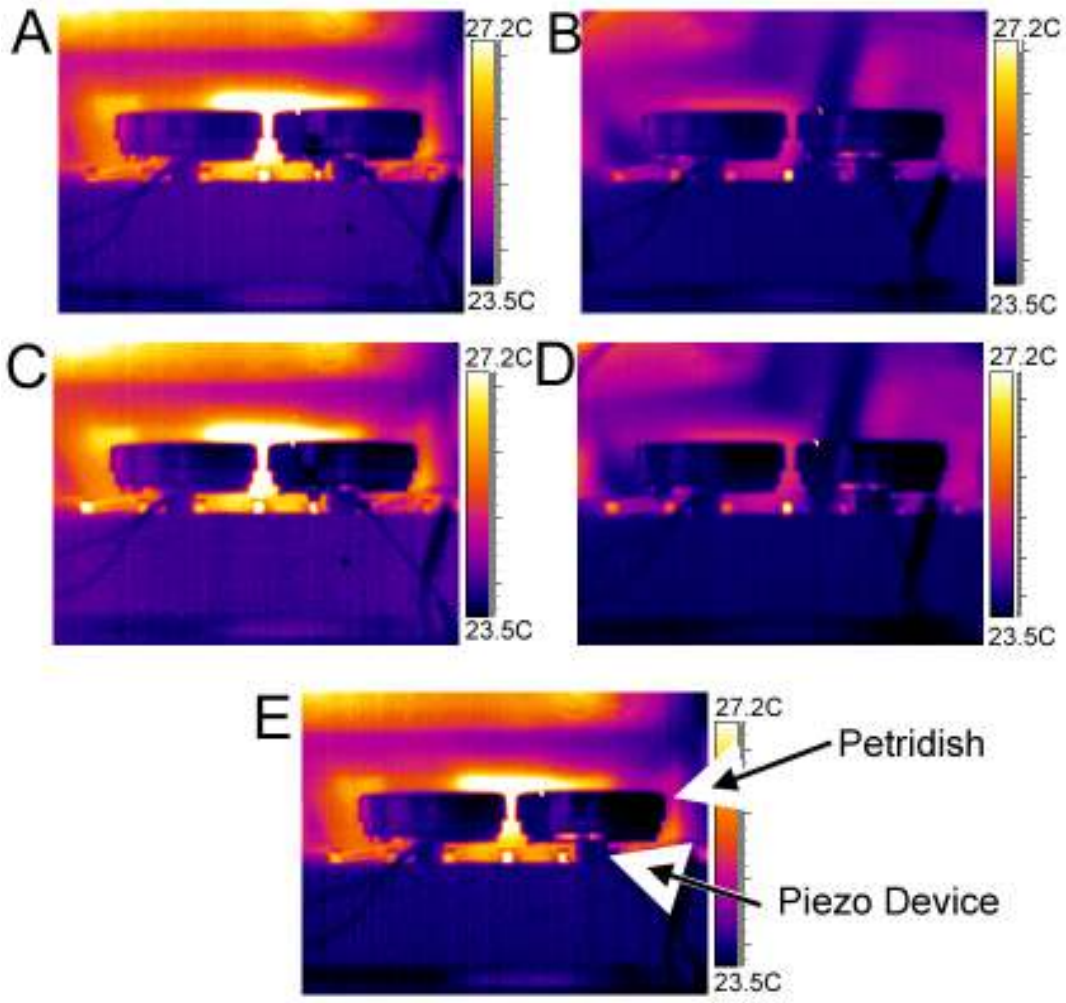

Figure 2.4: Temperature profile data, infrared images with experiments performed at room temperature. Piezo actuator on the left hand side is inactive and piezo actuator on right hand side is activated in diagrams (B), (C), and (E) : - (A) initial time point with no media in the Petri dishes, no piezo activation. (B) 5 mins of the piezo actuator activation at 5000 Hz and 20 V with no media in Petri dishes. (C) 10 mins of the piezo actuator activation at 5000 Hz and 20 V with no media in petri dish. (D) Initial time point with hepes media in petri dishes. (E) 5 mins of the piezo actuator activation at 20 V with hepes media in Petri dish. No thermal change was observed for any of the activated piezo devices relative to the inactivated devices, with or without media present in the Petri dish. This data provides thermal stability for the piezo actuator set up. All these samples were analysed in the bench. Figure used with permission from the publisher (Pemberton et al., 2015).

2.4.2 Piezo bioreactor mechanical integrity characterisation

Using ANSYS finite element modelling software, the vibration apparatus (aluminium, Petri dish and NSq-50) was modelled to determine the lowest resonant frequencies and potential physical deformations at 1000, 3000, 5000 and 10000 Hz. Resonances or deformations even at the nanometre level can alter the accelerative forces experienced by individual cells, and hence limit the reproducibility and control of the experiments. The modelled deformations, shown in **(Figure 2.5 D)**, indicate that the level of vibration control is diminished at 10000 Hz with even the polycarbonate substrate being expected to start physically deforming. The model shows that at 10000 Hz, two corners of the substrate move with amplitudes of 50 nm whilst the other two exhibited reduced amplitudes below 10 nm, which are also moving out of phase with the rest of the surface, see **(Figure 2.7)** for this data. This was supported by interferometric measurement which showed some corners moving at 18 nm whilst others moved at 76 nm giving large standard deviations (**see Figure 2.6 A)**. Deformation was also predicted at 5000 Hz in the corners of the polycarbonate substrates. Interferometry confirmed this with increased amplitudes up to 65 nm at the edges as opposed to 16 nm at the centre see **(Figure 2.7)**. The data however showed 1000 and 3000 Hz to be stable reproducible frequencies for use with this bioreactor set up. Peak acceleration can be calculated using the average amplitudes measured by interferometry and is given by $A_0\omega^2$ where A_0 is the amplitude and ω is the angular frequency. For 1000, 3000, 5000, and 10000 Hz this equates to peak accelerations of 0.1g, 1g, 1.6g and 14g respectively (6.5 g at the corners, 5000 Hz and 20 g at the corners, 10000 Hz). As per the interferometry characterisation in **(Figure 2.6 A)**, the nanometre level displacements measured at 20 V at the working frequencies used were as follows: 1000 Hz – 30 nm, 3000 Hz – 28 nm, and 5000 Hz – 16 nm.

The addition of multiple piezo actuators wired in parallel to the same signal generator power source was observed to have a negligible change on the height of the nanoscale displacements observed see **(Figure 2.6 B)**, and the results remained in line with the specification provided for the piezo actuator by PI.

Note the work for the ANSYS finite element modeling and interferometry measurements were performed in collaboration with Mr. Peter Childs, a physics PhD student from the University of West of Scotland.

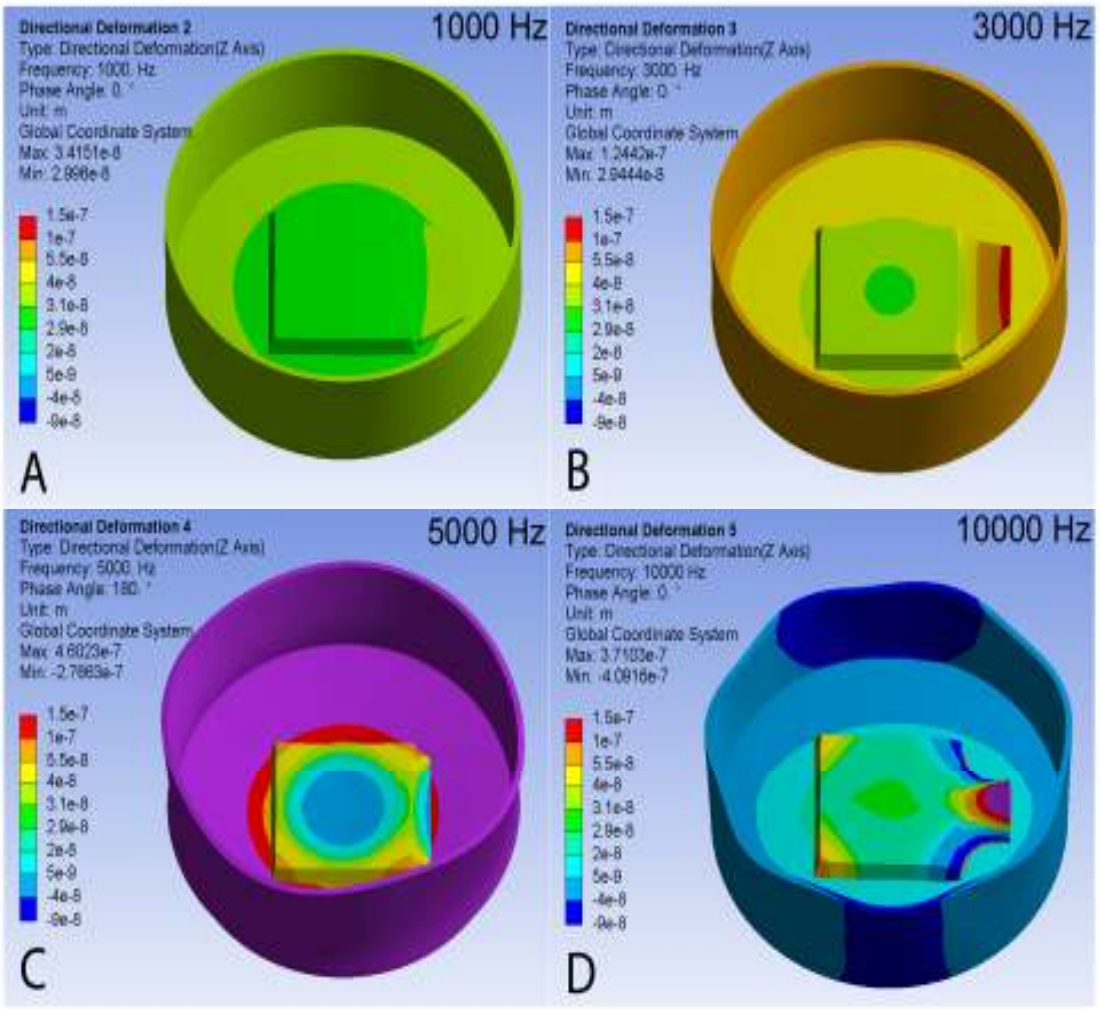

Figure 2.5: Characterisation of the 2D bioreactor: ANSYS harmonic response simulations of the vibration setup at (A) 1000 Hz, (B) 3000 Hz, (C) 5000 Hz and (D) 10000 Hz. Increasing deformation of the NSq-50 is seen as the frequency increases. Petri motion and piezo motion are out of phase at 5000 Hz due to resonant frequencies occurring lower than this (resonance causes an increase in magnitude of the displacement, which may cause poor reproducibility in future experiments). Figure used with permission from the publisher (Pemberton et al., 2015)

.

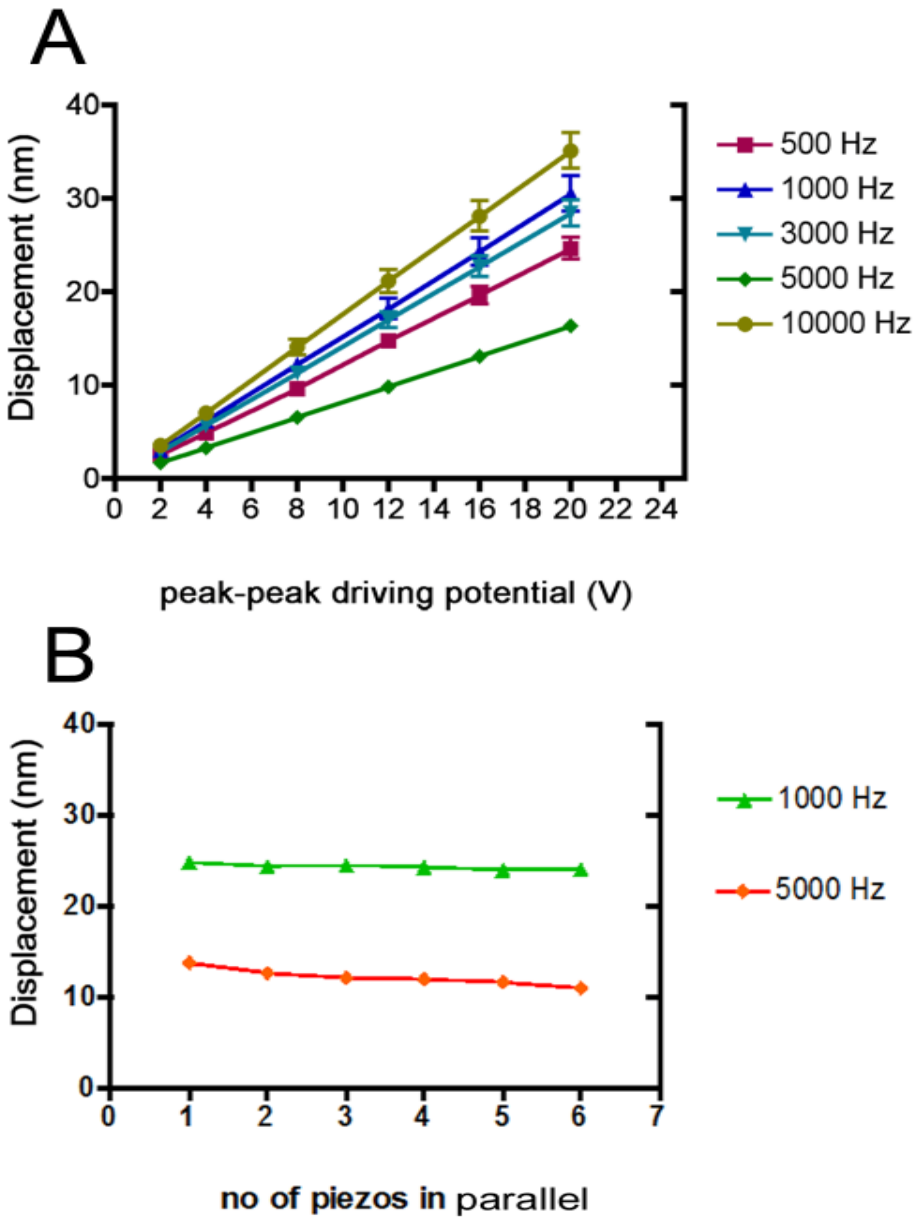

Figure 2.6: Empirical nanokicking displacement Assessment: (A) Graph showing the use of interferometry to determine displacement (nm) relative to peak to peak potential difference (V) of the piezo actuator. Determinations performed at varying frequencies from 500 Hz to 10000 Hz, N= 4 material replicates (average of 4 Petri dishes and piezo actuators, with each measurement being the average of 5 interferometry readings), a resonance at ~ 3000 Hz means that 3000 Hz has a higher displacement than 5000 Hz. (B) Determination of the effect of increasing the number of piezo actuators connected in parallel on the displacement (nm) of the piezo actuators at 20 V for 1000 Hz and 5000 Hz. The change was found to be negligible and within the specification of the piezo actuator apparatus. Figure used with permission from the publisher (Pemberton et al., 2015).

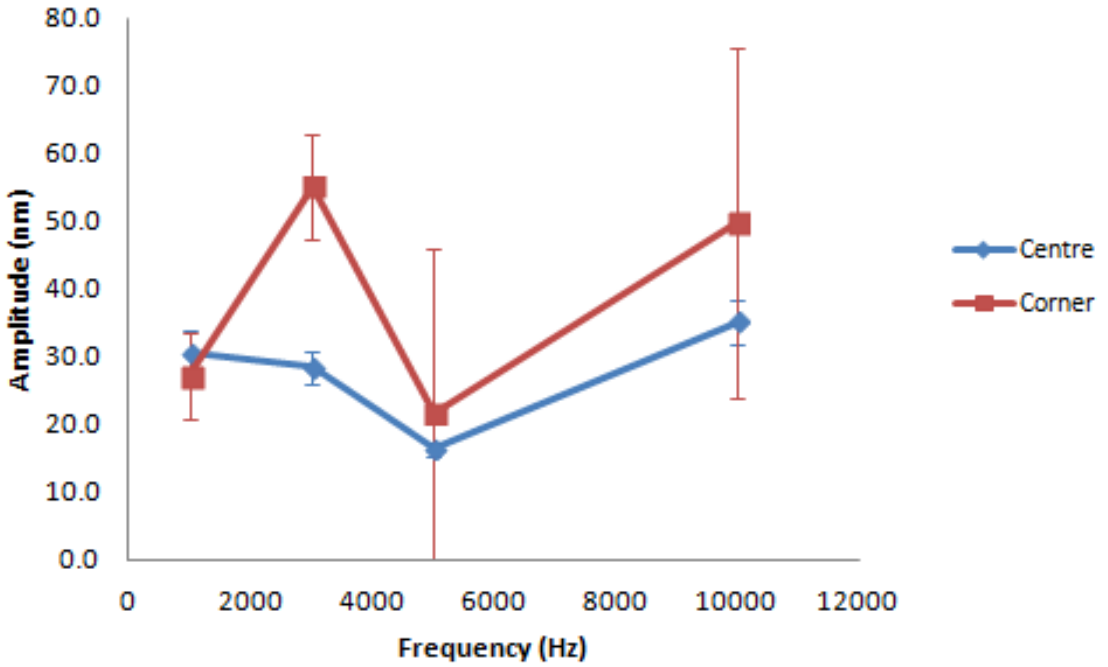

Figure 2.7: Interferometric measurement showing the standard deviation and range of amplitude displacement of the polycarbonate substrate motion comparing the corners and centres at the frequencies of 1000 Hz, 3000 Hz, 5000 Hz and 10000 Hz. The data shows that 10000 Hz has the most extreme level of variation in displacement, and is the most extreme frequency. Figure used with permission from the publisher (Pemberton et al., 2015).

.

2.4.3 Biological integrity of piezo vibration

Due to the fact that this research was novel and had not been attempted previously, it was important to confirm the selection of the correct housekeeping gene to be used as a biological internal reference standard for qRT-PCR analysis. Before commencing transcriptional analysis of high frequency nanokikced samples a qRT-PCR scouting experiment ensued. This entailed the piezo stimulation of fibroblast cells for 3 days at the extreme vibrational condition of 10000 Hz and 20 V peak to peak (equating to accelerations between 3.6 g and 20 g). The expressions of 5 well known qRT-PCR housekeeping genes were assessed against their unstimulated controls. As researched from the literature the genes chosen for the scouting experiment were *β*-actin, glyceraldehyde 3-phosphate dehydrogenase (GAPDH), hypoxanthine-guanine phosphoribosyltransferase (HPRT1), β-glucuronidase (GUSB) and the transferrin receptor (TFRC) (Bas et al., 2004; Bhoopathi et al., 2011; Iwaki et al., 2003; Rosales-Reyes et al., 2012; Thellin et al., 1999). Out of these, GAPDH was found to be the most stable gene with the lowest cycle threshold, as a result this was chosen as the internal reference housekeeping gene for all nanokicking stimulated qRT-PCR experiments throughout this PhD, see **(Figure 2.8)** for results.

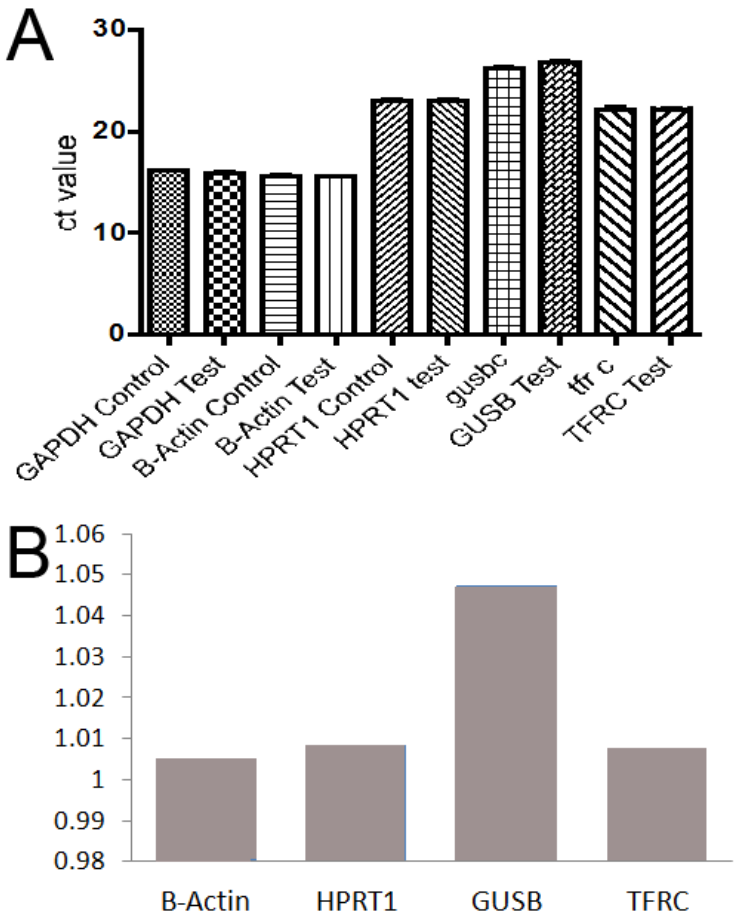

Figure 2.8: qRT-PCR housekeeping gene (internal genomic reference standard) scouting experiment: Fibroblast cells were nanokicked at extreme conditions for 3 days, following this the PCR cycle thresholds for specific housekeeping genes were compared against unstimulated controls. (A) GAPDH was found to be the most stable housekeeping gene with the lowest cycle threshold, other genes assessed included (B-Actin, HPRT1, GUSB and TFRC). (B) GAPDH was then used as a house keeping gene for comparison of all other genes. All experiments were carried out at 10000 Hz at an amplitude of 20 V peak to peak. N=5 (one experiment with 5 material replicates). Figure used with permission from the publisher (Pemberton et al., 2015).

2.5 Discussion of results

The mechanical integrity of the 2D piezo bioreactor which was constructed was found to be suitable for use when interrogated for thermal and mechanical stability and reproducibility. The design used was importantly not susceptible to shear force either. In terms of thermal consistency, it appeared that Physik Instrumente GmBH as an engineering company had

factored this potential issue into their construction of the piezo actuator and used the correct insulating materials. The use of heated polycaprolactone as a biocompatible glue was also suitable to securely fasten the polycarbonate NSq-50 nanotopographical substrates to the petri dish efficiently transferring the piezo nanodisplacement, as was confirmed by the interferomeotric measurements.

The interferometric empirical measurements matched closely with the results predicted by the ANSYS finite element modelling software, corroborating the expectation of innate resonances around 3000 - 4000 Hz, increased accelerations at 5000 and 10000 Hz and even physical deformations at 10000 Hz. The higher acceleration forces were made evident by the large standard deviations or differences in nanometre displacements between the centre and corners observed in the activated bioreactor.

By qRT-PCR the fibroblast cells (cells differentiated from MSCs which help to synthesis the extracellular matrix) were observed to have biological integrity for all the housekeeping genes that were assessed at an extreme condition of 10000 Hz. Even B-actin which comprises the microfilaments, which in part composes the cell cytoskeleton showed not to change to a large degree after 3 days of vibrational stimulation, when comparing cycle thresholds against unstimulated controls. As discussed in the introductory chapter it can also be further argued that it is in fact F-actin which is attached to the focal adhesion and it is primarily F and α - actin which play more significant roles in cell structure, contractility and movement.

Further resulting biological changes in the cells may perhaps then take initiative from the integrins and focal adhesions as nanokicking stimulation ensues. Out of all of the housekeeping genes assessed GAPDH was seen to have the lowest cycle threshold and was thought to be most stable, hence this was chosen as the biological internal reference standard which would be used for future qRT-PCR analyses to determination the genotype (transcriptome) of MSCs which had been stimulated by nanokicking.

2.6 Conclusion

The design which was engineered for 2D high frequency vibrations of MSCs was found to be fit for purpose, when interrogated for thermal, mechanical and biological integrity. This 2D bioreactor, see **(Figure 2.2)**, was hence suitable for introducing low amplitude high frequency nanometre displacements to a layer of MSCs cultured on an NSq-50 nanotopographical or flat surface.

Chapter III: Osteogenesis using the 2D bioreactor – nanotopography & nanokicking

3.1 Introduction

The work performed in chapter II included determining the most suitable housekeeping gene for genomic assessment; confirmation and validation of the mechanical integrity of the 2D bioreactor and assurance of the bioreactors suitability for biological experiments. Carrying on from this, chapter III provides an in depth assessment into the potential of the 2D vibrational bioreactor to differentiate multipotent MSCs into osteoblasts. To confirm this capacity, the flow of the biological information from genes to proteins to biological product was assessed. Finally, experimentation was subsequently performed at the mineralisation level for the presence of deposited calcium and phosphate – the constituents of apatite, the mineralised component of the bone matrix. It is hypothesised that this bioreactor in effect has the ability to provide a direct route to intramembranous ossification (ossification de novo) without the need for endochondral ossification or the preliminary formation of cartilage in the first instance.

3.2 Materials and methods

3.2.1 Materials

Note: Several of the reagents, protocols and the materials listed in chapter II were also prepared in the same fashion for chapter III; as a result these have not been relisted in **(Table 3.1)**. Only new methods, protocols and reagents distinctive to chapter III have been listed in **(Table 3.1)** and explained throughout section 3.2. Refer back to the original list of reagents from chapter II.

Materials and Reagents	Source / Supplier/ prepared
Osteocalcin mouse monoclonal IgG antibody	Santa Cruz Biotechnology, ABOC-5201, Lot: G3014
Osteopontin mouse monoclonal IgG antibody	Santa Cruz Biotechnology, AKM2A1 Lot:G1613 -
GAPDH rabbit monoclonal antibody	Abcam, ab128915, LotGR179384-1
anti-mouse IRDye 680 CW	LI-COR 926-68077
anti-rabbit IRDye 800 CW	LI-COR 926-32213
DAPI(4,6-diamidino-2-phenylindole)	Vector Laboratories H-1200
Phalloidin conjugated - FITC (Fluorescein)	Invitrogen R415
Streptavadin conjugated - rhodamine	Vector Laboratories SA-5001
Raman spectrometer	Renishaw InVia
Fluorescent and light microscope	Zeiss Axiophot BMBA011033
Silver nitrate	Sigma Aldrich 85228-50G
Sodium thiosulphate	BDH Analar 102684G
Aluminium sulphate	VWR Chemicals 12362.A1
Alizarin Red (ARS)	Sigma-aldrich A5533-25G
Ammonium hydroxide (5 M)	Centre for Cell Engineering, University of Glasgow
Bovine serum albumin (FBS)	Fisher Scientific – BP9700-100 Lot: 61-1247
Milk protein blocker	Marvel R.No.92962
Nuclear fast red	229113 Aldrich (CAS Number 6409-77-4)
1 x PBS	Centre for Cell Engineering, University of Glasgow
PBS/Tween 0.5%	Centre for Cell Engineering, University of Glasgow
Perm Buffer	Centre for Cell Engineering, University of Glasgow
Fixative	Centre for Cell Engineering, University of Glasgow
PBS/Tween 0.1%	Centre for Cell Engineering, University of Glasgow

Table 3.1: List of materials and reagents used in chapter III

3.2.2 Cell culture and media preparation

See section 2.3.4, for the methodology which was used to culture and feed the cells during the duration of the nanokicking stimulation and OSM stimulation. Although the cell culture preparation was the same, the durations which the experiments were carried out for were differed depending on whether transcription, protein or mineralisation was being assessed.

3.2.3 Quantitative real-time (qRT-) PCR

See section 2.3.7 of chapter II, for the methodology and preparation steps used to harvest the cells after experimental culture and isolation to quantify the RNA and perform quantitative polymer chain reaction analysis. **(Table 3.2)** below lists the specific gene primers which were used to perform the quantification experiments. GAPDH served as the house keeping gene or internal genetic reference standard for the transcription (mRNA) quantification.

Gene	Forward Primer	Reverse Primer
GAPDH	TCAAGGCTGAGAACGGGAA	TGGGTGGCAGTGATGGCA
BMP2	CCCACTTGGAGGAGAAACAA	AGCCACATTCCAGTCATTCC
RUNX2	GGTCAGATGCAGGCGGCCC	TACGTGTGGTAGCGCGTGGC
Osterix	GGCAAAGCAGGCACAAAGAAG	AATGAGTGGGAAAAGGGAGGG
Osteonectin (ONN)	AGAATGAGAAGCGCCTGGAG	CTGCCAGTGTACAGGGAAGA
Osteopontin (OPN)	AGCTGGATGACCAGAGTGCT	TGAAATTCATGGCTGTGGAA
Osteocalcin (OCN)	CAGCGAGGTAGTGAAGAGACC	TCTGGAGTTTATTTGGGAGCAG

Table 3.2: Primer sequences for genes used to perform qRT-PCR

3.2.4 In cell western

3.2.4.1 Preparation of in cell western reagents

Preparation of fixative

10 mL (38%) formaldehyde was placed into 90 mL PBS along with 2 g sucrose. The solution was then left at 37ºC for 15 minutes to dissolve the sucrose.

Preparation of perm buffer

The following compounds were added together: 10.3g sucrose, 0.292g NaCL, 0.06g MgCL2 (hexahydrate), 0.476g Hepes in 100 mL PBS. The solution was then adjusted to pH 7.2 using NaOH. 0.5 mL Triton X-100 was then added.

Preparation of blocking buffer

To 50 ml x 1 PBS was added 0.5 g milk protein (i.e. 1%), this was stirred for 5 minutes or alternatively the blocking buffer was heated to 37 º C to fully dissolve the milk powder.

Preparation of primary antibody

- **Osteocalcin or Osteopontin mouse:** 20 µL primary antibody was added to 1 mL of the blocking buffer prepared above, (1:50 dilution).
- **GAPDH rabbit:** 2 µL primary antibody GAPDH was added to 10 mL of the blocking buffer prepared above (1:5000 dilution)
- **Note:** these two were combined to make one primary antibody solution.

Preparation of secondary antibody

- **Osteocalcin or Osteopontin (donkey anti-mouse) 680 nm wavelength -** 1 µL secondary antibody was added into 10 mL of the blocking buffer prepared above, (1:10000 dilution). Note 0.2% Tween® 20 was added to the blocking buffer used as diluents for the secondary antibody. This was 20 µl Tween in 10 ml blocking buffer, which helped to lower the background fluorescence.
- **GAPDH (donkey anti-rabbit) 800 nm wavelength -** 1 µL secondary antibody was added into 10 mL of the blocking buffer prepared above, (1:10000 dilution). Note 0.2% Tween® 20 was added to the blocking buffer used as diluents for the secondary antibody. This was 20 ul Tween® 20 in 10 ml blocking buffer.
- **Note:** these two were combined to make one secondary antibody solution.

Preparation of wash buffer

To 1000 mL x 1 PBS was added 1 mL Tween® 20 (i.e. 0.1% Tween® 20).

3.2.4.2 In cell western procedure

- Fixative was used to fix the cells for 15 minutes at 37ºC.
- The cells were then permealised in perm buffer at 4ºC for 4 minutes.
- The perm buffer was then removed.

- The blocking buffer (PBS /1% milk protein) was added. The blocking procedure was performed for 1.5 hours at room temperature with moderate shaking on a plate shaker.
- The blocking solution was then removed.
- The primary antibody was then added and incubated at 37ºC in a warm room for 2 hours.
- The primary antibody was removed and the sample washed 5 separate times with wash buffer for 5 minutes each at room temperature with gentle shaking. Enough buffer was used to completely submerge the sample.
- The wash buffer was removed and the sample was washed once in blocking buffer.
- The secondary antibody was then added and left for 1 hour in a shaker, covered in tin foil.
- The secondary antibody was removed and the plate was washed 5 times with wash buffer, for 5 minutes for each wash. This included gentle shaking while covered in foil. The last wash was carried out solely in PBS so as to remove any bubbles caused by the surfactant Tween® 20.
- The 2 cm^2 polycarbonate substrates were then removed and lightly dried with white paper, turned upside down and moved to a newly labelled Corning 6 well plate.

3.2.5 Immunofluorescence

3.2.5.1 Preparation of the immunofluorescence reagents

Preparation of fixative

10 mL (38%) formaldehyde was placed into 90 mL PBS along with 2 g sucrose. The solution was then left at 37ºC for 15 minutes to dissolve the sucrose.

Preparation of perm buffer

The following compounds were added together: 10.3g sucrose, 0.292g NaCL, 0.06g MgCL2 (hexahydrate), 0.476g Hepes in 100 mL PBS. The solution was then adjusted to pH 7.2 using NaOH. 0.5 mL Triton X - 100 was then added.

Preparation of PBS/ 1%BSA

To 100 mL 1 x PBS was added 1 g bovine serum albumin (BSA). The solution was mixed to thoroughly dissolve the BSA in solution. The volume of solution prepared was scaled up or down depending on what was required. The solution was stored in the freezer when not in use.

Preparation of wash buffer

0.5 mL Tween 20 was added to 100 mL 1 x PBS (PBS/Tween 0.5%).

Preparation of primary antibody

3 uL phalloidin (to stain actin microfilaments) was added to 1 mL PBS/BSA solution (dilution 1 to 333). To the same volume was added 20 uL either osteopontin or osteopontin (rabbit) primary antibody, depending on which was being assessed per sample (dilution 1 to 50).

Preparation of secondary antibody

40 uL biotinylated anti-rabbit was added to 2 mL PBS/BSA (dilution 1 to 50).

Preparation of tertiary complex

40 uL streptavidin (conjugated rhodamine/texas red) was added to 2 mL PBS/BSA (dilution 1 to 50).

3.2.5.2 Immunofluorescence procedure

- The cells were first rinsed with 1 x PBS wash buffer.
- 38% formaldehyde solution was used to fix the MSCs directly onto the polycarbonate NSq-50 or flat substrate, at 4˚C for 5 minutes.
- Permeablisation buffer was used to permealise the cells, the substrates were incubated at 37˚C for 5 minutes.
- PBS/1%BSA was used as a blocking agent and the substrates were first incubated in the blocking buffer for 5 minutes at 37˚C. The solution was removed and the primary antibody was added, the samples were wrapped in foil and incubated at 37˚C for 1.5 hrs.

- The primary antibody was removed and the samples were washed for 3 x 5 minutes using the wash buffer. The final wash was performed with agitation on a shaker.
- The secondary antibody was then added and the samples were wrapped in foil and incubated at 37˚C for 1 hour.
- The secondary antibody was removed and the samples were once again washed for 3 x 5 minutes using wash buffer, with the last wash being performed with agitation.
- The wash buffer was removed and tertiary complex was added. The samples were once again wrapped in foil and incubated at 4˚C for 30 minutes.
- The tertiary complex was removed and the same wash procedure was once again undergone.
- Following on from this, a small drop of vectroshield-DAPI (to stain the nucleus) was added to the sample and they were subsequently inverted and fixed to a microscope coverslip. The samples were sealed using nitrocellulose/ butyl acetate (nail varnish).
- Microscopy was performed using an Axiophot-Zeiss Germany and where necessary the samples were stored at 4˚C.

3.2.6 Raman spectroscopy

- MSCs were cultured on either polycarbonate flat or NSq-50 substrates and exposed to piezo stimulation for the duration of 27 days.

- The substrates were removed and quickly dipped into deionised water to remove any excess basal media. The substrates were then directly introduced to the Raman system for assessment.

- Firstly, a sample of bovine cortical (compact) bone was scanned using the Raman spectrometer, to serve as a reference for perfectly mineralised bone.

- Subsequently, it was determined that 960 cm^{-1} was the dominant scattering wavenumber in the distinctive fingerprint region for bovine cortical bone, and hence all test samples were scanned at this wavenumber to determine the presence of phosphate.

- Visible spectroscopic scans were measured using a Renishaw InVia Raman spectrometer equipped with a 785 nm line-focus laser.
- A 0.25 cm^2 region of each substrate sample was assessed with a single static scan measurement with spectral acquisition at 960 cm^{-1}.
- A Leica microscope was used to observe the test samples at magnification x 20.
- No sample preparation was required before assessment by Raman spectroscopy.

3.2.7 Alizarin Red S staining

- Alizarin red solution was prepared at a concentration of 40 mM by adding 1.369 g Alizarin red powder to 100 mL of distilled water. The pH was then altered to 4.2 from 3.5 using NH_4OH.
- The solution was then filtered through a 0.2 μM filter.
- Following on from this MSCs which were cultured in basal media for 34 days exposed to vibrational stimulation were fixed using 38% formaldehyde at 37ºC for 15 minutes.
- The substrates were then covered with 1 ml Alazarin red S and placed on an orbital shaker for 1 hour at ambient temperature.
- The substrates were removed and rinsed 5× with deionised water. An extended rinse was then performed on an orbital shaker for 10 minutes.
- The substrates were allowed to dry and observed using an Axiophot-Zeiss (Germany0 microscope under white light.

3.2.8 Von Kossa staining

3.2.8.1 Preparation of Von Kossa reagents

- 5% silver nitrate was prepared by adding 5 g silver nitrate to 100 mL deionised water. The mixture was stirred to form a solution, which could be stored in the dark for up to 7 days.
- 5% sodium thiosulphate was prepared by adding 5 g of sodium thiosulphate to 100 mL deionised water. The mixture was once again thoroughly stirred. The solution could be stored for up to 6 months in the dark.

- Nuclear fast red counterstain was prepared at a concentration of 0.1% by adding 0.1 g nuclear fast red to 100 mL deionised water. To this solution was also added 5 g aluminium sulphate. The solution was boiled while stirring for approximately 10 minutes until a deep red colour change was observed. This solution was stable for up to 2 months.

3.2.8.2 Von Kossa staining procedure

- MSCs were cultured in basal media for 34 days exposed to piezo stimulation and were then fixed using 38% formaldehyde at 37ºC for 15 minutes.
- 5 % silver nitrate was used to immerse the substrates
- The substrates were then exposed to UV light for 20 minutes and rinsed in deionised water.
- Following this, 5% sodium thiosulphate was added to the substrates for 10 minutes and rinsed with tepid water for 5 minutes followed by deionised water.
- The substrates were then counterstained with nuclear fast red for 5 minutes and first rinsed 3× with deionised water followed by 70% ethanol.
- Nuclear fast red counterstained the cell nuclei in order to observe the position of the active osteoblast cells relative to the calcium phosphate nodules being deposited.
- The substrates were allowed to dry and were observed using an Axiophot-Zeiss (Germany) microscope under white light.

3.2.9 Statistics

To determine significance between controls and test samples the probability values have been quoted to an accuracy of 95% and 99% (*$p < 0.05$ and **$p < 0.01$ respectively), as an acceptable way to quote significant data. Kruskal-Wallis ANOVA, for use with non-parametric data, was used to compare significance in PCR experiments, using the Prism software package.

3.3 Results

3.3.1 Transcript analysis of nanokicking induced osteogenesis

In order to gain an understanding of the genetic changes which would be brought about through exposure to high frequency vibrational stimulation, transcriptional analysis of MSCs after nanokicking, with and without the added stimulation of the NSq-50 nanotopographical surface, was investigated. qRT-PCR was utilised as the technique of choice to assess various genes linked to osteogenesis. In particular the genes which were assessed were osteopontin (OPN), osteocalcin (OCN), osteonectin (ONN), BMP2, RUNX2 and osterix.

From the preliminary experiments performed, previous work has indicated that 500 Hz was a threshold frequency and was insufficient to bring about osteogenesis see **(Figure 3.1)**. Further to this, however, the samples which were cultured in osteogenic media, referred to as the positive control, did show an increased expression for some key specific osteogenic genes over both the 7 and 15 days time points **(Figure 3.2)**.

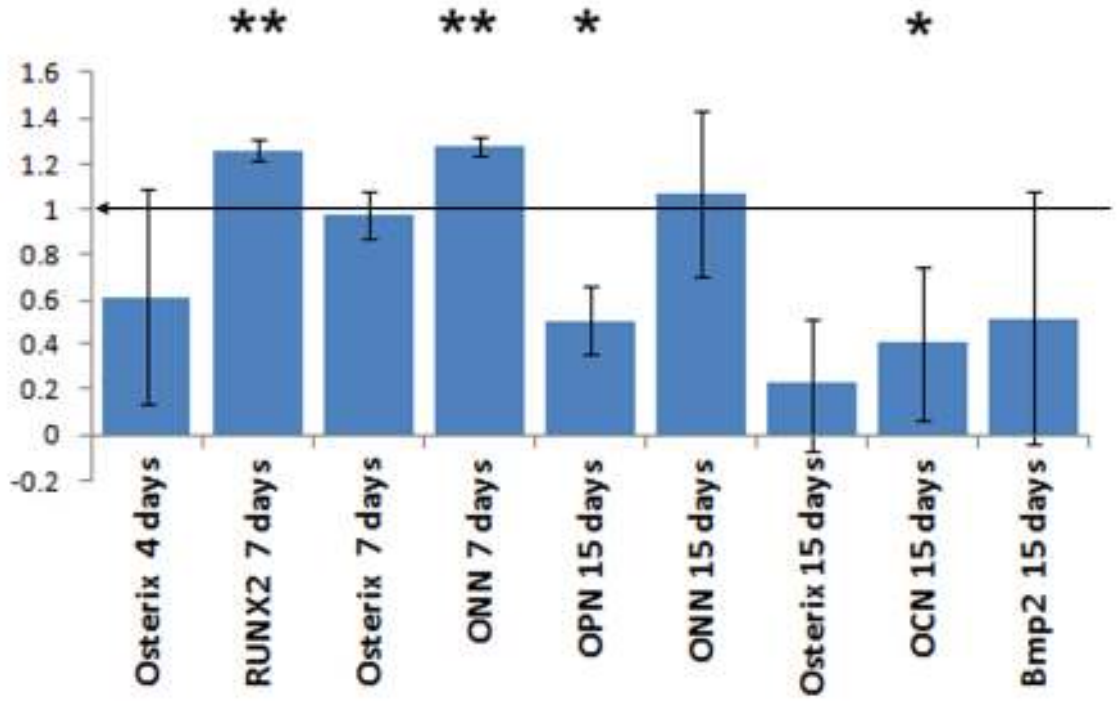

Figure 3.1: qRT-PCR: Nanokicking at 500 Hz after 4, 7 and 15 days time point on a flat polycarbonate surface. The data suggests that osteogenesis did not occur at a frequency of 500 Hz while there is some initial indication of gene induction, this fades at later timepoints. All experiments were carried out at an amplitude of 20 V peak to peak. N=3 (one experiment with three material replicates), results are mean ± standard deviation $*p < 0.05$ and $**p < 0.01$ by ANOVA. Figure used with permission from the publisher (Pemberton et al., 2015).

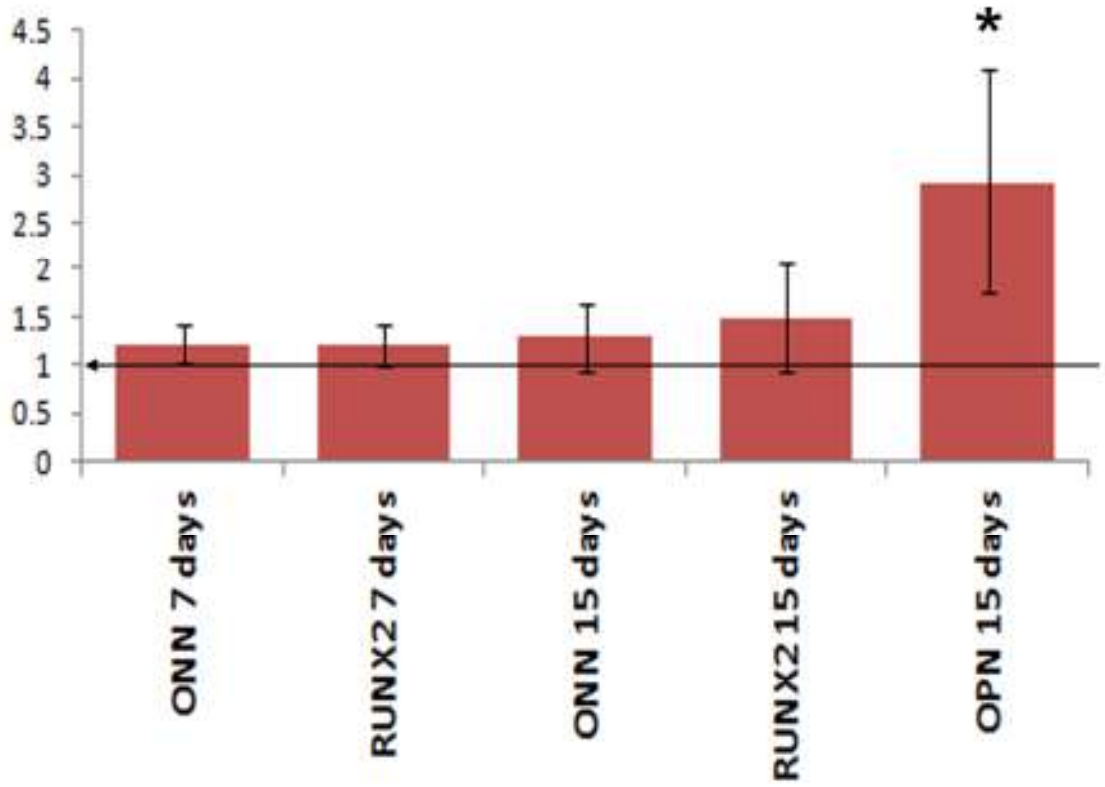

Figure 3.2: qRT-PCR showing osteogenic media, positive control samples showing an up-regulation in key osteogenic genes. N=3 (one experiment with three material replicates), results are mean ± standard deviation *$p < 0.05$ by ANOVA. Figure used with permission from the publisher (Pemberton et al., 2015) .

It was also important to this research to understand if there was a relationship between changes in frequency and the nanotopographical surface. To that end, further investigation of more osteogenic genes after 7 days of culture, exposed to increasing frequencies with and without NSq-50 nanotopography were assessed. This revealed that 1000, 3000 and 5000 Hz frequencies all had osteoinductive transcript effects. ONN was observed to be the most consistently up-regulated gene **(Figure 3.3)**. It was also observed that nanokicking at 5000 Hz further increased expression of osterix, OPN and OCN. The data suggested that nanokicking in its own right is very osteogenic, however coupling nanokicking together with the osteoinductive NSq-50 nanotopographical surface appeared to have a reductive or cancelling effect at the transcript level for the 7 days time point. This for the most part, appeared to be the result for all the genes assessed, and 5000 Hz in the absence of the nanotopographical surface appeared to provide the optimum osteogenic genetic increase. However, this

frequency is unreliable as it appears to be at the threshold of mechanical integrity of the bioreactor and hence would be inconsistent, as exhibited by the research performed in chapter II.

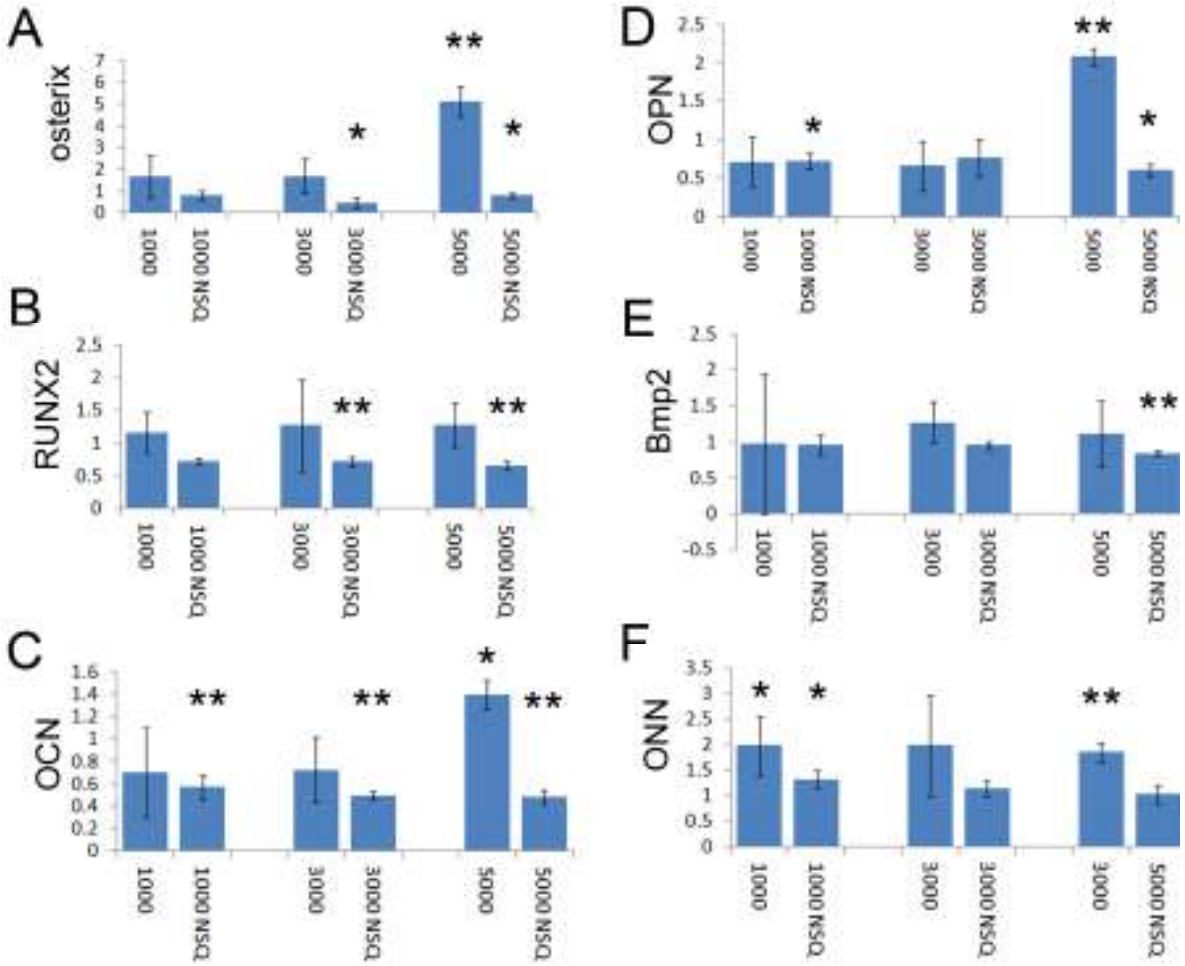

Figure 3.3: qRT-PCR for osteospecific gene expression: Nanokicking stimulation for 7 days comparing MSCs nanokicked on an NSq-50 surface against MSCs nanokicked on a flat surface. Samples were assessed at 1000 Hz, 3000 Hz and 5000 Hz (1, 3 and 5 kHz) for genes (A) osterix, (B) RUNX2 (C) osteocalcin (D) osteopontin (E) BMP2 and (F) osteonectin. NSq-50 with nanokicking had an overall reductive effect on these osteogenic genes while piezo stimulation on flat surfaces potentiated osteogenesis at the transcriptional level. Increasing frequency had an overall augmentative effect on osteogenic genes. All experiments were carried out at an amplitude of 20 V peak to peak. N=3, results are mean ± standard deviation *$p < 0.05$ and **$p < 0.01$ by ANOVA, the control are at a level of one. Figure used with permission from the publisher (Pemberton et al., 2015) .

3.3.2 Protein analysis of nanokicking induced osteogenesis

MSCs were nanokicked for 21 days and were assessed using quantitative in-cell western analysis by immunostaining for the proteins OPN and OCN. The protein GAPDH was once again used as an internal reference standard to quantitatively compare the expression of OPN and OCN as was the case for the qRT-PCR experiments. To remain in line with the genomic experiments, nanokicking was carried out both on a flat surface and also on an NSq-50 surface at 1000 Hz. MSCs were also cultured in OSM for the duration of 21 days and this served as a positive control. It was observed that at the protein level assessment, after 21 days of culture: the nanokicking; OSM induced differentiation and NSq-50 samples coupled with nanokicking all had a positive osteogenic effect.

Furthermore, it was noted that a combination of topography and nanokicking did not have the reductive effect which was observed at the earlier genetic level; but rather the highest expression of osteogenic proteins were noted at 1000 Hz of nanokicking coupled with the NSq-50 nanotopography.

The 1000, 3000 and 5000 Hz stimulation were all seen to be osteogenic at the protein level with nanokicking only, with the 3000 Hz providing the best expression of the three **(Figure 3.4A)**. Fluorescent microscopy of OCN and OPN revealed a similar trend see **(Figure 3.4B)**.

Interestingly, it was observed that whenever nanokicking was used; OCN appeared to be highly expressed, and in the osteogenic samples where nanokicking was not used (i.e. NSq-50 and OSM samples) OPN was observed to be the dominant protein expressed.

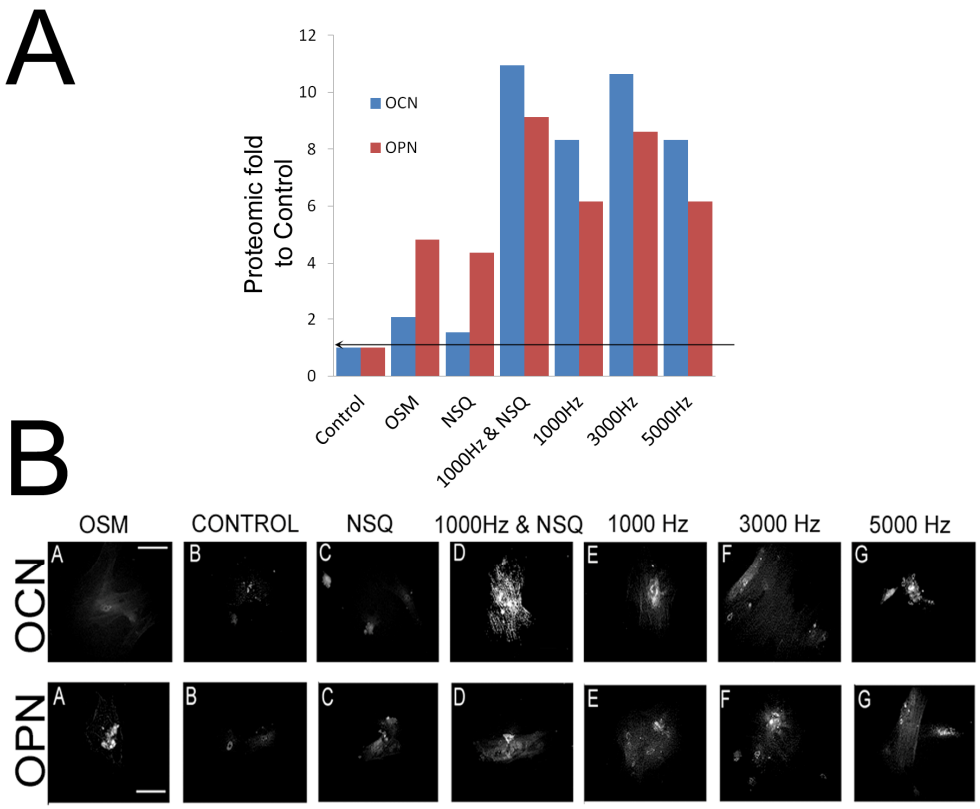

Figure: 3.4A - In cell western Assay quantitative proteomic analysis for OPN and OCN at the 21 day time point: OSM was the positive control. MSCs were cultured on an NSq-50 surface along with nanokicking at 1000 Hz. Samples were also nanokicked at 1000 Hz, 3000 Hz and 5000 Hz on a flat surface only. All stimulation was performed at 20 V and samples were compared relative to an unstimulated control, N = 2. 3.4B - Immunostaining, qualitative analysis for OPN and OCN at the 21 days time point, images chosen are representative of the entire sample population, low seeding density areas were chosen to ensure direct NSq-50 nanotopographical contact by the cells: (A) OSM, positive control, (B) Negative control - MSC cultured on a flat polycarbonate surface without nanokicking, (C) NSq-50 polycarbonate surface only, (D) NSq-50 with nanokicking at 1000 Hz, (E) 1000 Hz nanokicking only, (F) 3000 Hz nanokicking only, (G) 5000 Hz nanokicking only. Nanokicking at all frequencies was at 20 V. Mag 20×, scale bar =100 µm. Fixed cells were stained for OCN & OPN, N = 2. Figure used with permission from the publisher (Pemberton et al., 2015).

3.3.3 Bone matrix mineral deposition analysis of nanokicking induced osteogenesis

Following the flow of biological information from gene to protein; assessment of mineral deposition (osteogenesis) through nanokicking after 24 days of culture was determined. For this the presence of calcium phosphate deposition was investigated. Apatite deposition would only occur in the presence of active osteoblastic cells and this was assessed by three different techniques; i.e. Raman spectroscopy, Alizarin red stain (for calcium) and Von Kossa stain (for phosphate). The Alizarin red and Von Kossa results on controls (flat and NSq-50 piezo unstimulated) gave as expected results with little mineralisation noted on planar controls and mineralised nodules observed on NSq-50 see **(Figure 3.5A-D)**. Further to this, strong nodule formation was observed with higher piezo frequencies. In line with the protein-level data, the mineralization data confirms that the most distinctive nodules were formed at 1000 Hz piezo stimulation in tandem with the NSq-50 nanotopography **(Figure 3.5 G-H)**. The results also showed that nanokicking at 5000 Hz with and without the NSq-50 nanotopography see **(Figure 3.5 I-L)** also gave mineral deposition albeit to a less extent than what was observed at 1000 Hz.

Raman spectroscopic assessment was performed after 27 days of nanokicking by determining the unique scattering pattern of the fingerprint region of bovine cortical bone, i.e. perfectly mineralised bone. It was found that the predominant Raman peak for bone, (which is mainly comprised of hydroxyapatite $Ca_{10}(PO_4)_6(OH)_2$) had a wavenumber of 960 cm^{-1}. This data is provided in **(Figure 3.6D)**. By performing static scans at 960 cm^{-1} on test samples and controls **(Figure 3.6 A-C)** it was possible to use Raman to determine that 1000 Hz nanokicking even in the absence of the NSq-50 surface, was an ideal frequency for mineral deposition giving rise to large $Ca_{10}(PO_4)_6$ nodules; 5000 Hz also showed some mineral deposition but nodules were smaller and less distinctive. It was noted that the Raman results were corroborative with Alizarin red and Von Kossa, which gave further credence to the deposition of $Ca_{10}(PO_4)_6$ apatite through nanokicking.

These results together suggest that although nanokicking at 1000 Hz appears to provide the predominant osteoblastogenic effect, the combination with the NSq-50 surface may be optimum for osteoblast differentiation, growth and mineral deposition on a 2D geometry.

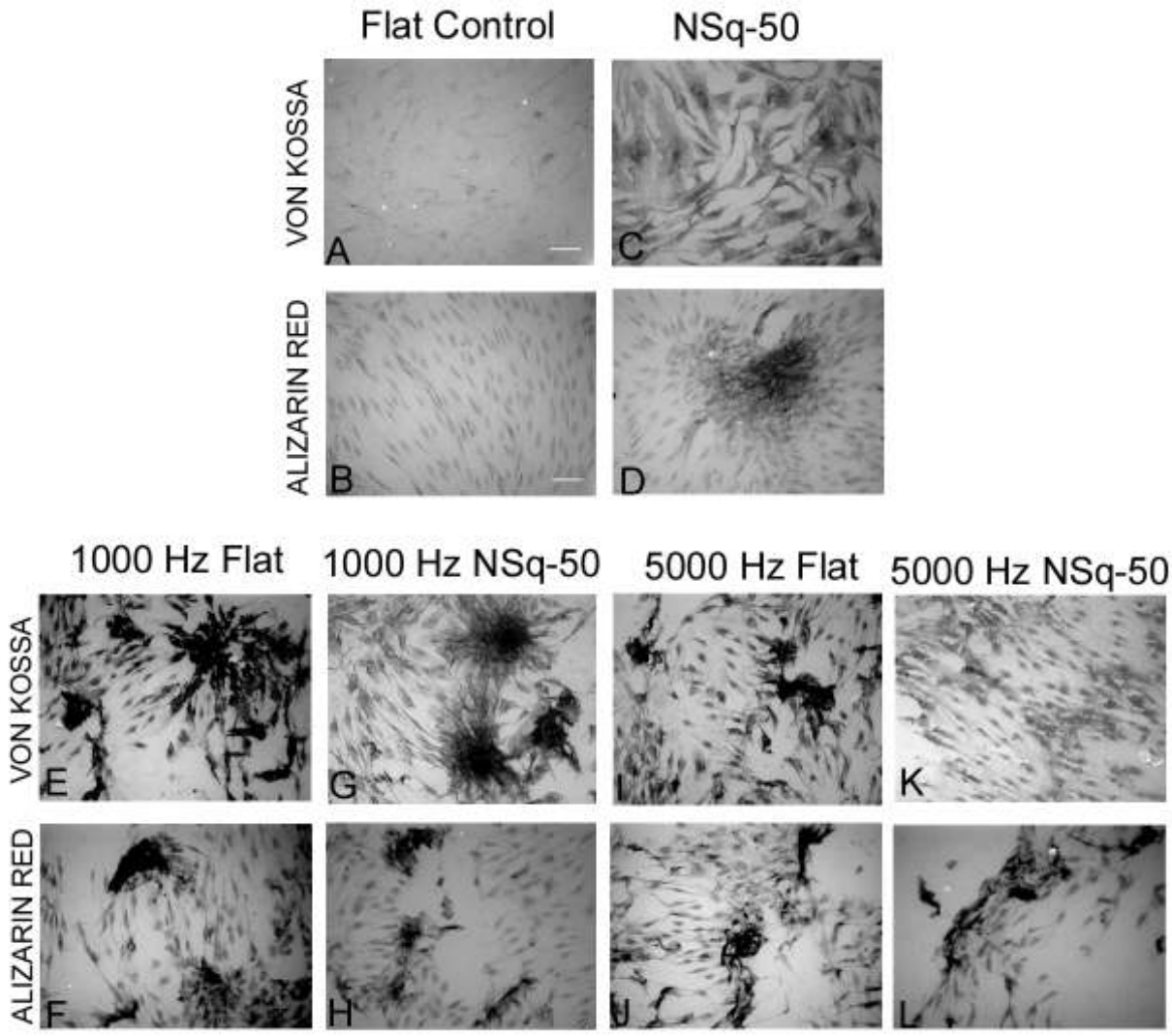

Figure 3.5: Bone mineral deposition assessment after 34 days: (A-B) MSCs grown on a blank polycarbonate surface only (negative control) showing no presence of $Ca_{10}(PO_4)_6$ nodules. (C-D) MSCs grown on an NSq-50 osteogenic surface showing an increased expression of mineralised nodules. (E-F) MSCs exposed to nanokicking at 1000 Hz on a blank polycarbonate surface, showing nodule formation. (G-H) 1000 Hz nanokicking on the NSq-50 surface showing the most distinct mineral nodule formation. (I-J) 5000 Hz nanokicking on a flat surface showing smaller nodules being formed. (K-L) MSCs exposed to nanokicking at 5000Hz on the NSq-50 surface showing evidence of nodule formation. For Von Kossa and Alizarin red stains Mag 10×, scale bar = 100 μm, N=2, same scale used for each picture. Figure used with permission from the publisher (Pemberton et al., 2015).

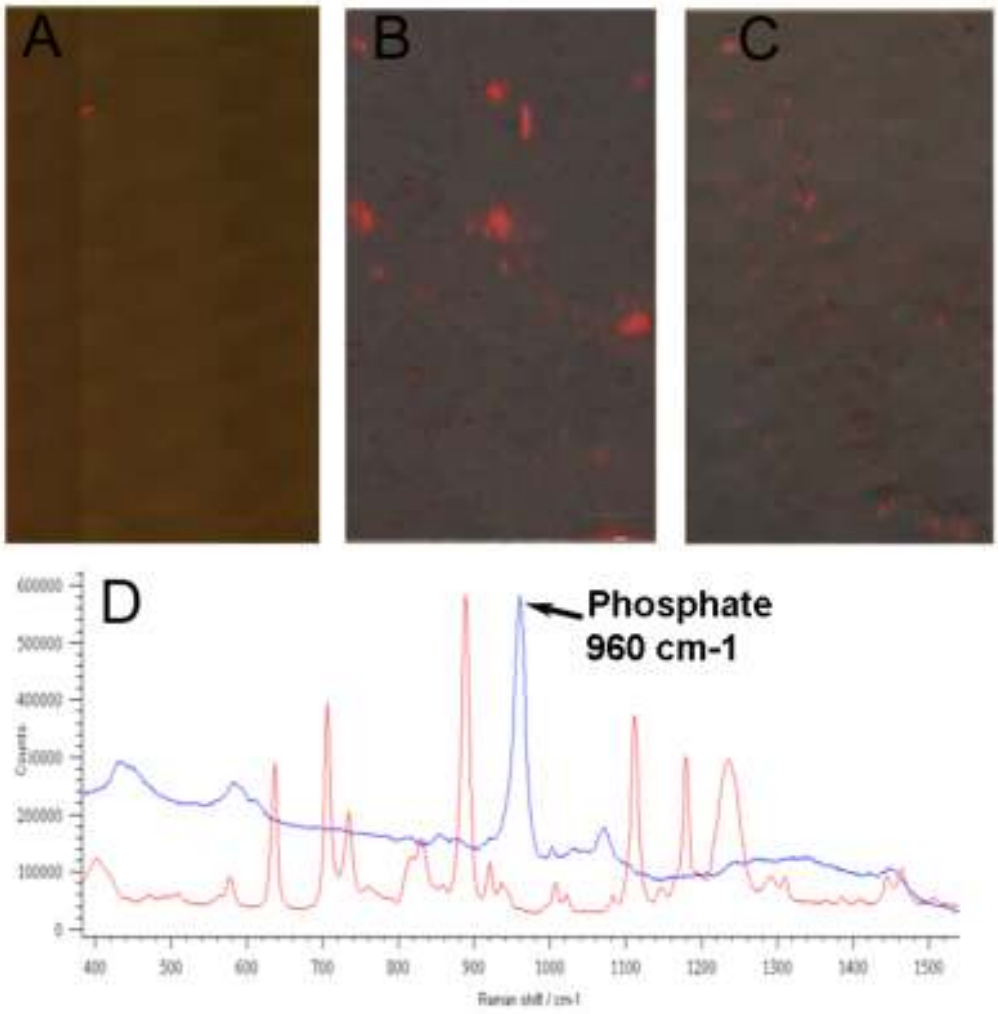

Figure 3.6: Raman visible spectroscopic scans for $Ca_{10}(PO_4)_6$ apatite mineral deposition after 27 days of nanokicking. Raman static single scan measurements with spectral acquisition at 960 cm^{-1} were taken for (A-C): (A) Scan of a blank polycarbonate surface (negative control). (B) Scan of a 1000 Hz nanokicking sample on a polycarbonate flat surface (C) Scan of 5000 Hz stimulated sample on an NSq-50 surface. Red areas show intense Raman scattering at 960 cm^{-1} indicating the presence of $Ca_{10}(PO_4)_2$ apatite. (D) the blue line shows the Raman scattering fingerprint region for bovine cortical bone with the predominant peak at 960 cm^{-1}, the red line shows the Raman scattering fingerprint region for the polycarbonate substrate with the predominant peak at 820 cm^{-1}, no over lapping of dominant peaks was observed. Due to the fact that the predominant fingerprint peak for $Ca_{10}(PO_4)_6$ was observed at 960 cm^{-1} the scans in (A), (B) and (C) were all performed at 960$cm^{-1}$to confirm the presence of calcium phosphate deposition. Note no spectra are shown due to the use of a static scan as described in the results. Figure used with permission from the publisher (Pemberton et al., 2015).

3.4 Discussion of results

The weight of gravity and constant motion while walking and running introduces mechanical stimulation at low frequency to the human skeletal system, which may be important in maintaining calcification of bone (Ahn and Grodzinsky, 2009). Conversely, astronauts exposed to a microgravity environment quickly find that their bones begin to atrophy and decalcify (Holick, 1998; Miyamoto et al., 1998). These low frequency vibrations naturally introduced to the ligaments, tendons and joints while running and the weight of the gravitational pull from the earth support the hypothesis that mechanical stimulation and weight bearing (Wolff's Law) may augment osteoblastogenesis (Chen et al., 2010; Stein and D'Ambrosia, 2008). This, in part, provided insight into a rationale to interrogate the potential of osteoblastogenesis using nanokicking vibrations. The experimental design, which has been discussed in chapter II and used here in chapter III, allows for both high frequency forces and weight to be introduced to a population of MSCs as the piezo actuator first expands or accelerates upwards and then contracts downwards (Curtis et al., 2013a).

When considering high-frequency, it is perhaps noteworthy that while bone is thought to be piezoelectric at low frequencies when dry, hydrated collagen is only piezoelectric at much higher frequencies, (Reinish and Nowick, 1975) and furthermore an electrical charge may stimulate skeletal repair and osteoblastogenesis (Goldstein et al., 2010; Noris-Suarez et al., 2007). Interestingly, Hakansson notes that one of the innate biological resonances of the protein complexes and minerals forming bone was found to be at an average of 972 Hz (Hakansson et al., 1994); it can hence be argued that this frequency is too close to one of the nanokicking frequencies we have employed (i.e. 1000 Hz) to simply be a biological coincidence.

After 7 days of mechanical stimulation, a marked increase in osteogenic related genes was observed, as the frequency was increased to 5000 Hz. The genes observed to be most up-regulated were OPN, OCN, ONN and osterix, with RUNX2 and BMP2 being less up-regulated at this time point. This osteoblastogenic genetic timeline is logical as BMP2 mediates RUNX2 (Jang et al., 2012; Kopf et al., 2012; Phimphilai et al., 2006) and RUNX2, which is a master transcription factor of osteogenesis (Gaur et al., 2005), proceeds to facilitate the increase of these later osteogenic genes like osterix (also an osteogenic transcription factor) and OCN, and is then itself down-regulated, as per the accepted transcript chronological order of osteogenesis see **(Figure 1.3)** (Stein and Lian, 1993).

It could be further argued that an increase in frequency also provides an increase in the force (through acceleration, where by force = mass of media above the cells × acceleration) being transmitted to the cells, which were adhered to the surface of the substrate. This would mean that as frequency increased the cells would, in effect 2D speaking, feel more 'gravity' and increasing gravity can be osteogenic (Holick, 1998; Miyamoto et al., 1998).

While in agreement that nanokicking was stimulatory to osteogenesis, the results at a transcript and protein level were a little out of sync. The transcriptional data indicated that nanokicking induced osteogenic gene transcription, but the response was generally not large apart from at 5000 Hz at the early time point assessed (7 days). It could be argued that this is perhaps from the extra amplitude predicted from the ANSYS modeling and tested resonant frequencies at the substrate edges at 5000 Hz, previously described in chapter 2, data provided in **(Figures 2.5 and 2.7).** It is noteworthy, that although the extra amplitude most likely caused by a resonant frequency at 5000 Hz provides a strongly positive osteogenic transcript response; due to lack of control and reproducibility of amplitude displacement, (from internal resonances), it would make consistently using a vibrational bioreactor calibrated to 5000 Hz challenging.

Perhaps surprisingly, it was observed that adding the nanotopography suppressed the nanokicking effect at this early transcriptomic time point **(Figure 3.3 A-F)**. However, protein level assessment at 21 days showed that nanokicking was more stimulatory than topography alone and that topography and nanokicking together could have an augmentative effect. This was confirmed by mineralisation assessment where topography and nanokicking both led to mature nodule formation, relative to the other conditions assessed, and the nodule formation was increased where both nanokicking and topography were used concomitantly. The protein level data and mineralisation data both also suggested that there was little extra osteogenic effect observed by using frequencies higher than 1000 Hz.

It is further interesting to note that without nanokicking, osteoinductive media and NSq-50 mostly induce OPN expression. However, whenever nanokicking is employed with or without the NSq-50 surface, OCN then assumes the most abundant expression. This could perhaps be explained by the fact that OPN, as well as aiding in binding of calcium, is also an Arg-Gly-Asp (RGD) containing glycoprotein which facilitates cellular adhesion (Bautista et

al., 1994; Zou et al., 2013). While OCN on the other hand, simply aids in bone mineralisation (Lee et al., 2007). One hypothesis is that nanokicking may potentially alter cell integrin attachments and potentially negate the need for additional RGD groups. This finding lends itself to work by Pierres *et al* demonstrating that cells vibrate on the nanoscale as they adhere; i.e. we supply the cells with nanoscale vibration and adhesion occurs via a different route compared to static samples (Pierres et al., 2008; Pierres et al., 2009). Also as an observation it is appealing that, as would be expected, proteins like OCN and OPN when immunostained were generally found around the Golgi apparatus and endoplasmic reticulum (sites of protein manufacture) before subsequently being transported to the extracellular matrix for use in mineral binding and cell attachment **(Figure 3.4 B)**. Further still it appears that ROCK/(RhoA kinase) pathway is involved and important for osteogenesis brought about through nanokicking further suggesting an adhesion dependant mechanism as the pathway can also be stimulated through the focal adhesions (Nikukar et al., 2013).

3.5 Conclusion

As would be expected from the canonical flow of biological data, an up-regulation of transcriptomics would lead to an up-regulation of proteins and subsequently a biological product, which in the case of osteogenesis would be $Ca_{10}(PO_4)_6$ deposition or the initial stages of the formation of mineralised bone (an osteon). This was the rationale used to determine if high frequency piezo vibrations (nanokicking) coupled with the also osteogenic nanotopographical surface (NSq-50) could augment the osteogenic phenotype. The data gave an affirmative result to this question and it was observed that an up-regulation of genes and proteins related to osteogenesis was determined; culminating with circular mineral $Ca_{10}(PO_4)_6$ deposits varying from 100 – 300 μm in diameter. Nano-kicking in its own right at a frequency of 1000 Hz was observed to be the most strongly osteogenic and when coupled with the NSq-50 surface also had a combined effect at the protein and most importantly at the mineralisation level. These positive data, grant confidence in the ability of high frequency vibrations resulting in nanometre level displacements, (driven by a piezo actuator) to stimulate MSCs to differentiate into osteoblastic cells, on a 2D surface.

Chapter IV: Validation of a novel nanokicking bioreactor for use with 3D collagen gels

4.1 Introduction

The work performed in chapter III, confirmed the ability of nanokicking (piezo technology) to bring about osteogenesis in 2D, and this was validated through genetic, protein and mineralisation results. Following on from this, the question was asked, could this technology i.e. nanokicking also be osteogenically inductive in 3D?

To facilitate finding an answer to this question a new reproducible and efficient bioreactor had to be developed and tested, which could harbour a 3D matrix such as collagen, in which MSCs could be grown. This would hence provide an *in vitro* /*ex vivo* bioreactor with cells grown more in line with the *in vivo* state. In the first instance it would be necessary to test and validate this new bioreactor once again, before initiating 3D osteogenic experiments.

4.2 Materials and methods

4.2.1 Materials

Note: Several of the reagents, protocols and the materials listed in chapter II were also prepared in the same fashion for chapter IV; as a result these have not been relisted in **(Table 4.1)**. Only new methods, protocols and reagents distinctive to chapter IV have been listed in **(Table 4.1)** and have been explained throughout section 4.2.

Materials and Reagents	Source / Supplier/ Prepared
Collagen Type 1 (Rats Tail) – 2.05 mg/mL	First Link UK, B/N:RTC6783, Cat: 60-30-810
10 X DMEM	First Link UK, B/N:MEM5813, Cat: 60-91-810
0.1 M NaOH	Fluka 72079-500mL, Lot: BCBL7951
Bovine serum albumin (FBS)	Fisher Scientific – BP9700-100 Lot: 61-1247
DMEM	Sigma Life Sciences, DR671, Lot:RNBD4946
Phosphorylated RUNX2 antibody – Rabbit	Abgent Cat no. Ap3559a, Lot: PS465
Laser inteferometer	SP-S, SIOS Meßtechnik GmbH, Ilmenau, Germany
Biotinylated anti-rabbit IgG (H+L)	Vector Laboratories BA-1100, Lot: W0614
Fluorescein streptavidin	Vector Laboratories SA-5001, Lot: W0408
Piezo actuator	Physik Instrumente, Karlsruhe, Germany – PL088.30
3 mm Fe_2O_3 ferrite magnets (700 gauss – 0.07T)	Magnet Expert, Tuxford, UK – F356F
6 well cell culture cluster	Corning Incorporated 3516, NY
Signal generator	Agilent, 33210A, CA
High voltage piezo driver amplifier	ENV 150, Piezosystemjena, Jena, Germany

Table 4.1: List of materials and reagents used in chapter IV

4.2.2 Setup/design of functioning novel bioreactor

As with the previous set up, an Agilent 33210A function generator served as the power source. However, to facilitate the new design a new model piezo actuator was required (PL088.30) and this meant that an amplifier (ENV 150) was also necessary for use along with the signal generator in order to give a voltage output of up to 80 V (160 V being the maximum voltage available). The continuous sinusoidal sine wave ranged between - 10 V to + 70 V, (80 V) in total and this caused 13 piezo actuators moving in unison to provide nano-displacement of the entire top platform of the new bioreactor design. The top plate of the platform was made of grade 420 magnetic stainless steel. On top of this the 6 well plate used to culture the cells had 6 x 30 mm Fe_2O_3 ferrite magnets adhered to the outside bottom (using 2 part epoxy glue – Henkel Dusseldorf, Germany). The 6 well plate was then magnetically attached to the top platform of the bioreactor.

An aluminum block served as the base of the bioreactor and facilitated the transference of the nanokicking displacements upwards instead of outward into the ambience. See **(Figure 4.3 A & C)** for the bioreactor design and setup along with **(Figure 4.3 B)** for an aerial view of the collagen gel seeded with cells in the 6 well plate, chapter IV results section.

4.2.3 Cell culture and media preparation

See section 2.3.4 page 36, for the methodology which was used to culture and feed the cells for the piezo samples. Although the cell culture preparation was the same, the duration which the experiments were carried out for was differed depending on whether it was transcriptional, protein or calcium phosphate mineralisation which was being assessed. To feed the MSCs that were cultured in the 3D collagen gels the bioreactor was carefully tilted to the side and the previous media was removed using a sterile pipette. Each individual well was then replenished with approximately 2 mL of fresh media. The media was changed every 3 – 4 days.

4.2.4 Quantitative real-time (qRT-) PCR

See section 2.3.7 of chapter II, pg 40 for the methodology and preparation steps used to harvest the cells after experimental culture, and to isolate and quantify the mRNA. **(Table 4.2)** below lists the specific gene primers which were used to perform the quantification experiments. GAPDH served as the house-keeping gene against which the relative presence of all the other genes (mRNA) listed in **(Table 4.2)** were quantified.

After 8 days of nanokicking MSCs cultured in either 6 or 24 well plates were assessed by qRT-PCR. The MSCs were harvested using trypsin and mechanical scrapping. The total RNA content was then extracted and DNase treated to remove any DNA present. For all sample conditions the RNA of three material triplicates were harvested using the Qiagen RNeasy extraction kit. The RNA content was quantified using the nanodrop system UV spectrophotometer and the levels of all samples were normalised. Following this the RNA was reverse transcribed to cDNA using the Qiagen quantiscript reverse transcription kit. The amplification of the cDNA was then carried out using the SYBR green PCR Kit.

Two frequencies (1000 Hz and 4000 Hz for both 6 and 24-well plates), with seeding performed at ~ 6,000 cells per well for the 24 well plates and ~25,000 cells per well for the 6-well plates were assessed. The plates were attached to the vibrational platform via magnets. (Note: 4 of the wells on the 24 well plate were combined to give one sample). The strength of the magnets was 0.07 T and a static magnetic field was only employed on the side of the vibrational surface i.e. not towards the cultured cells.

Given the strength of the magnets used and the setup which was employed, the weak magnetic field was expected to have negligible if any biological effect (Miyakoshi, 2006).

Note: these qRT-PCR experiments were performed in 2D as it was necessary to first perform bioequivalence testing of the new bioreactor, and confirm osteogenesis in 2D before progressing to 3D collagen gel experiments.

Gene	Forward Primer	Reverse Primer
GAPDH	TCAAGGCTGAGAACGGGAA	TGGGTGGCAGTGATGGCA
Alkaline Phosphatase	ATGAAGGAAAAGCCAAGCAG	CCACCAAATGTGAAGACGTG
RUNX2	GGTCAGATGCAGGCGGCCC	TACGTGTGGTAGCGCGTGGC
Osterix	GGCAAAGCAGGCACAAAGAAG	AATGAGTGGGAAAAGGGAGGG
Osteonectin	AGAATGAGAAGCGCCTGGAG	CTGCCAGTGTACAGGGAAGA
Osteocalcin	CAGCGAGGTAGTGAAGAGACC	TCTGGAGTTTATTTGGGAGCAG
PTK2	GTCTGCCTTCGCTTCACG	GCCGAGATCATGCCACTC
MAP2K1	TTTTAGGAAAAGTTAGCATTGCTGT	AGGGCTTGACATCTCTGTGC
MAP2K2	ACCAAAGTCCAGCACAGACC	ATGATCTGGTTCCGGATGG
ERK1	CCCTAGCCCAGACAGACATC	GCACAGTGTCCATTTTCTAACAGT
ERK2	TCTGCACCGTGACCTCAA	GCCAGGCCAAAGTCACAG

Table 4.2: Sequence for the qRT-PCR gene primers used.

4.2.5 Immunofluorescence procedure

- After 3 days piezo stimulation at 1000 Hz, the cells were rinsed with 1 x PBS wash buffer.
- A solution of 38% formaldehyde was then used to fix the MSCs inside the 6 well plate. This was performed at 4˚C for 5 minutes.
- Permeablising buffer was used to permealise the cells, and the wells were submerged and incubated at 37˚C for 5 minutes.
- PBS/1%BSA was used as a blocking agent and the wells were first incubated in the blocking buffer for 5 minutes at 37˚C. The solution was removed and a primary antibody, rabbit, specific to phosphorylated RUNX2 was added, the samples were incubated at 37˚C for 1.5 hrs.

- The primary antibody was then removed and the samples were washed for 3 x 5 minutes using the wash buffer (1 x PBS). The final wash was performed with agitation on a shaker.
- The secondary antibody, biotinylated anti-rabbit, was then added and the samples were incubated at 37˚C for 1 hour.
- The secondary antibody was removed and the samples were once again washed for 3 x 5 minutes using wash buffer, with the last wash being performed with agitation.
- The wash buffer was removed and tertiary complex, fluorescein streptadivin, was added. The samples were then wrapped in foil and incubated at 4˚C for 30 minutes.
- The tertiary complex was removed and the same wash procedure was once again undergone.
- Following on from this, a small drop of vectroshield-DAPI (to stain the nucleus) was added to the sample and a microscope coverslip was placed into the well.
- Microscopy was performed using an Axiophot-Zeiss, Germany.

4.2.6 Preparation of collagen gels

Collagen gels were prepared by adding collagen, which was acidic in nature, to 0.1 M NaOH in order to perform an acid base (phenol red indicator) titration. The change of pH towards a neutral level, caused self assembly or 3D rearrangement of the collagen structure to become more branched and cross linked in nature (Pogorelov and Selezneva, 2010). The gels were prepared by keeping a constant ratio between all reagents which would be used. This was as follows:

- Collagen - 40% total volume
- FBS – 8% total volume
- 10 X DMEM – 8% total volume
- Cells in media (basal media) – 8% total volume (A predetermined amount of cells (100,000 or 200,000 per well in a 6 well plate) was prepared by trypsinisation and counting using a hemocytometer. The cells were then resuspended in basal media.
- 0.1% NaOH - ~ 36% total volume

In the first instance the FBS, collagen and 10 X DMEM were added together and kept on ice. The cells in media were then added to the solution while being kept on ice. Following this the 0.1% NaOH was added, quickly at first and then drop wise, while stirring the solution until a permanent pink colour was observed. While kept on ice the gels were then added to the predefined 6 well plates which were used for the experiment. The gels were then quickly transferred to an incubator and allowed to set as increasing temperature further caused self assembly of the collagen 3D matrix. Four hours were allowed to elapse until nanokicking was initiated and the following day ~ 2 mL of fresh media was added to each well.

4.2.7 Laser vibrometry and nanokicking 3D characterisation

Laser interferometric vibrometry was again used to characterise the novel bioreactor with collagen gels used as a medium in which cells could be grown in 3D. See section 2.3.5, for an explanation of the laser vibrometer set up and use.

The aim of the new bioreactor set up was to enable the transference of the nanoscale vibrational stimulation from the piezo actuator through collagen gels in a 6 well plate. The collagen gels were rigid enough to allow a thin sheet of silica mirror to be placed on top of the gel. The laser from the interferometer could then be reflected from the top of the activated bioreactor to determine if the piezo driven nanoscale excursions could be permeated through the gels, and subsequently if the MSCs cultured within the gels in 3D, could also be stimulated by the nanokicking vertical vibrations. To assess this, and to concurrently characterise the novel 3D bioreactor system, two gel fills were determined; i.e. 2.5 mL and 5.0 mL and the nanoscale displacements were measured at the centre and at the corners of individual wells, within the 6 well plate.

The measurements were assessed (and the 3D bioreactor hence calibrated) at the varying voltages of 16, 32, 48, 64 and 80 V, and at the varying frequencies of 500, 1000, 2000, 3000 and 4000 Hz to determine if the 3D gel displacements were linear and consistent. A cell population of 100,000 cells per each well was used for the 2.5 mL collagen gel fill and 200,000 cells for the 5.0 mL collagen gel fill. The analyses were performed in triplicate with different wells being assessed. The assessment was performed at varying frequencies from 500 to 4000 Hz, determining both the centre and edge mean displacements for both the 2.5 and 5.0 mL collagen gel fills.

The nanometre displacements were taken at varying frequencies from 500 Hz to 4000 Hz but the amplitude was measured at 80 V. 80 V was the amplitude used for 3D piezo vibrational stimulation.

4.3 Results

4.3.1 Bioequivalence – The confirmation of nanokicking induced osteogenesis by the new platform in 2D

The first experiments on the new bioreactor were to determine if it in fact was able to induce osteogenesis in MSCs in 2D, and what's more to investigate what the optimum condition to do this was; i.e. would it be with use of a 6 well plate or a 24 well plate and would it be at 1000 Hz or 4000 Hz. To gain an answer to this question, in the first instance the technique of qRT-PCR was employed to assess any potential change in osteogenic transcripts between different sample sets of nanokicked samples and controls.

Nanokicking was performed for 8 days, and mRNA from unstimulated controls was used to assess the prevalence of the increase in osteogenic genes through the high frequency vibrations. So as to maintain consistency through the experiment and reduce variability the controls were also cultured with magnets beneath the plates, but were not stimulated by nanokicking.

The four osteogenic genes assessed included osterix, ALKP, OCN and ONN. At 1000 Hz in a 6 well plate all four genes were increased, with the gene ALKP encoding for alkaline phosphatease and the bone gamma carboxyglutamate protein (BGLAP) i.e. the gene coding for OCN showing significance relative to the controls, **(Figure 4.1 A)**. 1000 Hz vibration with a 6-well plate and 4000 Hz vibration with a 24 well plate respectively provided the best results, and incidentally these conditions are also most in line with the up-regualtion of the genes related to the ERK/MAPK pathway, **(Figure 4.2 A)**, and hence it is deemed will provide the most reproducible biological results. OCN is secreted mainly by osteoblasts and OCN is solely involved in bone mineralisation (Lee et al., 2007), which supports the prevalence of osteoblast differentiation using this vibrational bioreactor. Note both the 6 and 24 well plate experiments used the 30 mm diameter magnet in order to observe if one magnet type could be used with various plates. This may have also affected the results observed while using the 24 well plate.

On the contrary, the MSCs cultured in a 24 well plate with a 1000 Hz vibration, showed almost no up-regulation of the same osteogenic genes and the MSCs cultured at 4000 Hz with the 6-well plate provided a less consistent stimulation of these genes, albeit significant only ONN and ALKP were observed to be up-regulated out of the 4 genes assessed.

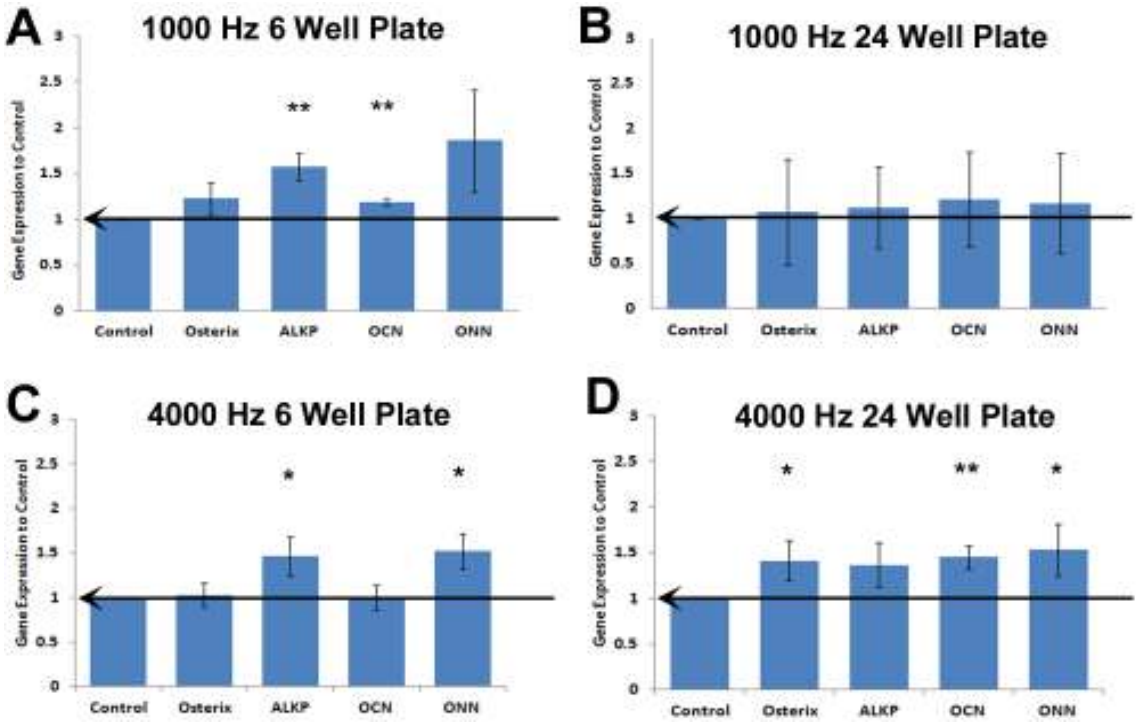

Figure 4.1: qRT-PCR for mRNA gene expression – Transcriptional Analysis. MSCs were nanokicked on the vibrational bioreactor for 8 days. (A) The MSCs were nanokicked at a frequency of 1000 Hz in a 6-well plate, (B) The MSCs were nanokicked at 1000 Hz in a 24 well plate, (C) The MSCs were nanokicked at 4000 Hz in a 6-well plate, (D) The MSCs were nanokicked at 4000 Hz in a 24 well plate. The subsequent gene expression of osterix, ALKP, osteocalcin and osteonection were assessed relative to an unstimulated control. All experiments were carried out at an amplitude of 80 V with a 22 nm vertical displacement. N = 3, results are mean ± standard deviation *$p < 0.05$ and **$p < 0.01$ by unpaired T-Test.

4.3.2 Biological mechanism of nanokicking induced osteogenesis

It was noteworthy to understand to some extent, how or by which mechanism nanokicked linked osteogenesis would occur. Although there undoubtedly are other pathways, it was believed that ERK/MAPK pathway would be critical.

After 8 days of nanokicking at 1000 Hz and 4000 Hz with cells seeded in a 6 and 24-well plate; qRT-PCR was used to determine the levels of the gene PTK2 encoding for focal adhesion kinase (FAK) relative to an unstimulated control and this was found to increase. Following the mechanistic cascade; other genes along the ERK/MAPK pathway including extracellular signal regulated kinases (ERK 1 and 2) showed an elevated expression. The activities of ERKs are linked to mitogen activated protein kinases (MAPKs) and subsequently, MAP2K1 and MAP2K2 were also observed to be up-regulated with MAP2K1 showing a significant increase in **(Figure 4.2 A)**, i.e. the stimulation of MSCs in a 6 well plate at 1000 Hz.

A downstream effector of this mechanistic cascade; i.e. the activated protein form of the osteogenic transcription factor phosphorylated RUNX2 (pRUNX2) was assessed by immunostaining, and unsurprisingly this too showed up-regulation after 3 days of nanokicking in a 6-well plate at 1000 Hz. **(Figure 4.2 I)** clearly showed the greatest increase being in or around the nucleus of the nanokicked MSCs.

The samples cultured at 4000 Hz in a 6 well plate and 4000 Hz in a 24 well plate showed only a negligible increase in the genes assessed related to the ERK/MAPK pathway and it was clear that this frequency was not MAPK inductive at the transcriptional level. The MSCs cultured at 1000 Hz in a 24 well plate also showed an equivalent increase of these genes relative to the samples at 1000 Hz in a 6 well plate, however, the standard deviations between the samples was much larger which meant less reproducible results **(Figure 4. 2 B)**. Of importance was the fact that the MSCs cultured at these conditions (1000 Hz in a 24 well plate), and assessed for osteogenesis showed almost no increase of any of the genes related to osteogenesis, **(Figure 4.1 B)**, i.e. at this condition (1000 Hz with a 24 well plate) a genetic up-regulation of MAPK and osteogenesis did not correlate.

On the contrary however, as was the case above with the osteogenic related genes, the results in **(Figure 4.2 A)** showed that the ideal condition for the increased expression of the

MEK/MAPK transcriptomics was from MSCs stimulated in a 6-well plate at a frequency 1000 Hz, i.e. the condition of 1000 Hz in a 6 well plate provided concurrent MAPK and osteogenic up-regulation confirming this to be the optimum condition.

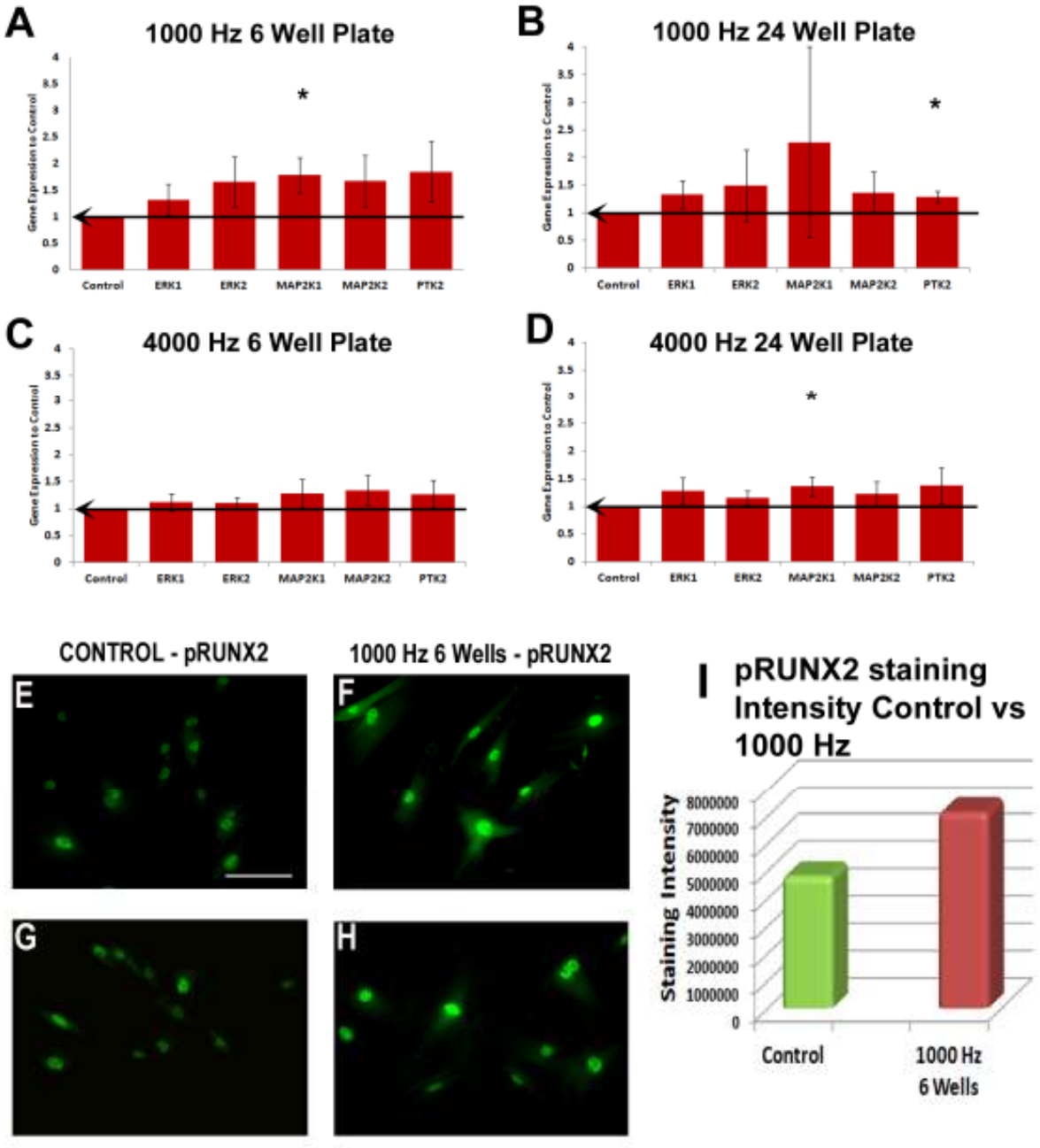

Figure 4.2: qRT-PCR for mRNA gene expression - Transcriptional Analysis. MSCs were nanokicked on the vibrational bioreactor for 8 days. (A) The MSCs were nanokicked at a frequency of 1000 Hz in a 6-well plate, (B) The MSCs were nanokicked at 1000 Hz in a 24

well plate, (C) The MSCs were nanokicked at 4000 Hz in a 6-well plate, (D) The MSCs were nanokicked at 4000 Hz in a 24 well plate. The expression of genes related to the, ERK/MAPK pathway, believed to be pivotal for mechanotransductive initiated osteoblastogenesis brought about through nanokicking; i.e. PTK2 (coding for FAK), ERK 1 and 2, MAP2K1 and MAP2K2, were assessed relative to an unstimulated control. All experiments were carried out at an amplitude of 80 V with a 22 nm vertical displacement. N = 3, results are mean ± standard deviation *$p < 0.05$ by unpaired t-test. (E & G): Immunostaining for phosphorylated RUNX2 for controls T1 and T2 after 3 days, showing unstimulated or basal levels of protein expression of phosphorylated RUNX2, (F & H) Immunsotaining for phosphorylated RUNX2 for nanokicked samples stimulated at 1000 Hz in a 6-well plate, T1 and T2 showing an increased expression of phosphorulated RUNX2 caused by high frequency nanokicking, Mag 20×, scale bar =100 μm. Fixed cells were stained for pRUNX2 (green), N = 2. (I) The subsequent quantitative representation of pRUNX2 immunostaining intensities, 1000 Hz piezo stimulated in a 6-well plate relative to the control with no stimulation, N=2.

4.3.3 Characterization of the new vibrational bioreactor using 3D collagen gel as an extracellular matrix

The parameter setting results for the new bioreactor performed in 2D showed that the optimal osteogenic condition for the bioreactor was at 1000 Hz using a 6 well plate. As a result of this the next set of experiments involved characterising the collagen gel with nanokicking using those conditions. The bioreactor and interferometer were set up as described in section 4.2.2 and **(Figure 4.3 A-C)**.

Collagen gel fills at 2.5 ml and 5.0 mL were compared using intereformetry to determine the level of displacement in a vertical direction. The data showed that when assessing 500, 1000, 2000, 3000 and 4000 Hz against amplitudes of 16, 32, 48, 64 and 80 V the nanolevel displacements were, in fact, linear for both 2.5 mL and 5.0 mL gel fills at each of these frequencies.

At 1000 Hz the 5 mL gel fill gave displacements which were on average 1/3rd that of the 2.5 mL gell fills. The maximum amplitude of 80 V providing a displacement of 5 nm for the 5 mL collagen samples and 15 nm for the 2.5 ml collagen samples. Average displacement were observed at approximately 3 nm and 1 nm, for 2.5 and 5.0 ml collagen gel fills respectively at the lowest amplitude of 16 V **(Figure 4.4 A & B).**

In order to understand the uniformity of the displacement across the entire surface of a well, interferometric measurements were taken at the centre and also at the edge of the gels for both 2.5 mL and 5.0 ml samples. The data gave evidence that any change between the centre and edges at the 1000 Hz frequency was negligible. At 80 V the 2.5 ml gels gave a displacement of approximately 15 nm **(Figure 4.5 C&D)** at both the centre and edges and this was the case when the mean data from both the edges and centre samples were combined, see **(Figure 4.5 A)**. The 5.0 mL gels gave a displacement at approximately 5.0 nm at 80 V for both the individual mean centre and edge values **(Figure 4.5 E&F)** and also approximately 5.0 nm for the centre and edge mean combined results **(Figure 4.5 B)**.

It is noteworthy that at the frequency of 3000 Hz a change in displacement was observed between the centre and edges, at both 2.5 and 5.0 mL gel fills with the edges showing an increased displacement with large SD, albeit the 5.0 mL edge displacements showed more variance than the 2.5 mL gel fill, see **(Figure 4.5 A-F)**.

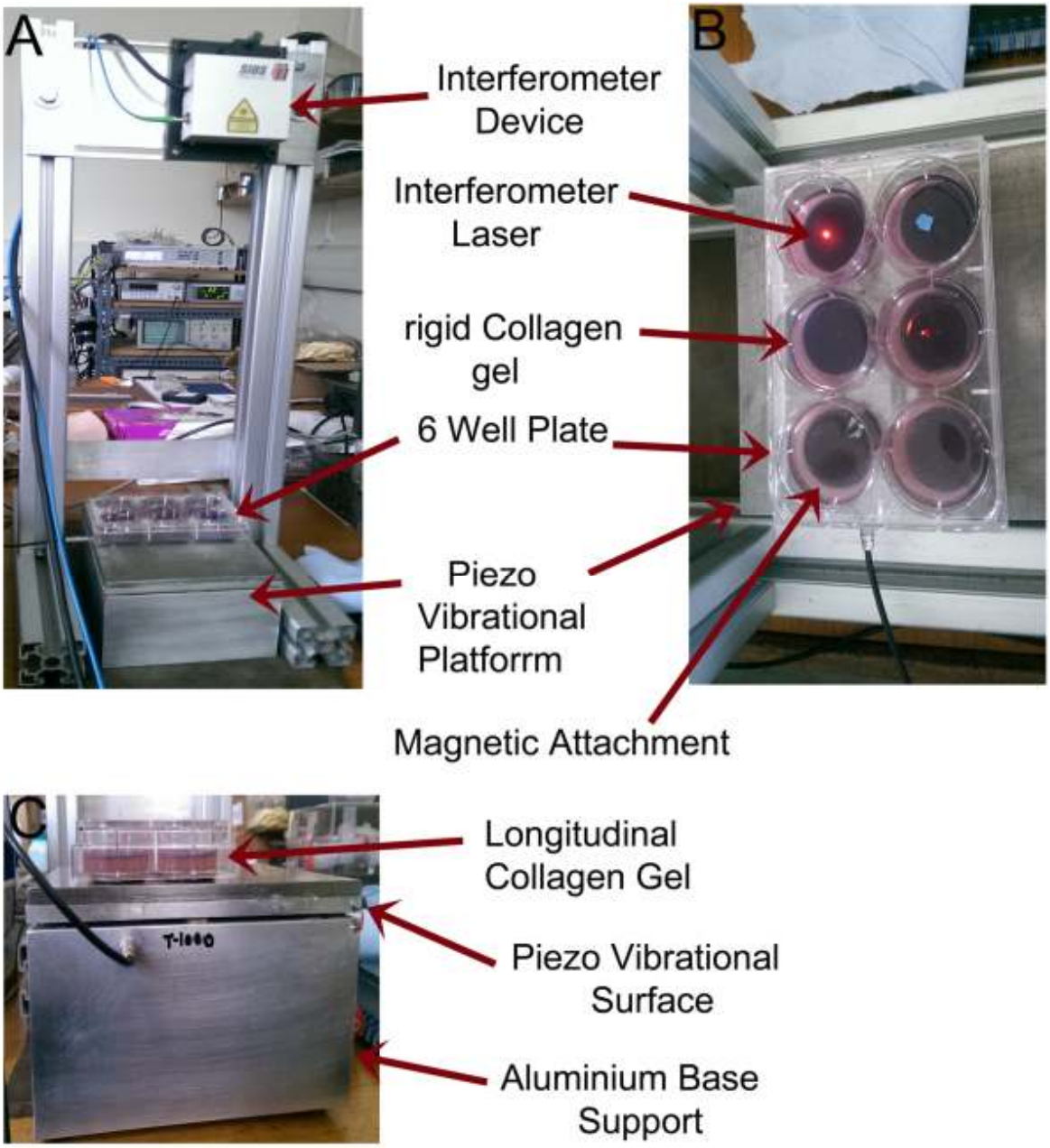

Figure 4.3: The nanokicking 3D collagen gel bioreactor (A) bioreactor set up for interferometric measurement, (B) aerial view of the 3D bioreactor showing the collagen gels set in a 6 well plate with the interferometric laser being shone over the gels for measurement, a silica mirror is used to reflect the laser for measurement, note: magnets were adhered to the outside of the 6 well plate to magnetically attach the 6 well plate to the surface, (C) cross sectional view of the 3D bioreactor showing the 6 well plate with 5 mL collagen gel fill, on top of the vibrational platform.

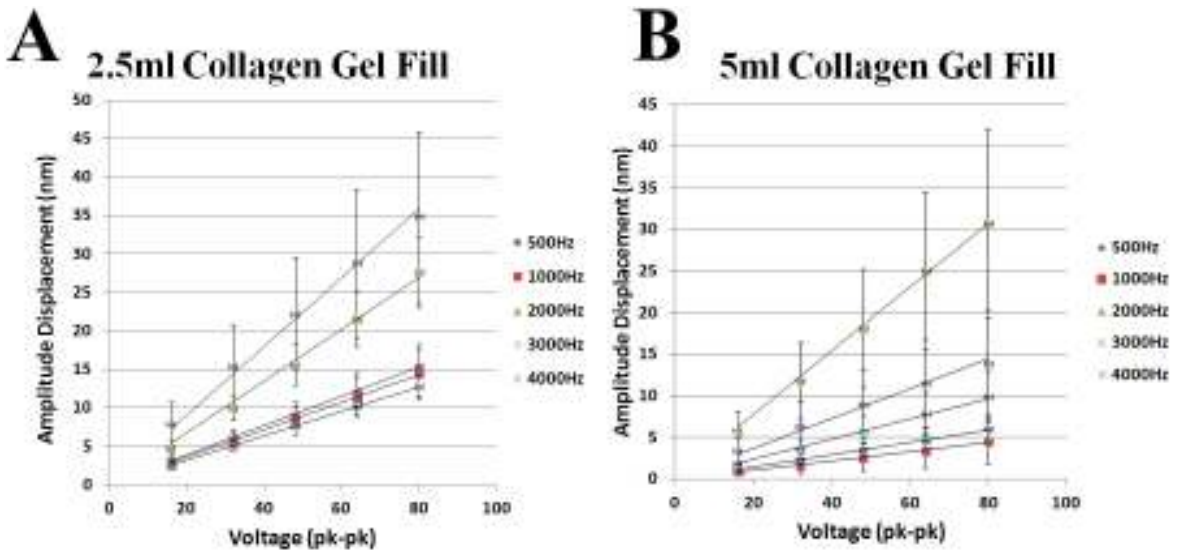

Figure 4.4: Summary collagen gel (centre and edges) interferometric measurements showing change in displacement (nm) relative to voltage at a particular frequency. (A) assessment performed on a 2.5 ml collagen gel fill (B) assessment performed on a 5 mL collagen gel fill. N = 6 piezo actuators (3 edge and 3 centre piezo actuators with 5 measurements for each piezo actuators). Frequencies assessed were 500, 1000, 2000 and 4000 Hz and mean measurements appeared to be linear across voltages measured i.e. 16, 32, 48, 64, and 80 V. 5 ml gel fills = 200000 MG-63 cells and 2.5 ml gel fills = 100000 MG-63 cells.

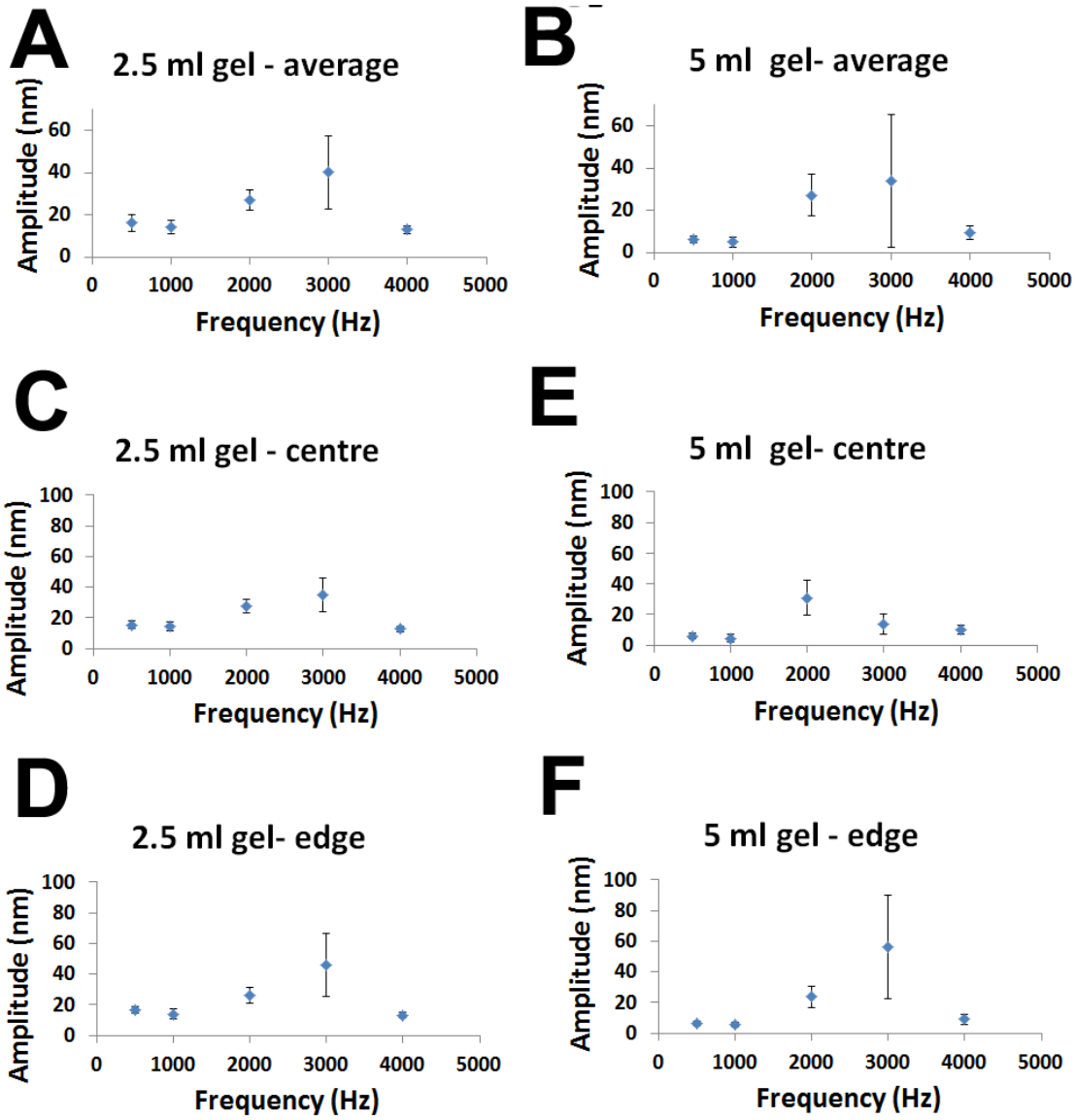

Figure 4.5: Collagen gel interferometric measurements for the 3D bioreactor, displacments were measured in 6 well plates (A) Summary of the edges and centre displacement in nm for a 2.5 mL gel fill (B) Summary of the edges and centre displacement in nm for a 5 mL gel fill. (C) 2.5 mL gel fill meansurements for centre only. (D) 2.5 mL gel fill measurements for edges only. (E) 5 mL gel fill measurement for centre only (F) 5 mL gel fill measurement for edges only. Voltage used was 80 V, Frequencies assessed were 500, 1000, 2000 and 4000 Hz. N = 6 piezo actuators for A-B, and N = 3 piezo actuators for C – F, with 5 measurements for each actuator, 5 mL gel fills = 200000 MG-63 cells and 2.5 mL gel fill = 100000 MG-63 cells.

4.4 Discussion of Results

The biological data from the parameter or specification setting experiments suggested that efficient and reproducible osteoblastic differentiation of MSCs occurred best using a 6-well plate at a frequency of 1000 Hz. This was confirmed through the 2D bioequivalence experiments, which proved that the previous and new bioreactor designs were osteogenically comparable. See Chapter II section 2.3.3, **(Figure 2.2)** for the previous design and characterisation of the bioreactor and **(Figure 4.3 C)** for the new design.

The interferometric data provided in **(Figure 4.4)** and **(Figure 4.5)** proves that having a magnet placed under each well relays a consistent uniform displacement mechanotransductively, which can then be biologically interpreted by the cultured cells as a cue for differentiation. This is not only confirmed by the osteogenic transcript data but also by the ERK/MAPK transcript data, which correlates well providing further confidence (Celil and Campbell, 2005; Zhu et al., 2012a). The fact that we have observed an increase in all the genes investigated related to the ERK/MAPK pathway, **(Figure 4.2 A)** at a transcriptomic level is reassuring, especially when the true biological expression of the ERK/MAPK pathway is observed at the protein level after post translation modification, primarily due to phosphorylation (Burack and Sturgill, 1997).

The mitogen activated protein kinase pathway is very important for cell division and hence proliferation, but here it appears that the downstream effector of this pathway is an up-regulation of pRUNX2 and hence osteogenic differentiation. This useful data provides us with not only a proof of concept for nanokicking induced osteogenesis, but we also begin to gain a preliminary understanding of a potential mechanism. It is worth stating however, that other mechanisms too such as the ROCK/RhoA pathway have also appeared to be fundamental (Xiao et al., 2002) (Nikukar et al., 2013).

Interestingly, the increase in intensity of the pRUNX2 at the protein level was observed at 3 days to be strongly centred around the nucleus of the cells. This too is logical as one would expect a transcription factor to be located near and around the nucleus, where it can facilitate promotion of the cells genetic machinery. This would cause a further up-regulation of other bone specific genes such as osterix and OCN, which is important for the binding and deposition of calcium and hence hydroxyapitite mineralisation (Lee et al., 2007).

The characterisation of the collagen gels with the new setup showed that the 5 mL gel fill had a displacement at 1/3rd that of the 2.5 mL gel fill, no doubt due to the increased height of the gels absorbing and dissipating the effect of nanokicking. This data guides the use of the new bioreactor towards the 2.5 mL collagen gel fill for 3D experiments, as the inteferometry shows this would still give a displacement at 1000 Hz equivalent of 15 nm **(Figure 4.5)**.

The unusually high displacements observed at 3000 Hz and 2000 Hz for the 2.5 mL and 5 mL gel fills could be attributed to innate resonances for the bioreactor. While this may provide an extra-vibrational effect it is believed that this would limit control and reproducibility in future piezo osteogenic experiments, hence is was decided that these frequency although perhaps strongly osteogenic would be inconsistent and provide limited control, an aspect that would not be tolerated under GMP conditions.

4.5 Conclusion

Through the use of interferometry, transcriptional and protein profiling related to osteogenesis in this chapter, I have confirmed the osteogenic capability of a novel bioreactor in 2D. What's more I have also confirmed that these sinusoidal waves can be transmitted through a collagen gel matrix to the surface providing evidence that 3D cultured MSCs would be exposed to this stimulation.

The bioreactor has been calibrated to 1000 Hz and 80 V, with a 3D collagen gel fill of 2.5 mL. This protocol will subsequently deliver a vertical displacement in the region of 15 nm. The next steps are now to assess this bioreactor *in situ*, cultured with MSCs in the 3D collagen matrix. This will be more closely aligned to their *in vivo* innate environment (*ex vivo*). The possibility of the differentiation of osteoblasts, and hence the formation of mineral deposits will be determined, i.e. if it is feasible to use this bioreactor to artificially engineer, in 3D, autologous human osteoblasts and calcium phosphate mineral deposits.

Chapter V: Osteogenesis in collagen gels by nanokicking using the 3D bioreactor

5.1 Introduction

The majority of the research related to regenerative medicine to date has centred on 2D culture experimentation, and although granting great insight, for the most part this research has been limited to cell engineering (Biggs et al., 2009; Huang et al., 2013; Peytour et al., 2013). It is evident that in order to truly harness the full potential of stem cells and to artificially grow and engineer tissue or organs, a knowledge and understanding of 3D culture is required (Petersen et al., 2010; Uygun et al., 2010). Classical osseous engineering attempts have utilised a source of osteogenic cells, a matrix material and the use of growth factors and osteogenic differentiation media such as dexamethasone and BMP-2 or other members of the transforming growth factor beta (TGF-β) superfamily (Xie and Han, 1996). When it comes to efforts made in the use of osseous bioreactors; maintenance of long term sterility, cost and difficulty operating present perfusion, spinner and rotating designs, as well as difficulties in clinical implementation have meant so far success in skeletal regenerative medicine has been limited (Laffosse et al., 2010; Langer et al., 2009; Rauh et al., 2011b). As a result, autografts and allografts, despite often being inadequate, have remained the best treatment available to clinicians.

It is of benefit to appropriate biomimetics in a potential matrix which can assume the physiological or mechanical characteristics of the *in vivo* natural state. In research into osteogenesis, be it endochondral or intramembranous bone formation, MSCs take a central role due to their mesodermal differentiation potential (Caplan, 1991; De Ugarte et al., 2003a). In bone tissue engineering the use of scaffolds or matrices which are osteoinductive or osteoconducive is the goal of biomimetics. To induce osteogenesis in 3D using MSCs an excellent matrix scaffold choice has been found to be Type I collagen (COL I). As far as osteo-biomimetics it is uniquely placed as greater than 90% of the organic composition of bone is made up of COL I. What's more like fibronectin, COL I also possesses the RGD (arginine-glycine-aspartic acid) adhesion sequence recognised by cell integrins, aiding not just cell attachment and migration but also proliferation. Further still an increased expression of mRNA and proteins related to OCN, OPN, ONN and COL I are almost a definitive indication of MSCs commitment to form osteoblasts. In particular OCN is directly regulated by the master transcription factor RUNX2, and is osteoblast specific, being secreted for calcium binding and deposition in bone modelling (and re-modelling in tandem with osteoclasts) (Lee et al., 2007; Weinreb et al., 1990).

Previously, it has been proven throughout this thesis and also published (Nikukar et al., 2013), that by mechanotransduction, nanokicking – i.e. high frequency low amplitude (nm scale) sinusoidal displacements can induce MSCs on a 2D surface to differentiate into osteoblasts. However, due to the limitations of 2D culture this work has been restricted to the development of an osteoblastic bioreactor. Collagen, as a 3D biomimetic matrix, has the potential to move towards bone tissue engineering. Interestingly, Sumanasinghe et al have researched the effect of uniaxial cyclic tensile (mechanical) strain on MSCs in a collagen construct and have found this to induce osteogenesis (Sumanasinghe et al., 2006). In line with this premise further work has shown that spontaneous osteogensis of MSCs cultured in a COL I matrix can also be achieved by simply altering the cytoskeletal tension of the gel (Kon et al., 2009). Also of note, very recent research has been performed using scaffolds composed of nanoparticulate mineralised collagen glycosaminoglycan, which was found to be osteogenic in its own right without the requirement of BMP-2 compared to controls. The success of this scaffold appeared to be in harmonising the combination of both the organic as well as the inorganic counterparts of bone (Ren et al., 2015).

In this chapter it is hypothesised that nanokicking MSCs cultured in a 3D collagen extracellular matrix, can *in vitro,* grow calcium phosphate ($Ca_{10}(PO_4)_6$) hydroxyapatite nodules *in situ*. These MSCs have been deliberately cultured without the addition of soluble factors or osteogenic chemical stimulation to singularly assess the osteogenic potential of nanokicking. This was achieved by engineering the novel vibrational osseous bioreactor already discussed in chapter IV. To interrogate this theory cultured MSCs were nanokicked and assessed at a genetic, protein and quantitative mineralisation levels relative to unstimulated controls (MSCs cultured in a collagen matrix which were not nanokicked).

5.2 Materials and methods

5.2.1 Materials

Materials and Reagents	Source / Supplier
Human mesenchymal stem cells, from bone marrow	Promocell GmBH, Germany
Collagen Type 1 (Rats Tail) – 2.05 mg/mL	First Link UK, B/N:RTC6783, Cat: 60-30-810
10 X DMEM	First Link UK, B/N:MEM5813, Cat: 60-91-810
0.1 M NaOH	Fluka 72079-500mL, Lot: BCBL7951
Bovine serum albumin (FBS)	Fisher Scientific – BP9700-100 Lot: 61-1247
Osteocalcin mouse monoclonal IgG antibody	Santa Cruz Biotechnology, ABOC-5201, Lot: G3014
Osteopontin mouse monoclonal IgG antibody	Santa Cruz Biotechnology, AKM2A1 Lot:G1613 -
GAPDH rabbit monoclonal antibody	Abcam, ab128915, LotGR179384-1
anti-mouse IRDye 680 CW	LI-COR 926-68077
anti-rabbit IRDye 800 CW	LI-COR 926-32213
Rnase free water	Qiagen, UK
Quantitech reverse transcriptase kit	Qiagen, UK
Spectrophotometer	Nanodrop ND-1000
7500 Real time PCR system	Applied Biosystems – S/N:275007079
Trizol	Life Technologies 15596-026
Chloroform	Sigma Aldrich 288306-100ML
Triton X-100	Sigma S/N:T-9284
Tween 20	Sigma Aldrich P9416-100mL
Permeability buffer	Centre for Cell Engineering, University of Glasgow
6 Well Cell Culture Cluster	Corning Incorporated 3516, NY
3 mm Fe_2O_3 ferrite magnets (700 gauss – 0.07T)	Magnet Expert, Tuxford, UK – F356F
Piezo Actuator	Physik Instrumente, Karlsruhe, Germany – PL088.30
Signal generator	Agilent 33210A
High Voltage Piezo Driver Amplifier	ENV 150, Piezosystemjena, Jena, Germany
Laser Interferometer Vibrometer	SIOS Meβtechnik GmBH Germany SP-S120

Table 5.1: Table of materials and reagents used for Chapter V

5.2.2 Quantitative Real-Time (qRT-) PCR

5.2.2.1 Trizol collagen gel extraction

- In order to extract the collagen matrix from the samples trizol was utilised and this extraction was carried out inside the fume hood. 1 mL of trizol reagent was added to each sample.
- The sample was then incubated at room temperature for 10 minutes to allow cell and matrix lysis. The samples were then centrifuged at 12000 g for 15 mins at 4°C.
- The supernatant was then transferred to a fresh Eppendorf tube to which was added 200 µL chloroform.
- Following this the samples were shaken vigorously stirred for 20 seconds and left to incubate at room temperature for 3 mins.
- The sample was then spun again at 12000 G for 15 mins at 4°C.

  The upper aqueous phase was then transferred to a clean Eppendorf tube, this volume was equivalent to 500-550 µL. This was done without disturbing the aqueous/organic interface.

Note: Now that the analyte (RNA) was in the aqueous phase the remainder of the qRT-PCR experimentation was carried out as outlined in Chapter II, section 2.3.7.2 – 2.3.7.5.

Gene Name	Forward Primer	Reverse Primer
GAPDH	TCAAGGCTGAGAACGGGAA	TGGGTGGCAGTGATGGCA
ONN	AGAATGAGAAGCGCCTGGAG	CTGCCAGTGTACAGGGAAGA
OPN	AGCTGGATGACCAGAGTGCT	TGAAATTCATGGCTGTGGAA
OCN	CAGCGAGGTAGTGAAGAGACC	TCTGGAGTTTATTTGGGAGCAG

Table 5.2: Sequence of gene primers used to perform qRT-PCR.

5.2.3 Rheology

Assessment of the physio-elastic properties of the collagen matrix was performed by carrying out dynamic frequency sweep experimentation. These frequency sweeps were performed by using a strain-controlled rheometer (Kinexus rotational rheometer system- Malvern). The parallel-plate used to perform the frequency sweep had a 20 mm diameter with a 0.25 mm gap. An integrated thermostat mechanism was used to maintain the sample temperature at 25°C. In order to keep the sample hydrated and prevent drying out through evaporation the internal atmosphere was kept saturated through the use of a solvent trap. An amplitude sweep was carried out and this confirmed no variation in elastic modulus (G′) and viscous modulus (G″). The amplitude sweep was performed up to a strain of 1% and these measurements were taken in a linear viscoelastic regime. The collagen matrix dynamic modulus was measured as a frequency function with a frequency range from 1 to 100 Hz. To ensure reproducibility all measurements per sample were performed in triplicates.

5.2.4 Raman spectroscopy

The 3D collagen gel matrix samples were nanokicked for 46 days, were partially dried and were directly assessed by Raman spectroscopy without further sample preparation. A Renishaw InVia Raman spectrometer with a 785 nm line focus laser was used to perform near IR spectroscopic scans. A reference standard of bovine cortical bone was used to assess the predominant finger print region spectrum for perfectly mineralised bone, and it was determined that 960 cm^{-1} and 1170 cm^{-1} were the predominant scattering wavenumbers. A light microscope (Leica) x 20 magnification was used to determine regions of interest and mineral deposition for assessment.

5.2.5 In cell western assay

The in cell western analysis was carried out as outlined in Section 3.2.4, Chapter 3. Note for the use of the collagen gels the primary antibody dilutions were increased to 1:20 for osteocalcin and osteopontin and 1:3500 for GAPDH. The secondary antibodies dilutions were prepared as 1:5000 for both osteocalcin and osteopontin and GAPDH.

5.2.6 Cell culture and collagen matrix preparation

MSCs were sourced from Promocell and expanded cells were used for culturing in passages 1-3. The basal media which was used to maintain the cells during experiments and for proliferation was DMEM (Sigma-Aldrich) supplemented with 10% FBS, 1% sodium pyruvate - Sigma (11 mg/ml), 1% MEM NEAA – Gibco (amino acids) and 2% antibiotics (6.74 U/mL penicillin-streptomycin, 0.2 µg/mL fungizone). MSCs were homogeneously seeded within a collagen matrix a population of approximately 1×10^5 per well. All culture was performed in an incubator at 37ºC with 5% CO_2. The basal culture media was removed and replenished 2-3 days. For the Osteogenic media positive control samples the DMEM basal media was also substituted with 100 µMol ascorbic acid and 50 nMol dexamethasone (Sigma). The collagen matrix was prepared by addition of 10x modified eagle's media (First Link UK), FBS, basal media with the appropriate number of cells and 2.05 mg/mL rats tail Type I collagen in 0.16% acetic acid (First Link UK). The solution was homogeneously mixed by pipetting. Following this 0.1 M NaOH was added while on ice, till a permanent pink/red colour change (phenol red indicator) was observed, to form a gel. The samples were then quickly placed in a 37°C incubator avoiding agitation.

5.2.7 Von Kossa assessment

The Von Kossa staining technique using silver nitrate to coordinate with the phosphate component of the calcium hydroxyapatite complex was performed after 28 days of nanokicking. This technique was carried out as per Section 3.2.8.2 pg 65, however for this experiment the nuclear fast red counter stain was not performed with the 3D collagen gels. Image J software package was used to determine the staining intensity.

5.2.8 Micro-computed tomography (micro-CT) analysis

MSCs were nanokicked in 3D at 1000 Hz in a collagen gel extracellular matrix for 35 days the samples were fixed using 10% formaldehyde and transferred into PBS and subsequently imaged using micro-CT. The scans were then compared against unstimulated controls. Each well (of the 6 well plate) was seeded with ~ 750,000 cells. In order to image the samples all the gels for both the test sample (stimulated at 1000 Hz) and controls were combined together

in a separate cryo tube manufactured by Nunc A/S, with an internal diameter of 9.8 mm (± 0.1 mm). Within the cryo tube polystyrene saturated with PBS was used to secure the gels in place. This ensured that the samples were unable to move during scanning. Polystyrene was utilised as it is radiolucent and allowed the gels to be imaged unobstructed. The micro-CT system which was used was a Skyscan 1172 (Orthopaedic engineering department University of Edinburgh S/N=08F01110). The data was reconstructed using Skyscan reconstruction software and scanning was performed with a 360° rotation (Resolution /pixel size = 2.9278 μm, Source Voltage = 58 kV, Source Current = 171 μA, Exposure = 1178 ms).

Note: The micro-CT work and the parameters chosen for analysis were carried out by Dr. Robert Wallace a member of the Orthopaedic engineering department at the University of Edinburgh.

5.2.9 Statistics

One way ANOVA was used to compare significance in PCR, in cell western and Von Kossa stain experiments. Two tailed, unpaired T-Tests were performed where a direct comparison was assessed between only two population groups. A sample population of between 3 and 6 replicates were always used. All results are quoted as mean ± Standard deviation and the probability values have been quoted to an accuracy of 95%, 99% and 99.9% (*$p < 0.05$, **$p < 0.01$ and *** $p \leq 0.001$ respectively).

5.3 Results

5.3.1 Rheology determination

Type I collagen was used as an osteoconducive extracellular matrix and MSCs were grown homogeneously spread within the 3D matrix. In order to confirm that a collagen gel matrix had been formed and not simply a viscous liquid, the elastic properties of the gel were determined. The incidence of a viscous liquid over a gel would negate the high frequency vibrational effect of the bioreactor and render osteogenesis unlikely. In order to assess the viscoelastic properties of the matrix rheology and modulus deformation was determined. For a gel the dynamic storage modulus is referred to as G′ and this term explains the amount of contortional strain required to deform or shear the elastic constituent of a gel. The loss

modulus is referred to as G″ and conversely this term explains the strain or force required to shear the viscous constituent of a gel. When G′ is equivalent to G″ this is the point at which liquefaction begins to occur. If G′>G″ the properties of a gel are present, and conversely if G′<G″ a liquid state is present.

Collagen gels were assessed for rheology both with and without cells, with a seeding density of approximately 100,000. The gel was allowed to set in a 6 well plate and then removed and measured. In both cases it was found that a soft gel was present indicated by the greater measurement of G′ over G″. In each case an elastic modulus of approximately 50 Pa was measured **(Figure 5.1 A)**.

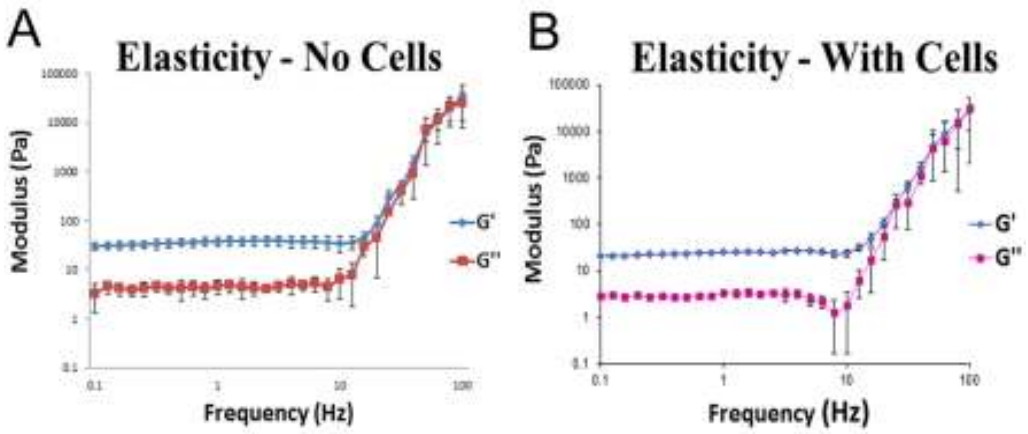

Figure 5.1: Characterisation of the collagen gel: (A) Rheology assessment for collagen gel without MSCs, elastic modulus equalling ~ 50 Pa. (B) Rheology assessment for collagen gel with MSCs seeded with ~ 100,000 cells, elastic modulus equalling ~ 50 Pa.

5.3.2 Transcript and protein assessment

The osteogenic bioreactor with collagen gels seeded at a density of approximately 100,000 MSCs was nanokicked (exposed to high frequency vertical displacements) at a frequency of 1000 Hz for 21 days. Following this the MSCs were harvested and the RNA was extracted in order to perform qRT-PCR and gain a transcriptomic understanding. The mRNA of 3 main osteogenic genes i.e. OCN, OPN and ONN were assessed for the nanokicked samples. It was found that all three of these genes were up-regulated relative to unstimulated controls.

Against a positive control - MSCs grown in osteogenic media without nanokicking (OSM); OPN and ONN were also up-regulated, with OPN being significant **(Figure 5.2 A).** However,

OCN was significantly over expressed for the positive control OSM samples. It also appeared that at 21 days time point the OPN and ONN were at lower expressed levels than the controls. This is simply due to the transcriptomic timeline for osteogenic expression by OSM. It is logical to deduce that if the assessment was performed a few days earlier these genes would certainly be upregulated. This unfortunately is one of the limitations of the technology.

Further to this, a quantitative osteogenic protein assessment was also carried out for nanokicked samples in the 3D collagen matrix, using the in cell Western technique. The protein expressions of OCN and OPN at the 21 days' time point was assessed relative to unstimulated controls and OSM positive controls. As per the transcriptional assessment, at the protein level GAPDH too was once again used as an internal reference biological standard. The data showed that both OCN and OPN in the nanokicked samples were up-regulated and also gave the largest expression of these osteogenic proteins compared to both unstimulated and positive controls. An increase in OCN and OPN both at a transcript and a protein level was a general trend which was observed by nanokicking. A population of 3 samples was used for both OCN and OPN **(Figure 5.2 B).** At a 2 weeks' time point a direct assessment of nanokicked samples relative to unstimulated controls was carried out at the protein level for OCN, using a larger population of 6 samples. This was again determined using the technique of in cell western for quantification. The protein expression of OCN was observed to be over expressed and increased by approximately 40%. The data was strongly significant for the nanokicked samples relative to the unstimulated controls **(Figure 5.2 C).**

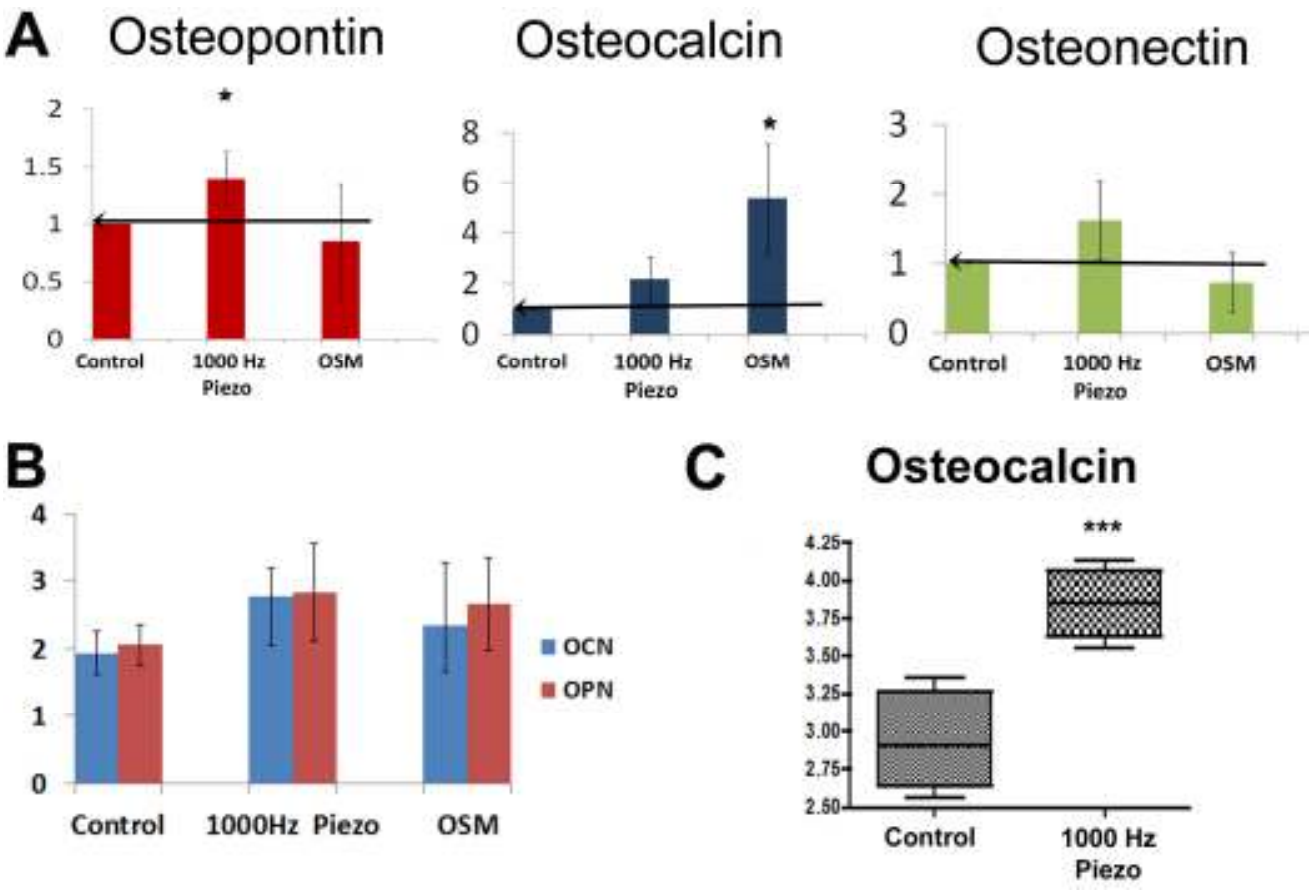

Figure 5.2: Transcriptomic assessment: (A) MSCs were exposed to nanokicking at 1000 Hz for the duration of 21 days in a collagen matrix. The transcriptomics were assessed against unstimulated controls and OSM positive controls (MSCs grown in osteogenic media) using the technique qRT-PCR. This showed an increase in OPN, OCN and ONN at this time point. N = 3 ±SD, * $p < 0.05$ by ANOVA, Protein assessment: (B) MSCs were exposed to nanokicking at 1000 Hz for 21 days in a collagen matrix, using in cell western the protein level expressions of OPN and OCN were assessed relative to unstimulated controls and positive controls OSM. Both OCN and OPN were observed to be increased relative to the controls, N = 3, results are mean ±SD. **(C)** MSCs exposed to nanokicking at 1000 Hz for 17 days using in cell western, compared to unstimulated controls. A significant increase was observed, N = 6, results are mean ± SD ***$p < 0.001$ by unpaired, 2 tailed T-Test.

5.3.3 Calcium phosphate ($Ca_{10}(PO_4)_6$) bone mineralisation determination:

Following on from affirmative osteogenic results at the transcriptomic and protein level, MSCs seeded in a collagen matrix were nanokicked for 28 days to determine the potential for bone mineralisation. The gel matrices including the cells were removed and then histologically stained for the presence of bound phosphate using the Von Kossa technique. The intensity of stain of the nanokicked samples were once again compared against the positive control, OSM samples and against unstimulated controls. Subsequently, the intensity of stain was quantified using the image J software package. The data showed that the phosphate deposition of the OSM and nanokicked samples was comparable and that the presence of phosphate was almost two fold relative to the unstimulated controls **(Figure 5.3 A and B).** Following on from this work, Raman spectroscopy was used to further assess, qualitatively and quantitatively, mineralisation in the gel matrix. MSCs were cultured for 46 days while being exposed to the vibrational bioreactor i.e. being nanokicked at a frequency of 1000 Hz. Relative to this, unstimulated controls were also cultured for the same duration of time. The test samples and control samples were then individually assessed in the Raman instrument using a laser attuned to the near IR to determine the presence of mineral deposits. The rationale for the long duration (46 days) of culture was two fold. Firstly, this was to assess the ability of the bioreactor to be cultured and maintain a sterile environment over a long period of time, and secondly to be certain that the MSCs had ample time to deposit mineralisation in the 3D collagen matrix, as the collagen matrix was a new condition being investigate.

In the first instance a sample of bovine cortical bone was determined in the Raman fingerprint region from 500 to 1500 cm^{-1}, which provides a specific profile for a particular compound. The resultant spectra showed that phosphate had a specific excitation scattering profile with a dominant peak at the 960 cm^{-1} wavenumber and subsequently a second peak at wavenumber 1072 cm^{-1} **(Figure 5.4 G)**. Given this data the Raman profile for the collagen gel matrix unstimulated control samples were assessed and this showed no noticeable Raman scattering at the wavelength/wavenumber of excitation used, and hence no peak interference between collagen and phosphate Raman spectra. **(Figure 5.4 A&D)**. Following this, the samples which were nanokicked were also assessed. These samples gave a scattering pattern which was consistent with the profile observed for cortical compact bone confirming the presence of

$Ca_{10}(PO_4)_6$ hydroxyapatite nodules, both the dominant peaks at wavenumber 960 cm^{-1} and 1072 cm^{-1} were observed **(Figure 5.4 B&E and C&F).** Quantification of these peaks showed that the value for the height and area for both peaks (960 cm^{-1} and 1072 cm^{-1}) were much higher in the cortical bone control compared to the nanokicked samples. Comparative quantification for width at half height gave a value for the cortical bone which was approximately half that for each nanokicked sample assessed using Raman spectroscopy. This value provides an indication of the mineral properties or crystalline structure (Gentleman et al., 2009; Tarnowski et al., 2002), **(Table 5.3).**

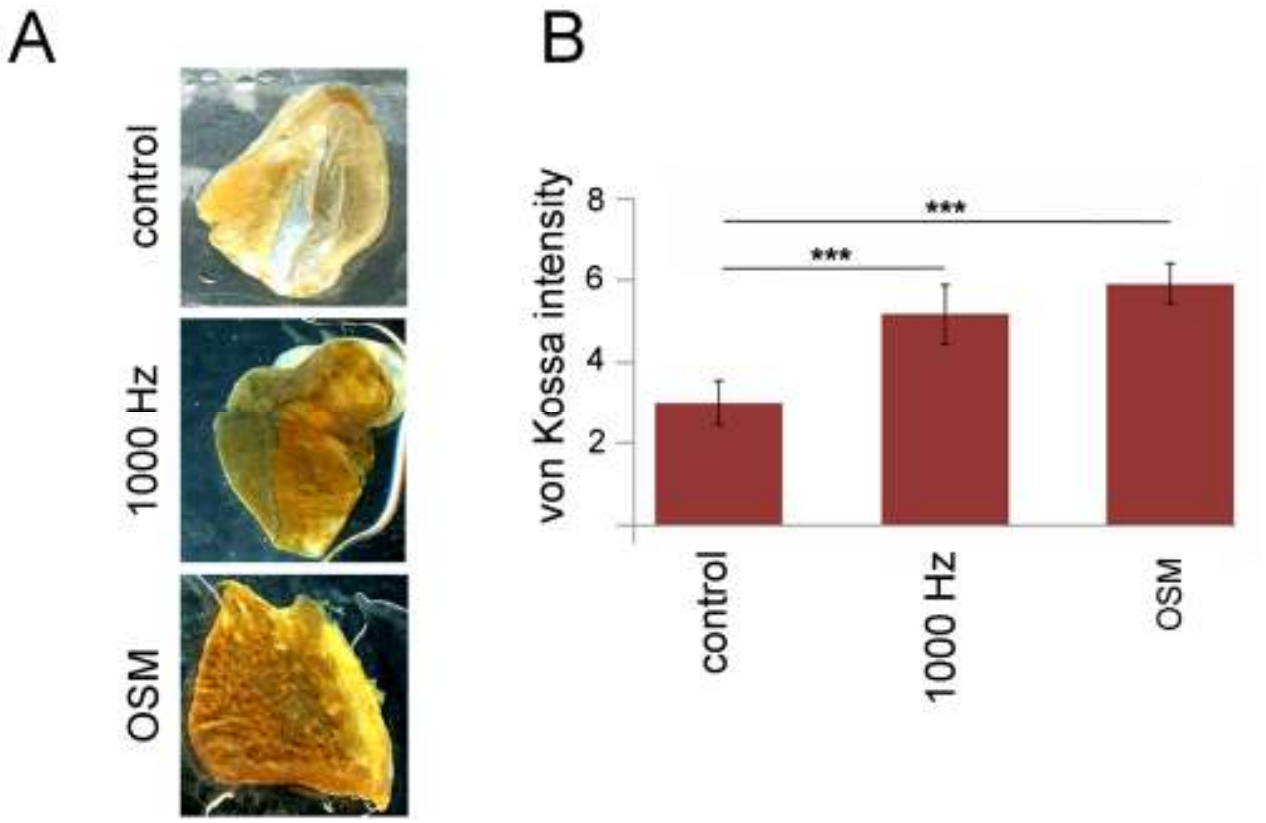

Figure 5.3: Bone mineralisation assessment: (A) Von Kossa staining was carried out after 28 days of nanokicking at 1000 Hz in a collagen matrix. The intensity of stain was compared against unstimulated controls and osteogenic media cultured MSCs. An increased intensity of staining was observed for nanokicked samples against unstimulated samples. This was comparable to the osteogenic media samples (OSM). (B) Quantitative representation of intensity of Von Kossa stains, N = 5, results are mean ± SD ***$p < 0.001$ by one way ANOVA.

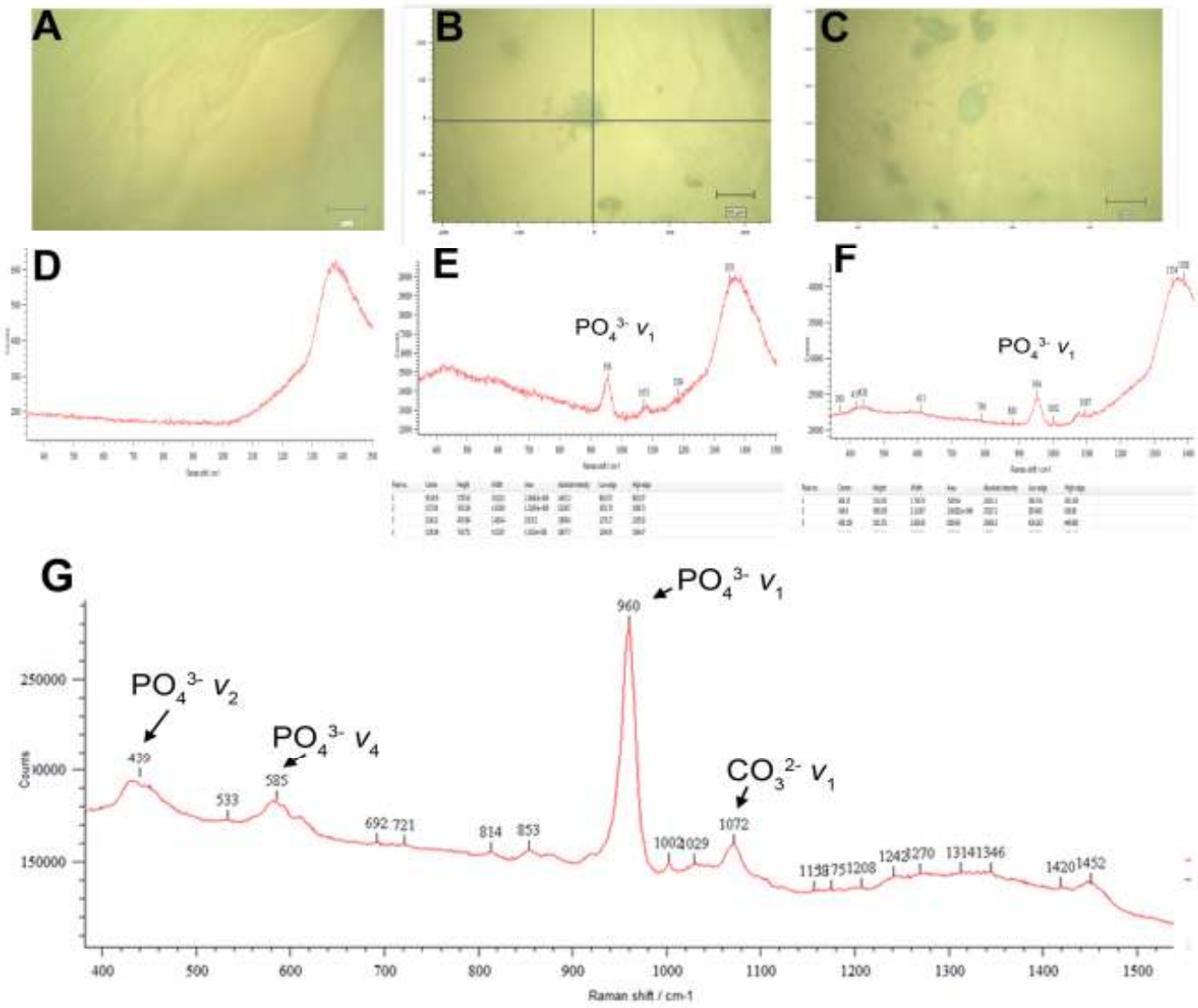

Figure 5.4: Bone mineralisation assessment: MSCs exposed to nanokicking at 1000 Hz for 46 days in a collagen matrix and compared against unstimulated controls for Raman scattering in the fingerprint identification region. (A&D): profile for unstimulated control. (B&E) profile for nanokicked sample. (C&F) profile of duplicate nanokicked sample, N = 3, scale bar = 50 µm. (G) Raman scattering for bovine cortical compact bone, this profile was used as a reference standard to characterise the Raman scattering pattern of bone.

	Bovine Cortical Bone (Perfectly Mineralised)	1000 Hz T1	1000 Hz T2	1000 Hz T3
Peak Raman Shift	960 cm^{-1}	960 cm^{-1}	960 cm^{-1}	960 cm^{-1}
Height	134510	1041	3951	1787
Area	3.030×10^7	1.11×10^6	3.84×10^6	2.17×10^6
FWHM	16.754	27.834	28.539	29.111

Table 5.3: Quantitative results of Raman scattering. Raman spectra results for nanokicked samples relative to the reference standard of cortical compact bovine mineralised bone. Values are shown for the Raman shift peak height, area and full width at half height maximum (FWHM).

Further to the results obtained when using Von Kossa and Raman spectroscopy to determine the formation of bone minerals, micro-CT was subsequently employed as a further confirmatory technique to assess the mineral deposits in the 3D collagen gel matrix. The samples were scanned (using X-rays) using a 360° rotation in horizontal transections through the collagen gel matrix. The light grey areas represent the collagen gel matrix with the black areas representing PBS or saturated polystyrene. The results showed that although on average only micro sized mineral deposits were observed there was a distinct difference in the presence or the amount of nodules observed between the test samples (i.e. nanokicked at 1000 Hz) and the controls see **(Figure 5.5)**. One of the largest nodules seen in the test sample had a diameter of approximately 500 μm with a depth of approximately 200 um **(Figure 5.5A)**. This data shows that, in line with the Raman assessment and Von Kossa staining, the high frequency stimulation at 1000 Hz has an extra-osteogenic effect on the MSCs within a 3D matrix relative to the controls.

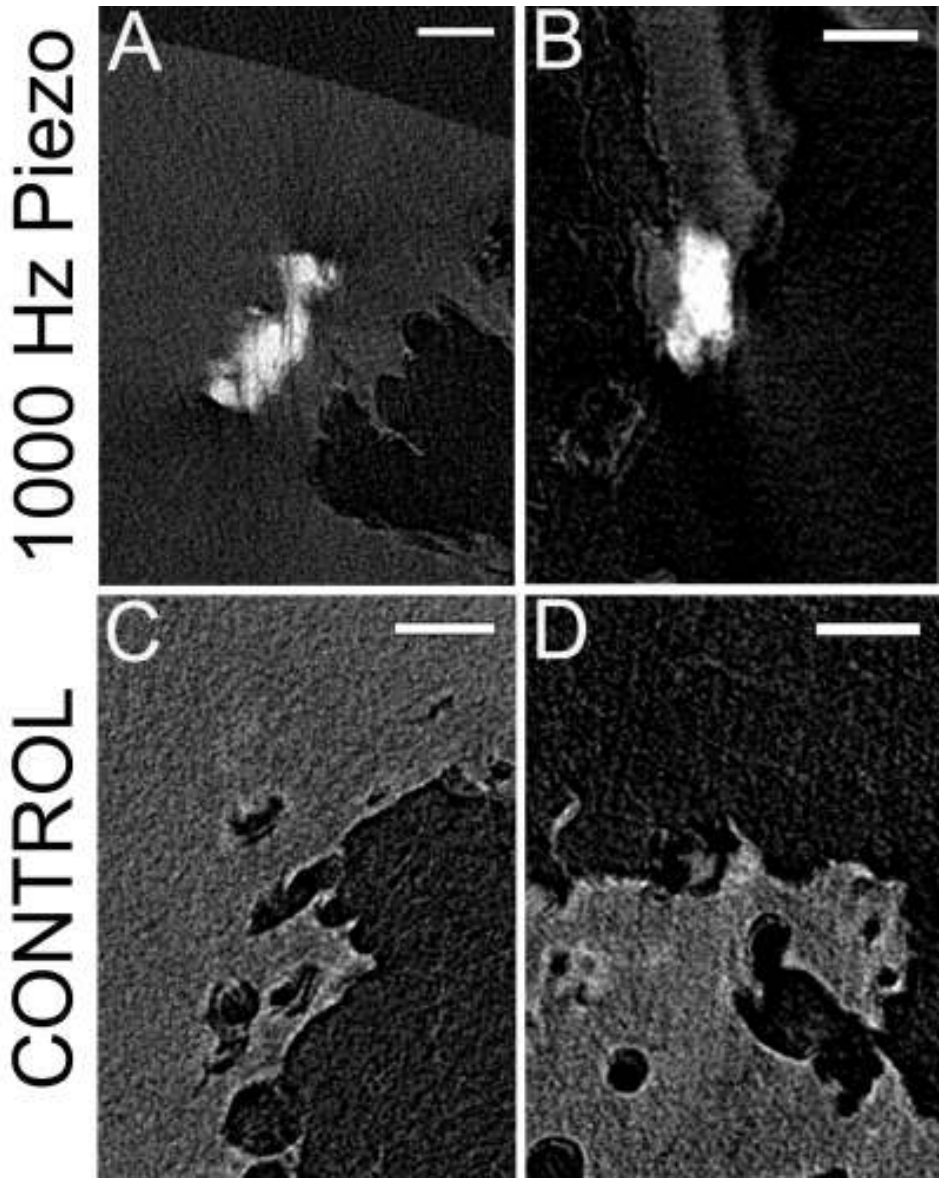

Figure 5.5: Calcium phosphate mineralisation assessment using micro-CT: MSCs cultured in a 3D collagen matrix were exposed to 1000 Hz nanokicking stimulation for 35 days. These samples were assessed against unstimulated controls. (A&B) micro-CT transectional scans through the collagen gel for the 1000 Hz test sample, small particulates of $Ca_{10}(PO_4)_6$ hydroxyapatite nodules observed. (C&D) micro-CT transectional scans through collagen gel of the control samples, scale bar = 200 μm, N=4 wells for the test samples and 3 wells for the controls.

5.4 Discussion

The assessment of the collagen matrix confirmed that a soft gel had been formed capable of suspending the MSCs in a 3D orientation. A comparable elastic modulus for the gels seeded with and without cells (i.e. ~50 Pa) was observed. Various publications have shown that MSCs seeded in a matrix with a higher Youngs modulus (equivalent to pre-calcified bone ~ 40 kPa) differentiate to osteoblasts (Engler et al., 2006; Engler et al., 2007). Although the stiffness of the gels used for the 3D matrix measured considerably lower than 40 kPa, it is likely that the modulus of the collagen matrix *in situ* tethered and strongly stretched within the 6 well plates is of a much higher stiffness than once removed. Hence MSCs seeded within gels in the bioreactor may be exposed to a much stiffer environment.

It has been previously surmised that in a 2D format, force through vibrational acceleration and the weight of the media on top of the MSCs could, in part, be inductive of osteogenesis (Pacicca et al., 2002; Stonemetz et al., 2011). However, in 3D it is theorised that a compression effect induced by the high frequency vibrations or in effect a constant pressure wave is perhaps created through the gelatinous matrix. This could be creating shearing or even an applied force through pressure and compression which, it has been published, aids skeletal regeneration and the induction of osteogenesis (Henstock et al., 2013; Kim et al., 2006; Neidlinger-Wilke et al., 2005). Unsurprisingly, we have also observed that an increased amount of collagen matrix (≥ 5 mL) also has a dissipating effect on the vibrational displacements which the MSCs are exposed to **(Figure 4.4)**.

The integrin attachments, focal adhesions and fibrillar adhesions which are formed in a 3D matrix differ from that formed in 2D. This is observed in the composition of α and β integrin subunits, protein complexes such as paxillin and the tyrosine phosphorylation of focal adhesion kinase (Bucci and Musitano, 2011). What's more, the morphology and lay out of cells is also altered assuming a slender and more spindle shape akin to the *in vivo* state (Cukierman et al., 2001). It is a possibility that this morphology may also expose a greater surface area of the MSCs to the vibrational nanokicking effect due to an increased surface area relative to 2D cultured cells which are flattened and more oval (Cukierman et al., 2001; Hakkinen et al., 2011). It is hence speculated that this increased vibrational exposure may also increase osteogenesis *in vivo*. Interestingly, Lund et al have shown that inhibiting ERK (which is usually increased as a key component in the MAPK pathway to augment

osteogenesis (Kapur et al., 2003; Xu et al., 2014)) promotes collagen gel compaction and fibrillogenesis in 3D resulting in an amplification of the osteogenic phenotype (Lund et al., 2009).

Bearing in mind that the harmonics emitted by our bioreactor at 1000 Hz is audible to the human ear, and hence is strong enough to vibrate the stereocilia inside the cochlea, it is considered that these sonic vibrations may also have some beneficial effect on the MSCs at the nanoscale, which is not yet fully understood. Indeed Yun-Kyong Choi and colleagues have published that acoustic vibration (sub-sonic, ≤ 40 Hz at 1.0 V) has the potential to induce neurogenesis in adipose derived MSCs while inhibiting adipogenesis, stem cell maintenance and proliferation (Choi et al., 2012). It is then logical to assume that higher acoustic vibrations such as have been used here (1000 Hz) may have further capacities for MSCs differentiation including osteogenesis.

The Raman quantification value of full width at half height maximum provides an indication of the crystalline structure or the density of mineralised bone $Ca_{10}(PO_4)_6$ in the samples being analysed by giving an indication of mineral crystalline structure (Gentleman et al., 2009). Although it is not a direct correlation the data indicates that the structure and density of the mineral in the perfectly formed bovine cortical bone reference standard is more mineralised and hence is more dense or well formed, compared to the bone particulates grown by the vibrational bioreactor. This is also indicated by a more sharply formed peak with a greater intensity or level of Raman scattering. This is particularly observed, in the 960 cm^{-1} wavenumber of the dominant peak provided by the stretching and bending motions created in the PO_4^{3-} V_1 bonds as it interacts with electromagnetic radiation . Although the data confirms that the cortical bone reference standard is more compact and crystalline it does not appear to be on orders of magnitude greater (Gentleman et al., 2009; Tarnowski et al., 2002).

The micro-CT results showed that in 3D, as is the case in 2D, the differentiated osteoblast cells will coalesce together to build or deposit ever increasing particulates of $Ca_{10}(PO_4)_6$, (Pemberton et al., 2015) as smaller particulates on the sub 20 µm size were observed ranging all the way to approximately 500 µm. Nevertheless, although there was a distinctive difference between the test samples and the controls, in effect the amount of mineral deposited in the test samples was on the microscale. It is thought that a limiting factor was that insufficient raw

material was made available, i.e. if more calcium and phosphate would be provided to the cells they could subsequently grow even larger $Ca_{10}(PO_4)_6$ particulates.

5.5 Conclusion

This unique research has shown that by using a novel bioreactor capable of providing sinusoidal high frequency (1000 Hz) displacements; it is possible to form mineral deposits *in vitro* in a 3D matrix. By histological staining it was clear that there was a significant increase in the deposition of mineral relative to unstimulated controls and further still the very specific technique of Raman spectroscopy also gave a definitive result that mineralisation did take place, and that the crystalline structure or density of the calcium phosphate minerals was not that much less than the cortical bone control. Further still by using the technique of micro-CT mineral deposits could be clearly observed *in situ* confirming the Raman and Von Kossa histological results.

Chapter VI: General Discussion

6.1 Introduction

The ability to orchestrate the function and phenotype of somatic cells or even stem cells, in particular MSCs, is not only important but also a fundamental part of cell engineering. Understanding the physiological workings at a cellular level is the first step to tissue engineering and the potential replacement of functional organs or even the replacement of osseous tissue (Chistiakov, 2012; Conrad and Huss, 2005). For the control of proliferation, migration, differentiation and also, importantly, the artificial maintenance of potential (stem cells in an undifferentiated state), research has been performed using several techniques. When referring specifically to osteogenesis these include nanotopographical surfaces in particular disorder and order patterns (Dalby et al., 2007d; Dalby et al., 2006a), the application of a magnetic or electrical field (Ahuja et al., 2005) and the manipulation of extracellular matrix stiffness and hydrostatic pressure (Engler et al., 2006; Liu et al., 2009a) and yet there are still other techniques (Prodanov et al., 2013).

Here; through these past 5 chapters, it has been demonstrated that the use of high frequency stimulation of displacements on the nanoscale can be introduced to MSCs using an artificially made bioreactor to induce differentiation. What's more it has been demonstrated that this bioreactor can be reproducibly and consistently made and that it can be used for both 2D and 3D long-term sterile cell culture. Although as yet unproven, it is theorised that it may also be possible to bring about several other types of physiological differentiation in adult stem cells which have not come from the bone marrow or perhaps even iPSC or ESC (Choi et al., 2012; Pre et al., 2011a), by attuning the bioreactor to different frequencies and amplitudes. This research, however, has concentrated solely on osteogenesis achieved through the use of bone marrow (from the iliac crest) derived MSCs.

6.2 Vibrational Inducement of Osteogenesis

A reasonable question is: how does nanokicking induced osteogeneis work? And although a definitive answer with all certainty cannot be given until even further work is carried out it is theorised that mechanotransduction must play a pivotal role.

The integrins bridge to the extracellular matrix at specific attachment points (e.g. RGD) helping to relate mechanical information which occurs outside of the cell to the intracellular compartments, in particular to the nucleus where transcription factors can be up/down-regulated to bring about a distinctive phenotype, See **(Figure 1.5)**, from the introduction**.** The data throughout this thesis suggests that this maybe a key means by which nanokicking mechanotransductively induces osteogenesis and differentiation in MSCs (Dalby et al., 2014a; Wang et al., 2009b). It has been observed that RUNX2 and OCN as well as other mRNA (gene transcripts) specific for osteoblast formation are related to the up-regulation of ERK1&2 and FAK which are closely linked to the MAPK pathway. This pathway is known to bring about a downstream increase in RUNX2 which commences in the focal adhesions which are physically linked to the intergins (Tsimbouri et al., 2012a). This research has also consistently shown a general trend of the increase of OCN and OPN (both genetic and protein) through nanokicking induced osteogenesis.

A physiological property of bone which may also add to osteogenesis is its piezoelectric attribute. We know that the inorganic component of bone is calcium phosphate hydroxyapatite $Ca_{10}(PO_4)_6(OH)_2$, while the organic content of bone is primarily made up of collagen. It has been previously published that collagen is piezo electric; however this property of collagen is only witnessed when it is dry. For this to occur when collagen is wet or hydrated it requires mechanical stimulation at much higher frequencies i.e. kHz or perhaps even the MHz range (Reinish and Nowick, 1975). Interestingly, the mechanical stimulation using the piezo actuator which has been carried out in this thesis was performed in the kHZ range. The unique effect of this is that an electric current also appears to have the ability to augment the growth or regeneration of osseous tissue (Goldstein et al., 2010) . An electrical charge also has the ability to induce or dictate polarization, and as a result, influence the directional movement of cells, a process referred to as galvanotaxis (Cohen et al., 2014). This could mean that an electric charge could also influence the direction or positioning of bone growth. A further

hypothesis is that the piezoelectric property of bone may also be used to orchestrate osteoblast movement and physiological activity (Finkelstein et al., 2007).

Just like the mechanical properties of the piezo actuator, the deformation of bone through weight bearing may also stimulate its piezo effect causing an electric dipole to form which would be observed by the osteoblasts on the surface of the bone and hence by the osteocytes which are connected to osteoblasts through canals called canaliculi see **(Figure 1.2**). Further still, the osteoclasts are also connected to the osteocytes through these canals. These connections and canals resemble the copper wire tubing and connections in an electrical circuit, or even the neuronal connections within brain and spinal tissue, which too incidentally, possess electrical activity (Salanki and Varanka, 1969). In effect there may possibly be an information (perhaps electrical, vibrational) network between the osteoblasts, osteocytes and osteoclasts which serves the purpose of modelling and remodelling at defined sites in growing bone or causing osteoblastic differentiation. Having explained these piezoelectric properties of collagen and bone and what might be an information network between the cells that make up bone; it is possible to deduce that our high frequency bioreactor may be stimulating these electrical and mechanical mechanisms through nanokicking: which could subsequently bring about osteogensis. Interestingly it has been suggested that through polarization a negative charge would result at regions of osteoclast proliferation and regions with a positive charge would cause osteoblast clustering (Fernandez et al., 2012). It is worth noting however, that different voltages/ currents may have altering affects and at the micro/nano scale the assumption would be that very low levels (≤ micro volts) would potentially be observed through nanokicking.

At the high frequencies of 1000 Hz – 5000 Hz which have been investigated, audible sonic vibrations can be detected by the human ear; hence these vibrations have a nanoscale acoustic effect also. It may be that this nanoacoustic effect may also provide an additive advantage for stem cell differentiation. It has been published that even lower sonic vibrations can affect stem cell lineage commitment, in particular neurogenesis from MSCs (Choi et al., 2012) . What's more, low intensity pulsed ultrasonography may also provide a beneficial effect on the regeneration of bone fractures (Claes and Willie, 2007).

In understanding osteogenic differentiation, we have observed in 3D that it is of importance to also consider the biomimetic attribute of any design or osteogenic scaffold, and hence efforts have been made to culture the MSCs as close as possible to the *in vivo* osseous natural state. Collagen, which is the dominant protein that makes up the organic component of bone, has been utilised as the extracellular matrix used in the 3D bioreactor model, and in line with biomimetics, collagen may to have an additive affect on the osteogenic phenotype when coupled with nanokicking (Ren et al., 2015; Sumanasinghe et al., 2006). In the osteogenic experiments performed in 2D, there was no collagen scaffold used, however MSCs do have the potential to form fibroblasts (they were first described by Friedenstein as colony forming unit fibroblasts) (Friedenstein, 1976; Friedenstein et al., 1968) which form the extracellular matrix including collagen. Hence the piezo electric properties of collagen described in the paragraphs above may have also been of importance even in the experiments performed with nanokicking in 2D.

Further to explain the design used in the 2D bioreactor and the osteogenic effect observed; it has been previously published that an increased weight or hypergravity (the weight of the media above the cells would be amplified by the force of nanokicking), and it has also been published that an increased weight would also be osteogenic (Kacena et al., 2004; Prodanov et al., 2013). It is hypothesised that this hypergravity effect may also be translated in the 3D culture system. The rheological assessments see **(Figure 5.1)**, has shown that, in effect, a very soft gel is surrounded by aqueous media. This design may provide a compression wave effect through the gel caused by the high frequency nanokicks. This compression could be interpreted as weight bearing by the cultured MSCs even in 3D, resulting in further osteogensis. Credence to this fact is also seen in that astronauts in a low gravity i.e. a low weight compressive effect on their bones suffer from musculoskeletal atrophy (Miyamoto et al., 1998) . Further, this hypothesis is in agreement with Wolff's Law, in that healthy osseous tissue will accommodate added strain or weight (activation and up-regulation of osteoblasts) by becoming fortified (Polk, 2011) .

6.3 Conception of the Novel 3D bioreactor: From 2D – 3D

The 2D piezo actuator bioreactor was found to be suitable for use when interrogated for thermal and mechanical stability. The design which was used was also importantly not susceptible to shear force (Nikukar et al., 2013). In terms of thermal consistency, the piezo actuators were made of ceramics which was an excellent insulator **(Figure 2.4)**. The use of heated polycaprolactone as a biocompatible glue was also suitable to securely fasten the polycarbonate NSq-50 nanotopographical substrates to the Petri dish efficiently transferring the piezo nanodisplacement, as was confirmed by the interferometric measurements **(Figure 2.6)**.

The interferometric empirical measurements also corroborated with the ANSYS finite element data and fortunately GAPDH was found to be a robust and suitable internal biological reference standard which could be used to assess osteogenic change both at a transcript expression and protein expression level. These data altogether provided confidence that the 2D bioreactor was capable of transferring a sustained mechanical vertical displacement at high frequency through a Petri dish to MSCs cultured on the surface, with the proven induction of osteogenesis (Pemberton et al., 2015).

Nevertheless, the use of the 2D bioreactor **(Figure 2.2)** which was inherited at the beginning of this PhD meant that the reproducibility between samples and in particular between individual piezo actuators could potentially be a source of error. What's more, the use of the 2D bioreactor with loose electrical wires meant that the bioreactor was cumbersome. Safety issues from loose wires, a time consuming set up for experiments, (in part due to using different glues for construction before every experiment), and the destruction of the individual piezo actuators over time through constant removal and attachment were some of the necessity drivers for change. A further problem was the need to change the media every 2 or 3 days within the incubator during long-term experiments i.e. a point at which sterility could be compromised. As a result of these shortcomings, the 3D bioreactor was conceived and designed to correct these failings with a plan which was conducive to eventual 3D GMP culture and ease of use with reproducible effect between all piezo actuators **(Figure 6.2)**. It was designed as a technologically novel genre of bioreactor (a nanovibrational bioreactor) as

opposed to the perfusion, spinner flasks, EMF etc. bioreactors which had previously been developed. This bioreactor does not require flow through but instead nutrient rich media would be added and removed from the top surface as and when required, depending on the vibrational mechanical forces for the movement of nutrients through diffusion. In part concepts learned from LEAN and 6 Sigma were employed in this design. These principles teach understandings in efficiency and productivity, and that if something is cumbersome or not value adding it should be dispensed with or optimised. They ask of one to keep in mind what is best for, or the need of the stakeholder and then this is incorporated into a thought process and then the design (Haenke and Stichler, 2015; Mason et al., 2015).

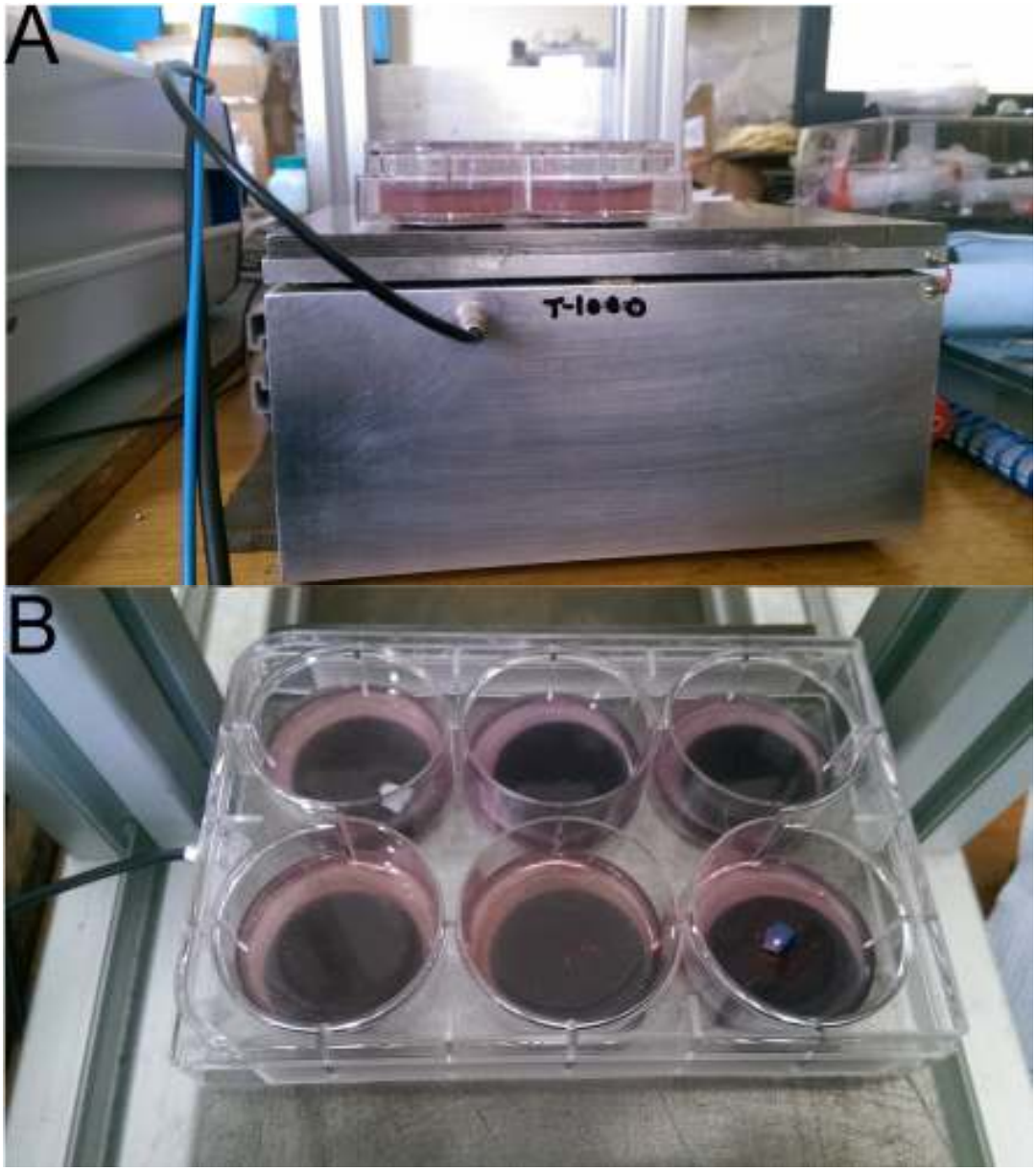

Figure 6.1: The novel 3D bioreactor (A) Shows a longitudinal section of the bioreactor which was designed and optimised from the bioreactor shown in figure 2.2 A. (B) Aerial view of the 3D bioreactor showing cultured MSCs within a collagen matrix in a 6 well plate.

Although there are several osteogenic bioreactors on the market already ranging from perfusion, centrifugal and rotating bioreactors, see **(Table 1.1)**, the uniqueness of the nanokicking bioreactor comes from the method in which it brings about osteoblast differentiation, it's cheaper running costs and perhaps most fundamental, the fact that it can bring about osteogenesis without the requirement of osteogenic media, growth factors, chemical compounds or intricate 3D scaffolds (e.g. dexamethasone, rhBMP2), (Ha et al., 2013; Rauh et al., 2011a; Yeatts et al., 2013). Hence for the most part the present commercial bioreactors require an osteogenic additive which also increases running cost and complexity. It is envisaged that long-term this bioreactor may possibly lend itself to clinical use and GMP manufacture of artificially produced autologous ossesous tissue for regenerative medicine or simply to produce autologous ossesous tissue for testing patient specific efficiency of a novel treatment in the burgeoning field of personalised medicine. This ambition however will require phase I – III clinical trials and collaboration with the pharmaceutical industry.

6.4 Conclusion

In conclusion, the hypothesis and aim of this thesis investigated over the past 3½ years has for the most part been met, nevertheless more research could still be performed. The design engineered for the 2D bioreactor facilitated high frequency vibrational stimulation of MSCs. This was found to be fit for purpose when interrogated for thermal, mechanical and biological integrity. This bioreactor was hence suitable to induce osteogenesis of MSCs in 2D and to enhance osteogenesis even further when coupled with an osteogenic (NSq-50) nanotopography. The 3D bioreactor; while having bioequivalence with the previous design is more simple and elegant to use and may have real world practical applications academically in research laboratories and clinically to be able to treat musculoskeletal conditions such as bone fractures, and potentially artificially grow replacement bone tissue for patients who have had osteosarcoma excisions.

6.5 Future Directions

The assessment of other sources of stem cells, such as hematopoietic, iPSC, ES may perhaps yield interesting results. A catalogued design of experiments should be performed, varying frequencies for each cell type, from 1 Hz – 5000 Hz and in the first instance assessing the

genetic landscape by microarray (or microRNA and mRNA determination). This could first be performed in 2D and then again in various 3D matrices. It is suggested that frequencies such as 396 Hz, 444 Hz, 639 Hz, 741 Hz and 852 Hz may be attuned to the resonance frequencies of the different tissues which make up the body and may have regenerative potential. It may be of interest to assess 528 Hz. It is theorised that this frequency may also have regenerative properties including DNA repair, delaying cell senescence.

Further research at the Schumann resonance frequency at 7.8 Hz may also provide interesting results for neurogenesis, as it is thought that the electrical impulses in the brain may resonate near that frequency also. Interestingly Nikola Tesla was also researching free wireless energy at an approximate frequency (7.8 Hz) in the Colorado Springs during the early 20th Century.

As far as osteogenic use of the bioreactor it would also be important to assess the potential of AD-MSC as these may be a more efficacious cell type than the BM-MSC. What's more they would be an easily retrievable source of MSCs, alleviating the patient distress caused by the removal of bone marrow aspirates. Research suggests that MSCs sourced from the adipose tissue may be more robust or viable (Dmitrieva et al., 2012a). It is also theorised that in 3D (and perhaps also in 2D) culture there may be other frequencies that have been overlooked which may be more osteogenic than 1000 Hz. It will hence be worthwhile to reinvestigate frequencies from 500 Hz – 5000 Hz. Furthermore, the adition of raw material for the osteoblasts (calcium and phosphate) particulates in the collagen matrix should expedite mineral deposition as well as increase the rigidity of the matrix making it more osteoinductive and vibrationally transductive.

Although the initial investigation of the bioreactor and piezo technology was to consider its affect on stem cells, it is believed that this technology may also lend itself favourably to several other biotechnological areas of research. Other future directions may include the determination of the affect of various frequencies and amplitude on several kinds of malignant cell types to observe if this may limit the rate of division of cancer cells. This may be achieved by aligning the frequency used with different biological resonant frequencies of cancer cell types. It is envisaged that this same modus operandi may be favourably used to assess the effect of vibrational and acoustic stimulation on pathogenic cell types; such as bacteria, viruses and protozoa.

VII: References

Ahn, A.C., and Grodzinsky, A.J. (2009). Relevance of collagen piezoelectricity to "Wolff's Law": a critical review. Medical engineering & physics *31*, 733-741.

Ahuja, Y.R., Bhargava, S.C., and Ratnakar, K.S. (2005). Electric and magnetic fields in stem cell research. Electromagnetic biology and medicine *24*, 121-134.

Allan, G., and Delerue, C. (2005). Unusual quantum confinement effects in IV-VI materials. Mat Sci Eng C-Bio S *25*, 687-690.

Amanda M. D. Malone, Charles T. Anderson, Padmaja Tummala, Roland Y. Kwon, Tyler R. Johnston, Tim Stearns and Christopher R. Jacobs (2007). Primary Cilia mediated mechanosensing in bone cells by a calcium-independant mechanism. PNAS 104, 13325-13330.

Andrew Thomas, R.B., Chiamaka Chuke-Okafor (2004). Applying lean six sigma in a small engineering company – a model for change. Journal of Manufacturing Technology Management *20*, 113 - 129.

Anton, F., Suck, K., Diederichs, S., Behr, L., Hitzmann, B., van Griensven, M., Scheper, T., and Kasper, C. (2008). Design and characterization of a rotating bed system bioreactor for tissue engineering applications. Biotechnology progress *24*, 140-147.

Angus K.T. Wann, Ning Zao, Courtney J. Haycraft, Cynthia G. Jensen, C. Anthony Poole, Susan R. McGlashan, and Martin M. Knight (2012), Primary Cilia mediate mechanotransduction through control of ATP-induced Ca^{2+} signalling in compressed chondrocytes. The FASEB Journal 26, 1663-1671.

Ballato, A. (1998). Historical development of piezoelectric materials and applications. Ceram Trans *88*, 1-14.

Bas, A., Forsberg, G., Hammarstrom, S., and Hammarstrom, M.L. (2004). Utility of the housekeeping genes 18S rRNA, beta-actin and glyceraldehyde-3-phosphate-dehydrogenase for normalization in real-time quantitative reverse transcriptase-polymerase chain reaction analysis of gene expression in human T lymphocytes. Scandinavian journal of immunology *59*, 566-573.

Basu, J., Genheimer, C.W., Guthrie, K.I., Sangha, N., Quinlan, S.F., Bruce, A.T., Reavis, B., Halberstadt, C., Ilagan, R.M., and Ludlow, J.W. (2011). Expansion of the human adipose-derived stromal vascular cell fraction yields a population of smooth muscle-like cells with markedly distinct phenotypic and functional properties relative to mesenchymal stem cells. Tissue engineering Part C, Methods *17*, 843-860.

Basu, J., Jayo, M.J., Ilagan, R.M., Guthrie, K.I., Sangha, N., Genheimer, C.W., Quinlan, S.F., Payne, R., Knight, T., Rivera, E.*, et al.* (2012). Regeneration of native-like neo-urinary tissue from nonbladder cell sources. Tissue engineering Part A *18*, 1025-1034.

Bautista, D.S., Xuan, J.W., Hota, C., Chambers, A.F., and Harris, J.F. (1994). Inhibition of Arg-Gly-Asp (RGD)-mediated cell adhesion to osteopontin by a monoclonal antibody against osteopontin. The Journal of biological chemistry *269*, 23280-23285.

Besunder, J.B., and Super, D.M. (2012). Lean Six Sigma: trimming the fat! Effectively managing precious resources. Critical care medicine *40*, 699-700.

Biggs, M.J.P., Richards, R.G., Gadegaard, N., Wilkinson, C.D.W., Oreffo, R.O.C., and Dalby, M.J. (2009). The use of nanoscale topography to modulate the dynamics of adhesion formation in primary osteoblasts and ERK/MAPK signalling in STRO-1+enriched skeletal stem cells. Biomaterials *30*, 5094-5103.

Burack, W.R., and Sturgill, T.W. (1997). The activating dual phosphorylation of MAPK by MEK is nonprocessive. Biochemistry *36*, 5929-5933.

Bharali, D.J., Yalcin, M., Davis, P.J., and Mousa, S.A. (2013). Tetraiodothyroacetic acid-conjugated PLGA nanoparticles: a nanomedicine approach to treat drug-resistant breast cancer. Nanomedicine *8*, 1943-1954.

Bhoopathi, P., Gondi, C.S., Gujrati, M., Dinh, D.H., and Lakka, S.S. (2011). SPARC mediates Src-induced disruption of actin cytoskeleton via inactivation of small GTPases Rho-Rac-Cdc42. Cellular signalling *23*, 1978-1987.

Bishop, M.R. (1997). Potential use of hematopoietic stem cells after radiation injury. Stem Cells *15*, 305-310.

Bjerre, L., Bunger, C., Baatrup, A., Kassem, M., and Mygind, T. (2011). Flow perfusion culture of human mesenchymal stem cells on coralline hydroxyapatite scaffolds with various pore sizes. Journal of biomedical materials research Part A *97*, 251-263.

Bjerre, L., Bunger, C.E., Kassem, M., and Mygind, T. (2008). Flow perfusion culture of human mesenchymal stem cells on silicate-substituted tricalcium phosphate scaffolds. Biomaterials *29*, 2616-2627.

Bobyn, J.D., McKenzie, K., Karabasz, D., Krygier, J.J., and Tanzer, M. (2009). Locally Delivered Bisphosphonate for Enhancement of Bone Formation and Implant Fixation. Journal of Bone and Joint Surgery-American Volume *91A*, 23-31.

Bonewald, L.F. (2007). Osteocytes as dynamic multifunctional cells. Ann Ny Acad Sci *1116*, 281-290.

Bucci, R.V., and Musitano, A. (2011). A Lean Six Sigma journey in radiology. Radiology management *33*, 27-33; quiz 34-25.

Bueno, E.M., and Glowacki, J. (2009). Cell-free and cell-based approaches for bone regeneration. Nature reviews Rheumatology *5*, 685-697.

Burack, W.R., and Sturgill, T.W. (1997). The activating dual phosphorylation of MAPK by MEK is nonprocessive. Biochemistry *36*, 5929-5933.

Caldwell, C. (2006). Lean-Six Sigma: tools for rapid cycle cost reduction. Healthcare financial management : journal of the Healthcare Financial Management Association *60*, 96-98.

Candiani, G., Raimondi, M.T., Aurora, R., Lagana, K., and Dubini, G. (2008). Chondrocyte response to high regimens of cyclic hydrostatic pressure in 3-dimensional engineered constructs. The International journal of artificial organs *31*, 490-499.

Caplan, A.I. (1991). Mesenchymal stem cells. Journal of orthopaedic research : official publication of the Orthopaedic Research Society *9*, 641-650.

Caplan, A.I. (1994). The mesengenic process. Clinics in plastic surgery *21*, 429-435.

Cauffman, G., De Rycke, M., Sermon, K., Liebaers, I., and Van de Velde, H. (2009). Markers that define stemness in ESC are unable to identify the totipotent cells in human preimplantation embryos. Human reproduction *24*, 63-70.

Celil, A.B., and Campbell, P.G. (2005). BMP-2 and insulin-like growth factor-I mediate osterix (Osx) expression in human mesenchymal stem cells via the MAPK and protein kinase D signaling pathways. Journal of Biological Chemistry *280*, 31353-31359.

Chistiakov, D.A. (2012). Liver regenerative medicine: advances and challenges. Cells, tissues, organs *196*, 291-312.

Chen, J.H., Liu, C., You, L., and Simmons, C.A. (2010). Boning up on Wolff's Law: mechanical regulation of the cells that make and maintain bone. Journal of biomechanics *43*, 108-118.

Choi, Y.K., Cho, H., Seo, Y.K., Yoon, H.H., and Park, J.K. (2012). Stimulation of sub-sonic vibration promotes the differentiation of adipose tissue-derived mesenchymal stem cells into neural cells. Life sciences *91*, 329-337.

Cifarelli, R.A., D'Onofrio, O., Grillo, R., Mango, T., Cellini, F., Piarulli, L., Simeone, R., Giancaspro, A., Colasuonno, P., Blanco, A.*, et al.* (2013). Development of a new wheat microarray from a durum wheat totipotent cDNA library used for a powdery mildew resistance study. Cellular & molecular biology letters *18*, 231-248.

Claes, L., and Willie, B. (2007). The enhancement of bone regeneration by ultrasound. Progress in biophysics and molecular biology *93*, 384-398.

Cohen, D.J., Nelson, W.J., and Maharbiz, M.M. (2014). Galvanotactic control of collective cell migration in epithelial monolayers. Nature materials *13*, 409-417.

Conese, M., Piro, D., Carbone, A., Castellani, S., and Di Gioia, S. (2014). Hematopoietic and mesenchymal stem cells for the treatment of chronic respiratory diseases: role of plasticity and heterogeneity. TheScientificWorldJournal *2014*, 859817.

Conrad, C., and Huss, R. (2005). Adult stem cell lines in regenerative medicine and reconstructive surgery. Journal of Surgical Research *124*, 201-208.

Coquelin, L., Fialaire-Legendre, A., Roux, S., Poignard, A., Bierling, P., Hernigou, P., Chevallier, N., and Rouard, H. (2012). In vivo and in vitro comparison of three different allografts vitalized with human mesenchymal stromal cells. Tissue engineering Part A *18*, 1921-1931.

Crisan, M., Yap, S., Casteilla, L., Chen, C.W., Corselli, M., Park, T.S., Andriolo, G., Sun, B., Zheng, B., Zhang, L.*, et al.* (2008). A perivascular origin for mesenchymal stem cells in multiple human organs. Cell stem cell *3*, 301-313.

Cronmiller, C., and Mintz, B. (1978). Karyotypic normalcy and quasi-normalcy of developmentally totipotent mouse teratocarcinoma cells. Developmental biology *67*, 465-477.

Crowder, S.W., Liang, Y., Rath, R., Park, A.M., Maltais, S., Pintauro, P.N., Hofmeister, W., Lim, C.C., Wang, X., and Sung, H.J. (2013). Poly(epsilon-caprolactone)-carbon nanotube composite scaffolds for enhanced cardiac differentiation of human mesenchymal stem cells. Nanomedicine *8*, 1763-1776.

Cukierman, E., Pankov, R., Stevens, D.R., and Yamada, K.M. (2001). Taking cell-matrix adhesions to the third dimension. Science *294*, 1708-1712.

Curtis, A., Reid, S., Martin, I., Vaidyanathan, R., Smith, C.A., Nikukar, H., and Dalby, M. (2013a). Cell Interactions at the Nanoscale:Piezoelectric Stimulation. IEEE Trans Nanobioscience *12*, 247-254.

Dahl, S.L.M., Kypson, A.P., Lawson, J.H., Blum, J.L., Strader, J.T., Li, Y.L., Manson, R.J., Tente, W.E., DiBernardo, L., Hensley, M.T.*, et al.* (2011). Readily Available Tissue-Engineered Vascular Grafts. Science translational medicine *3*.

Dalby, M.J., Gadegaard, N., and Oreffo, R.O. (2014). Harnessing nanotopography and integrin-matrix interactions to influence stem cell fate. Nature materials *13*, 558-569.

Dalby, M.J., Gadegaard, N., Tare, R., Andar, A., Riehle, M.O., Herzyk, P., Wilkinson, C.D., and Oreffo, R.O. (2007). The control of human mesenchymal cell differentiation using nanoscale symmetry and disorder. Nature materials *6*, 997-1003.

Dalby, M.J. (2005). Topographically induced direct cell mechanotransduction. Medical engineering & physics *27*, 730-742.

Dalby, M.J., Biggs, M.J., Gadegaard, N., Kalna, G., Wilkinson, C.D., and Curtis, A.S. (2007a). Nanotopographical stimulation of mechanotransduction and changes in interphase centromere positioning. Journal of cellular biochemistry *100*, 326-338.

Dalby, M.J., Gadegaard, N., Curtis, A.S.G., and Oreffo, R.O.C. (2007c). Nanotopographical control of human osteoprogenitor differentiation. Current stem cell research & therapy *2*, 129-138.

Dalby, M.J., Gadegaard, N., and Oreffo, R.O. (2014a). Harnessing nanotopography and integrin-matrix interactions to influence stem cell fate. Nature materials *13*, 558-569.

Dalby, M.J., McCloy, D., Robertson, M., Agheli, H., Sutherland, D., Affrossman, S., and Oreffo, R.O.C. (2006a). Osteoprogenitor response to semi-ordered and random nanotopographies. Biomaterials *27*, 2980-2987.

Dalby, M.J., McCloy, D., Robertson, M., Wilkinson, C.D., and Oreffo, R.O. (2006b). Osteoprogenitor response to defined topographies with nanoscale depths. Biomaterials *27*, 1306-1315.

David A. Hoey, Shane Tormey, Stacey Ramcharan, Fergal J. O'Brien, Christopher R. Jacobs (2012), Primary Cilia-Mediated Mechanotransduction in Human Mesenchymal Stem Cells. Stem Cells 30, 2561-2570.

De Ugarte, D.A., Morizono, K., Elbarbary, A., Alfonso, Z., Zuk, P.A., Zhu, M., Dragoo, J.L., Ashjian, P., Thomas, B., Benhaim, P.*, et al.* (2003). Comparison of multi-lineage cells from human adipose tissue and bone marrow. Cells, tissues, organs *174*, 101-109.

Dmitrieva, R.I., Minullina, I.R., Bilibina, A.A., Tarasova, O.V., Anisimov, S.V., and Zaritskey, A.Y. (2012). Bone marrow- and subcutaneous adipose tissue-derived mesenchymal stem cells Differences and similarities. Cell cycle *11*, 377-383.

Damasceno-Oliveira, A., Fernandez-Duran, B., Goncalves, J., Serrao, P., Soares-da-Silva, P., Reis-Henriques, M.A., and Coimbra, J. (2007). Effects of cyclic hydrostatic pressure on the brain biogenic amines concentrations in the flounder, Platichthys flesus. General and comparative endocrinology *153*, 385-389.

de Kretser, D. (2007). Totipotent, pluripotent or unipotent stem cells: a complex regulatory enigma and fascinating biology. Journal of law and medicine *15*, 212-218.

De Rooij, D.G., and Griswold, M.D. (2012). Questions About Spermatogonia Posed and Answered Since 2000. J Androl *33*, 1085-1095.

De Ugarte, D.A., Morizono, K., Elbarbary, A., Alfonso, Z., Zuk, P.A., Zhu, M., Dragoo, J.L., Ashjian, P., Thomas, B., Benhaim, P.*, et al.* (2003a). Comparison of multi-lineage cells from human adipose tissue and bone marrow. Cells, tissues, organs *174*, 101-109.

del Rio, A., Perez-Jimenez, R., Liu, R., Roca-Cusachs, P., Fernandez, J.M., and Sheetz, M.P. (2009). Stretching Single Talin Rod Molecules Activates Vinculin Binding. Science *323*, 638-641.

Deng, Y., Saucier-Sawyer, J.K., Hoimes, C.J., Zhang, J.W., Seo, Y.E., Andrejecsk, J.W., and Saltzman, W.M. (2014). The effect of hyperbranched polyglycerol coatings on drug delivery using degradable polymer nanoparticles. Biomaterials *35*, 6595-6602.

Dewey, M.J., Filler, R., and Mintz, B. (1978). Protein patterns of developmentally totipotent mouse teratocarcinoma cells and normal early embryo cells. Developmental biology *65*, 171-182.

Dewey, M.J., Gearhart, J.D., and Mintz, B. (1977). Cell surface antigens of totipotent mouse teratocarcinoma cells grown in vivo: their relation to embryo, adult, and tumor antigens. Developmental biology *55*, 359-374.

Dmitrieva, R.I., Minullina, I.R., Bilibina, A.A., Tarasova, O.V., Anisimov, S.V., and Zaritskey, A.Y. (2012a). Bone marrow- and subcutaneous adipose tissue-derived mesenchymal stem cells Differences and similarities. Cell cycle *11*, 377-383.

Dominici, M., Le Blanc, K., Mueller, I., Slaper-Cortenbach, I., Marini, F., Krause, D., Deans, R., Keating, A., Prockop, D., and Horwitz, E. (2006). Minimal criteria for defining multipotent mesenchymal stromal cells. The International Society for Cellular Therapy position statement. Cytotherapy *8*, 315-317.

Engler, A.J., Griffin, M.A., Sen, S., Bonnemann, C.G., Sweeney, H.L., and Discher, D.E. (2004). Myotubes differentiate optimally on substrates with tissue-like stiffness: pathological implications for soft or stiff microenvironments. The Journal of cell biology *166*, 877-887.

Engler, A.J., Sen, S., Sweeney, H.L., and Discher, D.E. (2006). Matrix elasticity directs stem cell lineage specification. Cell *126*, 677-689.

Engler, A.J., Sweeney, H.L., Discher, D.E., and Schwarzbauer, J.E. (2007). Extracellular matrix elasticity directs stem cell differentiation. Journal of musculoskeletal & neuronal interactions *7*, 335.

Etheridge, M.L., Campbell, S.A., Erdman, A.G., Haynes, C.L., Wolf, S.M., and McCullough, J. (2013). The big picture on nanomedicine: the state of investigational and approved nanomedicine products. Nanomedicine *9*, 1-14.

Fang, J., Liao, L., Yin, H.Z., Nakamura, H., Shin, T., and Maeda, H. (2014). Enhanced Bacterial Tumor Delivery by Modulating the EPR Effect and Therapeutic Potential of Lactobacillus casei. Journal of pharmaceutical sciences *103*, 3235-3243.

Fei, X.M., Wu, Y.J., Chang, Z., Miao, K.R., Tang, Y.H., Zhou, X.Y., Wang, L.X., Pan, Q.Q., and Wang, C.Y. (2007). Co-culture of cord blood CD34(+) cells with human BM mesenchymal stromal cells enhances short-term engraftment of cord blood cells in NOD/SCID mice. Cytotherapy *9*, 338-347.

Feinberg, A.P., Ohlsson, R., and Henikoff, S. (2006). The epigenetic progenitor origin of human cancer. Nature reviews Genetics *7*, 21-33.

Fernandez, J.R., Garcia-Aznar, J.M., and Martinez, R. (2012). Piezoelectricity could predict sites of formation/resorption in bone remodelling and modelling. Journal of theoretical biology *292*, 86-92.

Finger, A.R., Sargent, C.Y., Dulaney, K.O., Bernacki, S.H., and Loboa, E.G. (2007). Differential effects on messenger ribonucleic acid expression by bone marrow-derived human mesenchymal stem cells seeded in agarose constructs due to ramped and steady applications of cyclic hydrostatic pressure. Tissue engineering *13*, 1151-1158.

Finkelstein, E.I., Chao, P.H.G., Hung, C.T., and Bulinski, J.C. (2007). Electric field-induced polarization of charged cell surface proteins does not determine the direction of galvanotaxis. Cell Motil Cytoskeleton *64*, 833-846.

Fisher, M.B., and Mauck, R.L. (2013). Tissue engineering and regenerative medicine: recent innovations and the transition to translation. Tissue engineering Part B, Reviews *19*, 1-13.

Friedenstein, A.J. (1976). Precursor cells of mechanocytes. International review of cytology *47*, 327-359.

Friedenstein, A.J., Petrakova, K.V., Kurolesova, A.I., and Frolova, G.P. (1968). Heterotopic of bone marrow. Analysis of precursor cells for osteogenic and hematopoietic tissues. Transplantation *6*, 230-247.

Fernandez, J.R., Garcia-Aznar, J.M., and Martinez, R. (2012). Piezoelectricity could predict sites of formation/resorption in bone remodelling and modelling. Journal of theoretical biology *292*, 86-92.

Finkelstein, E.I., Chao, P.H.G., Hung, C.T., and Bulinski, J.C. (2007). Electric field-induced polarization of charged cell surface proteins does not determine the direction of galvanotaxis. Cell Motil Cytoskeleton *64*, 833-846.

Friedenstein, A.J. (1976). Precursor cells of mechanocytes. International review of cytology *47*, 327-359.

Freeman, F.E., Haugh, M.G., and McNamara, L.M. (2015). An in vitro bone tissue regeneration strategy combining chondrogenic and vascular priming enhances the mineralization potential of mesenchymal stem cells in vitro while also allowing for vessel formation. Tissue engineering Part A *21*, 1320-1332.

Friedenstein, A.J., Petrakova, K.V., Kurolesova, A.I., and Frolova, G.P. (1968). Heterotopic of bone marrow. Analysis of precursor cells for osteogenic and hematopoietic tissues. Transplantation *6*, 230-247.

Frost, H.M. (1994). Wolff's Law and bone's structural adaptations to mechanical usage: an overview for clinicians. The Angle orthodontist *64*, 175-188.

Gaur, T., Lengner, C.J., Hovhannisyan, H., Bhat, R.A., Bodine, P.V., Komm, B.S., Javed, A., van Wijnen, A.J., Stein, J.L., Stein, G.S*., et al.* (2005). Canonical WNT signaling promotes osteogenesis by directly stimulating Runx2 gene expression. The Journal of biological chemistry *280*, 33132-33140.

Gentleman, E., Swain, R.J., Evans, N.D., Boonrungsiman, S., Jell, G., Ball, M.D., Shean, T.A., Oyen, M.L., Porter, A., and Stevens, M.M. (2009). Comparative materials differences revealed in engineered bone as a function of cell-specific differentiation. Nature materials.

Goldstein, C., Sprague, S., and Petrisor, B.A. (2010). Electrical Stimulation for Fracture Healing: Current Evidence. Journal of orthopaedic trauma *24*, S62-S65.

Gardel, L.S., Serra, L.A., Reis, R.L., and Gomes, M.E. (2014). Use of Perfusion Bioreactors and Large Animal Models for Long Bone Tissue Engineering. Tissue Eng Part B-Re *20*, 126-146.

Garvin, K., Feschuk, C., Sharp, G., and Berger, A. (2007). Does the number of quality of pluripotent bone marrow stem cells decrease with age? Clinical orthopaedics and related research, 202-207.

Gaston, J., Quinchia Rios, B., Bartlett, R., Berchtold, C., and Thibeault, S.L. (2012). The response of vocal fold fibroblasts and mesenchymal stromal cells to vibration. PloS one *7*, e30965.

Goldfarb, S.M., and Morgan, H. (2013). Nanotechnology : select assessments of the National Nanotechnology Initiative (Hauppauge, N.Y.Lancaster: Nova Science ;Gazelle distributor).

Goldstein, A.S., Juarez, T.M., Helmke, C.D., Gustin, M.C., and Mikos, A.G. (2001). Effect of convection on osteoblastic cell growth and function in biodegradable polymer foam scaffolds. Biomaterials *22*, 1279-1288.

Goldstein, C., Sprague, S., and Petrisor, B.A. (2010). Electrical Stimulation for Fracture Healing: Current Evidence. Journal of orthopaedic trauma *24*, S62-S65.

Gomez-Lopez, S., Lerner, R.G., and Petritsch, C. (2014). Asymmetric cell division of stem and progenitor cells during homeostasis and cancer. Cellular and Molecular Life Sciences *71*, 575-597.

Gowen, M., Chapman, K., Littlewood, A., Hughes, D., Evans, D., and Russell, G. (1990). Production of Tumor Necrosis Factor by Human Osteoblasts Is Modulated by Other Cytokines, but Not by Osteotropic Hormones. Endocrinology *126*, 1250-1255.

Guo, L., Zhou, Y., Wang, S., and Wu, Y. (2014). Epigenetic changes of mesenchymal stem cells in three-dimensional (3D) spheroids. J Cell Mol Med.

Ha, Y.M., Amna, T., Kim, M.H., Kim, H.C., Hassan, M.S., and Khil, M.S. (2013). Novel silicificated PVAc/POSS composite nanofibrous mat via facile electrospinning technique: potential scaffold for hard tissue engineering. Colloids and surfaces B, Biointerfaces *102*, 795-802.

Haenke, R., and Stichler, J.F. (2015). Applying Lean Six Sigma for innovative change to the post-anesthesia care unit. The Journal of nursing administration *45*, 185-187.

Hakansson, B., Brandt, A., Carlsson, P., and Tjellstrom, A. (1994). Resonance frequencies of the human skull in vivo. The Journal of the Acoustical Society of America *95*, 1474-1481.

Hakkinen, K.M., Harunaga, J.S., Doyle, A.D., and Yamada, K.M. (2011). Direct comparisons of the morphology, migration, cell adhesions, and actin cytoskeleton of fibroblasts in four different three-dimensional extracellular matrices. Tissue engineering Part A *17*, 713-724.

Hashimoto, T., Yamada, M., Iwai, T., Saitoh, A., Hashimoto, E., Ukai, W., Saito, T., and Yamada, M. (2013). Plasticity-related gene 1 is important for survival of neurons derived from rat neural stem cells. Journal of neuroscience research *91*, 1402-1407.

Hassiotou, F., Filgueira, L., and Hartmann, P.E. (2013). Breastmilk is a novel source of stem cells with multi-lineage differentiation potential. Faseb Journal *27*.

Hathout, R.M. (2014). Using principal component analysis in studying the transdermal delivery of a lipophilic drug from soft nano-colloidal carriers to develop a quantitative composition effect permeability relationship. Pharm Dev Technol *19*, 598-604.

Hauptman A, S.Y. (2005). Envisioned developments in nanobiotechnology - Nano2Life expert survey report. Tel-Aviv, Israel: Interdisciplinary Centre for Technology Analysis and Forecasting, Tel-Aviv University.

Henstock, J.R., Rotherham, M., Rose, J.B., and El Haj, A.J. (2013). Cyclic hydrostatic pressure stimulates enhanced bone development in the foetal chick femur in vitro. Bone *53*, 468-477.

Henstock, J.R., Rotherham, M., Rose, J.B., and El Haj, A.J. (2013). Cyclic hydrostatic pressure stimulates enhanced bone development in the foetal chick femur in vitro. Bone *53*, 468-477.

Hernandez, L., Kozlov, S., Piras, G., and Stewart, C.L. (2003). Paternal and maternal genomes confer opposite effects on proliferation, cell-cycle length, senescence, and tumor formation. Proceedings of the National Academy of Sciences of the United States of America *100*, 13344-13349.

Himburg, H.A., Muramoto, G.G., Daher, P., Meadows, S.K., Russell, J.L., Doan, P., Chi, J.T., Salter, A.B., Lento, W.E., Reya, T.*, et al.* (2010). Pleiotrophin regulates the expansion and regeneration of hematopoietic stem cells. Nature medicine *16*, 475-482.

Hipp, J., and Atala, A. (2008). Sources of stem cells for regenerative medicine. Stem cell reviews *4*, 3-11.

Holick, M.F. (1998). Perspective on the impact of weightlessness on calcium and bone metabolism. Bone *22*, 105S-111S.

Huang, X., Zhang, F., Wang, H., Niu, G., Choi, K.Y., Swierczewska, M., Zhang, G., Gao, H., Wang, Z., Zhu, L.*, et al.* (2013). Mesenchymal stem cell-based cell engineering with multifunctional mesoporous silica nanoparticles for tumor delivery. Biomaterials *34*, 1772-1780.

Huangfu, D., Maehr, R., Guo, W., Eijkelenboom, A., Snitow, M., Chen, A.E., and Melton, D.A. (2008). Induction of pluripotent stem cells by defined factors is greatly improved by small-molecule compounds. Nature biotechnology *26*, 795-797.

Ishimi, Y., Miyaura, C., Jin, C.H., Akatsu, T., Abe, E., Nakamura, Y., Yamaguchi, A., Yoshiki, S., Matsuda, T., Hirano, T.*, et al.* (1990). Il-6 Is Produced by Osteoblasts and Induces Bone-Resorption. Journal of immunology *145*, 3297-3303.

Ito, Y., Kimura, T., Ago, Y., Nam, K., Hiraku, K., Miyazaki, K., Masuzawa, T., and Kishida, A. (2011). Nano-vibration effect on cell adhesion and its shape. Bio-medical materials and engineering *21*, 149-158.

Iwaki, N., Karatsu, K., and Miyamoto, M. (2003). Role of guanine nucleotide exchange factors for Rho family GTPases in the regulation of cell morphology and actin cytoskeleton in fission yeast. Biochemical and biophysical research communications *312*, 414-420.

Jung, Y.J., Kim, R., Ham, H.J., Park, S.I., Lee, M.Y., Kim, J., Hwang, J., Park, M.S., Yoo, S.S., Maeng, L.S.*, et al.* (2015). Focused low-intensity pulsed ultrasound enhances bone regeneration in rat calvarial bone defect through enhancement of cell proliferation. Ultrasound in medicine & biology *41*, 999-1007.

Jang, W.G., Kim, E.J., Kim, D.K., Ryoo, H.M., Lee, K.B., Kim, S.H., Choi, H.S., and Koh, J.T. (2012). BMP2 protein regulates osteocalcin expression via Runx2-mediated Atf6 gene transcription. The Journal of biological chemistry *287*, 905-915.

Jiang, J.X., Siller-Jackson, A.J., and Burra, S. (2007). Roles of gap junctions and hemichannels in bone cell functions and in signal transmission of mechanical stress. Frontiers in bioscience *12*, 1450-1462.

Judson, R.L., Babiarz, J.E., Venere, M., and Blelloch, R. (2009). Embryonic stem cell-specific microRNAs promote induced pluripotency. Nature biotechnology *27*, 459-461.

Jungreuthmayer, C., Donahue, S.W., Jaasma, M.J., Al-Munajjed, A.A., Zanghellini, J., Kelly, D.J., and O'Brien, F.J. (2009). A Comparative Study of Shear Stresses in Collagen-Glycosaminoglycan and Calcium Phosphate Scaffolds in Bone Tissue-Engineering Bioreactors. Tissue Eng Pt A *15*, 1141-1149.

Kacena, M.A., Todd, P., Gerstenfeld, L.C., and Landis, W.J. (2004). Experiments with osteoblasts cultured under hypergravity conditions. Microgravity science and technology *15*, 28-34.

Kanczler, J.M., Ginty, P.J., White, L., Clarke, N.M., Howdle, S.M., Shakesheff, K.M., and Oreffo, R.O. (2010). The effect of the delivery of vascular endothelial growth factor and bone morphogenic protein-2 to osteoprogenitor cell populations on bone formation. Biomaterials *31*, 1242-1250.

Kang, S.B., Olson, J.L., Atala, A., and Yoo, J.J. (2012). Functional Recovery of Completely Denervated Muscle: Implications for Innervation of Tissue-Engineered Muscle. Tissue Eng Pt A *18*, 1912-1920.

Kapur, S., Baylink, D.J., and Lau, K.H. (2003). Fluid flow shear stress stimulates human osteoblast proliferation and differentiation through multiple interacting and competing signal transduction pathways. Bone *32*, 241-251.

Karin, M., and Mintz, B. (1981). Receptor-mediated endocytosis of transferrin in developmentally totipotent mouse teratocarcinoma stem cells. The Journal of biological chemistry *256*, 3245-3252.

Kaufman, M.H., Robertson, E.J., Handyside, A.H., and Evans, M.J. (1983). Establishment of Pluripotential Cell-Lines from Haploid Mouse Embryos. J Embryol Exp Morph *73*, 249-261.

Kelley, R., Werdin, E.S., Bruce, A.T., Choudhury, S., Wallace, S.M., Ilagan, R.M., Cox, B.R., Tatsumi-Ficht, P., Rivera, E.A., Spencer, T.*, et al.* (2010). Tubular cell-enriched subpopulation of primary renal cells improves survival and augments kidney function in rodent model of chronic kidney disease. American journal of physiology Renal physiology *299*, F1026-1039.

Kilian, K.A., Bugarija, B., Lahn, B.T., and Mrksich, M. (2010). Geometric cues for directing the differentiation of mesenchymal stem cells. Proceedings of the National Academy of Sciences *107*, 4872-4877.

Kim, I.S., Song, Y.M., Lee, B., and Hwang, S.J. (2012). Human mesenchymal stromal cells are mechanosensitive to vibration stimuli. Journal of dental research *91*, 1135-1140.

Kim, J., Eligehausen, S., Stehling, M., Nikol, S., Ko, K., Waltenberger, J., and Klocke, R. (2014). Generation of functional endothelial-like cells from adult mouse germline-derived pluripotent stem cells. Biochemical and biophysical research communications *443*, 700-705.

Kim, U.K., Chung, I.K., Lee, K.H., Swift, J.Q., Seong, W.J., and Ko, C.C. (2006). Bone regeneration in mandibular distraction osteogenesis combined with compression stimulation. Journal of oral and maxillofacial surgery : official journal of the American Association of Oral and Maxillofacial Surgeons *64*, 1498-1505.

Klein-Nulend, J., Bakker, A.D., Bacabac, R.G., Vatsa, A., and Weinbaum, S. (2013a). Mechanosensation and transduction in osteocytes. Bone *54*, 182-190.

Ko, K., Tapia, N., Wu, G., Kim, J.B., Bravo, M.J., Sasse, P., Glaser, T., Ruau, D., Han, D.W., Greber, B.*, et al.* (2009). Induction of pluripotency in adult unipotent germline stem cells. Cell stem cell *5*, 87-96.

Kon, K., Shiota, M., Ozeki, M., Yamashita, Y., and Kasugai, S. (2009). Bone augmentation ability of autogenous bone graft particles with different sizes: a histological and micro-computed tomography study. Clinical oral implants research *20*, 1240-1246.

Kondo, M., Wagers, A.J., Manz, M.G., Prohaska, S.S., Scherer, D.C., Beilhack, G.F., Shizuru, J.A., and Weissman, I.L. (2003). Biology of hematopoietic stem cells and progenitors: implications for clinical application. Annual review of immunology *21*, 759-806.

Kopf, J., Petersen, A., Duda, G.N., and Knaus, P. (2012). BMP2 and mechanical loading cooperatively regulate immediate early signalling events in the BMP pathway. BMC Biol *10*, 37.

Korin, N., Bransky, A., Dinnar, U., and Levenberg, S. (2009). Periodic "flow-stop" perfusion microchannel bioreactors for mammalian and human embryonic stem cell long-term culture. Biomedical microdevices *11*, 87-94.

Krampera, M., Cosmi, L., Angeli, R., Pasini, A., Liotta, F., Andreini, A., Santarlasci, V., Mazzinghi, B., Pizzolo, G., Vinante, F.*, et al.* (2006). Role for interferon-gamma in the immunomodulatory activity of human bone marrow mesenchymal stem cells. Stem Cells *24*, 386-398.

Krause, D.S., Theise, N.D., Collector, M.I., Henegariu, O., Hwang, S., Gardner, R., Neutzel, S., and Sharkis, S.J. (2001). Multi-organ, multi-lineage engraftment by a single bone marrow-derived stem cell. Cell *105*, 369-377.

Krikorian, A.D., and Steward, F.C. (1978). Morphogenetic Responses of Cultured Totipotent Cells of Carrot (Daucus carota var. carota) at Zero Gravity. Science *200*, 67-68.

Kshitiz, Park, J., Kim, P., Helen, W., Engler, A.J., Levchenko, A., and Kim, D.H. (2012). Control of stem cell fate and function by engineering physical microenvironments. Integrative biology : quantitative biosciences from nano to macro *4*, 1008-1018.

Kurosawa, H. (2007). Methods for inducing embryoid body formation: in vitro differentiation system of embryonic stem cells. Journal of bioscience and bioengineering *103*, 389-398.

Kuwabara, T., and Asashima, M. (2012). Regenerative medicine using adult neural stem cells: the potential for diabetes therapy and other pharmaceutical applications. Journal of molecular cell biology *4*, 133-139.

Kacena, M.A., Todd, P., Gerstenfeld, L.C., and Landis, W.J. (2004). Experiments with osteoblasts cultured under hypergravity conditions. Microgravity science and technology *15*, 28-34.

Kapur, S., Baylink, D.J., and Lau, K.H. (2003). Fluid flow shear stress stimulates human osteoblast proliferation and differentiation through multiple interacting and competing signal transduction pathways. Bone *32*, 241-251.

Laffosse, J.M., Kinkpe, C., Gomez-Brouchet, A., Accadbled, F., Viguier, E., Sales de Gauzy, J., and Swider, P. (2010). Micro-computed tomography study of the subchondral bone of the vertebral endplates in a porcine model: correlations with histomorphometric parameters. Surgical and radiologic anatomy : SRA *32*, 335-341.

Langer, M., Prisby, R., Peter, Z., Boistel, R., Lafage-Proust, M.H., and Peyrin, F. (2009). Quantitative investigation of bone microvascularization from 3D synchrotron micro-computed tomography in a rat model. Conference proceedings : Annual International Conference of the IEEE Engineering in Medicine and Biology Society IEEE Engineering in Medicine and Biology Society Annual Conference *2009*, 1004-1007.

Lanza, R.P. (2006). Essentials of stem cell biology (Amsterdam ; Boston: Elsevier/Academic Press).

Larson, D.R., Zipfel, W.R., Williams, R.M., Clark, S.W., Bruchez, M.P., Wise, F.W., and Webb, W.W. (2003). Water-soluble quantum dots for multiphoton fluorescence imaging in vivo. Science *300*, 1434-1436.

Lau, E., Lee, W.D., Li, J., Xiao, A., Davies, J.E., Wu, Q., Wang, L., and You, L. (2011). Effect of low-magnitude, high-frequency vibration on osteogenic differentiation of rat mesenchymal stromal cells. Journal of orthopaedic research : official publication of the Orthopaedic Research Society *29*, 1075-1080.

Ledford, K.J., Murphy, N., Zeigler, F., and Bartel, R.L. (2013). Potential beneficial effects of ixmyelocel-T in the treatment of atherosclerotic diseases. Stem cell research & therapy *4*.

Lee, E., Grooms, R., Mamidala, S., and Nagy, P. (2014a). Six easy steps on how to create a lean sigma value stream map for a multidisciplinary clinical operation. Journal of the American College of Radiology : JACR *11*, 1144-1149.

Lee, M., Jeong, S.Y., Ha, J., Kim, M., Jin, H.J., Kwon, S.J., Chang, J.W., Choi, S.J., Oh, W., Yang, Y.S.*, et al.* (2014b). Low immunogenicity of allogeneic human umbilical cord blood-derived mesenchymal stem cells in vitro and in vivo. Biochemical and biophysical research communications *446*, 983-989.

Laffosse, J.M., Kinkpe, C., Gomez-Brouchet, A., Accadbled, F., Viguier, E., Sales de Gauzy, J., and Swider, P. (2010). Micro-computed tomography study of the subchondral bone of the vertebral endplates in a porcine model: correlations with histomorphometric parameters. Surgical and radiologic anatomy : SRA *32*, 335-341.

Langer, M., Prisby, R., Peter, Z., Boistel, R., Lafage-Proust, M.H., and Peyrin, F. (2009). Quantitative investigation of bone microvascularization from 3D synchrotron micro-computed tomography in a rat model. Conference proceedings : Annual International Conference of the IEEE Engineering in Medicine and Biology Society IEEE Engineering in Medicine and Biology Society Annual Conference *2009*, 1004-1007.

Lee, N.K., Sowa, H., Hinoi, E., Ferron, M., Ahn, J.D., Confavreux, C., Dacquin, R., Mee, P.J., Mckee, M.D., Jung, D.Y.*, et al.* (2007). Endocrine regulation of energy metabolism by the skeleton. Cell *130*, 456-469.

Liu, J., Zhao, Z.H., Li, J., Zou, L., Shuler, C., Zou, Y.W., Huang, X.J., Li, M.L., and Wang, J. (2009). Hydrostatic Pressures Promote Initial Osteodifferentiation With ERK1/2 Not p38 MAPK Signaling Involved. Journal of cellular biochemistry *107*, 224-232.

Lee KL, Hoey DA, Downs ME, Jacobs CR (2012). Primary Cilia-Mediated Mechanotransduction in Bone. Clini Rev Bone Miner Metab 8, 201-212.

Lewis, S., Singh, D., and Evans, C.E. (2009). Cyclic hydrostatic pressure and cotton particles stimulate synthesis by human lung macrophages of cytokines in vitro. Respiratory research *10*, 44.

Lin, T., Ambasudhan, R., Yuan, X., Li, W., Hilcove, S., Abujarour, R., Lin, X., Hahm, H.S., Hao, E., Hayek, A.*, et al.* (2009). A chemical platform for improved induction of human iPSCs. Nature methods *6*, 805-808.

Ling, G.Q., Chen, D.B., Wang, B.Q., and Zhang, L.S. (2012). Expression of the pluripotency markers Oct3/4, Nanog and Sox2 in human breast cancer cell lines. Oncology letters *4*, 1264-1268.

Litzinger, D.C., Buiting, A.M.J., Vanrooijen, N., and Huang, L. (1994). Effect of Liposome Size on the Circulation Time and Intraorgan Distribution of Amphipathic Poly(Ethylene Glycol)-Containing Liposomes. Bba-Biomembranes *1190*, 99-107.

Liu, J., Zhao, Z.H., Li, J., Zou, L., Shuler, C., Zou, Y.W., Huang, X.J., Li, M.L., and Wang, J. (2009a). Hydrostatic Pressures Promote Initial Osteodifferentiation With ERK1/2 Not p38 MAPK Signaling Involved. Journal of cellular biochemistry *107*, 224-232.

Liu, J., Zou, L., Wang, J., Schuler, C., Zhao, Z.H., Li, X.Y., Zhang, J.Y., and Liu, Y.R. (2009b). Hydrostatic pressure promotes Wnt10b and Wnt4 expression dependent and independent on ERK signaling in early-osteoinduced MSCs. Biochemical and biophysical research communications *379*, 505-509.

Liu, Y.Q., Berendsen, A.D., Jia, S.D., Lotinun, S., Baron, R., Ferrara, N., and Olsen, B.R. (2012). Intracellular VEGF regulates the balance between osteoblast and adipocyte differentiation. Journal of Clinical Investigation *122*, 3101-3113.

Lund, A.W., Stegemann, J.P., and Plopper, G.E. (2009). Inhibition of ERK promotes collagen gel compaction and fibrillogenesis to amplify the osteogenesis of human mesenchymal stem cells in three-dimensional collagen I culture. Stem cells and development *18*, 331-341.

Lysaght, M.J. (1995). Product development in tissue engineering. Tissue engineering *1*, 221-228.

Lysaght, M.J., and Hazlehurst, A.L. (2004). Tissue engineering: the end of the beginning. Tissue engineering *10*, 309-320.

Lysaght, M.J., and Reyes, J. (2001). The growth of tissue engineering. Tissue engineering *7*, 485-493.

Macchiarini, P., Jungebluth, P., Go, T., Asnaghi, M.A., Rees, L.E., Cogan, T.A., Dodson, A., Martorell, J., Bellini, S., Parnigotto, P.P.*, et al.* (2008). Clinical transplantation of a tissue-engineered airway. Lancet *372*, 2023-2030.

Mai, Q.Y., Yu, Y., Li, T., Wang, L., Chen, M.J., Huang, S.Z., Zhou, C.Q., and Zhou, Q. (2007). Derivation of human embryonic stem cell lines from parthenogenetic blastocysts. Cell research *17*, 1008-1019.

Mason, C., and Dunnill, P. (2008). A brief definition of regenerative medicine. Regenerative medicine *3*, 1-5.

Mason, S.E., Nicolay, C.R., and Darzi, A. (2015). The use of Lean and Six Sigma methodologies in surgery: a systematic review. The surgeon : journal of the Royal Colleges of Surgeons of Edinburgh and Ireland *13*, 91-100.

Matsubara, T., Kida, K., Yamaguchi, A., Hata, K., Ichida, F., Meguro, H., Aburatani, H., Nishimura, R., and Yoneda, T. (2008). BMP2 Regulates Osterix through Msx2 and Runx2 during Osteoblast Differentiation. Journal of Biological Chemistry *283*, 29119-29125.

Maumus, M., Peyrafitte, J.A., D'Angelo, R., Fournier-Wirth, C., Bouloumie, A., Casteilla, L., Sengenes, C., and Bourin, P. (2011). Native human adipose stromal cells: localization, morphology and phenotype. International journal of obesity *35*, 1141-1153.

McBeath, R., Pirone, D.M., Nelson, C.M., Bhadriraju, K., and Chen, C.S. (2004). Cell Shape, Cytoskeletal Tension, and RhoA Regulate Stem Cell Lineage Commitment. Developmental cell *6*, 483-495.

McMurray, R.J., Gadegaard, N., Tsimbouri, P.M., Burgess, K.V., McNamara, L.E., Tare, R., Murawski, K., Kingham, E., Oreffo, R.O.C., and Dalby, M.J. (2011). Nanoscale surfaces for the long-term maintenance of mesenchymal stem cell phenotype and multipotency. Nature materials *10*, 637-644.

McNamara, L.E., McMurray, R.J., Biggs, M.J., Kantawong, F., Oreffo, R.O., and Dalby, M.J. (2010). Nanotopographical control of stem cell differentiation. Journal of tissue engineering *2010*, 120623.

Meinel, L., Karageorgiou, V., Fajardo, R., Snyder, B., Shinde-Patil, V., Zichner, L., Kaplan, D., Langer, R., and Vunjak-Novakovic, G. (2004). Bone tissue engineering using human mesenchymal stem cells: Effects of scaffold material and medium flow. Annals of biomedical engineering *32*, 112-122.

Miller, N.L., Kleinschmidt, E.G., and Schlaepfer, D.D. (2014). RhoGEFs in cell motility: novel links between Rgnef and focal adhesion kinase. Current molecular medicine *14*, 221-234.

Mimeault, M., Hauke, R., and Batra, S.K. (2007). Stem cells: a revolution in therapeutics-recent advances in stem cell biology and their therapeutic applications in regenerative medicine and cancer therapies. Clinical pharmacology and therapeutics *82*, 252-264.

Minary-Jolandan, M., and Yu, M.F. (2009). Nanoscale characterization of isolated individual type I collagen fibrils: polarization and piezoelectricity. Nanotechnology *20*.

Mintz, B. (1985). Renewal and differentiation of totipotent hematopoietic stem cells of the mouse after transplantation into early fetuses. Progress in clinical and biological research *193*, 3-16.

Mason, S.E., Nicolay, C.R., and Darzi, A. (2015). The use of Lean and Six Sigma methodologies in surgery: a systematic review. The surgeon : journal of the Royal Colleges of Surgeons of Edinburgh and Ireland *13*, 91-100.

Miyamoto, A., Shigematsu, T., Fukunaga, T., Kawakami, K., Mukai, C., and Sekiguchi, C. (1998). Medical baseline data collection on bone and muscle change with space flight. Bone *22*, 79S-82S.

Miyakoshi, J. (2006). The review of cellular effects of a static magnetic field. Science and Technology of Advanced Materials *7*, 305-307.

Miyamoto, A., Shigematsu, T., Fukunaga, T., Kawakami, K., Mukai, C., and Sekiguchi, C. (1998). Medical baseline data collection on bone and muscle change with space flight. Bone *22*, 79S-82S.

Mintz, B., Anthony, K., and Litwin, S. (1984). Monoclonal derivation of mouse myeloid and lymphoid lineages from totipotent hematopoietic stem cells experimentally engrafted in fetal hosts. Proceedings of the National Academy of Sciences of the United States of America *81*, 7835-7839.

Miyakoshi, J. (2006). The review of cellular effects of a static magnetic field. Science and Technology of Advanced Materials *7*, 305-307.

Miyauchi, A., Alvarez, J., Greenfield, E.M., Teti, A., Grano, M., Colucci, S., Zambonin-Zallone, A., Ross, F.P., Teitelbaum, S.L., Cheresh, D.*, et al.* (1991). Recognition of osteopontin and related peptides by an alpha v beta 3 integrin stimulates immediate cell signals in osteoclasts. The Journal of biological chemistry *266*, 20369-20374.

Moler, F.W., Silverstein, F.S., Holubkov, R., Slomine, B.S., Christensen, J.R., Nadkarni, V.M., Meert, K.L., Clark, A.E., Browning, B., Pemberton, V.L.*, et al.* (2015). Therapeutic hypothermia after out-of-hospital cardiac arrest in children. The New England journal of medicine *372*, 1898-1908.

Morgani, S.M., Canham, M.A., Nichols, J., Sharov, A.A., Migueles, R.P., Ko, M.S., and Brickman, J.M. (2013). Totipotent embryonic stem cells arise in ground-state culture conditions. Cell reports *3*, 1945-1957.

Morishita, R. (2014). Regenerative medicine. BioMed research international *2014*, 431540.

Myers, K.A., Shrive, N.G., and Hart, D.A. (2007). A novel apparatus applying long term intermittent cyclic hydrostatic pressure to in vitro cell cultures. Journal of bioscience and bioengineering *103*, 578-581.

Nascimento, D.S., Mosqueira, D., Sousa, L.M., Teixeira, M., Filipe, M., Resende, T.P., Araujo, A.F., Valente, M., Almeida, J., Martins, J.P.*, et al.* (2014). Human umbilical cord tissue-derived mesenchymal stromal cells attenuate remodeling after myocardial infarction by proangiogenic, antiapoptotic, and endogenous cell-activation mechanisms. Stem cell research & therapy *5*.

National Research Council (U.S.). Committee to Review the National Nanotechnology Initiative., and National Academy Press (U.S.) (2006). A matter of size : triennial review of the National Nanotechnology Initiative (Washington, D.C.: National Academies Press).

Neidlinger-Wilke, C., Wurtz, K., Liedert, A., Schmidt, C., Borm, W., Ignatius, A., Wilke, H.J., and Claes, L. (2005). A three-dimensional collagen matrix as a suitable culture system for the comparison of cyclic strain and hydrostatic pressure effects on intervertebral disc cells. Journal of neurosurgery Spine *2*, 457-465.

Neidlinger-Wilke, C., Wurtz, K., Liedert, A., Schmidt, C., Borm, W., Ignatius, A., Wilke, H.J., and Claes, L. (2005). A three-dimensional collagen matrix as a suitable culture system for the comparison of cyclic strain and hydrostatic pressure effects on intervertebral disc cells. Journal of neurosurgery Spine *2*, 457-465.

Nikukar, H., Reid, S., Tsimbouri, P.M., Riehle, M.O., Curtis, A.S., and Dalby, M.J. (2013). Osteogenesis of mesenchymal stem cells by nanoscale mechanotransduction. ACS nano *7*, 2758-2767.

Nie, S. (2009). Biomedical nanotechnology for molecular imaging, diagnostics, and targeted therapy. Conference proceedings : Annual International Conference of the IEEE Engineering in Medicine and Biology Society IEEE Engineering in Medicine and Biology Society Annual Conference *2009*, 4578-4579.

Nikukar, H., Reid, S., Tsimbouri, P.M., Riehle, M.O., Curtis, A.S., and Dalby, M.J. (2013). Osteogenesis of mesenchymal stem cells by nanoscale mechanotransduction. ACS nano *7*, 2758-2767.

Noris-Suarez, K., Lira-Olivares, J., Ferreira, A.M., Feijoo, J.L., Suarez, N., Hernandez, M.C., and Barrios, E. (2007). In vitro deposition of hydroxyapatite on cortical bone collagen stimulated by deformation-induced piezoelectricity. Biomacromolecules *8*, 941-948.

O'Neal, D.P., Hirsch, L.R., Halas, N.J., Payne, J.D., and West, J.L. (2004). Photo-thermal tumor ablation in mice using near infrared-absorbing nanoparticles. Cancer letters *209*, 171-176.

Ostlund, C., Folker, E.S., Choi, J.C., Gomes, E.R., Gundersen, G.G., and Worman, H.J. (2009). Dynamics and molecular interactions of linker of nucleoskeleton and cytoskeleton (LINC) complex proteins. Journal of cell science *122*, 4099-4108.

Ott, H.C., Clippinger, B., Conrad, C., Schuetz, C., Pomerantseva, I., Ikonomou, L., Kotton, D., and Vacanti, J.P. (2010). Regeneration and orthotopic transplantation of a bioartificial lung. Nature medicine *16*, 927-U131.

Ozaki, S., Kaneko, S., Podyma-Inoue, K.A., Yanagishita, M., and Soma, K. (2005). Modulation of extracellular matrix synthesis and alkaline phosphatase activity of periodontal ligament cells by mechanical stress. Journal of periodontal research *40*, 110-117.

Pacicca, D.M., Moore, D.C., and Ehrlich, M.G. (2002). Physiologic weight-bearing and consolidation of new bone in a rat model of distraction osteogenesis. Journal of pediatric orthopedics *22*, 652-659.

Pang, X., Yang, H., and Peng, B. (2014). Human umbilical cord mesenchymal stem cell transplantation for the treatment of chronic discogenic low back pain. Pain physician *17*, E525-530.

Pappa, K.I., and Anagnou, N.P. (2009). Novel sources of fetal stem cells: where do they fit on the developmental continuum? Regenerative medicine *4*, 423-433.

Pemberton, G.D., Childs, P., Reid, S., Nikukar, H., Tsimbouri, P.M., Gadegaard, N., Curtis, A.S., and Dalby, M.J. (2015). Nanoscale stimulation of osteoblastogenesis from mesenchymal stem cells: nanotopography and nanokicking. Nanomedicine *10*, 547-560.

Petersen, T.H., Calle, E.A., Zhao, L.P., Lee, E.J., Gui, L.Q., Raredon, M.B., Gavrilov, K., Yi, T., Zhuang, Z.W., Breuer, C.*, et al.* (2010). Tissue-Engineered Lungs for in Vivo Implantation. Science *329*, 538-541.

Peytour, Y., Villacreces, A., Chevaleyre, J., Ivanovic, Z., and Praloran, V. (2013). Discarded leukoreduction filters: A new source of stem cells for research, cell engineering and therapy? Stem cell research *11*, 736-742.

Phimphilai, M., Zhoa, Z.R., Boules, H., Roca, H., and Franceschi, R.T. (2006). BMP signaling is required for RUNX2-dependent induction of the osteoblast phenotype. Journal of Bone and Mineral Research *21*, 637-646.

Phinney, D.G., and Prockop, D.J. (2007). Concise review: mesenchymal stem/multipotent stromal cells: the state of transdifferentiation and modes of tissue repair--current views. Stem Cells *25*, 2896-2902.

Pierres, A., Benoliel, A.M., Touchard, D., and Bongrand, P. (2008). How cells tiptoe on adhesive surfaces before sticking. Biophysical journal *94*, 4114-4122.

Pierres, A., Monnet-Corti, V., Benoliel, A.M., and Bongrand, P. (2009). Do membrane undulations help cells probe the world? Trends in Cell Biology *19*, 428-433.

Pimton.P (2013). Influence of Reduced Oxygen Tension on the Differentiation of Mouse Embryonic Stem Cells into Definitive Endoderm and Distal Lung Epithelial Cells. PhD Thesis. Philadelphia PA: Drexel University.

Pogorelov, A.G., and Selezneva, II (2010). Evaluation of collagen gel microstructure by scanning electron microscopy. Bulletin of experimental biology and medicine *150*, 153-156.

Polk, J.D. (2011). Lean Six Sigma, innovation, and the change acceleration process can work together. Physician executive *37*, 38-42.

Pollack, S.R., Meaney, D.F., Levine, E.M., Litt, M., and Johnston, E.D. (2000). Numerical model and experimental validation of microcarrier motion in a rotating bioreactor. Tissue engineering *6*, 519-530.

Porter, B.D., Lin, A.S., Peister, A., Hutmacher, D., and Guldberg, R.E. (2007). Noninvasive image analysis of 3D construct mineralization in a perfusion bioreactor. Biomaterials *28*, 2525-2533.

Phimphilai, M., Zhoa, Z.R., Boules, H., Roca, H., and Franceschi, R.T. (2006). BMP signaling is required for RUNX2-dependent induction of the osteoblast phenotype. Journal of Bone and Mineral Research *21*, 637-646.

Powell, R.J., Comerota, A.J., Berceli, S.A., Guzman, R., Henry, T.D., Tzeng, E., Velazquez, O., Marston, W.A., Bartel, R.L., Longcore, A.*, et al.* (2011). Interim analysis results from the RESTORE-CLI, a randomized, double-blind multicenter phase II trial comparing expanded autologous bone marrow-derived tissue repair cells and placebo in patients with critical limb ischemia. Journal of vascular surgery *54*, 1032-1041.

Pozzobon, M., Piccoli, M., and De Coppi, P. (2013). Sources of Mesenchymal Stem Cells: Current and Future Clinical Use. Advances in biochemical engineering/biotechnology *130*, 267-286.

Pre, D., Ceccarelli, G., Gastaldi, G., Asti, A., Saino, E., Visai, L., Benazzo, F., Cusella De Angelis, M.G., and Magenes, G. (2011a). The differentiation of human adipose-derived stem cells (hASCs) into osteoblasts is promoted by low amplitude, high frequency vibration treatment. Bone *49*, 295-303.

Prodanov, L., van Loon, J.J., te Riet, J., Jansen, J.A., and Walboomers, X.F. (2013). Substrate nanotexture and hypergravity through centrifugation enhance initial osteoblastogenesis. Tissue engineering Part A *19*, 114-124.

Rauh, J., Milan, F., Gunther, K.P., and Stiehler, M. (2011a). Bioreactor Systems for Bone Tissue Engineering. Tissue Eng Part B-Re *17*, 263-280.

Ren, X., Bischoff, D., Weisgerber, D.W., Lewis, M.S., Tu, V., Yamaguchi, D.T., Miller, T.A., Harley, B.A., and Lee, J.C. (2015). Osteogenesis on nanoparticulate mineralized collagen scaffolds via autogenous activation of the canonical BMP receptor signaling pathway. Biomaterials *50*, 107-114.

Rath, S.N., Strobel, L.A., Arkudas, A., Beier, J.P., Maier, A.K., Greil, P., Horch, R.E., and Kneser, U. (2012). Osteoinduction and survival of osteoblasts and bone-marrow stromal cells in 3D biphasic calcium phosphate scaffolds under static and dynamic culture conditions. J Cell Mol Med *16*, 2350-2361.

Reinish, G.B., and Nowick, A.S. (1975). Piezoelectric Properties of Bone as Functions of Moisture-Content. Nature *253*, 626-627.

Ren, G., Roberts, A.I., and Shi, Y. (2011). Adhesion molecules: key players in Mesenchymal stem cell-mediated immunosuppression. Cell adhesion & migration *5*, 20-22.

Ren, X., Bischoff, D., Weisgerber, D.W., Lewis, M.S., Tu, V., Yamaguchi, D.T., Miller, T.A., Harley, B.A., and Lee, J.C. (2015). Osteogenesis on nanoparticulate mineralized collagen

scaffolds via autogenous activation of the canonical BMP receptor signaling pathway. Biomaterials *50*, 107-114.

RikenCenter (2013). Riken Center of Biology "Information on proposed pilot study of the safety and feasibility of transplantation of autologous hiPSC-derived retinal pigment epithelium (RPE) cell sheets in patients with neovascular age-related macular degeneration".

Robert M. Davidson, Dimitris W. Tatakis, and Anthony L. Auerbach (1990), Multiple forms of mechanosensitive ion channels in osteoblast-like cells. European Journal of physiology 416, 646-651.

Robey, P.G., Young, M.F., Flanders, K.C., Roche, N.S., Kondaiah, P., Reddi, A.H., Termine, J.D., Sporn, M.B., and Roberts, A.B. (1987). Osteoblasts synthesize and respond to transforming growth factor-type beta (TGF-beta) in vitro. The Journal of cell biology *105*, 457-463.

Rosales-Reyes, R., Skeldon, A.M., Aubert, D.F., and Valvano, M.A. (2012). The Type VI secretion system of Burkholderia cenocepacia affects multiple Rho family GTPases disrupting the actin cytoskeleton and the assembly of NADPH oxidase complex in macrophages. Cellular microbiology *14*, 255-273.

Salanki, J., and Varanka, I. (1969). Analysis of the in situ electrical activity of nerves in fresh-water mussel (Anodonta cygnea L.). Acta biologica Academiae Scientiarum Hungaricae *20*, 437-450.

Salanki, J., and Varanka, I. (1969). Analysis of the in situ electrical activity of nerves in fresh-water mussel (Anodonta cygnea L.). Acta biologica Academiae Scientiarum Hungaricae *20*, 437-450.

Salter, E., Goh, B., Hung, B., Hutton, D., Ghone, N., and Grayson, W.L. (2012). Bone tissue engineering bioreactors: a role in the clinic? Tissue engineering Part B, Reviews *18*, 62-75.

Sanchez Alvarado, A., and Yamanaka, S. (2014). Rethinking differentiation: stem cells, regeneration, and plasticity. Cell *157*, 110-119.

Sanjeev, S. Ranade, Ruhma Syeda, and Ardem Patapoutian (2015), Mechanically Activated Ion Channels, Neuron 87, 1162-1176.

Sawada, Y., Tamada, M., Dubin-Thaler, B.J., Cherniavskaya, O., Sakai, R., Tanaka, S., and Sheetz, M.P. (2006). Force sensing by mechanical extension of the Src family kinase substrate p130Cas. Cell *127*, 1015-1026.

Schepers, E., de Clercq, M., Ducheyne, P., and Kempeneers, R. (1991). Bioactive glass particulate material as a filler for bone lesions. Journal of oral rehabilitation *18*, 439-452.

Schmeckebier, S., Mauritz, C., Katsirntaki, K., Sgodda, M., Puppe, V., Duerr, J., Schubert, S.C., Schmiedl, A., Lin, Q., Palecek, J.*, et al.* (2013). Keratinocyte Growth Factor and Dexamethasone Plus Elevated cAMP Levels Synergistically Support Pluripotent Stem Cell Differentiation into Alveolar Epithelial Type II Cells. Tissue Eng Pt A *19*, 938-951.

Schu, S., Nosov, M., O'Flynn, L., Shaw, G., Treacy, O., Barry, F., Murphy, M., O'Brien, T., and Ritter, T. (2012). Immunogenicity of allogeneic mesenchymal stem cells. J Cell Mol Med *16*, 2094-2103.

Sengenes, C., Lolmede, K., Zakaroff-Girard, A., Busse, R., and Bouloumie, A. (2005). Preadipocytes in the human subcutaneous adipose tissue display distinct features from the adult mesenchymal and hematopoietic stem cells. Journal of cellular physiology *205*, 114-122.

Sensebe, L., Bourin, P., and Tarte, K. (2011). Good manufacturing practices production of mesenchymal stem/stromal cells. Human gene therapy *22*, 19-26.

Sensebe, L., Gadelorge, M., and Fleury-Cappellesso, S. (2013). Production of mesenchymal stromal/stem cells according to good manufacturing practices: a review. Stem cell research & therapy *4*, 66.

Shabbir, A., Zisa, D., Lin, H., Mastri, M., Roloff, G., Suzuki, G., and Lee, T. (2010). Activation of host tissue trophic factors through JAK-STAT3 signaling: a mechanism of mesenchymal stem cell-mediated cardiac repair. American journal of physiology Heart and circulatory physiology *299*, H1428-1438.

Shabbir, A., Zisa, D., Suzuki, G., and Lee, T. (2009). Heart failure therapy mediated by the trophic activities of bone marrow mesenchymal stem cells: a noninvasive therapeutic regimen. American journal of physiology Heart and circulatory physiology *296*, H1888-1897.

Sharma, R.R., Pollock, K., Hubel, A., and McKenna, D. (2014). Mesenchymal stem or stromal cells: a review of clinical applications and manufacturing practices. Transfusion *54*, 1418-1437.

Singla V, Reiter JF (2006), The primary cilium as the cell's antenna: Signaling at a sensory organelle, Science 313, 629-633.

Sikavitsas, V.I., Bancroft, G.N., and Mikos, A.G. (2002). Formation of three-dimensional cell/polymer constructs for bone tissue engineering in a spinner flask and a rotating wall vessel bioreactor. Journal of biomedical materials research *62*, 136-148.

Sims, N.A., and Martin, T.J. (2014). Coupling the activities of bone formation and resorption: a multitude of signals within the basic multicellular unit. BoneKEy reports *3*, 481.

Slauson, S.R., Pemberton, R., Ghosh, P., Tantillo, D.J., and Aube, J. (2015). Domino Acylation/Diels-Alder Synthesis of N-Alkyl-octahydroisoquinolin-1-one-8-carboxylic Acids under Low-Solvent Conditions. The Journal of organic chemistry *80*, 5260-5271.

Song, K., Wang, H., Zhang, B., Lim, M., Liu, Y., and Liu, T. (2013). Numerical simulation of fluid field and in vitro three-dimensional fabrication of tissue-engineered bones in a rotating bioreactor and in vivo implantation for repairing segmental bone defects. Cell stress & chaperones *18*, 193-201.

Song, S., Park, J.T., Na, J.Y., Park, M.S., Lee, J.K., Lee, M.C., and Kim, H.S. (2014). Early expressions of hypoxia-inducible factor 1alpha and vascular endothelial growth factor increase the neuronal plasticity of activated endogenous neural stem cells after focal cerebral ischemia. Neural regeneration research *9*, 912-918.

Spaeth, E., Klopp, A., Dembinski, J., Andreeff, M., and Marini, F. (2008). Inflammation and tumor microenvironments: defining the migratory itinerary of mesenchymal stem cells. Gene therapy *15*, 730-738.

Spector, J.A., Mehrara, B.J., Greenwald, J.A., Saadeh, P.B., Steinbrech, D.S., Bouletreau, P.J., Smith, L.P., and Longaker, M.T. (2001). Osteoblast expression of vascular endothelial growth factor is modulated by the extracellular microenvironment. Am J Physiol-Cell Ph *280*, C72-C80.

Steeve, K.T., Marc, P., Sandrine, T., Dominique, H., and Yannick, F. (2004). IL-6, RANKL, TNF-alpha/IL-1: interrelations in bone resorption pathophysiology. Cytokine Growth F R *15*, 49-60.

Ahn, A.C., and Grodzinsky, A.J. (2009). Relevance of collagen piezoelectricity to "Wolff's Law": a critical review. Medical engineering & physics *31*, 733-741.

Ahuja, Y.R., Bhargava, S.C., and Ratnakar, K.S. (2005). Electric and magnetic fields in stem cell research. Electromagnetic biology and medicine *24*, 121-134.

Allan, G., and Delerue, C. (2005). Unusual quantum confinement effects in IV-VI materials. Mat Sci Eng C-Bio S *25*, 687-690.

Andrew Thomas, R.B., Chiamaka Chuke-Okafor (2004). Applying lean six sigma in a small engineering company – a model for change. Journal of Manufacturing Technology Management *20*, 113 - 129.

Anton, F., Suck, K., Diederichs, S., Behr, L., Hitzmann, B., van Griensven, M., Scheper, T., and Kasper, C. (2008). Design and characterization of a rotating bed system bioreactor for tissue engineering applications. Biotechnology progress *24*, 140-147.

Ballato, A. (1998). Historical development of piezoelectric materials and applications. Ceram Trans *88*, 1-14.

Bas, A., Forsberg, G., Hammarstrom, S., and Hammarstrom, M.L. (2004). Utility of the housekeeping genes 18S rRNA, beta-actin and glyceraldehyde-3-phosphate-dehydrogenase for normalization in real-time quantitative reverse transcriptase-polymerase chain reaction analysis of gene expression in human T lymphocytes. Scandinavian journal of immunology *59*, 566-573.

Basu, J., Genheimer, C.W., Guthrie, K.I., Sangha, N., Quinlan, S.F., Bruce, A.T., Reavis, B., Halberstadt, C., Ilagan, R.M., and Ludlow, J.W. (2011). Expansion of the human adipose-derived stromal vascular cell fraction yields a population of smooth muscle-like cells with markedly distinct phenotypic and functional properties relative to mesenchymal stem cells. Tissue engineering Part C, Methods *17*, 843-860.

Basu, J., Jayo, M.J., Ilagan, R.M., Guthrie, K.I., Sangha, N., Genheimer, C.W., Quinlan, S.F., Payne, R., Knight, T., Rivera, E.*, et al.* (2012). Regeneration of native-like neo-urinary tissue from nonbladder cell sources. Tissue engineering Part A *18*, 1025-1034.

Bautista, D.S., Xuan, J.W., Hota, C., Chambers, A.F., and Harris, J.F. (1994). Inhibition of Arg-Gly-Asp (RGD)-mediated cell adhesion to osteopontin by a monoclonal antibody against osteopontin. The Journal of biological chemistry *269*, 23280-23285.

Bharali, D.J., Yalcin, M., Davis, P.J., and Mousa, S.A. (2013). Tetraiodothyroacetic acid-conjugated PLGA nanoparticles: a nanomedicine approach to treat drug-resistant breast cancer. Nanomedicine *8*, 1943-1954.

Bhoopathi, P., Gondi, C.S., Gujrati, M., Dinh, D.H., and Lakka, S.S. (2011). SPARC mediates Src-induced disruption of actin cytoskeleton via inactivation of small GTPases Rho-Rac-Cdc42. Cellular signalling *23*, 1978-1987.

Biggs, M.J.P., Richards, R.G., Gadegaard, N., Wilkinson, C.D.W., Oreffo, R.O.C., and Dalby, M.J. (2009). The use of nanoscale topography to modulate the dynamics of adhesion formation in primary osteoblasts and ERK/MAPK signalling in STRO-1+enriched skeletal stem cells. Biomaterials *30*, 5094-5103.

Bishop, M.R. (1997). Potential use of hematopoietic stem cells after radiation injury. Stem Cells *15*, 305-310.

Bjerre, L., Bunger, C., Baatrup, A., Kassem, M., and Mygind, T. (2011). Flow perfusion culture of human mesenchymal stem cells on coralline hydroxyapatite scaffolds with various pore sizes. Journal of biomedical materials research Part A *97*, 251-263.

Bjerre, L., Bunger, C.E., Kassem, M., and Mygind, T. (2008). Flow perfusion culture of human mesenchymal stem cells on silicate-substituted tricalcium phosphate scaffolds. Biomaterials *29*, 2616-2627.

Bobyn, J.D., McKenzie, K., Karabasz, D., Krygier, J.J., and Tanzer, M. (2009). Locally Delivered Bisphosphonate for Enhancement of Bone Formation and Implant Fixation. Journal of Bone and Joint Surgery-American Volume *91A*, 23-31.

Bonewald, L.F. (2007). Osteocytes as dynamic multifunctional cells. Ann Ny Acad Sci *1116*, 281-290.

Bucci, R.V., and Musitano, A. (2011). A Lean Six Sigma journey in radiology. Radiology management *33*, 27-33; quiz 34-25.

Bueno, E.M., and Glowacki, J. (2009). Cell-free and cell-based approaches for bone regeneration. Nature reviews Rheumatology *5*, 685-697.

Burack, W.R., and Sturgill, T.W. (1997). The activating dual phosphorylation of MAPK by MEK is nonprocessive. Biochemistry *36*, 5929-5933.

Caldwell, C. (2006). Lean-Six Sigma: tools for rapid cycle cost reduction. Healthcare financial management : journal of the Healthcare Financial Management Association *60*, 96-98.

Candiani, G., Raimondi, M.T., Aurora, R., Lagana, K., and Dubini, G. (2008). Chondrocyte response to high regimens of cyclic hydrostatic pressure in 3-dimensional engineered constructs. The International journal of artificial organs *31*, 490-499.

Caplan, A.I. (1991). Mesenchymal stem cells. Journal of orthopaedic research : official publication of the Orthopaedic Research Society *9*, 641-650.

Caplan, A.I. (1994). The mesengenic process. Clinics in plastic surgery *21*, 429-435.

Cauffman, G., De Rycke, M., Sermon, K., Liebaers, I., and Van de Velde, H. (2009). Markers that define stemness in ESC are unable to identify the totipotent cells in human preimplantation embryos. Human reproduction *24*, 63-70.

Celil, A.B., and Campbell, P.G. (2005). BMP-2 and insulin-like growth factor-I mediate osterix (Osx) expression in human mesenchymal stem cells via the MAPK and protein kinase D signaling pathways. Journal of Biological Chemistry *280*, 31353-31359.

Chen, J.H., Liu, C., You, L., and Simmons, C.A. (2010). Boning up on Wolff's Law: mechanical regulation of the cells that make and maintain bone. Journal of biomechanics *43*, 108-118.

Chistiakov, D.A. (2012). Liver regenerative medicine: advances and challenges. Cells, tissues, organs *196*, 291-312.

Choi, Y.K., Cho, H., Seo, Y.K., Yoon, H.H., and Park, J.K. (2012). Stimulation of sub-sonic vibration promotes the differentiation of adipose tissue-derived mesenchymal stem cells into neural cells. Life sciences *91*, 329-337.

Cifarelli, R.A., D'Onofrio, O., Grillo, R., Mango, T., Cellini, F., Piarulli, L., Simeone, R., Giancaspro, A., Colasuonno, P., Blanco, A.*, et al.* (2013). Development of a new wheat microarray from a durum wheat totipotent cDNA library used for a powdery mildew resistance study. Cellular & molecular biology letters *18*, 231-248.

Claes, L., and Willie, B. (2007). The enhancement of bone regeneration by ultrasound. Progress in biophysics and molecular biology *93*, 384-398.

Cohen, D.J., Nelson, W.J., and Maharbiz, M.M. (2014). Galvanotactic control of collective cell migration in epithelial monolayers. Nature materials *13*, 409-417.

Conese, M., Piro, D., Carbone, A., Castellani, S., and Di Gioia, S. (2014). Hematopoietic and mesenchymal stem cells for the treatment of chronic respiratory diseases: role of plasticity and heterogeneity. TheScientificWorldJournal *2014*, 859817.

Conrad, C., and Huss, R. (2005). Adult stem cell lines in regenerative medicine and reconstructive surgery. Journal of Surgical Research *124*, 201-208.

Coquelin, L., Fialaire-Legendre, A., Roux, S., Poignard, A., Bierling, P., Hernigou, P., Chevallier, N., and Rouard, H. (2012). In vivo and in vitro comparison of three different allografts vitalized with human mesenchymal stromal cells. Tissue engineering Part A *18*, 1921-1931.

Crisan, M., Yap, S., Casteilla, L., Chen, C.W., Corselli, M., Park, T.S., Andriolo, G., Sun, B., Zheng, B., Zhang, L.*, et al.* (2008). A perivascular origin for mesenchymal stem cells in multiple human organs. Cell stem cell *3*, 301-313.

Cronmiller, C., and Mintz, B. (1978). Karyotypic normalcy and quasi-normalcy of developmentally totipotent mouse teratocarcinoma cells. Developmental biology *67*, 465-477.

Crowder, S.W., Liang, Y., Rath, R., Park, A.M., Maltais, S., Pintauro, P.N., Hofmeister, W., Lim, C.C., Wang, X., and Sung, H.J. (2013). Poly(epsilon-caprolactone)-carbon nanotube composite scaffolds for enhanced cardiac differentiation of human mesenchymal stem cells. Nanomedicine *8*, 1763-1776.

Cukierman, E., Pankov, R., Stevens, D.R., and Yamada, K.M. (2001). Taking cell-matrix adhesions to the third dimension. Science *294*, 1708-1712.

Curtis, A., Reid, S., Martin, I., Vaidyanathan, R., Smith, C.A., Nikukar, H., and Dalby, M. (2013a). Cell Interactions at the Nanoscale:Piezoelectric Stimulation. IEEE Trans Nanobioscience *12*, 247-254.

Curtis, A.S.G., Reid, S., Martin, I., Vaidyanathan, R., Smith, C.A., Nikukar, H., and Dalby, M.J. (2013b). Cell Interactions at the Nanoscale: Piezoelectric Stimulation. Ieee T Nanobiosci *12*, 247-254.

Dahl, S.L.M., Kypson, A.P., Lawson, J.H., Blum, J.L., Strader, J.T., Li, Y.L., Manson, R.J., Tente, W.E., DiBernardo, L., Hensley, M.T.*, et al.* (2011). Readily Available Tissue-Engineered Vascular Grafts. Science translational medicine *3*.

Dalby, M.J. (2005). Topographically induced direct cell mechanotransduction. Medical engineering & physics *27*, 730-742.

Dalby, M.J., Biggs, M.J., Gadegaard, N., Kalna, G., Wilkinson, C.D., and Curtis, A.S. (2007a). Nanotopographical stimulation of mechanotransduction and changes in interphase centromere positioning. Journal of cellular biochemistry *100*, 326-338.

Dalby, M.J., Biggs, M.J.P., Gadegaard, N., Kalna, G., Wilkinson, C.D.W., and Curtis, A.S.G. (2007b). Nanotopographical stimulation of mechanotransduction and changes in interphase centromere positioning. Journal of cellular biochemistry *100*, 326-338.

Dalby, M.J., Gadegaard, N., Curtis, A.S.G., and Oreffo, R.O.C. (2007c). Nanotopographical control of human osteoprogenitor differentiation. Current stem cell research & therapy *2*, 129-138.

Dalby, M.J., Gadegaard, N., and Oreffo, R.O. (2014a). Harnessing nanotopography and integrin-matrix interactions to influence stem cell fate. Nature materials *13*, 558-569.

Dalby, M.J., Gadegaard, N., and Oreffo, R.O.C. (2014b). Harnessing nanotopography and integrin-matrix interactions to influence stem cell fate. Nature materials *13*, 558-569.

Dalby, M.J., Gadegaard, N., Tare, R., Andar, A., Riehle, M.O., Herzyk, P., Wilkinson, C.D., and Oreffo, R.O. (2007d). The control of human mesenchymal cell differentiation using nanoscale symmetry and disorder. Nature materials *6*, 997-1003.

Dalby, M.J., McCloy, D., Robertson, M., Agheli, H., Sutherland, D., Affrossman, S., and Oreffo, R.O.C. (2006a). Osteoprogenitor response to semi-ordered and random nanotopographies. Biomaterials *27*, 2980-2987.

Dalby, M.J., McCloy, D., Robertson, M., Wilkinson, C.D., and Oreffo, R.O. (2006b). Osteoprogenitor response to defined topographies with nanoscale depths. Biomaterials *27*, 1306-1315.

Damasceno-Oliveira, A., Fernandez-Duran, B., Goncalves, J., Serrao, P., Soares-da-Silva, P., Reis-Henriques, M.A., and Coimbra, J. (2007). Effects of cyclic hydrostatic pressure on the brain biogenic amines concentrations in the flounder, Platichthys flesus. General and comparative endocrinology *153*, 385-389.

de Kretser, D. (2007). Totipotent, pluripotent or unipotent stem cells: a complex regulatory enigma and fascinating biology. Journal of law and medicine *15*, 212-218.

De Rooij, D.G., and Griswold, M.D. (2012). Questions About Spermatogonia Posed and Answered Since 2000. J Androl *33*, 1085-1095.

De Ugarte, D.A., Morizono, K., Elbarbary, A., Alfonso, Z., Zuk, P.A., Zhu, M., Dragoo, J.L., Ashjian, P., Thomas, B., Benhaim, P*., et al.* (2003a). Comparison of multi-lineage cells from human adipose tissue and bone marrow. Cells, tissues, organs *174*, 101-109.

De Ugarte, D.A., Morizono, K., Elbarbary, A., Alfonso, Z., Zuk, P.A., Zhu, M., Dragoo, J.L., Ashjian, P., Thomas, B., Benhaim, P*., et al.* (2003b). Comparison of multi-lineage cells from human adipose tissue and bone marrow. Cells, tissues, organs *174*, 101-109.

del Rio, A., Perez-Jimenez, R., Liu, R., Roca-Cusachs, P., Fernandez, J.M., and Sheetz, M.P. (2009). Stretching Single Talin Rod Molecules Activates Vinculin Binding. Science *323*, 638-641.

Deng, Y., Saucier-Sawyer, J.K., Hoimes, C.J., Zhang, J.W., Seo, Y.E., Andrejecsk, J.W., and Saltzman, W.M. (2014). The effect of hyperbranched polyglycerol coatings on drug delivery using degradable polymer nanoparticles. Biomaterials *35*, 6595-6602.

Dewey, M.J., Filler, R., and Mintz, B. (1978). Protein patterns of developmentally totipotent mouse teratocarcinoma cells and normal early embryo cells. Developmental biology *65*, 171-182.

Dewey, M.J., Gearhart, J.D., and Mintz, B. (1977). Cell surface antigens of totipotent mouse teratocarcinoma cells grown in vivo: their relation to embryo, adult, and tumor antigens. Developmental biology *55*, 359-374.

Dmitrieva, R.I., Minullina, I.R., Bilibina, A.A., Tarasova, O.V., Anisimov, S.V., and Zaritskey, A.Y. (2012a). Bone marrow- and subcutaneous adipose tissue-derived mesenchymal stem cells Differences and similarities. Cell cycle *11*, 377-383.

Dmitrieva, R.I., Minullina, I.R., Bilibina, A.A., Tarasova, O.V., Anisimov, S.V., and Zaritskey, A.Y. (2012b). Bone marrow- and subcutaneous adipose tissue-derived mesenchymal stem cells: differences and similarities. Cell cycle *11*, 377-383.

Dominici, M., Le Blanc, K., Mueller, I., Slaper-Cortenbach, I., Marini, F., Krause, D., Deans, R., Keating, A., Prockop, D., and Horwitz, E. (2006). Minimal criteria for defining multipotent mesenchymal stromal cells. The International Society for Cellular Therapy position statement. Cytotherapy *8*, 315-317.

Engler, A.J., Griffin, M.A., Sen, S., Bonnemann, C.G., Sweeney, H.L., and Discher, D.E. (2004). Myotubes differentiate optimally on substrates with tissue-like stiffness: pathological implications for soft or stiff microenvironments. The Journal of cell biology *166*, 877-887.

Engler, A.J., Sen, S., Sweeney, H.L., and Discher, D.E. (2006). Matrix elasticity directs stem cell lineage specification. Cell *126*, 677-689.

Engler, A.J., Sweeney, H.L., Discher, D.E., and Schwarzbauer, J.E. (2007). Extracellular matrix elasticity directs stem cell differentiation. Journal of musculoskeletal & neuronal interactions *7*, 335.

Etheridge, M.L., Campbell, S.A., Erdman, A.G., Haynes, C.L., Wolf, S.M., and McCullough, J. (2013). The big picture on nanomedicine: the state of investigational and approved nanomedicine products. Nanomedicine *9*, 1-14.

Fang, J., Liao, L., Yin, H.Z., Nakamura, H., Shin, T., and Maeda, H. (2014). Enhanced Bacterial Tumor Delivery by Modulating the EPR Effect and Therapeutic Potential of Lactobacillus casei. Journal of pharmaceutical sciences *103*, 3235-3243.

Fei, X.M., Wu, Y.J., Chang, Z., Miao, K.R., Tang, Y.H., Zhou, X.Y., Wang, L.X., Pan, Q.Q., and Wang, C.Y. (2007). Co-culture of cord blood CD34(+) cells with human BM mesenchymal stromal cells enhances short-term engraftment of cord blood cells in NOD/SCID mice. Cytotherapy *9*, 338-347.

Feinberg, A.P., Ohlsson, R., and Henikoff, S. (2006). The epigenetic progenitor origin of human cancer. Nature reviews Genetics *7*, 21-33.

Fernandez, J.R., Garcia-Aznar, J.M., and Martinez, R. (2012). Piezoelectricity could predict sites of formation/resorption in bone remodelling and modelling. Journal of theoretical biology *292*, 86-92.

Finger, A.R., Sargent, C.Y., Dulaney, K.O., Bernacki, S.H., and Loboa, E.G. (2007). Differential effects on messenger ribonucleic acid expression by bone marrow-derived human mesenchymal stem cells seeded in agarose constructs due to ramped and steady applications of cyclic hydrostatic pressure. Tissue engineering *13*, 1151-1158.

Finkelstein, E.I., Chao, P.H.G., Hung, C.T., and Bulinski, J.C. (2007). Electric field-induced polarization of charged cell surface proteins does not determine the direction of galvanotaxis. Cell Motil Cytoskeleton *64*, 833-846.

Fisher, M.B., and Mauck, R.L. (2013). Tissue engineering and regenerative medicine: recent innovations and the transition to translation. Tissue engineering Part B, Reviews *19*, 1-13.

Friedenstein, A.J. (1976). Precursor cells of mechanocytes. International review of cytology *47*, 327-359.

Friedenstein, A.J., Petrakova, K.V., Kurolesova, A.I., and Frolova, G.P. (1968). Heterotopic of bone marrow. Analysis of precursor cells for osteogenic and hematopoietic tissues. Transplantation *6*, 230-247.

Gardel, L.S., Serra, L.A., Reis, R.L., and Gomes, M.E. (2014). Use of Perfusion Bioreactors and Large Animal Models for Long Bone Tissue Engineering. Tissue Eng Part B-Re *20*, 126-146.

Garvin, K., Feschuk, C., Sharp, G., and Berger, A. (2007). Does the number of quality of pluripotent bone marrow stem cells decrease with age? Clinical orthopaedics and related research, 202-207.

Gaston, J., Quinchia Rios, B., Bartlett, R., Berchtold, C., and Thibeault, S.L. (2012). The response of vocal fold fibroblasts and mesenchymal stromal cells to vibration. PloS one *7*, e30965.

Gaur, T., Lengner, C.J., Hovhannisyan, H., Bhat, R.A., Bodine, P.V., Komm, B.S., Javed, A., van Wijnen, A.J., Stein, J.L., Stein, G.S.*, et al.* (2005). Canonical WNT signaling promotes osteogenesis by directly stimulating Runx2 gene expression. The Journal of biological chemistry *280*, 33132-33140.

Gentleman, E., Swain, R.J., Evans, N.D., Boonrungsiman, S., Jell, G., Ball, M.D., Shean, T.A., Oyen, M.L., Porter, A., and Stevens, M.M. (2009). Comparative materials differences revealed in engineered bone as a function of cell-specific differentiation. Nature materials.

Goldfarb, S.M., and Morgan, H. (2013). Nanotechnology : select assessments of the National Nanotechnology Initiative (Hauppauge, N.Y.

Lancaster: Nova Science ;

Gazelle distributor).

Goldstein, A.S., Juarez, T.M., Helmke, C.D., Gustin, M.C., and Mikos, A.G. (2001). Effect of convection on osteoblastic cell growth and function in biodegradable polymer foam scaffolds. Biomaterials *22*, 1279-1288.

Goldstein, C., Sprague, S., and Petrisor, B.A. (2010). Electrical Stimulation for Fracture Healing: Current Evidence. Journal of orthopaedic trauma *24*, S62-S65.

Gomez-Lopez, S., Lerner, R.G., and Petritsch, C. (2014). Asymmetric cell division of stem and progenitor cells during homeostasis and cancer. Cellular and Molecular Life Sciences *71*, 575-597.

Gowen, M., Chapman, K., Littlewood, A., Hughes, D., Evans, D., and Russell, G. (1990). Production of Tumor Necrosis Factor by Human Osteoblasts Is Modulated by Other Cytokines, but Not by Osteotropic Hormones. Endocrinology *126*, 1250-1255.

Guo, L., Zhou, Y., Wang, S., and Wu, Y. (2014). Epigenetic changes of mesenchymal stem cells in three-dimensional (3D) spheroids. J Cell Mol Med.

Ha, Y.M., Amna, T., Kim, M.H., Kim, H.C., Hassan, M.S., and Khil, M.S. (2013). Novel silicificated PVAc/POSS composite nanofibrous mat via facile electrospinning technique: potential scaffold for hard tissue engineering. Colloids and surfaces B, Biointerfaces *102*, 795-802.

Haenke, R., and Stichler, J.F. (2015). Applying Lean Six Sigma for innovative change to the post-anesthesia care unit. The Journal of nursing administration *45*, 185-187.

Hakansson, B., Brandt, A., Carlsson, P., and Tjellstrom, A. (1994). Resonance frequencies of the human skull in vivo. The Journal of the Acoustical Society of America *95*, 1474-1481.

Hakkinen, K.M., Harunaga, J.S., Doyle, A.D., and Yamada, K.M. (2011). Direct comparisons of the morphology, migration, cell adhesions, and actin cytoskeleton of fibroblasts in four different three-dimensional extracellular matrices. Tissue engineering Part A *17*, 713-724.

Hashimoto, T., Yamada, M., Iwai, T., Saitoh, A., Hashimoto, E., Ukai, W., Saito, T., and Yamada, M. (2013). Plasticity-related gene 1 is important for survival of neurons derived from rat neural stem cells. Journal of neuroscience research *91*, 1402-1407.

Hassiotou, F., Filgueira, L., and Hartmann, P.E. (2013). Breastmilk is a novel source of stem cells with multi-lineage differentiation potential. Faseb Journal *27*.

Hathout, R.M. (2014). Using principal component analysis in studying the transdermal delivery of a lipophilic drug from soft nano-colloidal carriers to develop a quantitative composition effect permeability relationship. Pharm Dev Technol *19*, 598-604.

Hauptman A, S.Y. (2005). Envisioned developments in nanobiotechnology - Nano2Life expert survey report. Tel-Aviv, Israel: Interdisciplinary Centre for Technology Analysis and Forecasting, Tel-Aviv University.

Henstock, J.R., Rotherham, M., Rose, J.B., and El Haj, A.J. (2013). Cyclic hydrostatic pressure stimulates enhanced bone development in the foetal chick femur in vitro. Bone *53*, 468-477.

Hernandez, L., Kozlov, S., Piras, G., and Stewart, C.L. (2003). Paternal and maternal genomes confer opposite effects on proliferation, cell-cycle length, senescence, and tumor formation. Proceedings of the National Academy of Sciences of the United States of America *100*, 13344-13349.

Himburg, H.A., Muramoto, G.G., Daher, P., Meadows, S.K., Russell, J.L., Doan, P., Chi, J.T., Salter, A.B., Lento, W.E., Reya, T.*, et al.* (2010). Pleiotrophin regulates the expansion and regeneration of hematopoietic stem cells. Nature medicine *16*, 475-482.

Hipp, J., and Atala, A. (2008). Sources of stem cells for regenerative medicine. Stem cell reviews *4*, 3-11.

Holick, M.F. (1998). Perspective on the impact of weightlessness on calcium and bone metabolism. Bone *22*, 105S-111S.

Huang, X., Zhang, F., Wang, H., Niu, G., Choi, K.Y., Swierczewska, M., Zhang, G., Gao, H., Wang, Z., Zhu, L.*, et al.* (2013). Mesenchymal stem cell-based cell engineering with multifunctional mesoporous silica nanoparticles for tumor delivery. Biomaterials *34*, 1772-1780.

Huangfu, D., Maehr, R., Guo, W., Eijkelenboom, A., Snitow, M., Chen, A.E., and Melton, D.A. (2008). Induction of pluripotent stem cells by defined factors is greatly improved by small-molecule compounds. Nature biotechnology *26*, 795-797.

Ishimi, Y., Miyaura, C., Jin, C.H., Akatsu, T., Abe, E., Nakamura, Y., Yamaguchi, A., Yoshiki, S., Matsuda, T., Hirano, T.*, et al.* (1990). Il-6 Is Produced by Osteoblasts and Induces Bone-Resorption. Journal of immunology *145*, 3297-3303.

Ito, Y., Kimura, T., Ago, Y., Nam, K., Hiraku, K., Miyazaki, K., Masuzawa, T., and Kishida, A. (2011). Nano-vibration effect on cell adhesion and its shape. Bio-medical materials and engineering *21*, 149-158.

Iwaki, N., Karatsu, K., and Miyamoto, M. (2003). Role of guanine nucleotide exchange factors for Rho family GTPases in the regulation of cell morphology and actin cytoskeleton in fission yeast. Biochemical and biophysical research communications *312*, 414-420.

Jang, W.G., Kim, E.J., Kim, D.K., Ryoo, H.M., Lee, K.B., Kim, S.H., Choi, H.S., and Koh, J.T. (2012). BMP2 protein regulates osteocalcin expression via Runx2-mediated Atf6 gene transcription. The Journal of biological chemistry *287*, 905-915.

Jiang, J.X., Siller-Jackson, A.J., and Burra, S. (2007). Roles of gap junctions and hemichannels in bone cell functions and in signal transmission of mechanical stress. Frontiers in bioscience *12*, 1450-1462.

Judson, R.L., Babiarz, J.E., Venere, M., and Blelloch, R. (2009). Embryonic stem cell-specific microRNAs promote induced pluripotency. Nature biotechnology *27*, 459-461.

Jungreuthmayer, C., Donahue, S.W., Jaasma, M.J., Al-Munajjed, A.A., Zanghellini, J., Kelly, D.J., and O'Brien, F.J. (2009). A Comparative Study of Shear Stresses in Collagen-Glycosaminoglycan and Calcium Phosphate Scaffolds in Bone Tissue-Engineering Bioreactors. Tissue Eng Pt A *15*, 1141-1149.

Kacena, M.A., Todd, P., Gerstenfeld, L.C., and Landis, W.J. (2004). Experiments with osteoblasts cultured under hypergravity conditions. Microgravity science and technology *15*, 28-34.

Kanczler, J.M., Ginty, P.J., White, L., Clarke, N.M., Howdle, S.M., Shakesheff, K.M., and Oreffo, R.O. (2010). The effect of the delivery of vascular endothelial growth factor and bone morphogenic protein-2 to osteoprogenitor cell populations on bone formation. Biomaterials *31*, 1242-1250.

Kang, S.B., Olson, J.L., Atala, A., and Yoo, J.J. (2012). Functional Recovery of Completely Denervated Muscle: Implications for Innervation of Tissue-Engineered Muscle. Tissue Eng Pt A *18*, 1912-1920.

Kapur, S., Baylink, D.J., and Lau, K.H. (2003). Fluid flow shear stress stimulates human osteoblast proliferation and differentiation through multiple interacting and competing signal transduction pathways. Bone *32*, 241-251.

Karin, M., and Mintz, B. (1981). Receptor-mediated endocytosis of transferrin in developmentally totipotent mouse teratocarcinoma stem cells. The Journal of biological chemistry *256*, 3245-3252.

Kaufman, M.H., Robertson, E.J., Handyside, A.H., and Evans, M.J. (1983). Establishment of Pluripotential Cell-Lines from Haploid Mouse Embryos. J Embryol Exp Morph *73*, 249-261.

Kelley, R., Werdin, E.S., Bruce, A.T., Choudhury, S., Wallace, S.M., Ilagan, R.M., Cox, B.R., Tatsumi-Ficht, P., Rivera, E.A., Spencer, T.*, et al.* (2010). Tubular cell-enriched subpopulation of primary renal cells improves survival and augments kidney function in rodent model of chronic kidney disease. American journal of physiology Renal physiology *299*, F1026-1039.

Kilian, K.A., Bugarija, B., Lahn, B.T., and Mrksich, M. (2010). Geometric cues for directing the differentiation of mesenchymal stem cells. Proceedings of the National Academy of Sciences *107*, 4872-4877.

Kim, I.S., Song, Y.M., Lee, B., and Hwang, S.J. (2012). Human mesenchymal stromal cells are mechanosensitive to vibration stimuli. Journal of dental research *91*, 1135-1140.

Kim, J., Eligehausen, S., Stehling, M., Nikol, S., Ko, K., Waltenberger, J., and Klocke, R. (2014). Generation of functional endothelial-like cells from adult mouse germline-derived pluripotent stem cells. Biochemical and biophysical research communications *443*, 700-705.

Kim, U.K., Chung, I.K., Lee, K.H., Swift, J.Q., Seong, W.J., and Ko, C.C. (2006). Bone regeneration in mandibular distraction osteogenesis combined with compression stimulation. Journal of oral and maxillofacial surgery : official journal of the American Association of Oral and Maxillofacial Surgeons *64*, 1498-1505.

Klein-Nulend, J., Bakker, A.D., Bacabac, R.G., Vatsa, A., and Weinbaum, S. (2013a). Mechanosensation and transduction in osteocytes. Bone *54*, 182-190.

Klein-Nulend, J., Bakker, A.D., Bacabac, R.G., Vatsa, A., and Weinbaum, S. (2013b). Mechanosensation and transduction in osteocytes. Bone *54*, 182-190.

Ko, K., Tapia, N., Wu, G., Kim, J.B., Bravo, M.J., Sasse, P., Glaser, T., Ruau, D., Han, D.W., Greber, B.*, et al.* (2009). Induction of pluripotency in adult unipotent germline stem cells. Cell stem cell *5*, 87-96.

Kon, K., Shiota, M., Ozeki, M., Yamashita, Y., and Kasugai, S. (2009). Bone augmentation ability of autogenous bone graft particles with different sizes: a histological and micro-computed tomography study. Clinical oral implants research *20*, 1240-1246.

Kondo, M., Wagers, A.J., Manz, M.G., Prohaska, S.S., Scherer, D.C., Beilhack, G.F., Shizuru, J.A., and Weissman, I.L. (2003). Biology of hematopoietic stem cells and progenitors: implications for clinical application. Annual review of immunology *21*, 759-806.

Kopf, J., Petersen, A., Duda, G.N., and Knaus, P. (2012). BMP2 and mechanical loading cooperatively regulate immediate early signalling events in the BMP pathway. BMC Biol *10*, 37.

Korin, N., Bransky, A., Dinnar, U., and Levenberg, S. (2009). Periodic "flow-stop" perfusion microchannel bioreactors for mammalian and human embryonic stem cell long-term culture. Biomedical microdevices *11*, 87-94.

Krampera, M., Cosmi, L., Angeli, R., Pasini, A., Liotta, F., Andreini, A., Santarlasci, V., Mazzinghi, B., Pizzolo, G., Vinante, F.*, et al.* (2006). Role for interferon-gamma in the immunomodulatory activity of human bone marrow mesenchymal stem cells. Stem Cells *24*, 386-398.

Krause, D.S., Theise, N.D., Collector, M.I., Henegariu, O., Hwang, S., Gardner, R., Neutzel, S., and Sharkis, S.J. (2001). Multi-organ, multi-lineage engraftment by a single bone marrow-derived stem cell. Cell *105*, 369-377.

Krikorian, A.D., and Steward, F.C. (1978). Morphogenetic Responses of Cultured Totipotent Cells of Carrot (Daucus carota var. carota) at Zero Gravity. Science *200*, 67-68.

Kshitiz, Park, J., Kim, P., Helen, W., Engler, A.J., Levchenko, A., and Kim, D.H. (2012). Control of stem cell fate and function by engineering physical microenvironments. Integrative biology : quantitative biosciences from nano to macro *4*, 1008-1018.

Kurosawa, H. (2007). Methods for inducing embryoid body formation: in vitro differentiation system of embryonic stem cells. Journal of bioscience and bioengineering *103*, 389-398.

Kuwabara, T., and Asashima, M. (2012). Regenerative medicine using adult neural stem cells: the potential for diabetes therapy and other pharmaceutical applications. Journal of molecular cell biology *4*, 133-139.

Laffosse, J.M., Kinkpe, C., Gomez-Brouchet, A., Accadbled, F., Viguier, E., Sales de Gauzy, J., and Swider, P. (2010). Micro-computed tomography study of the subchondral bone of the vertebral endplates in a porcine model: correlations with histomorphometric parameters. Surgical and radiologic anatomy : SRA *32*, 335-341.

Langer, M., Prisby, R., Peter, Z., Boistel, R., Lafage-Proust, M.H., and Peyrin, F. (2009). Quantitative investigation of bone microvascularization from 3D synchrotron micro-computed tomography in a rat model. Conference proceedings : Annual International Conference of the IEEE Engineering in Medicine and Biology Society IEEE Engineering in Medicine and Biology Society Annual Conference *2009*, 1004-1007.

Lanza, R.P. (2006). Essentials of stem cell biology (Amsterdam ; Boston: Elsevier/Academic Press).

Larson, D.R., Zipfel, W.R., Williams, R.M., Clark, S.W., Bruchez, M.P., Wise, F.W., and Webb, W.W. (2003). Water-soluble quantum dots for multiphoton fluorescence imaging in vivo. Science *300*, 1434-1436.

Lau, E., Lee, W.D., Li, J., Xiao, A., Davies, J.E., Wu, Q., Wang, L., and You, L. (2011). Effect of low-magnitude, high-frequency vibration on osteogenic differentiation of rat mesenchymal stromal cells. Journal of orthopaedic research : official publication of the Orthopaedic Research Society *29*, 1075-1080.

Ledford, K.J., Murphy, N., Zeigler, F., and Bartel, R.L. (2013). Potential beneficial effects of ixmyelocel-T in the treatment of atherosclerotic diseases. Stem cell research & therapy *4*.

Lee, M., Jeong, S.Y., Ha, J., Kim, M., Jin, H.J., Kwon, S.J., Chang, J.W., Choi, S.J., Oh, W., Yang, Y.S.*, et al.* (2014). Low immunogenicity of allogeneic human umbilical cord blood-derived mesenchymal stem cells in vitro and in vivo. Biochemical and biophysical research communications *446*, 983-989.

Lee, N.K., Sowa, H., Hinoi, E., Ferron, M., Ahn, J.D., Confavreux, C., Dacquin, R., Mee, P.J., Mckee, M.D., Jung, D.Y.*, et al.* (2007). Endocrine regulation of energy metabolism by the skeleton. Cell *130*, 456-469.

Lewis, S., Singh, D., and Evans, C.E. (2009). Cyclic hydrostatic pressure and cotton particles stimulate synthesis by human lung macrophages of cytokines in vitro. Respiratory research *10*, 44.

Lin, T., Ambasudhan, R., Yuan, X., Li, W., Hilcove, S., Abujarour, R., Lin, X., Hahm, H.S., Hao, E., Hayek, A.*, et al.* (2009). A chemical platform for improved induction of human iPSCs. Nature methods *6*, 805-808.

Ling, G.Q., Chen, D.B., Wang, B.Q., and Zhang, L.S. (2012). Expression of the pluripotency markers Oct3/4, Nanog and Sox2 in human breast cancer cell lines. Oncology letters *4*, 1264-1268.

Litzinger, D.C., Buiting, A.M.J., Vanrooijen, N., and Huang, L. (1994). Effect of Liposome Size on the Circulation Time and Intraorgan Distribution of Amphipathic Poly(Ethylene Glycol)-Containing Liposomes. Bba-Biomembranes *1190*, 99-107.

Liu, J., Zhao, Z.H., Li, J., Zou, L., Shuler, C., Zou, Y.W., Huang, X.J., Li, M.L., and Wang, J. (2009a). Hydrostatic Pressures Promote Initial Osteodifferentiation With ERK1/2 Not p38 MAPK Signaling Involved. Journal of cellular biochemistry *107*, 224-232.

Liu, J., Zou, L., Wang, J., Schuler, C., Zhao, Z.H., Li, X.Y., Zhang, J.Y., and Liu, Y.R. (2009b). Hydrostatic pressure promotes Wnt10b and Wnt4 expression dependent and independent on ERK signaling in early-osteoinduced MSCs. Biochemical and biophysical research communications *379*, 505-509.

Liu, Y.Q., Berendsen, A.D., Jia, S.D., Lotinun, S., Baron, R., Ferrara, N., and Olsen, B.R. (2012). Intracellular VEGF regulates the balance between osteoblast and adipocyte differentiation. Journal of Clinical Investigation *122*, 3101-3113.

Lund, A.W., Stegemann, J.P., and Plopper, G.E. (2009). Inhibition of ERK promotes collagen gel compaction and fibrillogenesis to amplify the osteogenesis of human mesenchymal stem cells in three-dimensional collagen I culture. Stem cells and development *18*, 331-341.

Lysaght, M.J. (1995). Product development in tissue engineering. Tissue engineering *1*, 221-228.

Lysaght, M.J., and Hazlehurst, A.L. (2004). Tissue engineering: the end of the beginning. Tissue engineering *10*, 309-320.

Lysaght, M.J., and Reyes, J. (2001). The growth of tissue engineering. Tissue engineering *7*, 485-493.

Macchiarini, P., Jungebluth, P., Go, T., Asnaghi, M.A., Rees, L.E., Cogan, T.A., Dodson, A., Martorell, J., Bellini, S., Parnigotto, P.P.*, et al.* (2008). Clinical transplantation of a tissue-engineered airway. Lancet *372*, 2023-2030.

Mai, Q.Y., Yu, Y., Li, T., Wang, L., Chen, M.J., Huang, S.Z., Zhou, C.Q., and Zhou, Q. (2007). Derivation of human embryonic stem cell lines from parthenogenetic blastocysts. Cell research *17*, 1008-1019.

Mason, C., and Dunnill, P. (2008). A brief definition of regenerative medicine. Regenerative medicine *3*, 1-5.

Mason, S.E., Nicolay, C.R., and Darzi, A. (2015). The use of Lean and Six Sigma methodologies in surgery: a systematic review. The surgeon : journal of the Royal Colleges of Surgeons of Edinburgh and Ireland *13*, 91-100.

Matsubara, T., Kida, K., Yamaguchi, A., Hata, K., Ichida, F., Meguro, H., Aburatani, H., Nishimura, R., and Yoneda, T. (2008). BMP2 Regulates Osterix through Msx2 and Runx2 during Osteoblast Differentiation. Journal of Biological Chemistry *283*, 29119-29125.

Maumus, M., Peyrafitte, J.A., D'Angelo, R., Fournier-Wirth, C., Bouloumie, A., Casteilla, L., Sengenes, C., and Bourin, P. (2011). Native human adipose stromal cells: localization, morphology and phenotype. International journal of obesity *35*, 1141-1153.

McBeath, R., Pirone, D.M., Nelson, C.M., Bhadriraju, K., and Chen, C.S. (2004). Cell Shape, Cytoskeletal Tension, and RhoA Regulate Stem Cell Lineage Commitment. Developmental cell *6*, 483-495.

McMurray, R.J., Gadegaard, N., Tsimbouri, P.M., Burgess, K.V., McNamara, L.E., Tare, R., Murawski, K., Kingham, E., Oreffo, R.O.C., and Dalby, M.J. (2011). Nanoscale surfaces for the long-term maintenance of mesenchymal stem cell phenotype and multipotency. Nature materials *10*, 637-644.

McNamara, L.E., McMurray, R.J., Biggs, M.J., Kantawong, F., Oreffo, R.O., and Dalby, M.J. (2010). Nanotopographical control of stem cell differentiation. Journal of tissue engineering *2010*, 120623.

Meinel, L., Karageorgiou, V., Fajardo, R., Snyder, B., Shinde-Patil, V., Zichner, L., Kaplan, D., Langer, R., and Vunjak-Novakovic, G. (2004). Bone tissue engineering using human mesenchymal stem cells: Effects of scaffold material and medium flow. Annals of biomedical engineering *32*, 112-122.

Miller, N.L., Kleinschmidt, E.G., and Schlaepfer, D.D. (2014). RhoGEFs in cell motility: novel links between Rgnef and focal adhesion kinase. Current molecular medicine *14*, 221-234.

Mimeault, M., Hauke, R., and Batra, S.K. (2007). Stem cells: a revolution in therapeutics-recent advances in stem cell biology and their therapeutic applications in regenerative medicine and cancer therapies. Clinical pharmacology and therapeutics *82*, 252-264.

Minary-Jolandan, M., and Yu, M.F. (2009). Nanoscale characterization of isolated individual type I collagen fibrils: polarization and piezoelectricity. Nanotechnology *20*.

Mintz, B. (1985). Renewal and differentiation of totipotent hematopoietic stem cells of the mouse after transplantation into early fetuses. Progress in clinical and biological research *193*, 3-16.

Mintz, B., Anthony, K., and Litwin, S. (1984). Monoclonal derivation of mouse myeloid and lymphoid lineages from totipotent hematopoietic stem cells experimentally engrafted in fetal hosts. Proceedings of the National Academy of Sciences of the United States of America *81*, 7835-7839.

Miyakoshi, J. (2006). The review of cellular effects of a static magnetic field. Science and Technology of Advanced Materials *7*, 305-307.

Miyamoto, A., Shigematsu, T., Fukunaga, T., Kawakami, K., Mukai, C., and Sekiguchi, C. (1998). Medical baseline data collection on bone and muscle change with space flight. Bone *22*, 79S-82S.

Miyauchi, A., Alvarez, J., Greenfield, E.M., Teti, A., Grano, M., Colucci, S., Zambonin-Zallone, A., Ross, F.P., Teitelbaum, S.L., Cheresh, D.*, et al.* (1991). Recognition of osteopontin and related peptides by an alpha v beta 3 integrin stimulates immediate cell signals in osteoclasts. The Journal of biological chemistry *266*, 20369-20374.

Morgani, S.M., Canham, M.A., Nichols, J., Sharov, A.A., Migueles, R.P., Ko, M.S., and Brickman, J.M. (2013). Totipotent embryonic stem cells arise in ground-state culture conditions. Cell reports *3*, 1945-1957.

Morishita, R. (2014). Regenerative medicine. BioMed research international *2014*, 431540.

Myers, K.A., Shrive, N.G., and Hart, D.A. (2007). A novel apparatus applying long term intermittent cyclic hydrostatic pressure to in vitro cell cultures. Journal of bioscience and bioengineering *103*, 578-581.

Nascimento, D.S., Mosqueira, D., Sousa, L.M., Teixeira, M., Filipe, M., Resende, T.P., Araujo, A.F., Valente, M., Almeida, J., Martins, J.P.*, et al.* (2014). Human umbilical cord

tissue-derived mesenchymal stromal cells attenuate remodeling after myocardial infarction by proangiogenic, antiapoptotic, and endogenous cell-activation mechanisms. Stem cell research & therapy *5*.

National Research Council (U.S.). Committee to Review the National Nanotechnology Initiative., and National Academy Press (U.S.) (2006). A matter of size : triennial review of the National Nanotechnology Initiative (Washington, D.C.: National Academies Press).

Neidlinger-Wilke, C., Wurtz, K., Liedert, A., Schmidt, C., Borm, W., Ignatius, A., Wilke, H.J., and Claes, L. (2005). A three-dimensional collagen matrix as a suitable culture system for the comparison of cyclic strain and hydrostatic pressure effects on intervertebral disc cells. Journal of neurosurgery Spine *2*, 457-465.

Nie, S. (2009). Biomedical nanotechnology for molecular imaging, diagnostics, and targeted therapy. Conference proceedings : Annual International Conference of the IEEE Engineering in Medicine and Biology Society IEEE Engineering in Medicine and Biology Society Annual Conference *2009*, 4578-4579.

Nikukar, H., Reid, S., Tsimbouri, P.M., Riehle, M.O., Curtis, A.S., and Dalby, M.J. (2013). Osteogenesis of mesenchymal stem cells by nanoscale mechanotransduction. ACS nano *7*, 2758-2767.

Noris-Suarez, K., Lira-Olivares, J., Ferreira, A.M., Feijoo, J.L., Suarez, N., Hernandez, M.C., and Barrios, E. (2007). In vitro deposition of hydroxyapatite on cortical bone collagen stimulated by deformation-induced piezoelectricity. Biomacromolecules *8*, 941-948.

O'Neal, D.P., Hirsch, L.R., Halas, N.J., Payne, J.D., and West, J.L. (2004). Photo-thermal tumor ablation in mice using near infrared-absorbing nanoparticles. Cancer letters *209*, 171-176.

Ostlund, C., Folker, E.S., Choi, J.C., Gomes, E.R., Gundersen, G.G., and Worman, H.J. (2009). Dynamics and molecular interactions of linker of nucleoskeleton and cytoskeleton (LINC) complex proteins. Journal of cell science *122*, 4099-4108.

Ott, H.C., Clippinger, B., Conrad, C., Schuetz, C., Pomerantseva, I., Ikonomou, L., Kotton, D., and Vacanti, J.P. (2010). Regeneration and orthotopic transplantation of a bioartificial lung. Nature medicine *16*, 927-U131.

Ozaki, S., Kaneko, S., Podyma-Inoue, K.A., Yanagishita, M., and Soma, K. (2005). Modulation of extracellular matrix synthesis and alkaline phosphatase activity of periodontal ligament cells by mechanical stress. Journal of periodontal research *40*, 110-117.

Pacicca, D.M., Moore, D.C., and Ehrlich, M.G. (2002). Physiologic weight-bearing and consolidation of new bone in a rat model of distraction osteogenesis. Journal of pediatric orthopedics *22*, 652-659.

Pang, X., Yang, H., and Peng, B. (2014). Human umbilical cord mesenchymal stem cell transplantation for the treatment of chronic discogenic low back pain. Pain physician *17*, E525-530.

Pappa, K.I., and Anagnou, N.P. (2009). Novel sources of fetal stem cells: where do they fit on the developmental continuum? Regenerative medicine *4*, 423-433.

Pemberton, G.D., Childs, P., Reid, S., Nikukar, H., Tsimbouri, P.M., Gadegaard, N., Curtis, A.S., and Dalby, M.J. (2015). Nanoscale stimulation of osteoblastogenesis from mesenchymal stem cells: nanotopography and nanokicking. Nanomedicine *10*, 547-560.

Petersen, T.H., Calle, E.A., Zhao, L.P., Lee, E.J., Gui, L.Q., Raredon, M.B., Gavrilov, K., Yi, T., Zhuang, Z.W., Breuer, C.*, et al.* (2010). Tissue-Engineered Lungs for in Vivo Implantation. Science *329*, 538-541.

Peytour, Y., Villacreces, A., Chevaleyre, J., Ivanovic, Z., and Praloran, V. (2013). Discarded leukoreduction filters: A new source of stem cells for research, cell engineering and therapy? Stem cell research *11*, 736-742.

Phimphilai, M., Zhoa, Z.R., Boules, H., Roca, H., and Franceschi, R.T. (2006). BMP signaling is required for RUNX2-dependent induction of the osteoblast phenotype. Journal of Bone and Mineral Research *21*, 637-646.

Phinney, D.G., and Prockop, D.J. (2007). Concise review: mesenchymal stem/multipotent stromal cells: the state of transdifferentiation and modes of tissue repair--current views. Stem Cells *25*, 2896-2902.

Pierres, A., Benoliel, A.M., Touchard, D., and Bongrand, P. (2008). How cells tiptoe on adhesive surfaces before sticking. Biophysical journal *94*, 4114-4122.

Pierres, A., Monnet-Corti, V., Benoliel, A.M., and Bongrand, P. (2009). Do membrane undulations help cells probe the world? Trends in Cell Biology *19*, 428-433.

Pimton.P (2013). Influence of Reduced Oxygen Tension on the Differentiation of Mouse Embryonic Stem Cells into Definitive Endoderm and Distal Lung Epithelial Cells. PhD Thesis. Philadelphia PA: Drexel University.

Pogorelov, A.G., and Selezneva, II (2010). Evaluation of collagen gel microstructure by scanning electron microscopy. Bulletin of experimental biology and medicine *150*, 153-156.

Polk, J.D. (2011). Lean Six Sigma, innovation, and the change acceleration process can work together. Physician executive *37*, 38-42.

Pollack, S.R., Meaney, D.F., Levine, E.M., Litt, M., and Johnston, E.D. (2000). Numerical model and experimental validation of microcarrier motion in a rotating bioreactor. Tissue engineering *6*, 519-530.

Porter, B.D., Lin, A.S., Peister, A., Hutmacher, D., and Guldberg, R.E. (2007). Noninvasive image analysis of 3D construct mineralization in a perfusion bioreactor. Biomaterials *28*, 2525-2533.

Powell, R.J., Comerota, A.J., Berceli, S.A., Guzman, R., Henry, T.D., Tzeng, E., Velazquez, O., Marston, W.A., Bartel, R.L., Longcore, A.*, et al.* (2011). Interim analysis results from the RESTORE-CLI, a randomized, double-blind multicenter phase II trial comparing expanded autologous bone marrow-derived tissue repair cells and placebo in patients with critical limb ischemia. Journal of vascular surgery *54*, 1032-1041.

Pozzobon, M., Piccoli, M., and De Coppi, P. (2013). Sources of Mesenchymal Stem Cells: Current and Future Clinical Use. Advances in biochemical engineering/biotechnology *130*, 267-286.

Pre, D., Ceccarelli, G., Gastaldi, G., Asti, A., Saino, E., Visai, L., Benazzo, F., Cusella De Angelis, M.G., and Magenes, G. (2011a). The differentiation of human adipose-derived stem cells (hASCs) into osteoblasts is promoted by low amplitude, high frequency vibration treatment. Bone *49*, 295-303.

Pre, D., Ceccarelli, G., Gastaldi, G., Asti, A., Saino, E., Visai, L., Benazzo, F., De Angelis, M.G.C., and Magenes, G. (2011b). The differentiation of human adipose-derived stem cells (hASCs) into osteoblasts is promoted by low amplitude, high frequency vibration treatment. Bone *49*, 295-303.

Prodanov, L., van Loon, J.J., te Riet, J., Jansen, J.A., and Walboomers, X.F. (2013). Substrate nanotexture and hypergravity through centrifugation enhance initial osteoblastogenesis. Tissue engineering Part A *19*, 114-124.

Rath, S.N., Strobel, L.A., Arkudas, A., Beier, J.P., Maier, A.K., Greil, P., Horch, R.E., and Kneser, U. (2012). Osteoinduction and survival of osteoblasts and bone-marrow stromal cells in 3D biphasic calcium phosphate scaffolds under static and dynamic culture conditions. J Cell Mol Med *16*, 2350-2361.

Rauh, J., Milan, F., Gunther, K.P., and Stiehler, M. (2011a). Bioreactor systems for bone tissue engineering. Tissue engineering Part B, Reviews *17*, 263-280.

Rauh, J., Milan, F., Gunther, K.P., and Stiehler, M. (2011b). Bioreactor Systems for Bone Tissue Engineering. Tissue Eng Part B-Re *17*, 263-280.

Reinish, G.B., and Nowick, A.S. (1975). Piezoelectric Properties of Bone as Functions of Moisture-Content. Nature *253*, 626-627.

Ren, G., Roberts, A.I., and Shi, Y. (2011). Adhesion molecules: key players in Mesenchymal stem cell-mediated immunosuppression. Cell adhesion & migration *5*, 20-22.

Ren, X., Bischoff, D., Weisgerber, D.W., Lewis, M.S., Tu, V., Yamaguchi, D.T., Miller, T.A., Harley, B.A., and Lee, J.C. (2015). Osteogenesis on nanoparticulate mineralized collagen scaffolds via autogenous activation of the canonical BMP receptor signaling pathway. Biomaterials *50*, 107-114.

RikenCenter (2013). Riken Center of Biology "Information on proposed pilot study of the safety and feasibility of transplantation of autologous hiPSC-derived retinal pigment epithelium (RPE) cell sheets in patients with neovascular age-related macular degeneration".

Robey, P.G., Young, M.F., Flanders, K.C., Roche, N.S., Kondaiah, P., Reddi, A.H., Termine, J.D., Sporn, M.B., and Roberts, A.B. (1987). Osteoblasts synthesize and respond to transforming growth factor-type beta (TGF-beta) in vitro. The Journal of cell biology *105*, 457-463.

Rosales-Reyes, R., Skeldon, A.M., Aubert, D.F., and Valvano, M.A. (2012). The Type VI secretion system of Burkholderia cenocepacia affects multiple Rho family GTPases disrupting the actin cytoskeleton and the assembly of NADPH oxidase complex in macrophages. Cellular microbiology *14*, 255-273.

Salanki, J., and Varanka, I. (1969). Analysis of the in situ electrical activity of nerves in fresh-water mussel (Anodonta cygnea L.). Acta biologica Academiae Scientiarum Hungaricae *20*, 437-450.

Salter, E., Goh, B., Hung, B., Hutton, D., Ghone, N., and Grayson, W.L. (2012). Bone tissue engineering bioreactors: a role in the clinic? Tissue engineering Part B, Reviews *18*, 62-75.

Sanchez Alvarado, A., and Yamanaka, S. (2014). Rethinking differentiation: stem cells, regeneration, and plasticity. Cell *157*, 110-119.

Sawada, Y., Tamada, M., Dubin-Thaler, B.J., Cherniavskaya, O., Sakai, R., Tanaka, S., and Sheetz, M.P. (2006). Force sensing by mechanical extension of the Src family kinase substrate p130Cas. Cell *127*, 1015-1026.

Schepers, E., de Clercq, M., Ducheyne, P., and Kempeneers, R. (1991). Bioactive glass particulate material as a filler for bone lesions. Journal of oral rehabilitation *18*, 439-452.

Schmeckebier, S., Mauritz, C., Katsirntaki, K., Sgodda, M., Puppe, V., Duerr, J., Schubert, S.C., Schmiedl, A., Lin, Q., Palecek, J.*, et al.* (2013). Keratinocyte Growth Factor and Dexamethasone Plus Elevated cAMP Levels Synergistically Support Pluripotent Stem Cell Differentiation into Alveolar Epithelial Type II Cells. Tissue Eng Pt A *19*, 938-951.

Schu, S., Nosov, M., O'Flynn, L., Shaw, G., Treacy, O., Barry, F., Murphy, M., O'Brien, T., and Ritter, T. (2012). Immunogenicity of allogeneic mesenchymal stem cells. J Cell Mol Med *16*, 2094-2103.

Sengenes, C., Lolmede, K., Zakaroff-Girard, A., Busse, R., and Bouloumie, A. (2005). Preadipocytes in the human subcutaneous adipose tissue display distinct features from the adult mesenchymal and hematopoietic stem cells. Journal of cellular physiology *205*, 114-122.

Sensebe, L., Bourin, P., and Tarte, K. (2011). Good manufacturing practices production of mesenchymal stem/stromal cells. Human gene therapy *22*, 19-26.

Sensebe, L., Gadelorge, M., and Fleury-Cappellesso, S. (2013). Production of mesenchymal stromal/stem cells according to good manufacturing practices: a review. Stem cell research & therapy *4*, 66.

Shabbir, A., Zisa, D., Lin, H., Mastri, M., Roloff, G., Suzuki, G., and Lee, T. (2010). Activation of host tissue trophic factors through JAK-STAT3 signaling: a mechanism of mesenchymal stem cell-mediated cardiac repair. American journal of physiology Heart and circulatory physiology *299*, H1428-1438.

Shabbir, A., Zisa, D., Suzuki, G., and Lee, T. (2009). Heart failure therapy mediated by the trophic activities of bone marrow mesenchymal stem cells: a noninvasive therapeutic regimen. American journal of physiology Heart and circulatory physiology *296*, H1888-1897.

Sharma, R.R., Pollock, K., Hubel, A., and McKenna, D. (2014). Mesenchymal stem or stromal cells: a review of clinical applications and manufacturing practices. Transfusion *54*, 1418-1437.

Sikavitsas, V.I., Bancroft, G.N., and Mikos, A.G. (2002). Formation of three-dimensional cell/polymer constructs for bone tissue engineering in a spinner flask and a rotating wall vessel bioreactor. Journal of biomedical materials research *62*, 136-148.

Sims, N.A., and Martin, T.J. (2014). Coupling the activities of bone formation and resorption: a multitude of signals within the basic multicellular unit. BoneKEy reports *3*, 481.

Song, K., Wang, H., Zhang, B., Lim, M., Liu, Y., and Liu, T. (2013). Numerical simulation of fluid field and in vitro three-dimensional fabrication of tissue-engineered bones in a rotating

bioreactor and in vivo implantation for repairing segmental bone defects. Cell stress & chaperones *18*, 193-201.

Song, S., Park, J.T., Na, J.Y., Park, M.S., Lee, J.K., Lee, M.C., and Kim, H.S. (2014). Early expressions of hypoxia-inducible factor 1alpha and vascular endothelial growth factor increase the neuronal plasticity of activated endogenous neural stem cells after focal cerebral ischemia. Neural regeneration research *9*, 912-918.

Spaeth, E., Klopp, A., Dembinski, J., Andreeff, M., and Marini, F. (2008). Inflammation and tumor microenvironments: defining the migratory itinerary of mesenchymal stem cells. Gene therapy *15*, 730-738.

Spector, J.A., Mehrara, B.J., Greenwald, J.A., Saadeh, P.B., Steinbrech, D.S., Bouletreau, P.J., Smith, L.P., and Longaker, M.T. (2001). Osteoblast expression of vascular endothelial growth factor is modulated by the extracellular microenvironment. Am J Physiol-Cell Ph *280*, C72-C80.

Steeve, K.T., Marc, P., Sandrine, T., Dominique, H., and Yannick, F. (2004). IL-6, RANKL, TNF-alpha/IL-1: interrelations in bone resorption pathophysiology. Cytokine Growth F R *15*, 49-60.

Stein, G.S., and Lian, J.B. (1993). Molecular mechanisms mediating proliferation/differentiation interrelationships during progressive development of the osteoblast phenotype. Endocrine reviews *14*, 424-442.

Stein, G.S., Lian, J.B., van Wijnen, A.J., Stein, J.L., Montecino, M., Javed, A., Zaidi, S.K., Young, D.W., Choi, J.Y., and Pockwinse, S.M. (2004). Runx2 control of organization, assembly and activity of the regulatory machinery for skeletal gene expression. Oncogene *23*, 4315-4329.

Stein, H., and D'Ambrosia, R. (2008). Wolff's law decoded. Orthopedics *31*, 213.

Stephen J. Szilvassy Albertus W, W. (2013). Hematopoietic stem and progenitor cells. Stemcell technologies mini review.

Stevens, M.M. (2008). Biomaterials for bone tissue engineering. Mater Today *11*, 18-25.

Stonemetz, J., Pham, J.C., Necochea, A.J., McGready, J., Hody, R.E., and Martinez, E.A. (2011). Reduction of regulated medical waste using lean sigma results in financial gains for hospital. Anesthesiology clinics *29*, 145-152.

Su, J., Chen, X., Huang, Y., Li, W., Li, J., Cao, K., Cao, G., Zhang, L., Li, F., Roberts, A.I.*, et al.* (2014). Phylogenetic distinction of iNOS and IDO function in mesenchymal stem cell-

mediated immunosuppression in mammalian species. Cell death and differentiation *21*, 388-396.

Sumanasinghe, R.D., Bernacki, S.H., and Loboa, E.G. (2006). Osteogenic differentiation of human mesenchymal stem cells in collagen matrices: effect of uniaxial cyclic tensile strain on bone morphogenetic protein (BMP-2) mRNA expression. Tissue engineering *12*, 3459-3465.

Surani, A., and Tischler, J. (2012). Stem cells: a sporadic super state. Nature *487*, 43-45.

Tachibana, M., Amato, P., Sparman, M., Gutierrez, N.M., Tippner-Hedges, R., Ma, H., Kang, E., Fulati, A., Lee, H.S., Sritanaudomchai, H*., et al.* (2013). Human embryonic stem cells derived by somatic cell nuclear transfer. Cell *153*, 1228-1238.

Takahashi, K., Tanabe, K., Ohnuki, M., Narita, M., Ichisaka, T., Tomoda, K., and Yamanaka, S. (2007). Induction of pluripotent stem cells from adult human fibroblasts by defined factors. Cell *131*, 861-872.

Takahashi, K., and Yamanaka, S. (2006). Induction of pluripotent stem cells from mouse embryonic and adult fibroblast cultures by defined factors. Cell *126*, 663-676.

Takashima, Y., Era, T., Nakao, K., Kondo, S., Kasuga, M., Smith, A.G., and Nishikawa, S. (2007). Neuroepithelial cells supply an initial transient wave of MSC differentiation. Cell *129*, 1377-1388.

Taran, R., Mamidi, M.K., Singh, G., Dutta, S., Parhar, I.S., John, J.P., Bhonde, R., Pal, R., and Das, A.K. (2014). In vitro and in vivo neurogenic potential of mesenchymal stem cells isolated from different sources. Journal of biosciences *39*, 157-169.

Tarnowski, C.P., Ignelzi, M.A., Jr., and Morris, M.D. (2002). Mineralization of developing mouse calvaria as revealed by Raman microspectroscopy. Journal of bone and mineral research : the official journal of the American Society for Bone and Mineral Research *17*, 1118-1126.

Tay, C.Y., Koh, C.G., Tan, N.S., Leong, D.T., and Tan, L.P. (2013). Mechanoregulation of stem cell fate via micro-/nano-scale manipulation for regenerative medicine. Nanomedicine *8*, 623-638.

Taylor, D., Hazenberg, J.G., and Lee, T.C. (2007). Living with cracks: damage and repair in human bone. Nature materials *6*, 263-268.

Teo, A.K.K., and Vallier, L. (2010). Emerging use of stem cells in regenerative medicine. Biochemical Journal *428*, 11-23.

Thellin, O., Zorzi, W., Lakaye, B., De Borman, B., Coumans, B., Hennen, G., Grisar, T., Igout, A., and Heinen, E. (1999). Housekeeping genes as internal standards: use and limits. J Biotechnol *75*, 291-295.

Tsimbouri, P.M., McMurray, R.J., Burgess, K.V., Alakpa, E.V., Reynolds, P.M., Murawski, K., Kingham, E., Oreffo, R.O., Gadegaard, N., and Dalby, M.J. (2012a). Using nanotopography and metabolomics to identify biochemical effectors of multipotency. ACS nano *6*, 10239-10249.

Tsimbouri, P.M., McMurray, R.J., Burgess, K.V., Alakpa, E.V., Reynolds, P.M., Murawski, K., Kingham, E., Oreffo, R.O.C., Gadegaard, N., and Dalby, M.J. (2012b). Using Nanotopography and Metabolomics to Identify Biochemical Effectors of Multipotency. ACS nano *6*, 10239-10249.

Tsimbouri, P.M., Murawski, K., Hamilton, G., Herzyk, P., Oreffo, R.O., Gadegaard, N., and Dalby, M.J. (2013). A genomics approach in determining nanotopographical effects on MSC phenotype. Biomaterials *34*, 2177-2184.

Uygun, B.E., Soto-Gutierrez, A., Yagi, H., Izamis, M.L., Guzzardi, M.A., Shulman, C., Milwid, J., Kobayashi, N., Tilles, A., Berthiaume, F*., et al.* (2010). Organ reengineering through development of a transplantable recellularized liver graft using decellularized liver matrix. Nature medicine *16*, 814-U120.

van der Kamp, A.W., Roza-de Jongh, E.J., Houwen, R.H., Magrane, G.G., van Dongen, J.M., and Evans, M.J. (1984). Developmental characteristics of somatic cell hybrids between totipotent mouse teratocarcinoma and rat intestinal villus cells. Experimental cell research *154*, 53-64.

Van Eerdenbrugh, B., Van den Mooter, G., and Augustijns, P. (2008). Top-down production of drug nanocrystals: Nanosuspension stabilization, miniaturization and transformation into solid products. Int J Pharmaceut *364*, 64-75.

Vlashi, E., and Pajonk, F. (2014). Cancer stem cells, cancer cell plasticity and radiation therapy. Seminars in cancer biology.

Vogel, V., and Sheetz, M. (2006). Local force and geometry sensing regulate cell functions. Nature reviews Molecular cell biology *7*, 265-275.

Voronov, R., VanGordon, S., Sikavitsas, V.I., and Papavassiliou, D.V. (2010). Computational modeling of flow-induced shear stresses within 3D salt-leached porous scaffolds imaged via micro-CT. Journal of biomechanics *43*, 1279-1286.

Vu, T.Q., Maddipati, R., Blute, T.A., Nehilla, B.J., Nusblat, L., and Desai, T.A. (2005). Peptide-conjugated quantum dots activate neuronal receptors and initiate downstream signaling of neurite growth. Nano letters *5*, 603-607.

Wang, L., Hu, Y.Y., Wang, Z., Li, X., Li, D.C., Lu, B.H., and Xu, S.F. (2009a). Flow perfusion culture of human fetal bone cells in large beta-tricalcium phosphate scaffold with controlled architecture. Journal of biomedical materials research Part A *91*, 102-113.

Wang, L., Ma, Z.S., Li, D.C., Lei, W., Hu, Y.Y., Wang, Z., Li, X., Zhang, Y., and Pei, G.X. (2013). [Three-dimensional flow perfusion culture enhances proliferation of human fetal osteoblasts in large scaffold with controlled architecture]. Zhonghua yi xue za zhi *93*, 1970-1974.

Wang, N., Tytell, J.D., and Ingber, D.E. (2009b). Mechanotransduction at a distance: mechanically coupling the extracellular matrix with the nucleus. Nat Rev Mol Cell Bio *10*, 75-82.

Wang, Y.K., Yu, X., Cohen, D.M., Wozniak, M.A., Yang, M.T., Gao, L., Eyckmans, J., and Chen, C.S. (2012). Bone morphogenetic protein-2-induced signaling and osteogenesis is regulated by cell shape, RhoA/ROCK, and cytoskeletal tension. Stem cells and development *21*, 1176-1186.

Weinreb, M., Shinar, D., and Rodan, G.A. (1990). Different pattern of alkaline phosphatase, osteopontin, and osteocalcin expression in developing rat bone visualized by in situ hybridization. Journal of bone and mineral research : the official journal of the American Society for Bone and Mineral Research *5*, 831-842.

Weissman, I.L. (2000). Stem cells: units of development, units of regeneration, and units in evolution. Cell *100*, 157-168.

Wildemann, B., Lubberstedt, M., Haas, N.P., Raschke, M., and Schmidmaier, G. (2004). IGF-I and TGF-beta 1 incorporated in a poly(D,L-lactide) implant coating maintain their activity over long-term storage-cell culture studies on primary human osteoblast-like cells. Biomaterials *25*, 3639-3644.

Wilshaw, S.P., Rooney, P., Berry, H., Kearney, J.N., Homer-Vanniasinkam, S., Fisher, J., and Ingham, E. (2012). Development and Characterization of Acellular Allogeneic Arterial Matrices. Tissue Eng Pt A *18*, 471-483.

Wingate, K., Bonani, W., Tan, Y., Bryant, S.J., and Tan, W. (2012). Compressive elasticity of three-dimensional nanofiber matrix directs mesenchymal stem cell differentiation to vascular cells with endothelial or smooth muscle cell markers. Acta biomaterialia *8*, 1440-1449.

Wu, X., Liu, H., Liu, J., Haley, K.N., Treadway, J.A., Larson, J.P., Ge, N., Peale, F., and Bruchez, M.P. (2003). Immunofluorescent labeling of cancer marker Her2 and other cellular targets with semiconductor quantum dots. Nature biotechnology *21*, 41-46.

Xiao, G., Jiang, D., Gopalakrishnan, R., and Franceschi, R.T. (2002). Fibroblast growth factor 2 induction of the osteocalcin gene requires MAPK activity and phosphorylation of the osteoblast transcription factor, Cbfa1/Runx2. The Journal of biological chemistry *277*, 36181-36187.

Xie, Q., Wang, Z., Bi, X.P., Zhou, H.F., Wang, Y.F., Gu, P., and Fan, X.Q. (2014). Effects of miR-31 on the osteogenesis of human mesenchymal stem cells. Biochemical and biophysical research communications *446*, 98-104.

Xie, Y., and Han, R. (1996). Bulk modulus calculations based on perturbation self-consistency. Journal of physics Condensed matter : an Institute of Physics journal *8*, 7199-7204.

Xu, D., Xu, L., Zhou, C., Lee, W.Y., Wu, T., Cui, L., and Li, G. (2014). Salvianolic acid B promotes osteogenesis of human mesenchymal stem cells through activating ERK signaling pathway. The international journal of biochemistry & cell biology *51*, 1-9.

Yamasaki, K. (1983). The Role of Cyclic-Amp, Calcium, and Prostaglandins in the Induction of Osteoclastic Bone-Resorption Associated with Experimental Tooth Movement. Journal of dental research *62*, 877-881.

Yeatts, A.B., Choquette, D.T., and Fisher, J.P. (2013). Bioreactors to influence stem cell fate: augmentation of mesenchymal stem cell signaling pathways via dynamic culture systems. Biochimica et biophysica acta *1830*, 2470-2480.

Yezhelyev, M.V., Qi, L., O'Regan, R.M., Nie, S., and Gao, X. (2008). Proton-sponge coated quantum dots for siRNA delivery and intracellular imaging. J Am Chem Soc *130*, 9006-9012.

Yu, B., Zhao, X.L., Yang, C.Z., Crane, J., Xian, L.L., Lu, W., Wan, M., and Cao, X. (2012). Parathyroid hormone induces differentiation of mesenchymal stromal/stem cells by enhancing bone morphogenetic protein signaling. Journal of Bone and Mineral Research *27*, 2001-2014.

Zhang, Z., and Alexanian, A.R. (2014). The neural plasticity of early-passage human bone marrow-derived mesenchymal stem cells and their modulation with chromatin-modifying agents. Journal of tissue engineering and regenerative medicine *8*, 407-413.

Zhou, H.Y., Wu, S.L., Joo, J.Y., Zhu, S.Y., Han, D.W., Lin, T.X., Trauger, S., Bien, G., Yao, S., Zhu, Y.*, et al.* (2009). Generation of Induced Pluripotent Stem Cells Using Recombinant Proteins. Cell stem cell *4*, 381-384.

Zhou, T., Benda, C., Dunzinger, S., Huang, Y., Ho, J.C., Yang, J., Wang, Y., Zhang, Y., Zhuang, Q., Li, Y.*, et al.* (2012). Generation of human induced pluripotent stem cells from urine samples. Nature protocols *7*, 2080-2089.

Zhu, F.C., Friedman, M.S., Luo, W.J., Woolf, P., and Hankenson, K.D. (2012a). The transcription factor osterix (SP7) regulates BMP6-induced human osteoblast differentiation. Journal of cellular physiology *227*, 2677-2685.

Zhu, X.S., Jing, D., and Gang, L. (2012b). The Comparison of Multilineage Differentiation of Bone Marrow and Adipose-Derived Mesenchymal Stem Cells. Clin Lab *58*, 897-903.

Zolochevska, O., Yu, G., Gimble, J.M., and Figueiredo, M.L. (2012). Pigment Epithelial-Derived Factor and Melanoma Differentiation Associated Gene-7 Cytokine Gene Therapies Delivered by Adipose-Derived Stromal/Mesenchymal Stem Cells are Effective in Reducing Prostate Cancer Cell Growth. Stem cells and development *21*, 1112-1123.

Zou, C., Luo, Q., Qin, J., Shi, Y., Yang, L., Ju, B., and Song, G. (2013). Osteopontin promotes mesenchymal stem cell migration and lessens cell stiffness via integrin beta1, FAK, and ERK pathways. Cell biochemistry and biophysics *65*, 455-462.

Stein, H., and D'Ambrosia, R. (2008). Wolff's law decoded. Orthopedics *31*, 213.

Stephen J. Szilvassy Albertus W, W. (2013). Hematopoietic stem and progenitor cells. Stemcell technologies mini review.

Stevens, M.M. (2008). Biomaterials for bone tissue engineering. Mater Today *11*, 18-25.

Stonemetz, J., Pham, J.C., Necochea, A.J., McGready, J., Hody, R.E., and Martinez, E.A. (2011). Reduction of regulated medical waste using lean sigma results in financial gains for hospital. Anesthesiology clinics *29*, 145-152.

Su, J., Chen, X., Huang, Y., Li, W., Li, J., Cao, K., Cao, G., Zhang, L., Li, F., Roberts, A.I.*, et al.* (2014). Phylogenetic distinction of iNOS and IDO function in mesenchymal stem cell-mediated immunosuppression in mammalian species. Cell death and differentiation *21*, 388-396.

Sumanasinghe, R.D., Bernacki, S.H., and Loboa, E.G. (2006). Osteogenic differentiation of human mesenchymal stem cells in collagen matrices: effect of uniaxial cyclic tensile strain on bone morphogenetic protein (BMP-2) mRNA expression. Tissue engineering *12*, 3459-3465.

Surani, A., and Tischler, J. (2012). Stem cells: a sporadic super state. Nature *487*, 43-45.

Tachibana, M., Amato, P., Sparman, M., Gutierrez, N.M., Tippner-Hedges, R., Ma, H., Kang, E., Fulati, A., Lee, H.S., Sritanaudomchai, H.*, et al.* (2013). Human embryonic stem cells derived by somatic cell nuclear transfer. Cell *153*, 1228-1238.

Takahashi, K., Tanabe, K., Ohnuki, M., Narita, M., Ichisaka, T., Tomoda, K., and Yamanaka, S. (2007). Induction of pluripotent stem cells from adult human fibroblasts by defined factors. Cell *131*, 861-872.

Takahashi, K., and Yamanaka, S. (2006). Induction of pluripotent stem cells from mouse embryonic and adult fibroblast cultures by defined factors. Cell *126*, 663-676.

Takashima, Y., Era, T., Nakao, K., Kondo, S., Kasuga, M., Smith, A.G., and Nishikawa, S. (2007). Neuroepithelial cells supply an initial transient wave of MSC differentiation. Cell *129*, 1377-1388.

Taran, R., Mamidi, M.K., Singh, G., Dutta, S., Parhar, I.S., John, J.P., Bhonde, R., Pal, R., and Das, A.K. (2014). In vitro and in vivo neurogenic potential of mesenchymal stem cells isolated from different sources. Journal of biosciences *39*, 157-169.

Tarnowski, C.P., Ignelzi, M.A., Jr., and Morris, M.D. (2002). Mineralization of developing mouse calvaria as revealed by Raman microspectroscopy. Journal of bone and mineral research : the official journal of the American Society for Bone and Mineral Research *17*, 1118-1126.

Tay, C.Y., Koh, C.G., Tan, N.S., Leong, D.T., and Tan, L.P. (2013). Mechanoregulation of stem cell fate via micro-/nano-scale manipulation for regenerative medicine. Nanomedicine *8*, 623-638.

Taylor, D., Hazenberg, J.G., and Lee, T.C. (2007). Living with cracks: damage and repair in human bone. Nature materials *6*, 263-268.

Teo, A.K.K., and Vallier, L. (2010). Emerging use of stem cells in regenerative medicine. Biochemical Journal *428*, 11-23.

Thellin, O., Zorzi, W., Lakaye, B., De Borman, B., Coumans, B., Hennen, G., Grisar, T., Igout, A., and Heinen, E. (1999). Housekeeping genes as internal standards: use and limits. J Biotechnol *75*, 291-295.

Tarnowski, C.P., Ignelzi, M.A., Jr., and Morris, M.D. (2002). Mineralization of developing mouse calvaria as revealed by Raman microspectroscopy. Journal of bone and mineral research : the official journal of the American Society for Bone and Mineral Research *17*, 1118-1126.

Tseng, P.C., Young, T.H., Wang, T.M., Peng, H.W., Hou, S.M., and Yen, M.L. (2012). Spontaneous osteogenesis of MSCs cultured on 3D microcarriers through alteration of cytoskeletal tension. Biomaterials *33*, 556-564.

Tsimbouri, P.M., McMurray, R.J., Burgess, K.V., Alakpa, E.V., Reynolds, P.M., Murawski, K., Kingham, E., Oreffo, R.O., Gadegaard, N., and Dalby, M.J. (2012). Using nanotopography and metabolomics to identify biochemical effectors of multipotency. ACS nano *6*, 10239-10249.

Tsimbouri, P.M., Murawski, K., Hamilton, G., Herzyk, P., Oreffo, R.O., Gadegaard, N., and Dalby, M.J. (2013). A genomics approach in determining nanotopographical effects on MSC phenotype. Biomaterials *34*, 2177-2184.

Uygun, B.E., Soto-Gutierrez, A., Yagi, H., Izamis, M.L., Guzzardi, M.A., Shulman, C., Milwid, J., Kobayashi, N., Tilles, A., Berthiaume, F*., et al.* (2010). Organ reengineering

Uygun, B.E., Soto-Gutierrez, A., Yagi, H., Izamis, M.L., Guzzardi, M.A., Shulman, C., Milwid, J., Kobayashi, N., Tilles, A., Berthiaume, F*., et al.* (2010). Organ reengineering through development of a transplantable recellularized liver graft using decellularized liver matrix. Nature medicine *16*, 814-U120.

through development of a transplantable recellularized liver graft using decellularized liver matrix. Nature medicine *16*, 814-U120.

van der Kamp, A.W., Roza-de Jongh, E.J., Houwen, R.H., Magrane, G.G., van Dongen, J.M., and Evans, M.J. (1984). Developmental characteristics of somatic cell hybrids between totipotent mouse teratocarcinoma and rat intestinal villus cells. Experimental cell research *154*, 53-64.

Van Eerdenbrugh, B., Van den Mooter, G., and Augustijns, P. (2008). Top-down production of drug nanocrystals: Nanosuspension stabilization, miniaturization and transformation into solid products. Int J Pharmaceut *364*, 64-75.

Vlashi, E., and Pajonk, F. (2014). Cancer stem cells, cancer cell plasticity and radiation therapy. Seminars in cancer biology.

Vogel, V., and Sheetz, M. (2006). Local force and geometry sensing regulate cell functions. Nature reviews Molecular cell biology *7*, 265-275.

Voronov, R., VanGordon, S., Sikavitsas, V.I., and Papavassiliou, D.V. (2010). Computational modeling of flow-induced shear stresses within 3D salt-leached porous scaffolds imaged via micro-CT. Journal of biomechanics *43*, 1279-1286.

Vu, T.Q., Maddipati, R., Blute, T.A., Nehilla, B.J., Nusblat, L., and Desai, T.A. (2005). Peptide-conjugated quantum dots activate neuronal receptors and initiate downstream signaling of neurite growth. Nano letters *5*, 603-607.

Wang, L., Hu, Y.Y., Wang, Z., Li, X., Li, D.C., Lu, B.H., and Xu, S.F. (2009a). Flow perfusion culture of human fetal bone cells in large beta-tricalcium phosphate scaffold with controlled architecture. Journal of biomedical materials research Part A *91*, 102-113.

Wang, L., Ma, Z.S., Li, D.C., Lei, W., Hu, Y.Y., Wang, Z., Li, X., Zhang, Y., and Pei, G.X. (2013). [Three-dimensional flow perfusion culture enhances proliferation of human fetal osteoblasts in large scaffold with controlled architecture]. Zhonghua yi xue za zhi *93*, 1970-1974.

Wang, N., Tytell, J.D., and Ingber, D.E. (2009b). Mechanotransduction at a distance: mechanically coupling the extracellular matrix with the nucleus. Nat Rev Mol Cell Bio *10*, 75-82.

Wang, Y.K., Yu, X., Cohen, D.M., Wozniak, M.A., Yang, M.T., Gao, L., Eyckmans, J., and Chen, C.S. (2012). Bone morphogenetic protein-2-induced signaling and osteogenesis is regulated by cell shape, RhoA/ROCK, and cytoskeletal tension. Stem cells and development *21*, 1176-1186.

Weinreb, M., Shinar, D., and Rodan, G.A. (1990). Different pattern of alkaline phosphatase, osteopontin, and osteocalcin expression in developing rat bone visualized by in situ hybridization. Journal of bone and mineral research : the official journal of the American Society for Bone and Mineral Research *5*, 831-842.

Weissman, I.L. (2000). Stem cells: units of development, units of regeneration, and units in evolution. Cell *100*, 157-168.

Wildemann, B., Lubberstedt, M., Haas, N.P., Raschke, M., and Schmidmaier, G. (2004). IGF-I and TGF-beta 1 incorporated in a poly(D,L-lactide) implant coating maintain their activity over long-term storage-cell culture studies on primary human osteoblast-like cells. Biomaterials *25*, 3639-3644.

Wilshaw, S.P., Rooney, P., Berry, H., Kearney, J.N., Homer-Vanniasinkam, S., Fisher, J., and Ingham, E. (2012). Development and Characterization of Acellular Allogeneic Arterial Matrices. Tissue Eng Pt A *18*, 471-483.

Wingate, K., Bonani, W., Tan, Y., Bryant, S.J., and Tan, W. (2012). Compressive elasticity of three-dimensional nanofiber matrix directs mesenchymal stem cell differentiation to vascular cells with endothelial or smooth muscle cell markers. Acta biomaterialia *8*, 1440-1449.

Wu, X., Liu, H., Liu, J., Haley, K.N., Treadway, J.A., Larson, J.P., Ge, N., Peale, F., and Bruchez, M.P. (2003). Immunofluorescent labeling of cancer marker Her2 and other cellular targets with semiconductor quantum dots. Nature biotechnology *21*, 41-46.

Xian, C.J., Zhou, F.H., McCarty, R.C., and Foster, B.K. (2004). Intramembranous ossification mechanism for bone bridge formation at the growth plate cartilage injury site. Journal of orthopaedic research : official publication of the Orthopaedic Research Society *22*, 417-426.

Xiao, G., Jiang, D., Gopalakrishnan, R., and Franceschi, R.T. (2002). Fibroblast growth factor 2 induction of the osteocalcin gene requires MAPK activity and phosphorylation of the osteoblast transcription factor, Cbfa1/Runx2. The Journal of biological chemistry *277*, 36181-36187.

Xie, Q., Wang, Z., Bi, X.P., Zhou, H.F., Wang, Y.F., Gu, P., and Fan, X.Q. (2014). Effects of miR-31 on the osteogenesis of human mesenchymal stem cells. Biochemical and biophysical research communications *446*, 98-104.

Xie, Y., and Han, R. (1996). Bulk modulus calculations based on perturbation self-consistency. Journal of physics Condensed matter : an Institute of Physics journal *8*, 7199-7204.

Xu, D., Xu, L., Zhou, C., Lee, W.Y., Wu, T., Cui, L., and Li, G. (2014). Salvianolic acid B promotes osteogenesis of human mesenchymal stem cells through activating ERK signaling pathway. The international journal of biochemistry & cell biology *51*, 1-9.

Yamasaki, K. (1983). The Role of Cyclic-Amp, Calcium, and Prostaglandins in the Induction of Osteoclastic Bone-Resorption Associated with Experimental Tooth Movement. Journal of dental research *62*, 877-881.

Yeatts, A.B., Choquette, D.T., and Fisher, J.P. (2013). Bioreactors to influence stem cell fate: augmentation of mesenchymal stem cell signaling pathways via dynamic culture systems. Biochimica et biophysica acta *1830*, 2470-2480.

Yezhelyev, M.V., Qi, L., O'Regan, R.M., Nie, S., and Gao, X. (2008). Proton-sponge coated quantum dots for siRNA delivery and intracellular imaging. J Am Chem Soc *130*, 9006-9012.

Yu, B., Zhao, X.L., Yang, C.Z., Crane, J., Xian, L.L., Lu, W., Wan, M., and Cao, X. (2012). Parathyroid hormone induces differentiation of mesenchymal stromal/stem cells by enhancing bone morphogenetic protein signaling. Journal of Bone and Mineral Research *27*, 2001-2014.

Zhang, Z., and Alexanian, A.R. (2014). The neural plasticity of early-passage human bone marrow-derived mesenchymal stem cells and their modulation with chromatin-modifying agents. Journal of tissue engineering and regenerative medicine *8*, 407-413.

Zhou, H.Y., Wu, S.L., Joo, J.Y., Zhu, S.Y., Han, D.W., Lin, T.X., Trauger, S., Bien, G., Yao, S., Zhu, Y.*, et al.* (2009). Generation of Induced Pluripotent Stem Cells Using Recombinant Proteins. Cell stem cell *4*, 381-384.

Zhou, T., Benda, C., Dunzinger, S., Huang, Y., Ho, J.C., Yang, J., Wang, Y., Zhang, Y., Zhuang, Q., Li, Y.*, et al.* (2012). Generation of human induced pluripotent stem cells from urine samples. Nature protocols *7*, 2080-2089.

Zhu, F.C., Friedman, M.S., Luo, W.J., Woolf, P., and Hankenson, K.D. (2012a). The transcription factor osterix (SP7) regulates BMP6-induced human osteoblast differentiation. Journal of cellular physiology *227*, 2677-2685.

Zhu, X.S., Jing, D., and Gang, L. (2012b). The Comparison of Multilineage Differentiation of Bone Marrow and Adipose-Derived Mesenchymal Stem Cells. Clin Lab *58*, 897-903.

Zolochevska, O., Yu, G., Gimble, J.M., and Figueiredo, M.L. (2012). Pigment Epithelial-Derived Factor and Melanoma Differentiation Associated Gene-7 Cytokine Gene Therapies Delivered by Adipose-Derived Stromal/Mesenchymal Stem Cells are Effective in Reducing Prostate Cancer Cell Growth. Stem cells and development *21*, 1112-1123.

Zou, C., Luo, Q., Qin, J., Shi, Y., Yang, L., Ju, B., and Song, G. (2013). Osteopontin promotes mesenchymal stem cell migration and lessens cell stiffness via integrin beta1, FAK, and ERK pathways. Cell biochemistry and biophysics *65*, 455-462.